

**CHARACTERIZATION OF MAGNETO-RHEOLOGICAL
FLUID AND MONOTUBE DAMPER THROUGH
EXPERIMENTAL AND COMPUTATIONAL ANALYSIS**

Thesis

Submitted in partial fulfillment of the requirements for the degree of
DOCTOR OF PHILOSOPHY

by

Gurubasavaraju T.M.



DEPARTMENT OF MECHANICAL ENGINEERING
NATIONAL INSTITUTE OF TECHNOLOGY KARNATAKA,
SURATHKAL, MANGALORE – 575025

May 2018

DECLARATION

I hereby *declare* that the Research Thesis entitled “**CHARACTERIZATION OF MAGNETO-RHEOLOGICAL FLUID AND MONOTUBE DAMPER THROUGH EXPERIMENTAL AND COMPUTATIONAL ANALYSIS**” which is being submitted to the **National Institute of Technology Karnataka, Surathkal** in partial fulfillment of the requirements for the award of the Degree of **Doctor of Philosophy** in **Department of Mechanical Engineering** is a *bonafide report of the research work carried out by me*. The material contained in this Research Thesis has not been submitted to any University or Institution for the award of any degree.

Register Number : **145077ME14F06**

Name of the Research Scholar : **Gurubasavaraju T.M.**

Signature of the Research Scholar :

Department of Mechanical Engineering

Place : **NITK, Surathkal**

Date :

C E R T I F I C A T E

This is to *certify* that the Research Thesis entitled “**CHARACTERIZATION OF MAGNETO-RHEOLOGICAL FLUID AND MONOTUBE DAMPER THROUGH EXPERIMENTAL AND COMPUTATIONAL ANALYSIS**” submitted by **Mr. Gurubasavaraju T.M. (Register Number: 145077ME14F06** as the record of the research work carried out by him, is *accepted as the Research Thesis submission* in partial fulfillment of the requirements for the award of degree of **Doctor of Philosophy**.

Research Guide(s)

Dr. Hemantha Kumar

Assistant Professor

Department of Mechanical Engineering

NITK, Surathkal

Dr. Arun M.

Assistant Professor

Department of Mechanical Engineering

NITK, Surathkal

Chairman - DRPC

Date:

ACKNOWLEDGEMENTS

With a deep sense of gratitude, I wish to express my sincere thanks to my supervisors **Dr. Hemantha Kumar** and **Dr. Arun M.**, Department of Mechanical Engineering, National Institute of Technology Karnataka (N.I.T.K), Surathkal, for their excellent guidance and support throughout my resesarch work. I received very useful, encouraging and excellent academic feedback from them, which has helped me in coming up with this thesis. Their constant encouragement, help and review of the entire work during the course of the investigation were invaluable. I profoundly thank them.

I take this opportunity to thank **Dr. Narendranath S.**, Professor and Head, Department of Mechanical Engineering for his continuous and timely suggestions.

I acknowledge the funding support from **IMPRINT** project No. **IMPRINT/2016/7330**, titled with “Development of Cost Effective Magneto-Rheological (MR) Fluid Damper in Two wheelers and Four Wheelers Automobile to Improve Ride Comfort and Stability” under Ministry of Human Resource Development and Ministry of Road Transfer and Highways, Govt. of India.

I wish to thank all the members of the Research Program Assessment Committee members, **Prof. Ravikiran Kadoli**, Department of Mining Engineering and **Dr. A.S. Balu**, Assistant Professor, Department of Civil Engineering for their appreciation and valuable suggestions for this research work.

I wish to express my sincere gratitude to all the faculty members of the Department of Mechanical Engineering, N.I.T.K Surathkal for their help, encouragement and support all through this research work.

My sincere thanks to all my lab mates Dr. Madhusudan C.K, Mr. Kiran Vernekar, Dr. Gangadhar N, Mr. Subash Acharya, Mr. Puneeth N.P., Mr. Rangaraj M Desai., Mr. Ravikumar., Mr. J. Vipin Allien, Mr. Srinivasa N and Mr. Radhe Shyam, Dr. Hemant K for their help and support to carry out this dissertation work.

I am indebted to my batchmates Mr. Balanarasimha Mr. Praveen Shenoy, Mr. Mallikarjuna B, Mr. Susheel Kumar and my MTech project guide Mr. Madev Nagaral for their constant help and encouragement during the entire research work.

Finally, I would like to thank my parents who have trusted me throughout my life. I would like to share this moment of happiness with my mother, Savithramma T.M; My brothers Dr. Vishwaradhya T.M and Mr. Siddalinga Swamy T.M.; My uncle Mr. Gurusuddaiah T.S. for their constant encouragement.

Gurubasavaraju T.M.

ABSTRACT

Magnetorheological fluid belongs to a class of smart materials which exhibit change in their rheological properties, when exposed to an external magnetic field and these properties are completely reversible. By utilizing these special characteristics, the damping force of the MR damper can be controlled and varied in real time applications. The main objective of this research work is to investigate the characteristics of MR fluid and MR damper through experimental as well as computational methods and to evaluate the semi-active suspension with MR dampers performance in terms of ride comfort and road holding of vehicles, when subjected to random road conditions. The rheological characterization of the MR fluid samples under different magnetic fields and fluid gap has been evaluated through experimentation. The measured fluid properties were used for computing the damping force of MR damper. Using single and multi-objective particle swarm optimization techniques, the optimal proportion of iron particles for MR damper application was determined to maximize the shear stress and damping force.

The dynamic characterization of MR damper through experimental approach using dynamic test facility at 1.5 Hz and 2 Hz frequencies has been carried out. Also, the influence of material properties of MR damper components on the induced magnetic flux density and geometrical parameters on the damping force was investigated through finite element analysis as well as analytical methods. Multi-objective genetic algorithm and screening optimization techniques were employed to maximize the magnetic flux density and to identify the optimal values of the design variables. Using the analytical method, damping force of the damper was computed for the obtained optimal values of the design variables. It was observed that the damping force of the MR damper whose cylinder is made up of magnetic material was 2.79 times greater than that of MR damper whose cylinder is made up of non-magnetic material.

Further, a coupled finite element analysis (FEA) and computational fluid dynamics (CFD) analysis was used for estimating the magnetic flux density and damping force for different input currents. The credibility of the shear mode monotube MR damper

analysis results were validated with experimental results. To overcome certain limitations of shear mode damper, an attempt has been made to realize the mixed mode damper by combining the flow and shear mode operations. The variations in the damping characteristics of flow and mixed mode MR damper under different input were compared with shear mode MR damper. Results showed that combination of two modes of operation could enhance the damping force to a significant level. The damping force of mixed mode MR damper was found to be 3 times greater than that of shear mode MR damper at 2 Hz frequency and 0.4 A current.

Based on results obtained from computational analyses, a non-parametric representative model exhibiting the hysteretic behavior of MR damper was developed. The developed nonparametric model was implemented in a quarter car semi-active suspension to determine the dynamic response of the vehicle subjected to random road excitations. Further, this model was implemented in three-wheeler vehicle semi-active suspension system to evaluate its dynamic performance. The outcome showed that the vehicle with non-parametric based MR suspension system provided good vibration isolation for semi-active suspension than passive suspension system in terms of ride comfort and road holding.

Keywords: MR damper, Optimization, CFD, FEA, Semi-active suspension system, Quarter car model, Random road profile, Three-wheeler model.

CONTENTS

Declaration	
Certificate	
Acknowledgements	
Abstract	
List of contents	i
List of figures	vii
List of tables	xiii
Abbreviations	xv

1. INTRODUCTION

1.1 INTRODUCTION	1
1.2 MR FLUID	1
1.3 COMPONENTS OF MR FLUID	3
1.3.1 Carrier fluid phase	3
1.3.2 Magnetisable particles	3
1.3.3 Additives	4
1.4 PROPERTIES OF MR FLUIDS	5
1.4.1 Off state viscosity	5
1.4.2 Yield stress	5
1.4.3 Magnetic flux density and Magnetic flux intensity (B-H) Relationship	5
1.4.4 Durability and In-Use Thickening	6
1.4.5 Pre-yield and Post-yield behavior	6
1.5 MR FLUID OPERATION MODES	7
1.5.1 Flow/Valve Mode	7
1.5.2 Squeeze-flow mode	8
1.5.3 Shear Mode	9
1.5.4 Pinch mode	10
1.6 MAGNETORHEOLOGICAL DAMPER	10
1.6.1 Monotube MR damper	11
1.6.2 Twin tube MR damper	12

1.6.3	Double ended MR damper	13
1.7	VIBRATION SUSPENSION SYSTEM	13
1.7.1	Passive suspension system	14
1.7.2	Active suspension system	14
1.7.3	Semi-active suspension system	15
1.8	MATHEMATICAL MODEL OF MR DAMPER	17
1.8.1	Quasi-static models	17
1.8.2	Dynamic models	18
1.8.2.1	<i>Parametric models</i>	18
1.8.2.2	<i>Non-parametric models</i>	19
1.8.3	Inverse dynamic models	19
1.8.4	Vehicle models	19
1.9	OUTLINE OF THE THESIS	20
2.	LITERATURE REVIEW	22
2.1	INTRODUCTION	22
2.2	FLOW MODELS OF MR FLUID	22
2.2.1	Bingham fluid model	23
2.2.2	Herschel-Bulkley fluid model	23
2.2.3	Casson Fluid model	23
2.3	CHARACTERISATION OF MAGNETORHEOLOGICAL (MR) FLUID	24
2.3.1	Viscoelastic behavior of MR fluid	25
2.4	APPLICATIONS OF MR FLUIDS	27
2.4.1	MR Bearings	27
2.4.2	MR mounts	28
2.4.3	MR fluid brake and MR clutch	29
2.4.4	MR fluid polishing	30
2.4.5	MR dampers in various applications	31
2.5	COMPUTATIONAL ANALYSIS OF MR DAMPER	33
2.5.1	Geometric optimization of MR damper	35
2.5.2	FEA and CFD analysis	38
2.6	MR DAMPER MODELS	40

2.6.1	Quasi-static models	41
2.6.2	Parametric models	41
2.6.3	Non-parametric model	46
2.7	SEMI-ACTIVE VIBRATION CONTROL OF VEHICLES	49
2.8	MOTIVATION	51
2.9	OBJECTIVES	51
2.10	SCOPE	52
2.11	SUMMARY	52
3.	METHODOLOGY AND EXPERIMENTAL SETUP	53
3.1	INTRODUCTION	53
3.2	METHODOLOGY	53
3.2.1	Preparation of MR fluid and Evaluation of optimum proportion of MR fluid	55
3.2.2	Dynamic characterization of an MR damper	55
3.2.3	Optimization of an MR damper	56
3.2.4	Coupled FEA and CFD analysis of MR damper	56
3.2.5	Development of nonparametric model of MR damper and dynamic analysis of vehicle suspension	57
3.3	EXPERIMENTAL SETUP	57
3.3.1	Rheological characterization	57
3.3.1.1	<i>Measuring tool (PP-20)</i>	57
3.3.1.2	<i>MRD cell</i>	59
3.3.2	Damper test facility	59
3.3.2.1	<i>Electric motor driven shaker</i>	60
3.3.2.2	<i>DC Power supply</i>	61
3.3.2.3	<i>Data acquisition System</i>	61
3.3.2.4	<i>Displacement transducer</i>	62
3.3.2.5	<i>Force transducer</i>	62
3.4	SUMMARY	63
4.	PREPARATION AND RHEOLOGICAL CHARACTERIZATION OF MR FLUID	64
4.1	INTRODUCTION	64

4.2 SAMPLE PREPARATION	64
4.3 APPARATUS	65
4.4 COMPUTATION OF DAMPING FORCE OF MR DAMPER	66
4.5 OPTIMISATION THROUGH PARTICLE SWARM OPTIMISATION (PSO)	68
4.6 DESIGN OF EXPERIMENTS (DOE)	70
4.7 ANALYSIS OF VARIANCE (ANOVA)	71
4.8 RESULTS AND DISCUSSIONS	71
4.8.1 Influence of particle concentration	71
4.8.2 Influence of parallel plate gap	73
4.8.2.1 <i>Polynomial equation</i>	75
4.8.3 Dynamic characteristics	77
4.8.4 Statistical analysis	79
4.8.5 Response surface method	84
4.9 SUMMARY	87
5. FABRICATION AND CHARACTERISATION OF MONOTUBE MR DAMPER	88
5.1 INTRODUCTION	88
5.2 SHEAR MODE TYPE MONOTUBE MR DAMPER	88
5.2.1 MR damper characteristics	88
5.2.1.1 <i>Controllable damping force</i>	88
5.2.1.2 <i>Effective stiffness</i>	89
5.2.1.3 <i>Energy dissipation</i>	89
5.2.1.4 <i>Equivalent damping coefficient</i>	90
5.2.2 Components of MR damper	90
5.2.3 Material Selection	90
5.2.4 Geometric details of monotube MR damper	91
5.3 EXPERIMENTAL SETUP	93
5.4 RESULTS AND DISCUSSION	94
5.5 SUMMARY	97
6. GEOMETRIC OPTIMIZATION OF MR DAMPER AND STATISTICAL ANALYSIS OF DESIGN PARAMETERS	98

6.1 INTRODUCTION	98
6.2 METHODOLOGY OF OPTIMIZATION	98
6.3 MAGNETOSTATIC ANALYSIS	99
6.4 ESTIMATION OF DAMPING FORCE OF MR DAMPER	102
6.5 OPTIMIZATION OF MONOTUBE MR DAMPER	104
6.5.1 Design of Experiments	104
6.5.2 Response surface and optimization	105
6.6 RESULTS AND DISCUSSIONS	106
6.6.1 Results of Magnetostatic analysis	106
6.6.2 Damping force results	107
6.6.3 Optimization results	109
6.6.3.1 <i>Analysis of variance (ANOVA)</i>	109
6.6.3.2 <i>Normality test</i>	113
6.6.3.3 <i>Homoscedasticity</i>	114
6.6.3.4 <i>Run chart</i>	115
6.6.3.5 <i>Sensitivity and Response surfaces</i>	115
6.7 SUMMARY	121
7. COMPUTATIONAL FLUID DYNAMIC ANALYSIS OF MR DAMPER	122
7.1 INTRODUCTION	122
7.2 COMPUTATIONAL ANALYSIS	122
7.2.1 Magnetostatic analysis of monotube MR damper	123
7.2.2 CFD analysis of MR Damper	126
7.3 RESULTS AND DISCUSSION	130
7.3.1 Magnetostatic analysis results	130
7.3.2 CFD analysis results	132
7.3.3 Validating the CFD results with experimental results of monotube MR damper	133
7.3.4 Influence of the frequency on damping force (using CFD analysis)	135
7.3.5 Influence of effective gap length on damping force (using CFD analysis)	138

7.3.6	Comparison of modes of MR damper	139
7.4	SUMMARY	142
8.	DYNAMIC ANALYSIS OF A VEHICLE WITH SEMI-ACTIVE SUSPENSIONS SYSTEM	144
8.1	INTRODUCTION	144
8.2	NON-PARAMETRIC MODELLING OF MR DAMPER	144
8.2.1	Random road profile model	146
8.2.2	Performance indices	148
8.3	MATHEMATICAL MODELING OF VEHICLE	148
8.3.1	Semi-active control strategies	148
8.3.1.1	Fuzzy logic control strategy	149
8.3.1.2	Proportional-Integral-Derivative (PID) control strategy	151
8.3.2	Dynamic analysis of quarter car model	153
8.3.2.1	Dynamic response analysis of quarter car model subjected to random road	155
8.3.3	Dynamic analysis of three-wheeler passenger vehicle	159
8.4	SUMMARY	164
9.	SUMMARY AND CONCLUSIONS	165
9.1	SUMMARY	165
9.2	CONTRIBUTIONS	166
9.3	CONCLUSIONS	167
9.4	SCOPE OF FUTURE WORK	169
	REFERENCES	170
	APPENDIX	193

LIST OF FIGURES

Figure No.	Description	Page No.
Figure 1.1	MR fluid particles (a) Off -state and (b) On state	2
Figure 1.2	B-H curve (a) General model (b) MRF-132DG	6
Figure 1.3	Shear stress vs shear rate plot of (a) Bingham Plastic and (b) MR fluid	7
Figure 1.4	Flow Mode	8
Figure 1.5	Squeeze-flow mode	9
Figure 1.6	Shear mode	9
Figure 1.7	Pinch mode	10
Figure 1.8	Magnetorheological damper	11
Figure 1.9	Schematic diagram of Monotube MR damper	12
Figure 1.10	Schematic diagram of Twin tube MR damper	12
Figure 1.11	Schematic diagram of Double ended MR damper	13
Figure 1.12	Passive suspension system	14
Figure 1.13	Active suspension system	15
Figure 1.14	Semi-active suspension system	16
Figure 1.15	(a) Variable orifice damper and (b) MR damper	17
Figure 1.16	Classification of MR damper models	18
Figure 1.17	Generalized vehicle model	20
Figure 2.1	Viscometer (a) Disc type (b) Coaxial cylinder	26
Figure 2.2	MR fluid based bearing	27
Figure 2.3	MR mount	28
Figure 2.4	MR fluid brake-Disk type	29
Figure 2.5	MR fluid clutches	30
Figure 2.6	MR polishing device	30
Figure 2.7	Monotube MR fluid damper	31
Figure 2.8	MR damper used for recoil in buffer gun	31
Figure 2.9	Landing gear	32
Figure 2.10	MR damper in structural application	32

Figure 2.11	MR damper for vibration reduction in washing machine	32
Figure 2.12	MR damper in prosthetic leg application	33
Figure 2.13	MR damper in tool vibration isolation application	33
Figure 2.14	MR damper suspension for vehicle application	33
Figure 2.15	Velocity profile of MR fluid through an annular gap	39
Figure 2.16	Bingham model	42
Figure 2.17	Stiffness viscosity elasto slide model	43
Figure 2.18	Modified Bouc-wen model	44
Figure 2.19	Non-parametric modelling	47
Figure 2.20	Schematic of non-parametric modelling	47
Figure 2.21	System identification of MR damper using Neural Network	48
Figure 3.1	Research methodology	54
Figure 3.2	Rotational plate type rheometer	58
Figure 3.3	Measuring tool PP20	58
Figure 3.4	Magnetorheological device cell	59
Figure 3.5	Schematic representation of damper testing machine	60
Figure 3.6	Programmable DC power supply	61
Figure 3.7	Displacement transducer	63
Figure 3.8	Force transducer	63
Figure 4.1	Rheometer MCR 302 with MRD Cell	66
Figure 4.2	MR damper model	67
Figure 4.3	(a) Flow curve and (b) Magnetic flux density versus current	72
Figure 4.4	Rheological properties of MR fluid in current sweep for three MR fluid samples. (a), (c), (e) Variation of shear stress and (b), (d), (f) Variation of torque	74
Figure 4.5	Normal stress variation against current for (a) 25 % MRF sample and (b) 35 % MRF sample	76

Figure 4.6	Frequency dependency of (a) Storage modulus, (b) Loss modulus and (c) Complex viscosity	78
Figure 4.7	Normality plot of residuals	82
Figure 4.8	Run chart of shear stress and damping force	83
Figure 4.9	Residuals versus fitted value	83
Figure 4.10	3D response surface of damping force versus Gap and particle concentration	84
Figure 4.11	3D response surface of damping force versus Gap and DC current	85
Figure 4.12	3D response surface of Shear stress versus Gap and particle concentration	85
Figure 4.13	3D response surface of Shear stress versus Gap and DC current	86
Figure 5.1	Monotube MR Damper	92
Figure 5.2	Damper testing facility	93
Figure 5.3	Force versus displacement plot at 1 Hz frequency	94
Figure 5.4	Force versus displacement plot at 1.5 Hz frequency	95
Figure 5.5	Force versus displacement plot at 2 Hz frequency	95
Figure 5.6	(a) Energy dissipation of MR damper per stroke and (b) Equivalent damping	96
Figure 6.1	Methodology flow chart	99
Figure 6.2	Figure 6.2 Damper model (a) Boundary conditions (b) Dimensions of MR damper model and (c) Model of composite outer cylinder	100
Figure 6.3	B-H Curve of (a) MRF-132 DG (b) SA1018	101
Figure 6.4	Flowchart for damping force estimation	102
Figure 6.5	Central composite design	105
Figure 6.6	Magnetic flux density induced in the annular gap for (a) Damper model 1 (b) Damper model 2 (c) Damper model 3 and (d) Comparison of three models	107

Figure 6.7	Force versus velocity - MR damper <i>model 1</i> at velocity, (a) 5mm/s, (b) 10mm/s, (c) 15mm/s and (d) 20mm/s	108
Figure 6.8	Force versus velocity - MR damper <i>model 3</i> at velocity, (a) 5mm/s, (b) 10mm/s, (c) 15mm/s and (d) 20mm/s	109
Figure 6.9	Normal plot of (a) Model 1 and (b) Model 3 MR dampers	114
Figure 6.10	Residuals plot of (a) Model 1 and (b) Model 3 MR dampers	114
Figure 6.11	Run chart of (a) Model 1 and (b) Model 3 MR dampers	115
Figure 6.12	Local sensitivity chart for (a) <i>Model 1</i> and (b) <i>Model 3</i> MR dampers	116
Figure 6.13	3D Response surface of magnetic flux, flow gap and number of turns for <i>model 1</i> MR damper	117
Figure 6.14	3D Response surface of magnetic flux, flow gap and coil height for <i>model 3</i> MR damper	117
Figure 6.15	(a) Number of turn versus magnetic flux density for <i>model 1</i> MR damper (b) <i>Model 3</i> MR damper	118
Figure 6.16	Magnetic flux density versus DC current (a) <i>Model 1</i> MR damper and (b) <i>Model 3</i> MR damper	118
Figure 6.17	Force versus velocity curve for optimised MR damper	121
Figure 7.1	Procedure of Computational method	123
Figure 7.2	Monotube damper model (a) Dimensions and (b), (c), (d) mesh of <i>Model-shear</i> , <i>Model-flow</i> and <i>Model-mixed</i> MR damper respectively	125
Figure 7.3	Computational Fluid domain (a) Model and Boundaries, (b) Meshed model	127
Figure 7.4	Bingham Model	129

Figure 7.5	Contours and magnetic flux lines induced for (a) Model-Shear, (b) Model-Flow and (c) Model-Mixed	131
Figure 7.6	Magnetic flux density in the shear flow region of monotube MR damper for applied currents	132
Figure 7.7	Contours under downward motion (a ₁ , a ₂ , a ₃) Pressure contours (b ₁ , b ₂ , b ₃) velocity streamlines	133
Figure 7.8	Contours under upward motion (a ₁ , a ₂ , a ₃) Pressure contours (b ₁ , b ₂ , b ₃) velocity streamlines respectively	133
Figure 7.9	Force v/s Displacement plot for MR damper at 1.5 Hz frequency for different currents (a) 0.1 A, (b) 0.2 A, (c) 0.3 A and (d) 0.4 A	134
Figure 7.10	Force v/s Displacement plot for MR damper for 2 Hz frequency (a) 0.1 A, (b) 0.2 A, (c) 0.3 A and (d) 0.4 A	135
Figure 7.11	Force versus time history curve of monotube MR damper at (a) 1 Hz, (b) 1.5 Hz, (c) 2 Hz (d) 2.5 Hz and (e) 3 Hz frequency	138
Figure 7.12	Effect of fluid flow gap length	139
Figure 7.13	Force and Pressure variation with respect to time in cylinder of MR damper (a, b) 1 Hz, (c, d) 2 Hz and (e, f) 3 Hz for all three models	140
Figure 7.14	Equivalent damping for (a) 0.1 A, (b) 0.2 A, (c) 0.3 A, (d) 0.4 A and (e) Energy dissipation for three damper models	142
Figure 8.1	Non-parametric modelling flow chart	145
Figure 8.2	Random road roughness profile in (a) Time domain and (b) PSD	147
Figure 8.3	Control structure for quarter car model with fuzzy logic controller	150
Figure 8.4	Fuzzy membership functions (a, b) Input membership and (c) Output membership	151
Figure 8.5	Control structure for three-wheeler car model with PID controller	152

Figure 8.6	Quarter car model with semi-active suspension	154
Figure 8.7	Response of vehicle with MR damper for good road condition, (a) Root mean square acceleration v/s velocity (b) RMS road holding v/s Velocity	156
Figure 8.8	Response of vehicle with MR damper for poor road condition, (a) Root mean square acceleration v/s velocity (b) RMS road holding v/s Velocity	157
Figure 8.9	Sprung mass acceleration response in time domain	158
Figure 8.10	Sprung mass acceleration response in frequency domain	159
Figure 8.11	Three-wheeler vehicle model	161
Figure 8.12	(a) RMS Road holding versus velocity and (b) Unsprung mass RMS acceleration	162
Figure 8.13	PSD of sprung mass displacement and acceleration for (a, b) Bounce (c, d) Pitch and (e, f) Roll motion of the vehicle	164

LIST OF TABLES

Table No.	Description	Page No.
Table 3.1	Specifications of DC power supply	61
Table 3.2	Specification of the displacement transducer	62
Table 3.3	Specifications of the force transducer	62
Table 4.1	Composition of MR fluid samples	65
Table 4.2	Dimensions of MR damper	67
Table 4.3	Parameters of PSO	70
Table 4.4	Range of parameters	71
Table 4.5	Polynomial model functions for different MR fluid samples	75
Table 4.6	Regression model	79
Table 4.7	Design of Experiments	80
Table 4.8	Analysis of Variance for shear stress	81
Table 4.9	Analysis of Variance for damping force	81
Table 4.10	Summary of optimal variable parameters from Single objective PSO.	87
Table 4.11	Summary of Optimal parameters obtained from Multi objective PSO	87
Table 5.1	Magnetic permeability of different materials	91
Table 5.2	Dimensions of the MR damper	92
Table 6.1	Damper model details	100
Table 6.2	Material properties of the MR damper components	101
Table 6.3	Properties of MR Fluid- 132 DG (Lord co.)	103
Table 6.4	Design parameters range and sensitivity	104
Table 6.5	Design of experiments	110
Table 6.6	ANOVA table for damper <i>Model 1</i>	111
Table 6.7	ANOVA table for damper <i>Model 3</i>	111
Table 6.8	Summary of statistics	113

Table 6.9	ANOVA Coefficient Estimate	113
Table 6.10	Candidate points obtained through optimisation using screening algorithm for <i>Model 1</i> damper	119
Table 6.11	Candidate points obtained through optimisation using screening algorithm for <i>Model 3</i> damper	119
Table 6.12	Candidate points obtained through optimisation using MOGA algorithm for <i>Model 1</i> damper	119
Table 6.13	Candidate points obtained through optimisation using MOGA algorithm for <i>Model 3</i> damper	120
Table 6.14	Optimised design parameters based on MOGA and screening method for <i>Model 1</i> damper	120
Table 6.15	Optimised design parameters based on MOGA and screening method for <i>Model 3</i> damper	120
Table 7.1	Dimensions of the monotube damper	124
Table 7.2	Material Properties of the MR damper components	126
Table 7.3	CFD analysis details	126
Table 7.4	Boundary conditions of CFD analysis	127
Table 7.5	Mesh dependency check	130
Table 7.6	Magnetostatic analysis results of Monotube MR damper	132
Table 8.1	Coefficient of polynomial equation	146
Table 8.2	Road roughness detail	147
Table 8.3	Fuzzy rules	149
Table 8.4	Optimal parameter of PID controller	153
Table 8.5	Parameters of quarter car suspension system	155
Table 8.6	Parameter values of the three-wheeler	161

ABBREVIATIONS

τ	Shear stress
μ	Dynamic viscosity
$\dot{\gamma}$	Shear Rate
IUT	In Use Thickening
τ_y	Static yield stress
S	Relative motion between plates
Q	volumetric flow rate
μ_∞	viscosity at infinite shear rate
G'	Storage modulus
G''	Loss modulus
C_0	Damping coefficient
f_c	Frictional force
f_0	offset force
f_{ve}	Viscoelastic force
F_s	Stiction effect
$\sigma_{0a}, \sigma_{0b}, \sigma_{2a}, \sigma_{2b}, \sigma_1$	constant parameters relating properties of MR Fluid
MRD	Magnetorheological device
F_f	Frictional force
$F_{f\mu}, F_{f\tau}$	Force due to shear stress and viscosity
c_f	Flow rate dependent coefficient
w	Circumference
A_{fp}	Area of piston head
c_1, c_2	Acceleration coefficient
r_1, r_2	Uniformly distributed decimal number
μ_0	Magnetic permeability of free space
μ_r	Relative permeability of material
t_d	Gap between the plate
Nc	Number of turns

d	Parallel plate diameter
S_x	Shear stress
F_x	Damping force
PSO	Particle swarm optimization
h	Annular Gap
L	Length of annular gap
$F_{Max} F_{min}$	maximum and minimum damping force
K_{eff}	effective field dependent stiffness
E_d	Energy dissipation
C_e	Equivalent damping coefficient
B	Magnetic flux density
J	Current flux density
H	Magnetic field intensity
ρ	Free electric charge
D	Electric flux density
L_t	Total effective axial pole length
d_0	Diameter of piston head
CCD	central composite design
MOGA	Multi objective genetic algorithm
<i>CFD</i>	Computational Fluid Dynamics
FEMM	Finite Element Method Magnetic
τ_B	Field dependent yield stress
<i>CEL</i>	Command Expression Language
<i>CCL</i>	CFX command language
U	velocity
P	static pressure
SST	shear stress transport
γ_c	Critical shear strain rate
t_s	Time step
ω	Angular velocity
f	Frequency

n	Order of polynomial
γ	Shear strain rate
PSD	power spectral density
$G_q(\Omega)$	spatial power spectral density
$G_q(\Omega_0)$	coefficient of road roughness
Ω, Ω_0	spatial and reference spatial angular frequency
$Z_r(t)$	road roughness amplitude
$w(t)$	white noise signal
ω_o	lowest cutoff angular frequency
PID	Proportional Integral Derivative
$C_1,$	Suspension damping coefficient
C_2, C_a, C_b, C_c	Tyre damping coefficient
$U, U_{ta}, U_{tb}, U_{tc},$ U_{bc}, U_{ba}, U_{bb}	Bounce displacement
Z_1, Z_2, Z_3	Road amplitude
β	Sprung mass displacement (Pitch)
α	Sprung mass displacement (Roll)
C_v	Viscous damping coefficient
ER	Electro-rheological
f_0	Accumulator force
I	Applied current
I_x	Roll Axis Moment of Inertia
I_y	Pitch Axis Moment of Inertia
K_0 and K_1	Stiffness in Bouc-Wen model
K_{eff}	Effective field dependent stiffness
$K_1, K_{a1}, K_{b1}, K_{c1}$	Suspension Stiffness
$K_2, K_{a2}, K_{b2}, K_{c2}$	Tire stiffness
LVDT	Linear variable differential transducer
LQG	linear quadratic Gaussian
LQR	Linear quadratic regulator
MR	Magneto rheological

M_1, M_s

Sprung mass

M_2, M_a, M_b, M_c

Unsprung mass

CHAPTER 1

INTRODUCTION

1.1 INTRODUCTION

Materials which can sense the external stimuli such as temperature, magnetic field, electric field, light etc. and adapt to the variations in external conditions are referred to as smart materials. Due to external stimulus, material environmental conditions are varied resulting in change of material properties. Utilising this behaviour of smart materials, smart systems/components are designed in such a manner that response can be controlled as desirable for particular applications. Some of the examples of smart materials are magnetorheological fluids (MR), electrorheological fluids (ER) and MR elastomers.

New technologies have been developed by adopting smart materials are used to overcome the vibration and undesirable disturbances in the machine or equipment. The smart fluids such as MR fluids, MR elastomers and ER fluids can be used for developing such an advanced device. The MR fluid based devices could offer better performance compared to the conventional devices.

1.2 MR Fluid

Magnetorheological fluids consist of fine, non-colloidal, low coercivity ferromagnetic particles in a carrier fluid. These are belonging to a class of smart materials, which exhibits change in rheological properties when exposed to the external magnetic field. The magnetorheological fluids exhibit spontaneous change in rheological properties upon subjecting to external stimulus or magnetic field and these properties are completely reversible. These smart materials were first reported by Rabinow in the year 1948. The parameters such as composition of MR constituents, concentration of particles, magnetic flux density and applied current significantly influences the

change in rheological properties such as field dependent dynamic yield stress and viscosity. The field dependent yield stress could reach up to about 100 kPa (Phulé 1999). These advantages make MR fluid to play an important role in various applications such as MR dampers, MR brakes, bearings, clutches and valves.

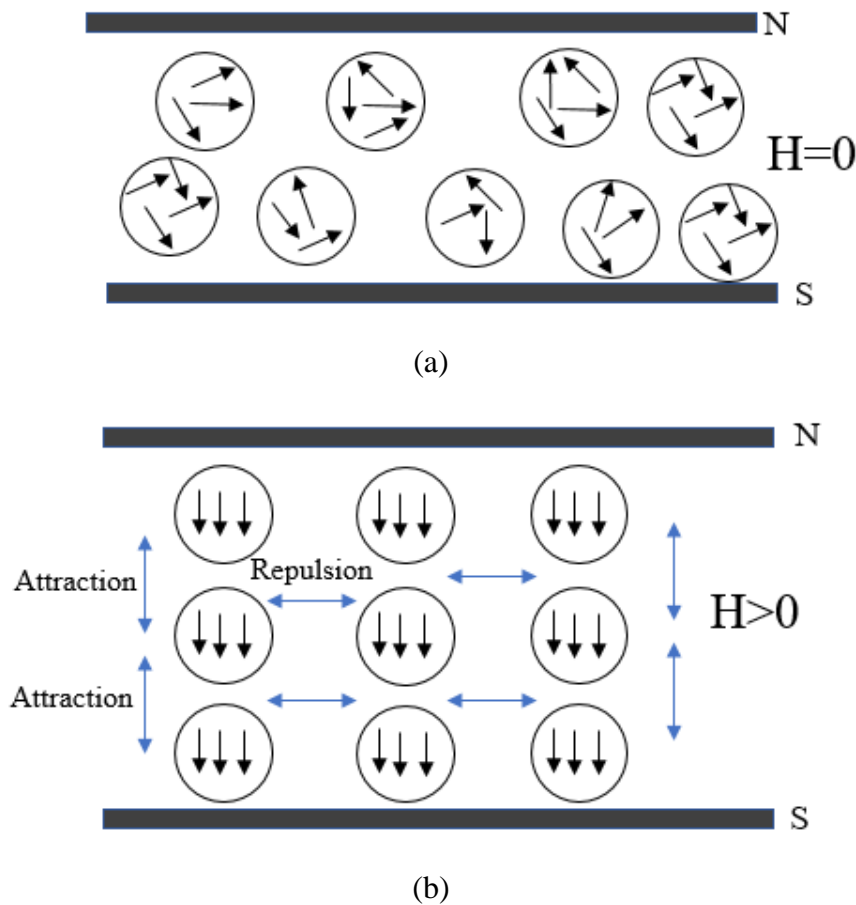


Figure 1.1 MR fluid particles (a) Off -state and (b) On state (Agraval et al. 2001)

Due to the difference in the value of magnetic permeability of carrier fluid and the ferromagnetic particles, the MR effect can be observed on application of magnetic field. The particles act as multi domain, each domain has randomly aligned with dipole moment under the absence of magnetic field as shown in figure 1.1 (a). Under external magnetic field, all the domains in a particle align in the direction of magnetic flux lines. Each particle gets attract in the direction parallel to the magnetic flux lines and repulsion occurs in the perpendicular direction as shown in figure 1.1 (b). This results in construction of chain like structures in the direction of flux lines.

1.3 COMPONENTS OF MR FLUID

The magnetorheological fluid consists of three major components. They are,

1. Carrier fluid phase
2. Magnetisable particles
3. Additives

The selection of these three components and their weight or volume proportion is critically important, since they have significant influence on the physical (operating temperature, settling time) and rheological characteristics (yield stress, off state viscosity, viscoelastic properties) of the MR fluid. It also has a prime importance in the selection for various application.

1.3.1 Carrier fluid phase

The magnetisable particles are suspended in carrier fluid. The selection of carrier fluid is based on various factors and it is distinctive for various applications. The important factors to be considered during the selection of carrier fluid are viscosity, stability to temperature, compatibility to magnetic particles, chemical stability and surface tension. The type of carrier fluid, which is considered as most desirable for the MR fluid preparation must exhibit low viscosity, offering wide range of operating temperature and redispersibility of particles (Jolly et al. 1998). It is also an important fact to be taken care that too low viscous fluid may cause instability and sedimentation problem, while on the other hand, too high viscosity leads to higher off state viscosity which is undesirable (Fang et al. 2009). The most common carrier fluid used are silicone oil, petroleum based oil, mineral oils, polyester, polyether, water, glycerol, hydrocarbon oil etc. The silicone oil has got a wide range of operating temperature and it is the most compatible fluid with other materials of the MR devices (Jiang et al. 2011).

1.3.2 Magnetisable particles

The dispersed phase of magnetorheological fluid are ferromagnetic solid particles and these can be made of various metals, alloys and ceramics. Few examples are ferrite

polymers, carbonyl iron, iron and its compounds, iron cobalt alloys, nickel zinc ferrite etc. The important properties which should be exhibited by the particles are saturation magnetization, low magnetic coercivity and magnetically multi domain. The saturation magnetization of particles can enhance the attraction between the particles and the attraction is equal to square of the magnetization (Carlson and Jolly, 2000). Low magnetic coercivity materials are magnetically soft materials. These are temporary magnets, which do not retain magnetic effect after the removal of external magnetic field and can be easily magnetized and demagnetized. Other physical parameters which impact the MR effect are particle size, particle shape, density and volume fraction. The highly spherical particles of size in range of 1-10 micron make fluid to be less abrasive, durable and more robust. Also, upon increasing or reducing the size, MR effect can be enhanced in higher magnetic fields (Black and Carlson, 2006).

Higher volume fraction of particles in the carrier fluid can increase the viscosity to a significant level and a researcher found that the upper level of particle concentration in mineral oil is 50 percentage of volume fraction. The insights in the studies implemented in the literature in context to MR fluids suggested that carbonyl iron particles with an average size of 1 to 4 microns is the most desirable for synthesis of MR fluid as they exhibit higher magnetic saturation and can be easily manufactured (Chiriac et al. 2009).

1.3.3 Additives

The major objectives for usage of additives in the MR fluid is to prevent the sedimentation, to obtain stable suspensions, to increase lubrication, to prevent particle oxidation, agglomeration and increase durability of the fluid. Among these, most important aspects are increasing the stability and durability of the MR fluid. The particle settling is not a critical issue in devices like MR damper in which the fluid is in constant motion. The findings of the research reveal that the fluid kept for very long period (one year) can regain its initial properties after one cycle of stroke in MR damper (Burson 2006). But the agglomeration of particles in the absence of magnetic field still remains as a concern. Enhancement in stability and reduction of

abrasion/erosion can be achieved by utilizing the materials such as grease, thixotropic agents, antifriction and anti-erosion compounds. The thixotropic agents build a weak structure at low shear rate and reduce the sedimentation. To reduce the agglomeration of particles, iron naphthenate can be added to the MR fluid (Charles and Olabi 2007).

1.4 PROPERTIES OF MR FLUIDS

1.4.1 Off state viscosity

The viscosity of an MR fluid under the absence of magnetic field is called as off state viscosity. The velocity dependent minimum force of an MR device is depending on the off-state viscosity. It is also depending on the viscosity of the base fluid and the particle volume fraction. At room temperature, the off-state viscosity of a regular MR fluid is in the range of 0.05 to 0.2 Pa-s (Carlson, 2009). The off-state viscosity is characterized by Newtons law of viscosity,

$$\tau = \mu\dot{\gamma} \quad (1.1)$$

where τ is shear stress (Pa), μ is dynamic viscosity (Pa.s) and $\dot{\gamma}$ is shear rate (1/s)

1.4.2 Yield stress

The yield stress of the MR fluid under the influence of magnetic field is referred as field dependent yield stress since yield stress can be varied upon change in magnetic field. The maximum output of MR devices is depending on the yield stress (Lopez et al. 2012). The yield stress is depending not only on the magnetic field but also on type of dispersed particles, volume fraction of the particles and particle size distribution (Philips 1969, Chin et al. 2001).

1.4.3 Magnetic flux density and Magnetic flux intensity (B-H) Relationship

Generally, the relationship between the magnetic flux density and magnetic flux intensity is nonlinear in nature. If the magnetisable particles are made of very low coercive materials (magnetically soft materials) having good mobility, very little or no hysteresis can be seen in the curve. The B-H curve is represented as shown in figure 1.2.

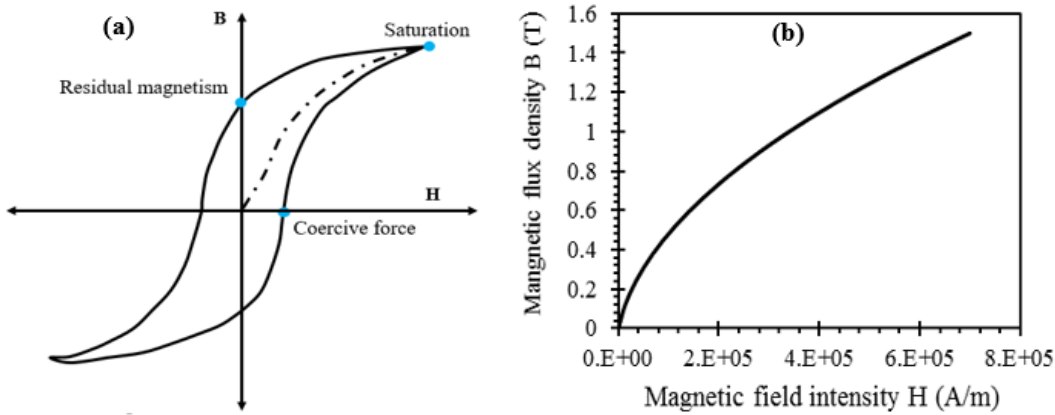


Figure 1.2 B-H curve (a) General model (b) MRF-132DG (Lord Corporation Ltd.)

1.4.4 Durability and In-Use Thickening

When the fluid undergoes high shear for a very long period of time, the fluid will get thickened. This phenomenon is called as in-use thickening (IUT). The durability of the MR fluid reduces due to this phenomenon. The main reason for IUT is peeling of friable surface of the particle subjected to high shear resulting in breaking of particles. The IUT of a fluid can be reduced by the use of particle of higher hardness and using antifriction additives (Goncalves et al. 2006).

1.4.5 Pre-yield and Post-yield behavior

Typical MR fluid has an initial viscosity (0.2 to 0.3 Pa-s), density (3 to 4 g/cm³), magnetic field strength (50 to 250 kA/m), maximum yield strength (50 to 100 kPa), supply voltage (2 to 25 V) and current intensity (1 to 2 A). The MR fluid behaves as a Newtonian fluid in the absence of external magnetic field, while in presence of the magnetic field it exhibits non-Newtonian behavior, similar to distinct Bingham fluid. The MR fluid model is expressed by Bingham model as (Parlak et al. 2012)

$$\tau = \tau(B) + \mu\dot{\gamma} \quad \tau > \tau_y \quad (1.2)$$

$$\dot{\gamma} = 0 \quad \tau < \tau_y \quad (1.3)$$

where $\dot{\gamma}$ = Shear Rate, τ_y = Static yield stress, μ = Dynamic Viscosity

τ = Local Shear stress, $\tau(B)$ = Field dependent shear stress

The dynamic yield shear stress $\tau(B)$ increases with external magnetic field. Magnetic field dependent yield shear stress of the fluid is evaluated by adopting two regions, Pre-yield and Post-yield regions are as shown in figure 1.3. In the pre-yield region, MR fluid behaves like linear viscoelastic materials, where dynamic yield stress dominates the local shear stress. In the post yield region, MR fluid behaves like plastic material where local yield stress dominates the dynamic yield stress. In the post yield region, fluid behaves as nonlinear viscoelastic material.

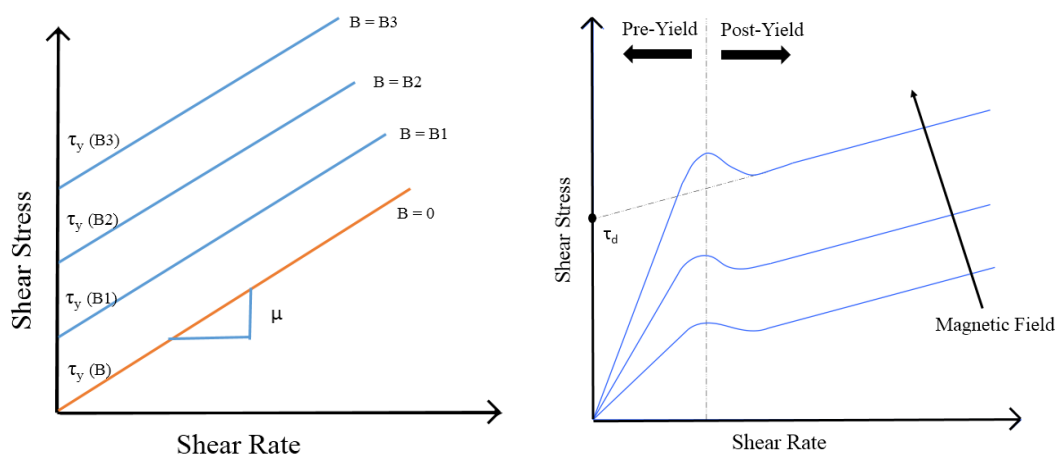


Figure 1.3 Shear stress vs shear rate plot of (a) Bingham Plastic and (b) MR fluid (Choi et al. 2013)

1.5 MR FLUID OPERATION MODES

There are four main modes of operations of MR fluids application in the controllable devices. They are

1. Flow mode
2. Squeeze mode
3. Shear mode
4. Pinch mode

1.5.1 Flow/Valve Mode

In flow/valve mode, there is a pressure drop across the fluid, as it flows through the device. Gap between the two stationary plates is filled with MR fluid (Grunwald and Olabi 2008). Magnetic field is varied in a direction perpendicular to the flow as

shown in figure 1.4. Flow mode is the most common of the four operational modes of MR fluid and serves as the primary method used in MR dampers. Among MR devices, MR dampers have been most widely studied and developed for commercial applications.

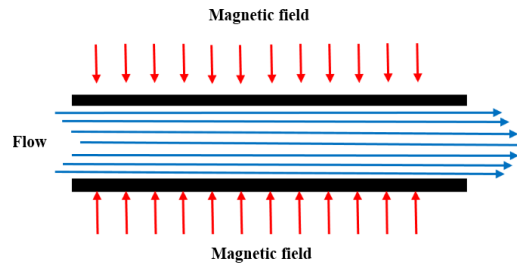


Figure 1.4 Flow Mode (Choi et al. 2013).

The pressure drop occurring in the flow mode resist the force induced in the device. There are two independent components which are main cause of pressure drop. They are (i) viscous component due to pure rheology (ΔP_μ) and (ii) magnetorheology (ΔP_{mr}). This can be expressed as.

$$\Delta P = \Delta P_\mu + \Delta P_{mr} = \frac{\mu}{\tau_b^2} \left[\frac{12}{f^2} \right] \left[\frac{\Delta P_{mr}}{\Delta P_\mu} \right] Q \quad (1.4)$$

where μ dynamic viscosity, τ_b is field dependent yield stress, Q is volumetric flow rate of MR fluid

1.5.2 Squeeze-flow mode

The MR fluid is placed between the two moving plates as shown in figure 1.5 and the relative displacement is perpendicular to the flow direction. In this mode, the ferrous particle chains undergo forces similar to columnar buckling. The force acting is axial to the magnetic flux lines and particle chain. The force developed in this mode is greatly dependent on the particle chain rather than the viscosity of the MR fluid. Typically, in squeeze mode devices there is a little or no flow of MR fluid and it is employed in controlling the small displacement vibration applications. The magnitude of resistive force can be controlled by varying magnetic field between the plates. Usual gap between the two plates is around 0.5mm. Recent studies on this mode revealed that, it is capable of producing compression and tensile stress at same time

and generate higher force compare to other mode types (Kim et al. 2008, Olabi and Grunwald 2007).

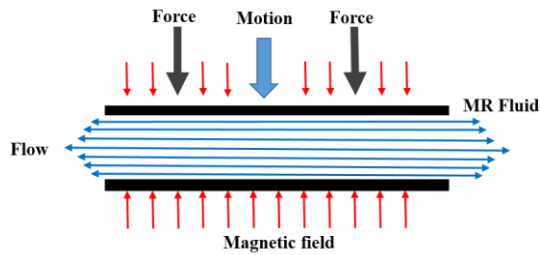


Figure 1.5 Squeeze-flow mode (Choi et al. 2013)

1.5.3 Shear Mode

Shear mode is also known as direct shear mode. In this mode, one of the pole plates moves parallel to the other causing a shearing force to develop across the fluid gap as shown in figure 1.6. Difference between shear mode and valve mode is that, the pole plates are not stationary in shear mode. Here, the motion between the two plates may be either translational or rotational. Drag force and viscosity of the excited MR fluid are the resistances for moving plates. The thickness of MR fluid sandwich between two moving plates is of the order of 0.13 to 0.4 mm. This mode of operation can be seen in clutches, brakes and locking devices. The total force in shear mode can be written as,

$$F = F_{\mu} + F_{mr} = \left[\frac{\mu \cdot S \cdot A}{g} \right] + \tau_b \cdot A \quad (1.5)$$

$$A = L \cdot w \quad (1.6)$$

where S is the relative speed of two plates, g is the gap size and A is surface area, L and w is length of the flow gap, τ_b is magnetic field dependent shear stress.

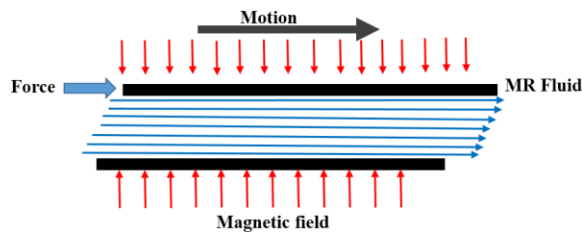


Figure 1.6 Shear mode (Choi et al. 2013)

1.5.4 Pinch mode

In pinch mode, the magnetic poles are separated by a nonmagnetic material spacer as shown in figure 1.7. The magnetic flux lines are nearly parallel to the flow of the fluid and magnetic poles are placed axially. The magnetic field is highly non-uniform throughout the MR fluid in this mode. Instead of making MR fluid into semisolid throughout the valve gap, the fluid gets excited by external magnetic field only near the walls.

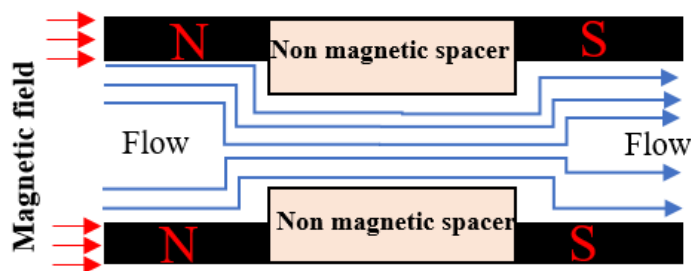


Figure 1.7 Pinch mode (Goncalves and Carlson 2009)

1.6 MAGNETORHEOLOGICAL DAMPER

In recent years, the MR dampers have gained more popularity in the field of semi-active control systems. Enormous research has been carried out in the field of magnetorheological dampers. MR dampers have attracted the interest of researchers, because of their variable damping features, mechanical simplicity, low power consumption, fast response and compatibility with electronic control. This type of semi-active dampers is controlled using magnetic field. The magnetorheological damper construction is almost similar to conventional hydraulic damper. The difference between MR damper and conventional hydraulic damper is that the MR damper consists of an electromagnetic coil wound inside the piston head. Figure 1.8 shows the schematic diagram of a prototype MR damper consisting of two chambers in the cylinder separated by a floating piston. The chamber above the floating piston is filled with MR fluid and the chamber below is called as accumulator. The accumulator is filled with pressurized nitrogen gas and its function is to compensate the volume changes induced by the up and down movement of the piston and to offer rebounding force. When the piston is under action, the fluid flows through the annular

gap in the piston head. Piston head consists of an electromagnetic coil which is wound inside with copper wire. The wires used for electromagnetic coil is heat-resistant and electrically insulated. When electrical current is applied to the copper coil, a magnetic field is induced around the piston head. The magnetic field can be varied upon supplying controlled current.

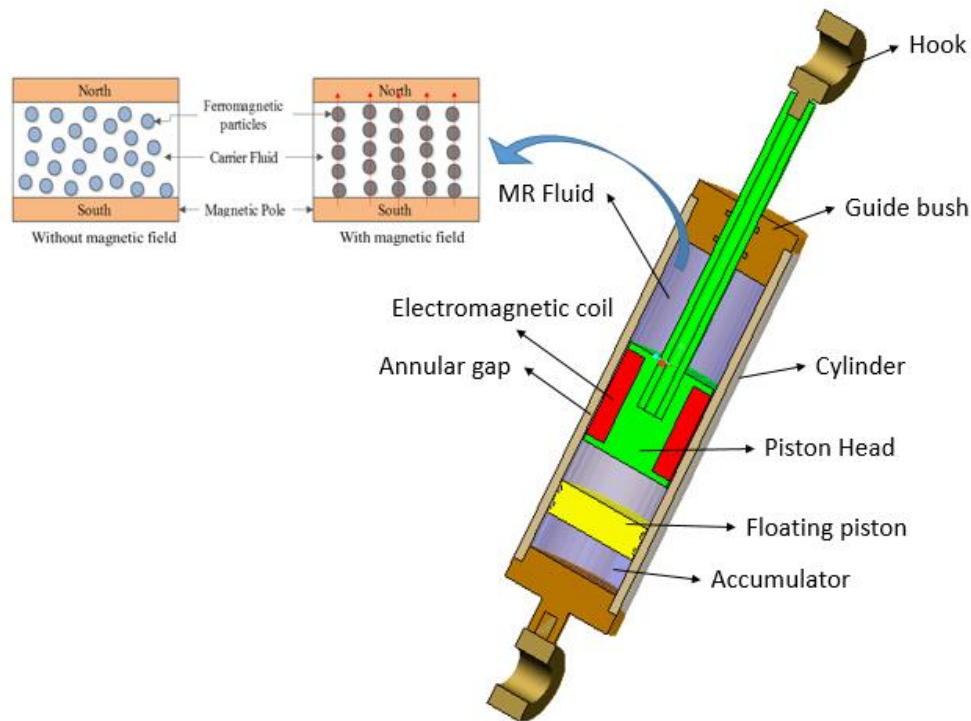


Figure 1.8 Magnetorheological damper

The MR damper is classified into three types as follows:

1. Monotube MR damper
2. Twin Tube MR damper
3. Double ended MR damper

1.6.1 Monotube MR damper

A monotube MR damper (figure 1.9) has only one reservoir for the MR fluid and an accumulator mechanism to accommodate the change in volume that results from piston rod movement. The monotube dampers are greatly used, since these can be

installed in any orientation and are compact in size. The floating piston provides a barrier between the MR fluid and a compressed gas/spring (usually nitrogen), which is used to accommodate the volume change that occurs when the piston is under action.

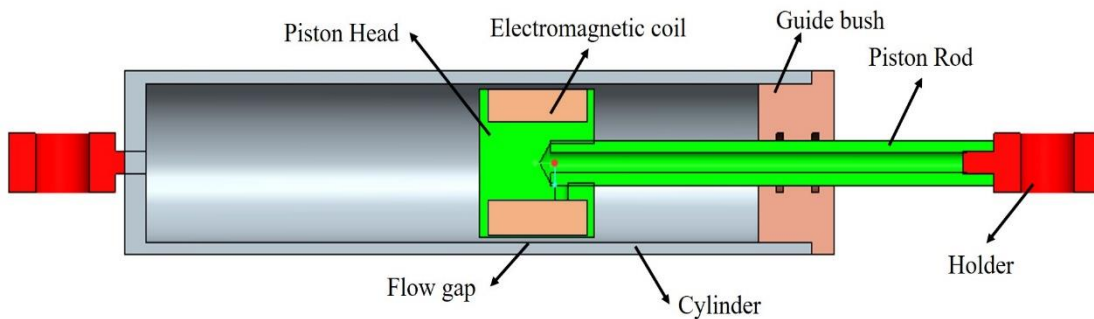


Figure 1.9 Schematic diagram of Monotube MR damper

1.6.2 Twin tube MR damper

The twin tube MR damper (figure 1.10) consists of two reservoirs/housings for MR fluid. The guide bush guides the piston rod assembly in exactly the same manner as in a monotube damper. The volume enclosed by the inner housing is referred as the inner reservoir. Likewise, the volume that is defined by the space between the inner housing and the outer housing is termed as the outer reservoir. The inner reservoir is filled with MR fluid so that no air pockets exist and ensures flow of fluid from inner to outer tube/ reservoir and vice versa through a base valve provided at the bottom of the inner tube.

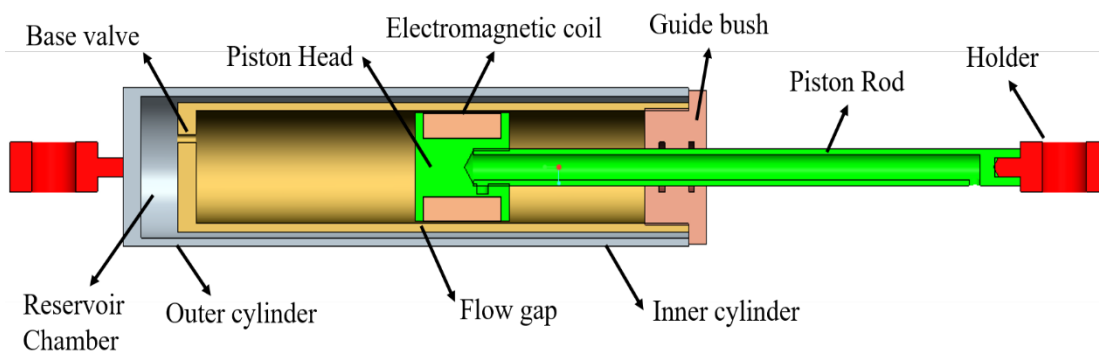


Figure 1.10 Schematic diagram of Twin tube MR damper

1.6.3 Double ended MR damper

The double-ended damper consists of two piston rods of equal diameter protruding from both ends of the damper housing.

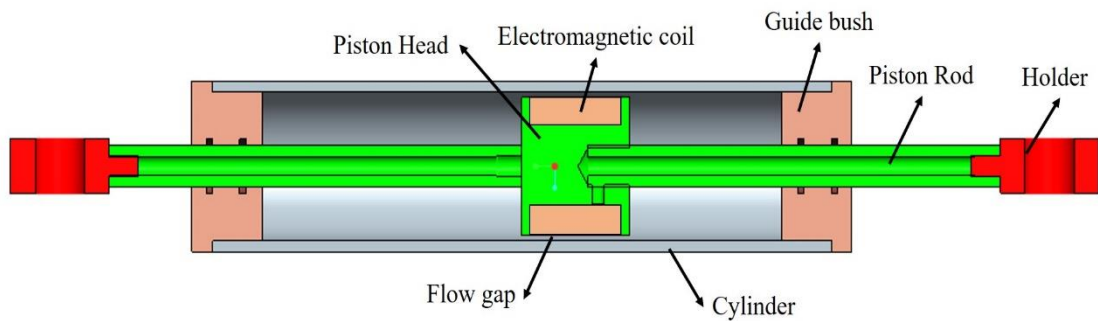


Figure 1.11 Schematic diagram of Double ended MR damper

Figure 1.11 shows a section view of a typical double-ended MR damper. Since there is no change in volume as the piston rod moves relative to the damper body, the double-ended damper does not require an accumulator mechanism (James et al. 2001).

1.7 VIBRATION SUSPENSION SYSTEM

The vibration isolation in many industrial machineries, automobiles and structural buildings needs an advanced damping system in dissipating the energy from the externally and internally induced vibrations to improve ride comfort, structural safety and system performance. Dampers are the most commonly used vibration isolation components which work on the energy dissipation principle. In automobiles, the vibration is induced from road surface irregularities, engine vibration, structural vibration and aerodynamic forces. The problem due to road induced vibration of vehicle systems are generally solved by placing the suspension system between the wheel and the chassis. In such cases, it is required to adopt the suspension system which can perform satisfactorily under different operating conditions. Basically, there are three types of suspension systems. They are,

1. Passive suspension system
2. Active suspension system
3. Semi-active suspension System

1.7.1 Passive suspension system

The passive suspension systems as shown in figure 1.12 are the most commonly used system for vibration isolation. Design of such damping system consists of a simple rubber or synthetic material and springs. Most of the passive systems have low manufacturing cost. Thorough understanding of vibration problem and properties of the material is necessary in order to design the passive suspension for a particular application. Apart from ease of fabrication and inexpensiveness, passive systems have several limitations such as bulky size, heavy weight, lack of versatility and require re-tuning of tuned treatments. These are ineffective when the frequencies of induced vibration vary with the time.

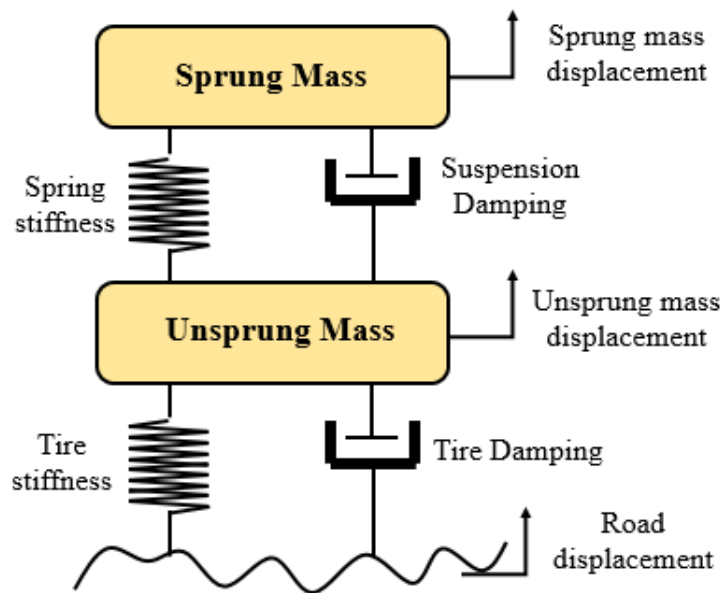


Figure 1.12 Passive suspension system

1.7.2 Active suspension system

An active suspension system has the capability to adjust itself continuously for the changes in road profile or conditions. An active element or actuators is used to apply

the desired force to sprung and un-sprung mass as shown in figure 1.13. The desired force is calculated by an advanced control system used in the vehicle.

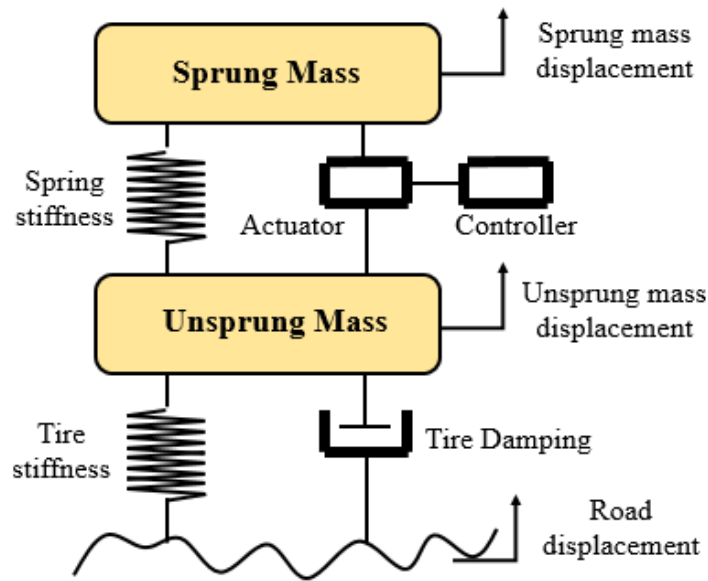


Figure 1.13 Active suspension system

By changing its characteristics to respond to varying road conditions, active suspension offers superior handling, road comfort, responsiveness and safety. In spite of many advantages, the active systems have several limitations as well. These systems are quite expensive and complex which need a force actuator, sensors and processors for its functioning.

1.7.3 Semi-active suspension system

The limitations of passive and active suspension systems are overcome by adapting the semi-active or adaptive suspension systems. It is less expensive than active system and more versatile than passive system. The actuator and fixed damping is replaced by a variable force damper in semi-active suspension systems. By changing the damping force, rate of energy dissipation can be changed. An illustration of semi-active suspension system is shown in figure 1.14. In semi-active suspension system, damping force can be controlled in real time and it offers very quick response. These systems consist of damping controller and system controller, which are used to monitor and control the performance of the system. Depending upon the input

obtained from the response of the vehicle, the system controller generates the desired damping force. In case, if there is no supply of current or if control system fails, the system can still function like a passive suspension system. Hence, semi-active suspensions are referred as fail-safe mode systems.

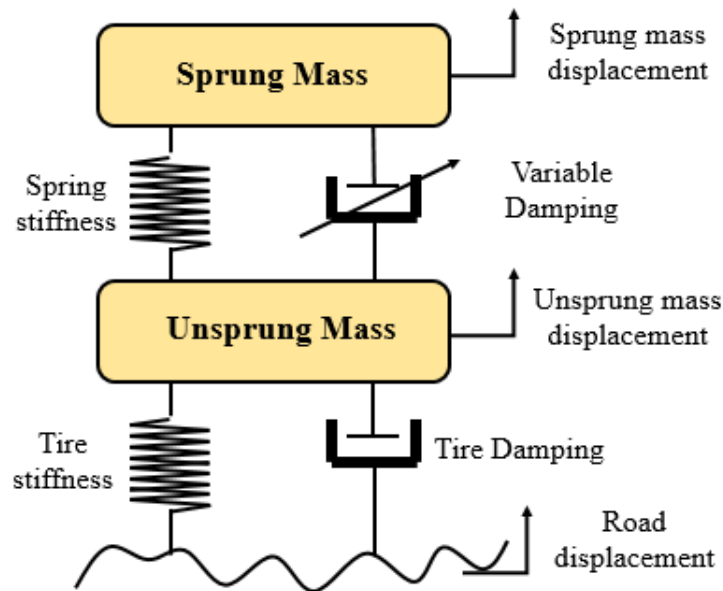


Figure 1.14 Semi-active suspension system

The semi-active suspension consists of a variable damper which can be controlled. Basically, there are two types of variable damper. They are (i) MR/ER damper and (ii) Variable orifice damper. The basic principle behind the variable orifice damper is that the orifice gap can be controlled and varied to achieve the desired damping force. A larger orifice provides less dissipative resistance, while a smaller orifice provides increased dissipative resistance. The opening of the orifice is determined in real time by feedback control laws. Figure 1.15 (a) shows the illustrative diagram of variable orifice damper. The second variable damper is MR/ER dampers as shown in figure 1.15 (b). It consists of magnetically sensitive fluid whose rheological properties can be varied with respect to an external magnetic field generated with help of an electromagnetic coil.

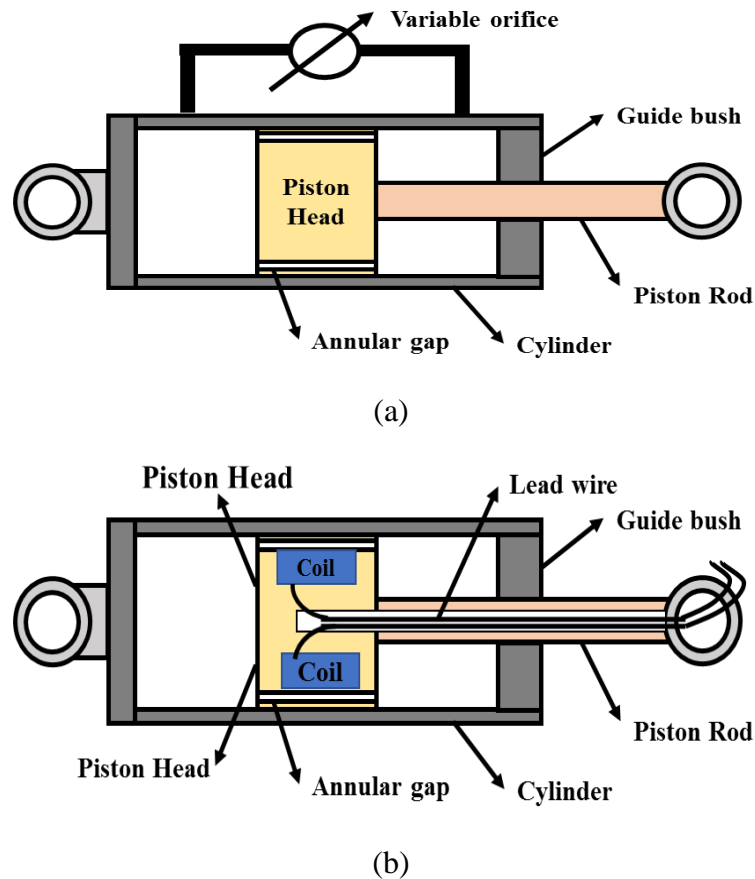


Figure 1.15 (a) Variable orifice damper and (b) MR damper

1.8 MATHEMATICAL MODEL OF MR DAMPER

The behavior of MR damper is nonlinear and hysteretic in nature. The response is a nonlinear function of the input parameters. The nonlinearity, linearity and hysteretic behavior of the MR damper can be represented by various models. These models are characterized based on three features i.e., characteristics of representative models, based on adaptability and reversibility. Figure 1.16 illustrates the complete classification of MR damper models.

1.8.1 Quasi-static models

The quasi-static models are employed to model the characteristic of MR damper using different fluid flow models such as Bingham, Hershel Bulkley and Casson models. These models are used in preliminary design of MR damper. The main

disadvantage of these models is that they don't completely describe the nonlinear behaviors and dynamic loading. In order to overcome this limitation, the dynamic models have been developed. (Yang et al. 2011)

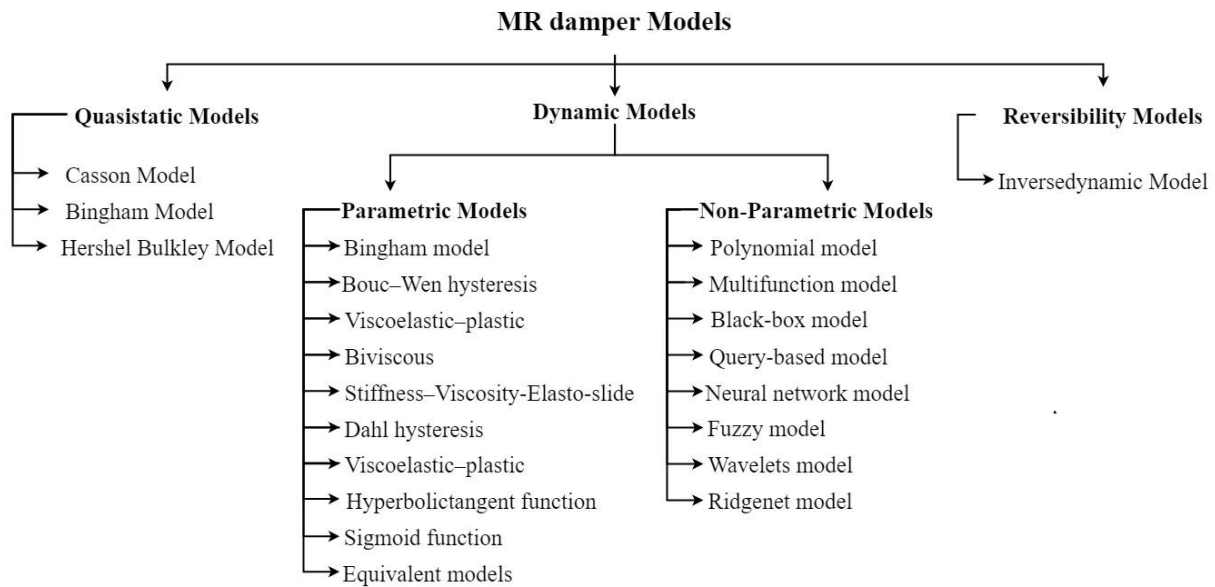


Figure 1.16 Classification of MR damper models

1.8.2 Dynamic models

Dynamic models are classified into two types i.e parametric and non-parametric models. These models are used for describing the dynamic behaviour of the MR damper.

1.8.2.1 Parametric models

This technique categorises the models as a combination of spring, damper and physical elements. The values of parametric models are identified by minimising the error between experimental and simulation results. The accuracy of these models depends on the initial assumption regarding the structure of the mechanical model which simulates the behaviour of the system. There is a chance of negative mass or stiffness occurring if the assumptions and constraints are not applied precisely (Ehrgot and Masri 1992). The parametric model which predicts the behaviour of MR damper

is complex in real time applications. To overcome the limitations of the parametric modelling, the non-parametric models has been developed.

1.8.2.2 Non-parametric models

These models were proposed by Marsi and Caughey (1979) to overcome the limitations of the parametric models. This approach uses analytical expression to predict the characteristics of the MR damper. The expression is a polynomial equation, which represent the damping force as the function of displacement and applied current. The method requires information regarding the displacement, velocity, and the restoring force acting on the system to FORMULATE an approximate expression for the value of the restoring force in terms of the system state variables using regression techniques.

1.8.3 Inverse dynamic models

These models are contradiction to the forward dynamics models, where the force is calculated by using the current (or voltage). In these models, current or command voltage required is estimated and the required damping force is the input given to the model. Most of the developed controllers determine the damping force produced by the MR damper. But the force exerted by the MR damper cannot be controlled directly; it can only be controlled in terms of the applied current (or voltage). Thus, inverse dynamic models make it possible to estimate the current for the required damping force.

1.8.4 Vehicle models

The vehicle models represent the free body diagram and are used to formulate the mathematical model. Main parts of vehicle models are sprung mass, unsprung mass, springs, tire and axial systems. Figure 1.17 illustrates generalized vehicle model. The mass of vehicle body and the interior parts are referred as sprung mass and masses of tire-axles are represented as unsprung mass. The suspension system consisting of mechanical elements such as spring and viscous damper is the intermediate system which connects the sprung mass and unsprung mass. The suspension system is used to

isolate the vibration being transmitted from the road disturbances to vehicle body in order to provide better ride comfort and road holding to the vehicle when travelling over rough road.

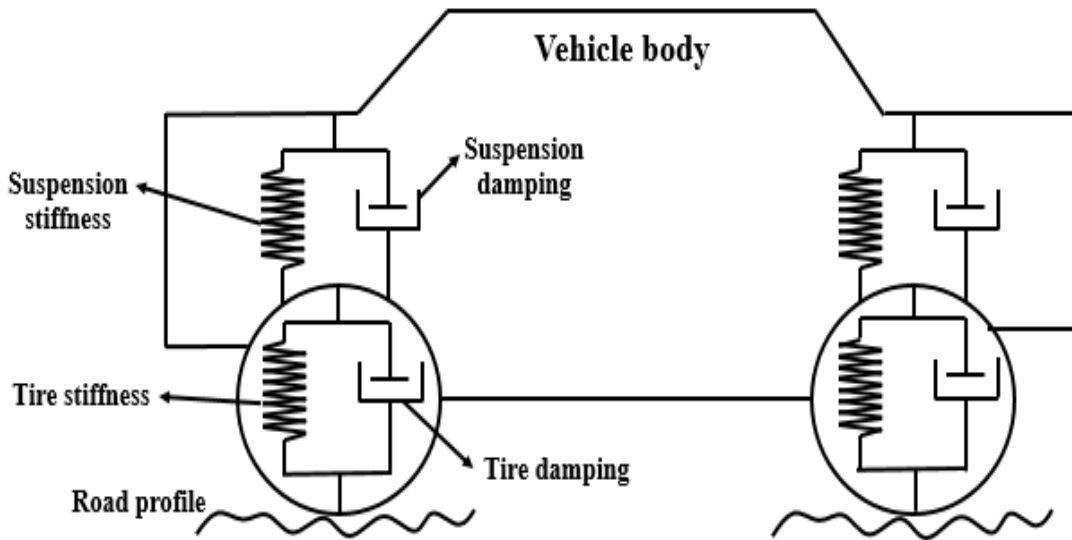


Figure 1.17 Generalized vehicle model

1.9 OUTLINE OF THE THESIS

There are totally nine chapters in this thesis. The brief summary of each chapter is discussed below.

First chapter will provide introduction to the technology and overview of the magnetorheological principles. The constituents of MR fluid, rheological properties, modes of operation of MR devices, MR damper and different modelling methods are discussed.

In the second chapter, provides state of art literature reviews on characterising MR fluid, application of MR fluid in various engineering domains, dynamic performance evaluation of MR damper, computational method involved in the MR damper analysis and modelling of MR dampers and controllers in relevant fields are elaborated.

Research work flow and methodology involved is presented in the third chapter. The experimental setups, components, features, functions of the sensors and data acquisition system are discussed.

The preparation and rheological characterisation of MR fluid is discussed in the fourth chapter. The effect of fluid gap, magnetic flux density and the proportion of particle volume fraction on damping effect are analysed. The optimisation techniques such as particle swarm optimisation and response surface methods are used for evaluating the optimal proportion of particle volume fraction in carrier fluid. Statistical analysis of the parameters is also discussed.

In the fifth chapter, details of fabricated MR damper and characterisation through experimental methods are discussed. The variation in damping force due to application of DC current and the energy dissipation in the MR damper are presented.

The magnetic flux density induced at the shear gap of MR damper is the prominent factor for developing desired damping force. The optimal parameters influencing the magnetic flux density and interaction between these parameters are elaborated in the sixth chapter. Also, an optimisation technique used for maximising the magnetic flux density and damping force is discussed in detail.

A computational approach involved in coupled FE and CFD analysis to characterise the MR damper is demonstrated in the eighth chapter. Detailed analysis of the variation of pressure, velocity and damping characteristics under different inputs are elaborated.

Non-parametric modelling of MR damper and interfacing the model with quarter car and three-wheeler semi-active suspension systems are presented in chapter 8. The vertical dynamic analysis of quarter car and three-wheeler vehicle subjected to random road input conditions are presented and their performance is compared with passive suspension system.

Important conclusions of the investigation, main contribution, scope for future work have been presented in ninth chapter.

CHAPTER 2

LITERATURE REVIEW

2.1 INTRODUCTION

An overview and detailed introduction to MR fluid, modes of operation of MR devices, MR damper and its applications in semi-active vehicle suspension systems are discussed in the previous chapter. This chapter discusses state-of-the-art literature review on characterisation of MR fluid dynamic characterisation of MR damper, optimization of the MR damper, computational analysis of MR damper, predicting the behaviour of MR damper through development of parametric and non-parametric modelling, passive and semi-active vibration control of vehicle suspension system.

2.2 FLOW MODELS OF MR FLUID

The magnetorheological fluids exhibit spontaneous change in rheological properties, when they are subjected to external stimulus or magnetic field and these properties are completely reversible. These smart materials were first reported by Rabinow in the year 1948. The parameters such as composition of MR fluid constituents, concentration of particles, magnetic flux density and applied current cause a significant change in rheological properties such as field dependent dynamic yield stress and viscosity. The field dependent yield stress can reach up to about 100 kPa (Phule and Ginder (1999)). Owing to these advantages, MR fluids play an important role in various applications such MR dampers, MR brakes, bearings, clutches and valves.

There are three prominent models for viscoplastic fluids, which are Bingham plastic, Herschel-Bulkley and Casson fluid models. These models are used for characterisation and to interpret the parameters.

2.2.1 Bingham fluid model

Bingham model describes the fluid behaviour under shear stress. This model defines that, MR fluid acts as solid within the region of critical shear stress referred to as yield point and it behaves as Newtonian fluid beyond this point (Sidpara et al. 2009). The transition of MR fluid from solid to viscous fluid is occurs at a critical value and yield stress at this point is defined as dynamic yield stress. Mathematically the Bingham model is expressed as

$$\tau = \tau_y + \mu\dot{\gamma} \quad \text{for } \tau > \tau_y \quad (2.1)$$

where, μ = Viscosity of the fluid, τ = Shear stress, $\dot{\gamma}$ = Shear rate, τ_y = Critical shear yield stress.

2.2.2 Herschel-Bulkley fluid model

This model too defines the behaviour of MR fluid as solid below critical shear stress (within the yield point). The expression representing the Herschel-Bulkley model is,

$$\tau = \tau_y + \mu_H\dot{\gamma}^n \quad \text{for } \tau > \tau_y \quad (2.2)$$

where, μ_H is viscosity, n is power law index or flow behaviour index. If n is greater than 1, it indicates shear thickening fluid and when n is less than 1, it indicates shear thinning fluid.

2.2.3 Casson Fluid model

Casson model assumes that at zero shear rate, the shear thinning fluids have viscosity of infinite level and zero viscosity at infinite shear rate (Jha and Jain (2009)). It is known that the ferrous particles in the fluid get polarised along the magnetic field lines by formation a chain like structure. Under flow condition, this chain is subjected to tension and the chain breaks when the tension reaches a value beyond the critical value. Based on this, an expression has been formulated to obtain a relation between the shear stress and shear rate. The constituent equation of Casson fluid model is expressed as,

$$\sqrt{\tau} = \sqrt{\tau_y} + \sqrt{\mu_\infty\dot{\gamma}} \quad \text{for } \tau > \tau_y \quad (2.3)$$

where, μ_∞ is the suspension viscosity at infinite shear rate.

2.3 CHARACTERISATION OF MAGNETORHEOLOGICAL (MR) FLUID

Characterization of MR fluid is an essential requirement to implement it in the devices for industrial and commercial applications. The damping characteristics and performance evaluation of fluid under working condition is essential. The behavior of the MR fluid changes when it is subjected to magnetic field, due to polarization of particles in the magnetic field. This makes the fluid much thicker than the fluid under no magnetic field. The viscosity of the MR fluid depends on the strength of magnetic field applied to it. Hence, by varying the applied magnetic field, viscosity can be controlled.

The behaviour of MR fluids under various conditions has been reported extensively in the literature. Experiments on steady state and dynamic properties involving viscoelasticity of MR fluids have been performed. The dynamic studies of MR fluids subjected to low strain rate enables to evaluate the influence of parameters on the rheological properties (Claracq et al. 2004). Wang and Gordaninejd (2006) conducted experiments on commercial MR fluid, MR polymeric fluid and ferro fluid based MR fluid using flow mode type rheometer and compared their rheological properties. Among these three samples, ferro fluid based MR fluid exhibited higher shear yield stress than other two samples (132LD and MR polymeric gel based MR fluid). Genc and Phule (2002) described impact of saturation magnetisation of dispersed particle phase, particle concentration, particle size and magnetic field on the properties of MR fluid. They reported that MR fluid consisting of finer particle size exhibited lower yield stress due to lesser saturation magnetisation of finer particles. De Vicente et al. (2004) predicted the low shear flow behaviour of MR fluid using a single width chain model and wall deflection effects were identified under low external magnetic fields and different fluid flow gaps. Guo et al. (2012) considered four different volume fractions of MR fluid samples for studying normal force behaviour of the fluid.

The settling of the particle in the MR fluid is not a major problem as long as the fluid is under constant motion or if allowed to disperse the settled particles. A good quality of MR fluid used for MR damper application can serve the nominal force after a stroking cycle even after prolonged storage (Burson 2006). Phule and Ginder (1999)

synthesised nickel zinc ferrite and magnetic iron based MR fluid along with nanoscale additive. The enhancement in sedimentation stability and redispersibility of the synthesised MR fluid was demonstrated. López-López et al. (2006) carried out an investigation on sedimentation, aggregation and redispersibility of three MR samples consisting of three different additives i.e oleic acid, aluminium stearate and nanoparticles of silica. They found an interesting fact that oleic acid and aluminium stearate did not offer any privilege for reduction in settling time, but on other hand they could play an enhanced role in improving the redispersibility of the particle. Jang et al. (2005) used poly vinyl butyral (PVB) as the coating material for CI particles for reducing the sedimentation time of the particles. Lim et al. (2004) employed fumed silica as the sedimentation agent in carbonyl iron particle based MR fluid and characterised its rheological properties. They found that sedimentation of particles is inhibited upon usage of fumed silica. López-López et al. (2005) studied the stability and redispersibility of MR fluid samples consisting of oleate-covered magnetite nanoparticle dispersed in kerosene through electromagnetic induction method. Pu and Jiang (2005) demonstrated reduction of particle settlement upon usage of nanotube composites (CNT) surface covered with magnetite (Fe_3O_4) as the suspension in carrier fluid. They concluded that, CST/ Fe_3O_4 particles are superior to magnetite particles as suspension in MR fluid. Shah et al. (2013) characterised MR fluid consisting of plate like iron particles of micron size and presented their role in improvement of stability and rheological properties. Zuzhi et al. (2016) synthesised MR fluid by using silane and bentonite as the additives to enhance the performance of the fluid. Through design of experiment and optimisation process they found that MR fluid with additives of 2.88 % mass fraction of silane and 3.60 % mass fraction of bentonite exhibited improved sedimentation stability. Ngatu and Wereley (2007) demonstrated the performance of MR fluid samples consisting of combination of nano and micron sized particles referred as bidisperse particles in MR fluid.

2.3.1 Viscoelastic behaviour of MR fluid

Viscoelastic behaviour of MR fluids can be seen under the pre-yield region and these properties are essential for understanding MR devices particularly in MR damper. The viscoelastic properties such as storage modulus (G') and loss modulus (G'') depends

upon the applied magnetic field and volume fraction of MR fluid. Values of G' and G'' increase with increase in both magnetic field and volume fraction (Li et al. 1999). Eshaghi et al. (2015) proposed a phenomenological model for characterisation of MR fluid (MR 122EG and 132 DG Lord corporation) and obtained a relationship between complex shear modulus, magnetic flux density and frequency of excitation from experimental results. Figure 2.1 shows the two-common type of viscometer used in the rheological characterisation.

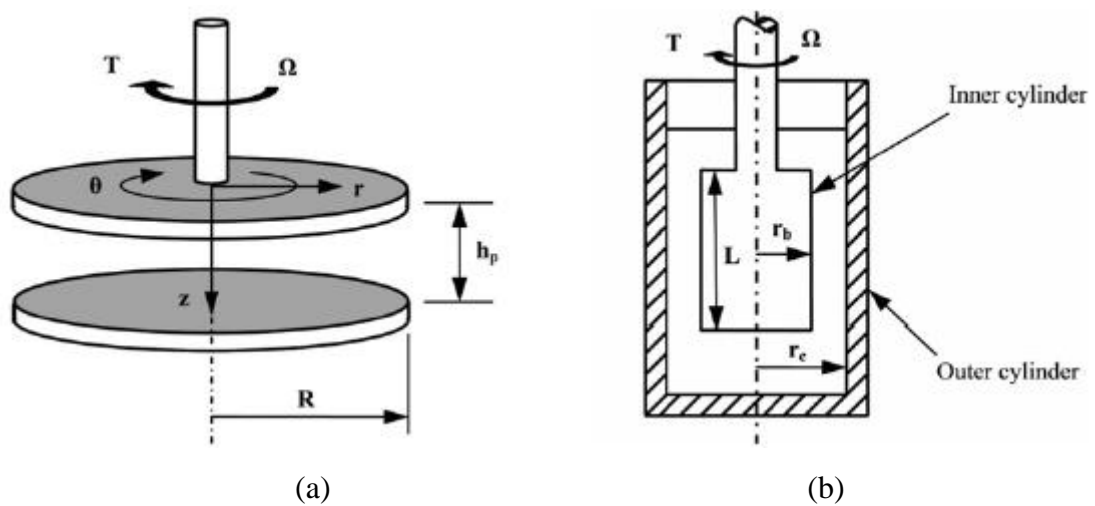


Figure 2.1 Viscometer (a) Disc type (b) Coaxial cylinder

Susan-Resiga (2016) examined dependence of static and dynamic yield stress on the volume fraction of magnetite nanoparticles and iron particles under different magnetic fields. De Gans et al. (2000) carried out investigation on influence of particle size on rheological properties of MR fluid. Bell et al. (2007) manufactured MR fluid by considering silicone as carried fluid and nickel microwires as suspensions and studied dispersion stability of MR fluid with respect to particle shapes. Zhang et al. (2008) synthesized a shear thickening MR fluid consisting of carbonyl iron powder and nano sized silica particles suspended in ethylene glycol. From experimentation, they observed that there is an increase in complex viscosity of MR samples crossing the critical dynamic shear rate. Choi et al. (2005) analysed magnetic field dependent fluid characteristics of MR fluid using two viscometers i.e. rotational coaxial cylinder and parallel plate viscometers. Also, carried out theoretical studies by developing a relationship between shear stress, torque shear rate and angular velocity.

2.4 APPLICATIONS OF MR FLUIDS

2.4.1 MR Bearings

The dynamic characteristics such as stiffness and damping of bearing can be enhanced by adopting advanced technologies while designing them. One such area is employing smart material lubricants in journal bearing to improve its controlling ability and overall performance. A typical MR fluid bearing is as shown in figure 2.2. Hesselbach and Abel-Keilhack (2003) presented a concept to overcome the disadvantages of conventional hydrostatic bearing by adopting MR fluid based hydrostatic bearings. Forte et al. (2004) presented numerical simulation and experimental analysis of MR fluid based damped rotor dynamic behavior. Gertzos et al. (2008) demonstrated CFD analysis of hydrodynamic bearing by considering non-Newtonian behaviour of MR fluid as Bingham fluid model. The performance of the bearing was evaluated using CFD analysis and experimental analysis. Both methods found a good agreement. Bompos and Nikolakopoulos (2011) presented specific procedure for conducting the coupled CFD and FE analysis to evaluate the journal bearing characteristics. Bompos and Nikolakopoulos (2016) carried out performance evaluation of MR fluid based bearings through experiments and dynamic properties were estimated by employing impact excitation method. Laukiavich et al. (2014) presented application of ferro magnetorheological fluid in controlling fluid flow and enhancement in dynamic behaviour of hydrodynamic bearings. Bompos and Nikolakopoulos (2016) investigated the influence of ferrous particle size on the rotodynamic behaviour of shaft with bearing through coupled FE and CFD simulation and concluded that nano sized particle based MR fluid significantly benefited the static and dynamic performance.

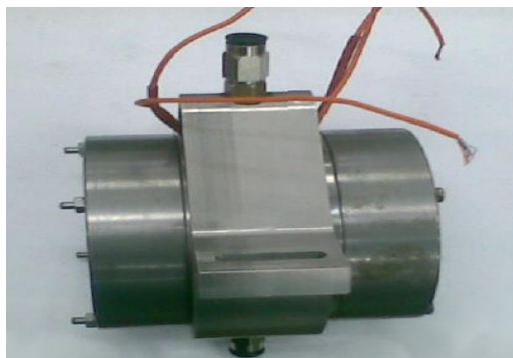


Figure 2.2 MR fluid based bearing (Bompos and Nikolakopoulos, 2014)

2.4.2 MR mounts

The magnetorheological fluid based mounts are particularly used as engine mounts in industrial applications to mitigate the shocks and vibration associated due to switching on and off of engines. Figure 2.3 shows the schematic of an engine mount. These mounts operate under squeeze mode. Ahmadian and Ahn (1999) investigated the effect of MR mount parameters such as fluid resistance, volumetric stiffness and rubber stiffness on its transmissibility. They showed that the variation of these parameter values has significant effect on the vibration performance of the mount. Barber and Carlson (2010) designed valve based MR mount and evaluated its dynamic stiffness and damping under on and off state conditions. Also, effect of particle concentration on mount performance was estimated by considering 22 % and 36 % particle volume fraction and concluded that damping and stiffness could be tuned by varying the magnetic field. Elahinia et al. (2013) elaborated a review on designing, modelling and controlling of MR and ER fluid based mounts and their advantages over the conventional pneumatic and hydraulic mounts. Chen et al. (2016) presented a mathematical model of semi-active vehicle engine MR mount to estimate the field dependent force and dynamic stiffness. Further, they validated experimental results with simulation results. Recently Porsche an automotive company, adopted magnetorheological engine mounts for its new model 119 turbo (SAE 2009).

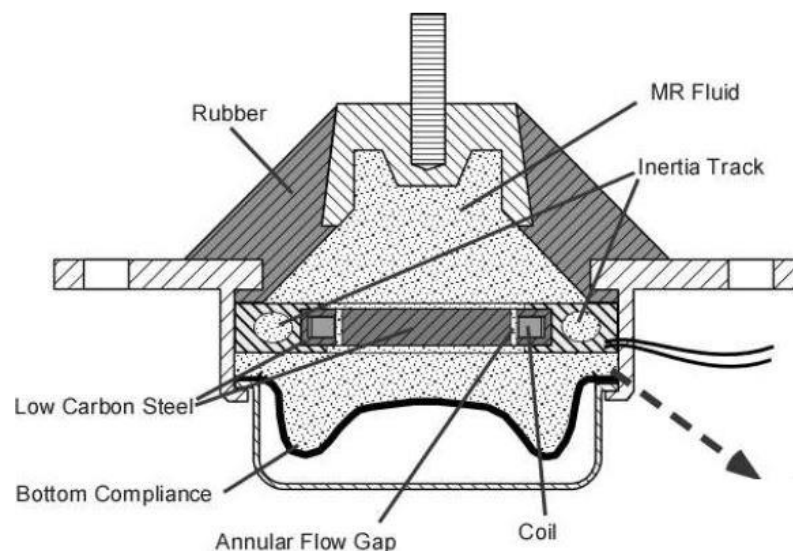


Figure 2.3 MR mount (Barber and Carlson, 2009)

2.4.3 MR fluid brake and MR clutch

MR fluid used in automobile brakes, which are referred to as MR brakes. There are five major types of MR brakes i.e, drum brake, disk brake, inverted brake, T-shaped single and multidisc rotor and multidisc brake. Figure 2.4 shows the disk type MR brake and its components, which is the type of MR brake described in the literature by Rabinow (1948). Typically, MR brakes operate under shear mode. These brakes consist of stator, rotor, electromagnetic coil and MR fluid filled in gap between the stator and rotor. The performance of MR brake and also their design, modelling and implementation in various applications were discussed in many research papers.

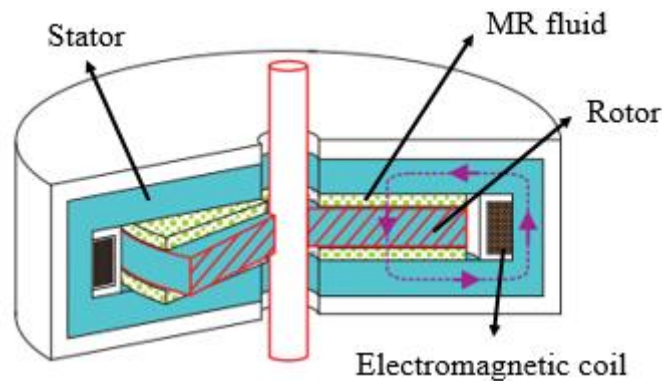
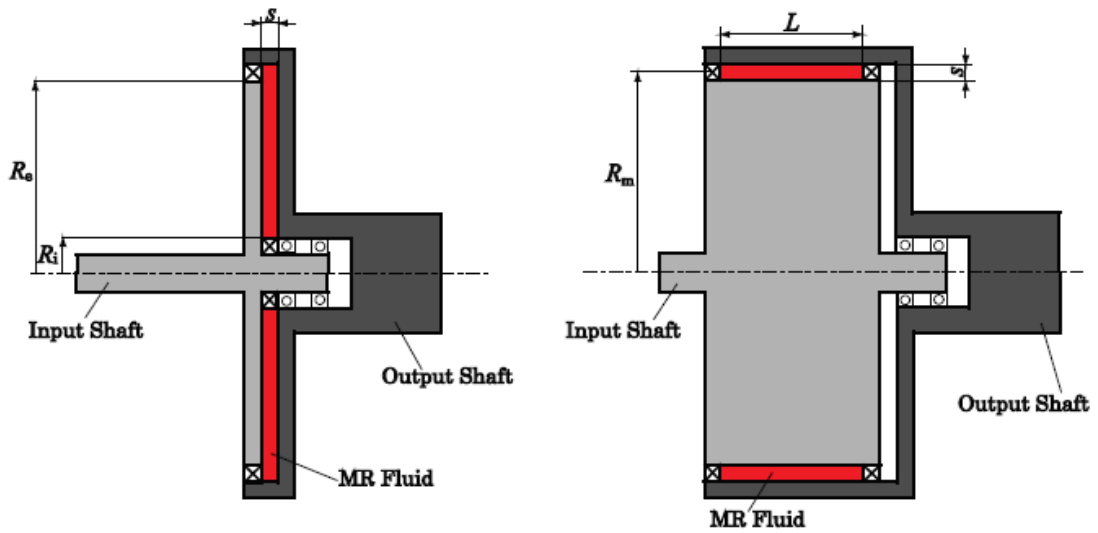


Figure 2.4 MR fluid brake-Disk type (Avraam, 2009)

The MR clutches operate under shear mode type and these are used for transmitting torque from engine to the transmission. The electromagnetic coil is wound on output shaft and MR fluid is filled in shearing gap provided (Bose et al. 2013) between input and output shafts. Basically, there are two configurations of clutches i.e, disk shaped and cylindrical clutches as shown in figure 2.5. The fluid filled in the gap get excited by external magnetic flux induced by the electromagnetic coil and fluid becomes semisolid. The semisolid fluid has higher yield stress which offers higher torque transmission capability to device.



(a) Disk type

(b) Cylindrical type

Figure 2.5 MR fluid clutches (Bucchi et al. 2014)

2.4.4 MR fluid polishing

In MR fluid polishing, MR fluid acts as an abrasive fluid. It flows through a predefined converging fluid flow gap provided between working surface and moving wall to polish the materials (Xiu et al. 2017). These are used mainly for polishing optical glasses, ceramics, plastic and non-magnetic materials (Wang and Meng, 2001). Figure 2.6 shows the schematic diagram of MR polishing device.

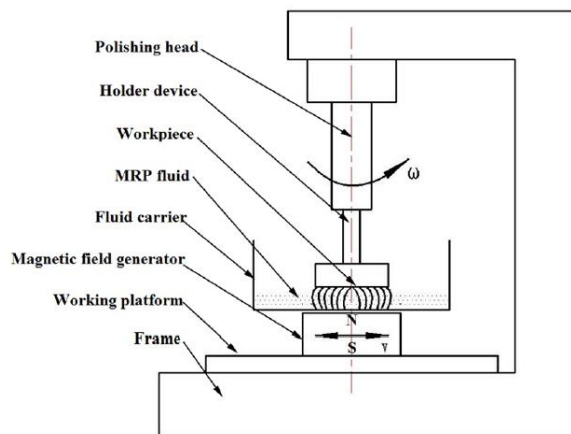


Figure 2.6 MR polishing device (Xiu et al. 2017)

2.4.5 MR dampers in various applications

Magnetorheological fluid damper (Figure 2.7) is one of the semi-active devices filled with magnetorheological fluid. In MR dampers, the damping forces are controlled by the action of magnetic field on the MR fluid. This allows the damping characteristics of the damper to be continuously controlled by varying the magnetic field.

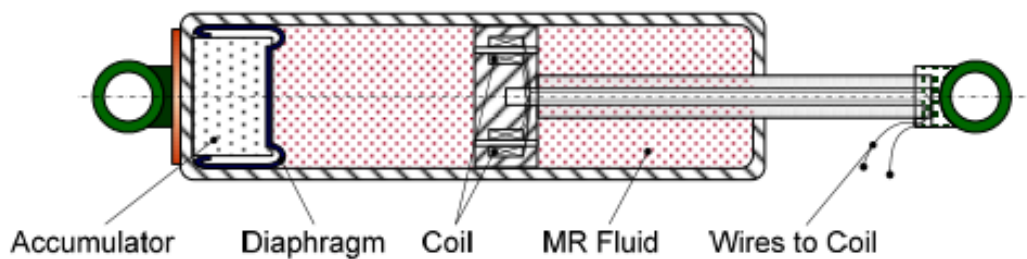


Figure 2.7 Monotube MR fluid damper (Truong and Ahn, 2012)

The applications of MR dampers are found in various fields such as civil structures in earthquake resistant buildings and bridges, vehicles, household applications such as washing machine, prosthetic leg and hard turning machine tool vibration isolation applications. Figures 2.8 to 2.14 illustrate different applications of MR fluid damper. Ahamed et al. (2016) developed an MR damper model for vehicular application and demonstrated the energy generation ability of the damper.

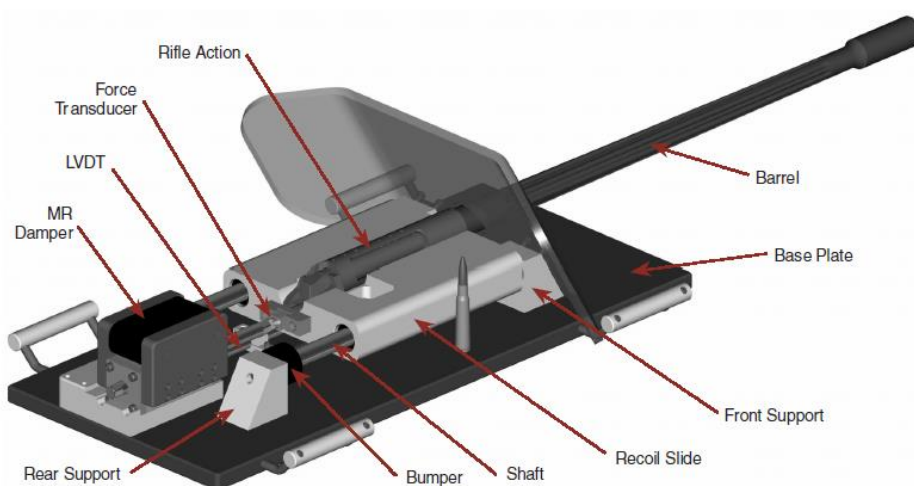


Figure 2.8 MR damper used for recoil in buffer gun (Ahmadian and Poynor, 2001)

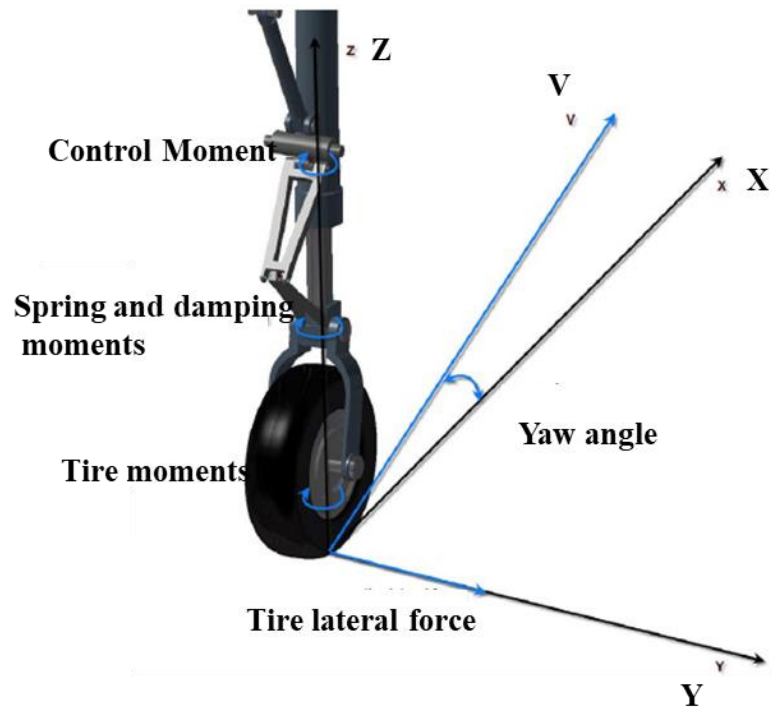


Figure 2.9 Landing gear (Chen et al. 2001)

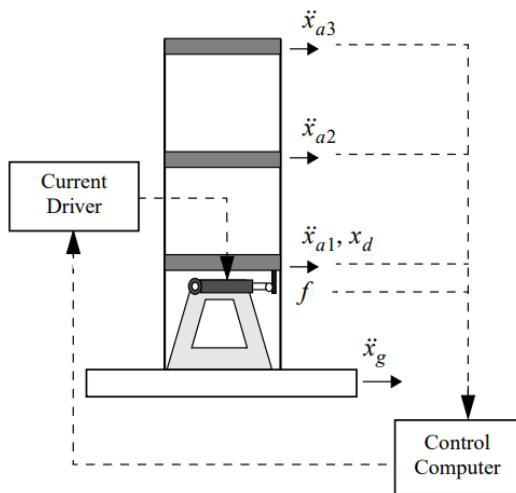


Figure 2.10 MR damper in structural application (Dyke et al. 1998)

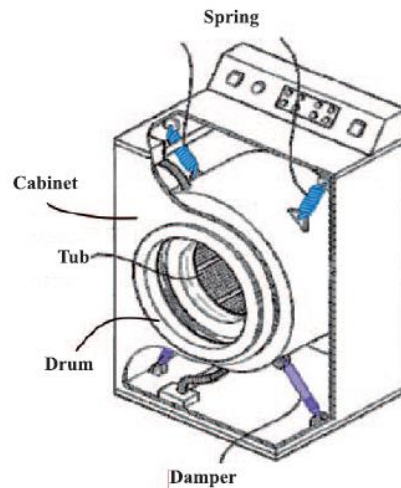


Figure 2.11 MR damper for vibration reduction in washing machine (Nguyen et al. 2014)

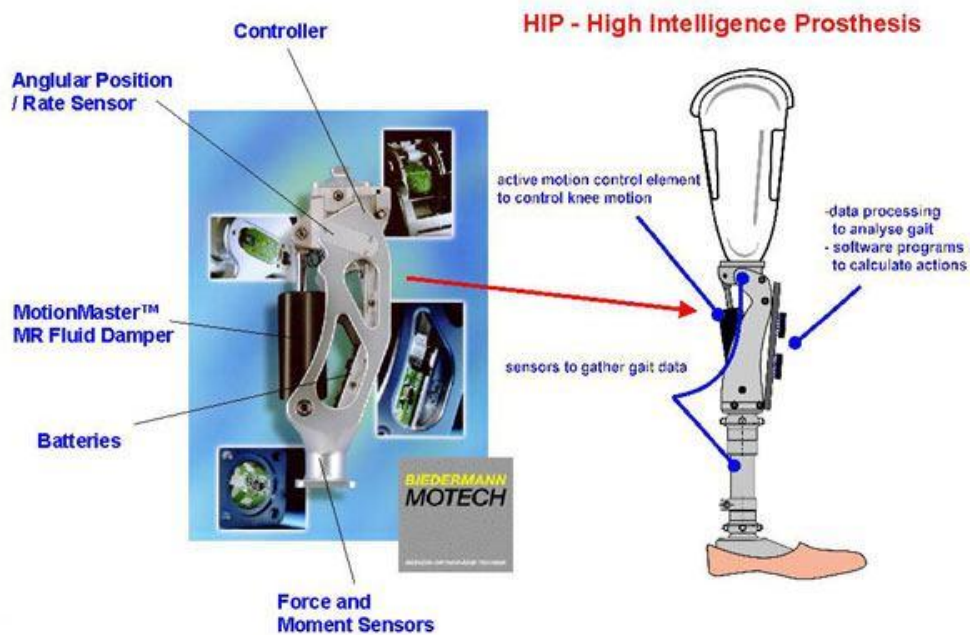


Figure 2.12 MR damper in prosthetic leg application (Klingenberg, 2001)

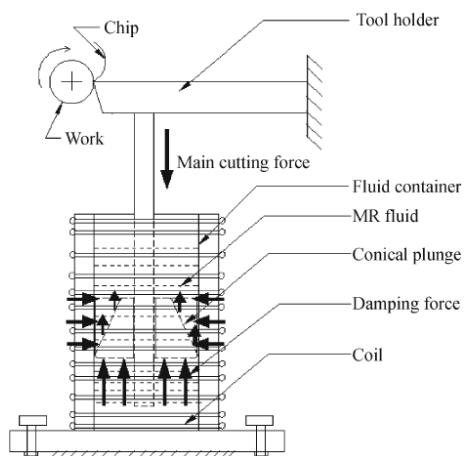


Figure 2.13 MR damper in tool vibration isolation application (Paul et al. 2012)

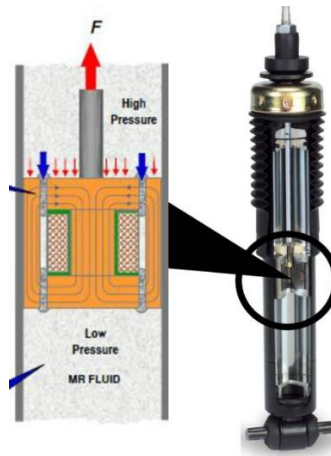


Figure 2.14 MR damper suspension for vehicle application (Magneride)

2.5 COMPUTATIONAL ANALYSIS OF MR DAMPER

Magnetorheological damper is a semi-active device employed to control the vibration of a system with suitable control strategy. The controllable damping force in MR

damper is produced by applying appropriate magnetic field to the MR fluid and variable damping can be achieved in real time. The design aspect of MR damper is electromagnetic coil incorporated in the piston head and the fluid flow gap. The characteristics of MR damper are expressed in the form of force versus velocity and force versus displacement curves. These characteristics can be obtained from experimentation using sophisticated dynamic testing machines and computational performing analysis.

Anakwa et al. (1998) developed a prototype pneumatic active suspension system using a pneumatic actuator for active control of vibration. Liao and Lai (2002) studied the single degree of freedom (SDOF) system with an MR fluid damper under harmonic excitations. They proposed mathematical models of SDOF with MR damper and validated it with experimental investigations. They also compared results obtained from mathematical model of MR damper with those of conventional viscous damper. Yang et al. (2002) designed and developed a large-scale MR damper and proposed two quasi-static models such as axi-symmetric and parallel plate models to predict the hysteresis behavior of MR damper. Gravatt (2003) designed and fabricated an MR damper for super-sport motorcycle applications and characterized its performance both experimentally and analytically. Kulkarni et al. (2003) designed and studied the performance of MR damper with different currents, operating frequencies and amplitudes under squeeze mode, torsional mode and combined mode. Ahmadian and Norris (2008) characterized an MR damper under impact and shock loading. They developed drop tower to apply impact load on the MR damper and studied the damper performance by dropping the mass from different heights. Sahasrabudhe et al. (2005) developed a smart sliding isolation system using controllable MR damper and its performance was evaluated analytically as well as experimentally. Ali and Ramaswamy (2009) developed two nonlinear model based control algorithms to monitor the magneto-rheological damper voltage required to control the structural vibration. Costa and Branco (2009) conducted experimental and analytical studies of MR damper to evaluate the dynamic performance and also, they studied the friction force effect between MR fluid and the device wall. Liu et al. (2006) proposed a new configuration of suspension system using two controllable dampers and two constant springs for

controlling the variable stiffness. Cronje et al. (2005) developed a variable stiffness and vibration damping MR isolator with a closed-loop displacement and velocity feedback control system.

Kciuk et al. (2010) experimentally investigated the response of a prototype magneto rheological damper at various magnitudes of control current. Kim et al. (2011) estimated the performance of MR damper by using a vehicle. They have obtained the dynamic responses of the vehicle by using single-lane change and rapid braking test. Potter et al. (2011) studied the quasi-active damping method of coupled mechanical and control system design using multiple semi-active dampers. Ashfak et al. (2011) designed, fabricated and evaluated the performance of an MR damper. Imaduddin et al. (2013) presented an overview of recent developments in rotary MR damper in terms of different proposed concepts of structural design, magnetic circuit configuration and modelling techniques. Dutta and Dutta (2014) studied the effectiveness of vibration isolation by using nonlinearity in the magnetorheological damper under harmonic excitation. McLaughlin et al. (2014) evaluated the performance of a magnetorheological damper with spiral channel bypass valve under sinusoidal excitation. Esteki et al. (2014) studied dynamic analysis of electrorheological and magnetorheological fluid dampers in flow and mixed mode configurations under harmonic and random excitations. Avinash et al. (2014) developed a twin tube MR damper and conducted experiments to analyze the damping characteristics of the MR damper under different input conditions. Berasategui et al. (2014) evaluated the power dissipation capacity of MR damper in pre-yield and post-yield damping region under imposed and unrestrained harmonic excitations. Hu et al. (2015) developed linear variable differential sensor based magnetorheological damper and evaluated its performance under static and dynamic conditions.

2.5.1 Geometric optimization of MR damper

Force developed in the MR damper is highly influenced by the magnetic flux density induced in the fluid flow gap. In the recent past, optimization of MR damper by considering various geometric parameters, electric parameters and damping force has been conducted by researchers. Gavin et al. (2001) compared electrorheological and

magnetorheological fluid devices with the electrical power requirement and optimized the MR damper in order to minimize the electrical power consumption. Rosenfield and Wereley (2004) proposed an analytical optimization design method for MR valves and dampers based on the assumption of constant magnetic flux density throughout the magnetic circuit. Shivaram and Gangadharan (2007) designed a statistical model of MR damper using the Design of Experiments approach by which various factors such as magnetic field strength, volume fraction of the magnetic particle, shearing gap between piston and cylinder, amplitude and frequency of vibration were considered in their experimentation. Nguyen et al. (2008) determined the optimal geometrical dimensions of MR valve to improve the valve performance and pressure drop by using golden section algorithm and local quadratic fitting technique through FEM. Park et al. (2008) developed an electromechanical brake system using magnetorheological fluid and performed multidisciplinary finite element analysis which involved magnetostatic, computational fluid dynamics and heat transfer analysis to study the behavior of the system.

Nguyen and Choi (2009) determined the optimal level of geometrical parameters such as coil width, flange thickness, piston radius and flow gap of MR shock absorber to maximize the damping force, dynamic range and inductive time constant of the damper by using FEA. Zhang et al. (2009) carried out electromagnetic circuit analysis using FEM and performed optimisation of a new vane MR damper. Nguyen et al. (2009) developed a quasi-static model using Bingham fluid model for the MR valve and demonstrated geometric optimisation of the design parameters to maximise the yield stress and damping force. Gudmundsson et al. (2010) evaluated the rheological properties of prefluorinated polyether based MR fluid. They also conducted geometrical optimization study of MR brake to maximize the brake torque. Parlak et al. (2010) studied the geometrical optimization of MR damper to achieve optimal vibration control by using Taguchi experimental design. The optimal solutions of the MR damper were evaluated using analytical equations. Sallom and Samad (2011) designed an MR valve, based on the optimization result, which could maximize the magnetic flux density at the valve gap. Yu et al. (2007) conducted the optimization study of the magnetic circuit in MR dampers by adjusting the fluid flow gap in order to achieve a

greater magnetic field strength. Parlak et al. (2012) geometrically optimized the MR damper by considering maximization of damper force and maximum magnetic flux density as objective function using goal driven optimization. Tu et al. (2007) designed an MR damper for an automobile front suspension, wherein magnetic circuit in the piston was examined by using FEM and properties of the designed damper were determined by conducting experiments. Parlak and Engin (2012) analyzed the fluid flow through the annular gap by quasi-static analysis and conducted CFD analysis of the MR damper. Tu et al. (2007) conducted FE analysis using MR damper axisymmetric model in ANSYS to calculate the total magnetic field developed in the MR damper.

Thakkar et al. (2013) conducted electromagnetic analysis of MR damper to identify the saturation limit of supplied current by using FEM. Zhou and Zhang (2013) conducted multi-objective optimization of electromagnetic circuit of an MR damper in order to minimize the area of magnetic circuit and to enhance the damper force by using finite element method. Parlak et al. (2013) carried out geometric optimization of MR damper using the Taguchi design of experiments. This work focused on maximizing the magnetic flux density at the annular gap of the MR damper and classifying the design variables, which had high influence on the objective function. The optimal damper configurations obtained from this study were fabricated and tested for verification. Nguyen et al. (2014) optimized the MR damper of front loaded washing machine using finite element analysis in conjunction with golden section algorithm. Mangal and Ashwin (2014) conducted the optimization of geometrical parameters of MR damper to maximize the damper force by using statistical tool (Taguchi design of experiment approach) coupled with the finite element method (FEM). Ferdous et al. (2014) conducted studies on optimization of MR damper for different configurations of damper piston, fluid flow gap and damper housing by using finite element analysis (FEA) and then, validated the analysis results with experimental results. Djavarehshkian et al. (2015) analytically investigated the effect of parameters such as number of turns, pole length, gap thickness and spool length of MR damper. They also conducted optimization study of these parameters for minimization of electrical power consumption and improvement of damper force by using response surface method. Hu et al. (2015) proposed a double coil MR damper which could obtain force and dynamic

range though quasi-static model. They also considered seven different configurations of piston head for investigating the performance of double coil damper and obtained optimal parameters.

2.5.2 FEA and CFD analysis

Damping force is one of the key parameters for estimation of dynamic performance of the MR damper. The fluid flow in the annular gap is simulated using CFD tool to obtain damping force versus velocity plot. Snyder et al. (2001) discussed the hysteresis behavior of the linear MR damper by considering different nonlinear models such as nonlinear Bingham plastic model, biviscous model, nonlinear hysteresis biviscous and viscoelastic plastic model. They observed that the energy dissipation error of the non-linear viscoelastic plastic model was better than the other nonlinear models. Zschunke et al. (2004) evaluated magnetic flux through finite element analysis and computed flow resistance in the orifice of damper using CFD analysis. Zhu (2005) conducted experiments on disk type MR damper and performed magnetic field analysis by using FEM. The effect of current applied to the electromagnetic coil on induced magnetic flux density in the fluid flow gap was analyzed through theoretical and experimental studies. Yasrebi et al. (2006) presented finite element analysis and fluid flow analysis to predict the performance of the MR damper. Further, computationally obtained results were verified with the experimental results. Shams et al. (2007) evaluated the force acting on the valve of automotive shock absorbers using CFD and FEA. Samali et al. (2003) carried out experimentation on prototype MR damper in shear mode. They also investigated dynamic behavior of MR damper by using quasi-static method. Park et al. (2008) developed an electromechanical brake system using magnetorheological fluid and performed multidisciplinary finite element analysis, which involved magnatostatic, computational fluid dynamics and heat transfer analysis to study the behavior of the system. Various optimization tools were used to obtain the optimum parameters of the damper. Li et al. (2009) carried out investigation on vibrational isolation ability of developed MR fluid damper with variable stiffness and damping. Weng et al. (2008) developed a general expression corresponding to exact flow of fluid in the fluid flow gap and conducted CFD simulation. The results obtained from simulation and general expressions were compared with experimental results.

Bullough et al. (2008) conducted CFD simulation for steady and unsteady flow for various applications such as piezo driven outlet flow, 2D clutch, 1D clutch, 1D valve and Rayleigh step bearings. Case et al. (2011) conducted a multiphysics modelling of magnetorheological dampers by using COMSOL, focusing on the objective to develop a semi-active control scheme in medical orthosis. Goldasz and Sapinski (2011) conducted magnetostatic analysis of MR damper by using FEM and numerical simulation for two different operation modes namely flow and squeeze mode. Bompos et al. (2011) presented an integrated simulation study of a magnetorheological fluid journal bearing by using CFD and FEM. The journal bearing characteristics such as eccentricity, attitude angle, oil flow and friction coefficients were calculated and presented as functions of the magnetic field.

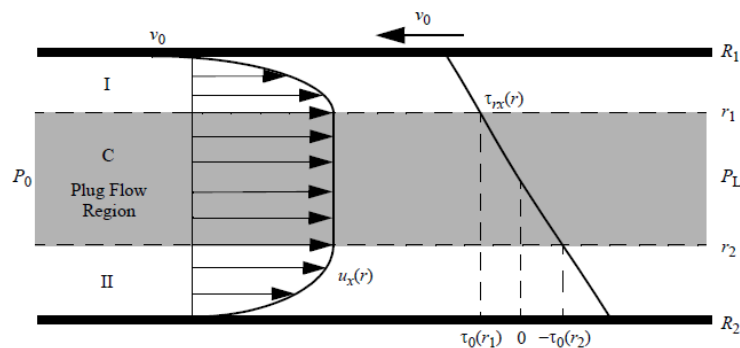


Figure 2.15 Velocity profile of MR fluid through an annular gap (Parlak et al. 2012).

The velocity profile of MR fluid flow across the annular gap is as shown in the figure 2.15. Parlak et al. (2012) conducted FE analysis to optimize the damper geometry based on maximum magnetic flux density and coupled it with computational fluid dynamics analysis using CFX to obtain the damping force. Further, the simulation results were compared with the experimental results. Parlak et al. (2012) investigated the non-Newtonian flow in the annular gap using quasi-static analysis and evaluated plug thickness and damper force. They also carried out CFD analysis of MR damper by using transient and deformed mesh, which can enable the piston sinusoidal movement considering non-Newtonian region. Also, effect of stroke and velocity on the damper performance were examined. Gedik et al. (2012) conducted two dimensional CFD simulation of steady state, viscous, laminar flow of magnetorheological fluid through

the gap between two fixed parallel plates under uniform magnetic field using magnetohydrodynamic (MHD) module. Omidbeygi et al. (2013) investigated hydrodynamic characteristics of magnetorheological fluid flow within the eccentric flow gap in shear mode by using numerical and analytical techniques. The influence of MR effect on fluid flow, caused by applied magnetic field on flow field have been analyzed. Diudea et al. (2013) conducted computational fluid dynamics analysis of vehicle shock absorber and carried out further investigation on improving the ride comfort and steering ability. Gedik et al. (2013) performed a CFD analysis of liquid-metal (electrically conducting) fluid flow in a circular non-conducting pipe, by considering steady state, laminar, incompressible viscous flow using magnetohydrodynamic (MHD) model. Liu et al. (2015) investigated shear performance of metal foam magnetorheological damper by considering a key factor such as damping force and reported that the damping force increase with increment in current. Sternberg et al. (2014) designed and tested large capacity MR damper and used multi-physics finite element models to investigate the coupled magnetic and fluid-dynamic behavior of the designed damper. They concluded that new external coil design could be used for the MR damper. Yazid et al. (2014) presented the design of MR damper with a combination of a squeeze and shear mode. They showed that a higher damping force can be obtained from mixed mode as compared to the single mode dampers. Zheng et al. (2014) designed and analyzed a new MR damper with multistage piston and separate input currents. They used finite element method to investigate magnetic flux density distribution in the fluid flow gap. Paul et al. (2014) used COMSOL software for CFD analysis of the MR damper and compared the results with experimental results.

2.6 MR DAMPER MODELS

Development of representative dynamic models, which can exhibit exact inherent non-linearity of MR damper is a prominent aspect for reaching high performance. The need of these models is for predicting the dynamic behaviour and damper design. The models which are developed can serve the purpose in numerical simulation for evaluating the performance of the semi-active systems with associated controllers. It is necessary to understand the semi-active systems prior to developing and employing them in service.

Some of the important parameters which should be considered while designing these models are accuracy, simplicity, robustness, adaptation and reversibility.

MR damper models are classified based on three parameters i.e., properties, method adopted for modelling and reversibility. Quasi-static models are categorised based on the properties of the MR fluid. Parametric and non-parametric models are categorised based on the modelling method and inverse model is based on the reversibility.

2.6.1 Quasi-static models

These models are very much useful in preliminary design of an MR damper, but the main limitation of these models lies in inefficiency of describing the nonlinear behavior under dynamic loading conditions particularly in case of hysteretic nature. To overcome the disadvantages of these models, new dynamic models have been developed. There are three important quasi-static models namely, Bingham model, Casson model and Hershel Bulkley model.

2.6.2 Parametric models

Parametric models are developed by considering the physical elements such as linear and nonlinear springs, dash pots, friction elements and other mechanical elements. Most of the parametric models developed so far have concentrated on hysteresis characteristics of the MR damper. The important parametric models which are extensively used in the research are Bingham model, biviscous model, viscoelastic plastic model, stiffness viscosity elasto slide model, Bouc-wen model, Dahl hysteresis model, Luge model, hyperbolic tangent function model, sigmoid function, equivalent model and phase transition models.

Bingham model was proposed and developed by Stanway et al. (1987) using combination of friction element and viscous damper. Figure 2.16 shows the schematic of Bingham MR damper model. This model is mathematically expressed as below (Spencer et al. 1997),

$$F(t) = C_0\dot{x} + f_c \text{sgn}(\dot{x}) + f_0 \quad (2.4)$$

where, \dot{x} is the velocity, C_0 is the damping coefficient, f_c is the frictional force, f_0 is the offset force.

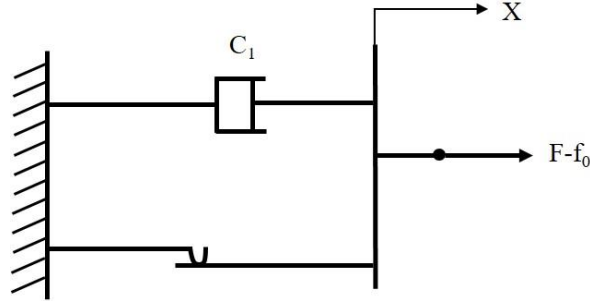


Figure 2.16 Bingham model

Wereley et al. (1998) proposed an idealized Bingham plastic model by modifying the existing Bingham model. This model was developed based on the parallel plate approximation and considering the yield force (F_y) and pre-yield damping (C_{po}). Mathematical expression to describe this model is given as,

$$F(t) = \begin{cases} C_{po}v + F_y & v > 0 \\ -F_y < F < F_y & v = 0 \\ C_{po}v - F_y & v < 0 \end{cases} \quad (2.5)$$

Kamath et al. (1997) developed a nonlinear dynamic model by considering pre-yield and post yield behavior. To capture the characteristics under this region a viscoelastic fluid element and viscous fluid was used. Ang et al. (2004) formulated relationship for hysteretic loop based on its symmetric nature by expressing each stage of motion through an equation. Sims et al. (2000) demonstrated efficiency of a model, which was developed by using spring and mass connected in series. It was represented as a lumped parameter which directly relates to the device geometry.

Gamato filisko (1991) worked on the viscoelastic plastic models by considering pre-yield, post yield and yield response of the fluid. Pang et al. (1998) presented nonlinear viscoelastic plastic model considering the effect of response in pre-yield and yield region. They have used combination of linear mechanism using linear shape function.

The mathematical expression of viscoelastic plastic model under sinusoidal displacement is written as

$$F(t) = \begin{cases} f_{ve} + F_s & |F(t) \leq F_y| \\ C_1 \dot{x} + R\ddot{x} + F_y \operatorname{sgn}(x) & |F(t) \geq F_y| \end{cases} \quad (2.6)$$

where, f_{ve} = Viscoelastic force, F_s = Stiction effect, R = Equivalence inertial motion, F_y = Yield force.

Wereley et al. (1999) developed two models to predict the nonlinear characteristics of MR damper i.e, viscoelastic plastic model with stiffness and stiffness viscosity elasto slide model. The method for identifying the unknown parameters of each model was also presented, which was achieved by minimizing the mean square error difference of predicted and experimental results. The schematic representation of stiffness viscosity elasto slide model is as shown in figure 2.17.

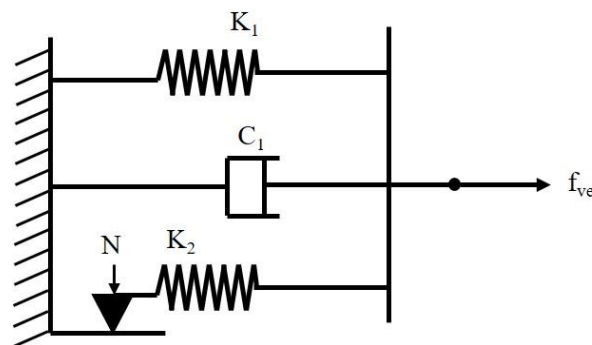


Figure 2.17 Stiffness viscosity elasto slide model

Hu et al. (2003) demonstrated the usage of rate dependent elastic slide model to describe the non-linearity of MR elastomer damper. Wen (1976) proposed a new modelling method of hysteretic systems. Bouc (1971) formulated an analytical expression of hysteretic model and this model was generalized by Wen (1976), popularly referred as Bouc-Wen model and is extensively used in hysteresis modelling. Spencer et al. (1998) used Bouc-Wen model to express the hysteretic nature of MR damper and damping force, which is expressed as

$$F(t) = C_0 \dot{x} + K_0(x - x_0) + \alpha Z \quad (2.7)$$

where α is parameter of Bouc-wen model and Z is evolutionary variable Phenomenological models are proposed in order to accurately predict the behavior of MR damper, which are referred as modified Bouc-Wen model and it is illustrated in shown in figure 2.18. This model consists of a set of constant parameters that relate characteristics to excitation current which is needed to be identified. These parameters are as follows,

$$\theta = (C_0, C_1, K_0, K_1, L, x_0, \gamma, \beta, A, n)$$

where K_0 is control stiffness, K_1 is accumulator stiffness, C_0, C_1 are damping coefficient, x_0 is initial displacement, γ, β, A, n are parameters of Bouc-wen model.

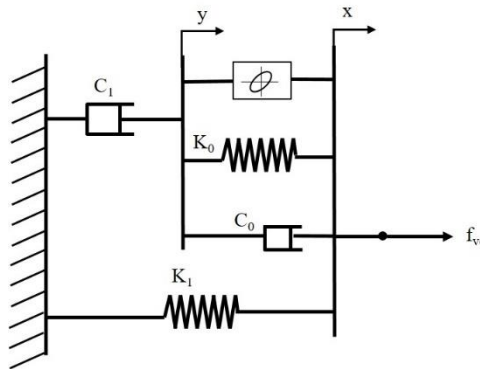


Figure 2.18 Modified Bouc-wen model

Yang et al. (2004) proposed a dynamic model based on the Bouc-Wen model to evaluate the dynamic characteristic of a large-scale MR damper in civil engineering applications. Yang et al. (2002) developed a dynamic model by realizing the model parametric function as a third order polynomial and identified associated equations as a function of current. Ali and Ramaswamy (2009) proposed modified Bouc-Wen model based on consideration of amplitude, effect of current on the parameters and presented quadratic relation for the parameters. Yao et al. (2002) carried out performance evaluation of MR damper by adapting Bouc-Wen model and obtained the parameters using optimization technique. Kwok et al. (2007) developed a dynamic model by

modifying the existing Bouc-Wen model for considering the non-symmetric hysteresis behavior and identified the parameters using the genetic algorithm. Particle swarm optimization was also used for identifying the values of parameters by Kwok et al. (2007). The non-symmetrical Bouc wen model is expressed as,

$$\dot{z} = [-\gamma \operatorname{sgn}\{\dot{x} - \mu \operatorname{sgn}(x)\}z]|z|^n - \beta|z|^n + A](\dot{x} \operatorname{sgn}(x)) \quad (2.8)$$

where, μ = scale factor.

Dahl (1976) proposed a model by considering the frictional effect such as Coulomb friction and solid friction in a controllable system. This model is expressed through a differential equation which is given as,

$$\frac{dF(t)}{dx} = \sigma \left[1 - \frac{F(t)}{f_c} \operatorname{sgn}(\dot{x}) \right]^\zeta \quad (2.9)$$

σ is stiffness coefficient, ζ is shaping parameter, $F(t)$ is friction force, f_c is coulomb friction force.

This model uses Bouc-Wen operator and hence there are too many parameters to be determined. Zhou et al. (2006) modified this model by adopting the Dahl operator in place of Bouc-Wen operator to effectively capture the damper characteristics. Ikhouane and Dyke (2007) considered viscous friction for developing a model for shear mode type MR damper. It is also referred to as viscous Dahl model and can be expressed as

$$F(t) = C_0 \dot{x} + \alpha z \quad (2.10)$$

where, z is the non-dimensional variable, C_0 and α are voltage dependent constant.

By combining steady state friction and stiction characteristics, a new model was proposed by de Wit (1995). This model is also known as Lugre friction model. Jimenez and Alvarez (2005) modified this model to develop a simple and accurate model which is similar. Its properties as well as efficiency were also investigated. Jimenez and Alvarez (2002) presented an MR damper model by computing the internal state with a nonlinear absorber. Sakai et al. (2003) proposed a predictive model which can be

employed as inverse model to find voltage required for obtaining desirable damper force. The proposed model was developed by modifying the existing Lugre dynamic model and this model was found to offer higher performance when compared to existing model. The modified Lugre model of MR damper is expressed as,

$$F(t) = (\sigma_{0a} + \sigma_{0b})z + \sigma_1\dot{z} + (\sigma_{2a} + \sigma_{2b}v)\dot{x} \quad (2.11)$$

where, \dot{x} is relative velocity, v is the applied voltage, σ_{0a} , σ_{0b} , σ_{2a} , σ_{2b} , σ_1 are the constant parameters relating properties of MR fluid, z is the internal variable. First two terms in the above equation are related to friction force and third term is related to the viscous force.

Kwok et al. (2006) proposed a hyperbolic tangent function based model to predict the MR damper behavior by considering hyperbolic tangent function for representing the viscous nature and linear function for stiffness. Guo et al. (2006) presented a model to interpret the hysteretic and bi-viscous characteristics of MR damper with accuracy and precision. Also, application of this model in vibrational mitigation was investigated. Wang et al. (2003) developed a generalized representative model of MR damper by using symmetric and asymmetric sigmoid functions and the performance of the generalized model was evaluated under various excitations. Ma et al. (2006) developed a model which was independent of current function by utilizing bi-viscous, polynomial, extended Bouc-wen and sigmoid function models.

2.6.3 Non-parametric model

Non-parametric models are used as the representative dynamic models of MR damper which are obtained based on the results of analysis data and operation principle of the devices. Basically, non-parametric modelling is associated with developing and formulating of an accurate function which could predict and represent the dynamic characteristics of controllable devices. The construction of this model is shown in the figure 2.19 (Bogdon, 2003). The limitations of the parametric models can be overcome by adopting non-parametric models. These models are robust and can be employed to linear, nonlinear and hysteretic systems (Ehrgott et al. 1992). There are many non-parametric models developed for MR damper application such as polynomial model,

multifunctional model, back box model, query based model, neural network model, fuzzy model, wavelet model and ridgent model.

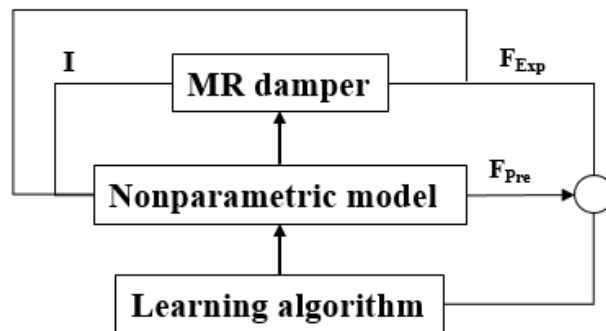


Figure 2.19 Non-parametric modelling

Choi et al. (2005) developed a hysteretic model which was dependent on the external field and expressed through a polynomial model. Also, a comparative study of parametric and non-parametric models was carried out and they observed that higher order polynomial models were efficient in capturing the hysteresis behavior. Figure 2.20 shows the proposed non-parametric model. Kim et al. (2008) studied a squeeze mode type MR damper behavior under external excitation using non-parametric model.

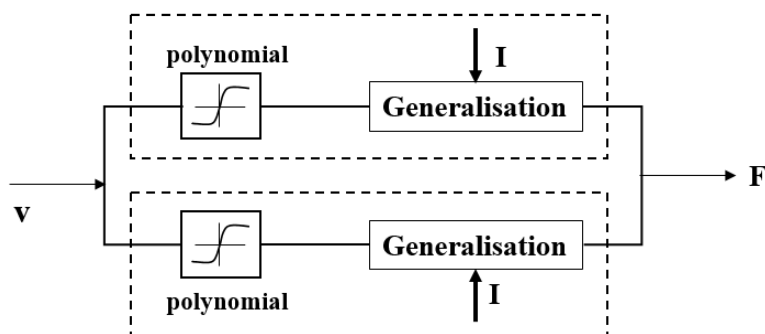


Figure 2.20 Schematic of non-parametric modelling

Song et al. (2005) proposed efficient non-parametric model developed using a series of mathematical functions and also verified its performance with parametric model. Song et al. (2007) employed nonparametric model of MR damper with adaptive control algorithm to evaluate the dynamic performance of the controlled system. Huang et al. (2006) carried out numerical analysis of MR devices using a fourth order auto

regressive model and trispectrum function, which are obtained from displacement and velocity characteristics of experimental test. Koga and Sano (2006) proposed a new approach for predicting the dynamic behavior of MR damper which is referred to as query based approach. Wang and liao (2004) studied the dynamic performance of an MR damper using online trained neural network and demonstrated that desirable damping force can be obtained by voltage signal generated from proposed inverse dynamic based neural network algorithm. Figure 2.21 shows the flow chart of system identification of MR damper using neural network.

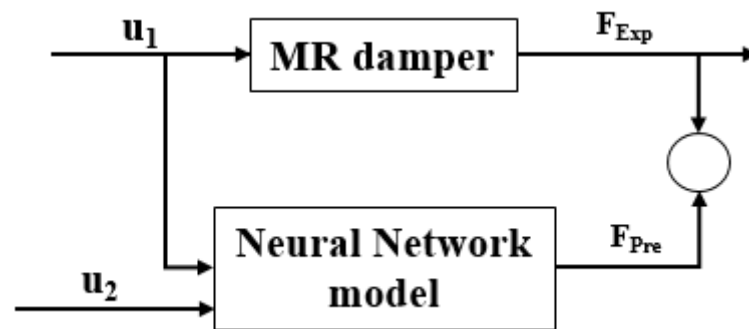


Figure 2.21 System identification of MR damper using Neural Network

Narendra and Parthasarathy (1990) discussed about effective implementation of neural network in identification and control of nonlinear systems. Yang and Lee (1997) carried out investigation on implementing neural network in vibration isolation of a system by developing three neural networks. Each model is assigned for system identification, online monitoring and vibration isolation respectively.

Schurter et al. (2000) presented a new approach to develop nonlinear model using adaptive neuro fuzzy interference system and carried out numerical analysis to validate the model representing an MR damper. Schurter et al. (2001) utilized experimental data to develop a trained fuzzy representative model of MR damper and found that proposed model could accurately predict the device characteristics with minimal simulation time. Jin et al. (2002) carried out investigation on implementation of ridge network to capture the non-linearity of the system and developed a predictive model of MR damper using ridge approach. Jin et al. (2005) presented an alternative modelling technique which was developed by using radial basis function network by combining forward and

inverse dynamic approach. Jan (2003) investigated the usage and efficiency of developed model by combining the neural network with parametric modelling.

2.7 SEMI-ACTIVE VIBRATION CONTROL OF VEHICLES

Eski and Yildirim (2009) designed a neural network based controller to control the vibration of seven degrees of freedom (DOF) active full car model subjected to random road roughness. The neural network control system consists of robust controller and feed forward neural network predictive controller. They have also evaluated the performance of active suspension system by using proportional integral derivative (PID) controller and compared results between them. Priyandoko et al. (2009) developed hybrid controller to isolate the vibration of active quarter car suspension system. Hybrid controller comprised of two different controllers such as sky-hook and adaptive neuro active force controller (SANAC). The performances of the active quarter car suspension system with SANAC controller were evaluated experimentally as well as mathematically and results were compared. Amato and Viassolo (2000) developed a controller for active suspension system to improve the passenger ride comfort. Control system consisted of inner loop and the outer loop controller, where the inner loop controller reduces the actuator nonlinearity and outer loop controller controls hydraulic actuator to achieve the desirable force to provide better performance. Fateh and Alavi (2009) developed impedance control strategy for controlling the vibration of active suspension system. In this control, an impedance rule prescribes the desired behavior of the suspension system in the form of second order linear system. Sharkawy (2005) used the adaptive fuzzy control (AFC) and fuzzy logic control (FLC) for active suspension system to provide better ride comfort and road holding qualities. They also evaluated the responses of the active suspension system with linear quadratic regulator (LQR) control and compared the results with passive suspension system. Yeh and Tsao (1994) proposed fuzzy preview controller to control the vibration of active suspension system. In this, control action was achieved by sensing the road irregularities ahead of vehicle and control signal was provided to the actuator to develop required force to isolate the vibration of a vehicle system. Lam et al. (2002) proposed a semi-active control for quarter car suspension with MR damper. They used PID controller for system control and they also analysed the performance of the quarter car

model subjected to road bump as excitation. Jeon et al. (1999) studied the vibration isolation performance of an MR damper with on-off skyhook control strategy. Chen (2009) proposed skyhook surface sliding mode control method in semi-active vehicle suspension system for its ride comfort enhancement. Rao and Narayanan (2009) reported dynamic response studies of two-degree freedom quarter car model with nonlinear passive elements traversing on a rough road with sky-hook control strategy. Khiavi et al. (2013) proposed an optimal nonlinear control strategy for a semi-active suspension system with MR damper in order to improve the ride quality and stability of the vehicle. Here, a non-parametric (polynomial) model was used to represent the MR damper in semi-active suspension system. Nguyen et al. (2015) developed neuro-fuzzy controller (NFC) based on ANFIS for controlling the vibration of quarter car suspension system. They have also analysed the performance of a quarter car suspension with sky-hook control strategy and compared the results between them.

Prabakar et al. (2009) studied the optimal preview control of half car model with MR damper under random road excitation. MR damper was modelled using modified Bouc-Wen model. Rossi and Lucente (2004) used H-infinity control strategy on quarter car and half car semi-active suspension system in order to improve the ride comfort and road holding performance. Karkoub et al. (2006) conducted analytical study to evaluate the effectiveness of the MR damper in reduction of vibration by using half car model with optimal control strategy. Kasprzyk et al. (2014) evaluated the performance of semi-active half car model with sky-hook and LMS control algorithms and compared the results between them. Hrovat (1993) compared the performances of active and passive suspension systems on quarter, half and full car models using linear quadratic optimal control. Talib et al. (2013) evaluated the performance of the half car active suspension system with self-tuning PID controller under different road conditions.

Jahromi and Zabihollah (2010) designed linear quadratic regulator (LQR) and fuzzy logic controller for full car model with MR damper in order to reduce the amplitude of the sprung mass and the results were compared with the results of passive suspension system. Paksoy et al. (2014) developed intelligent controllers using self-tuning fuzzy logic controller as a semi-active control strategy in a full car vehicle model with MR

damper to reduce the vibration of vehicle. The performances of full car model with these controllers were evaluated under road bump as input and compared the results of developed controller and regular controller. Zhang et al. (2013) studied the dynamic behaviour of MR damper based on full car vehicle model with sky-hook control strategy. They have considered modified Bouc-Wen model for representing MR damper.

2.8 MOTIVATION

Though enormous research works have been reported in the field of experimental and computational analysis of MR damper, the following studies are worth investigating in order to improve the performance of MR damper.

- The optimal proportion of MR fluid constituent plays a crucial role in enhancing the performance of MR damper; hence there is still a scope for considerable work to be carried out in this area. Also, the parameters influencing the rheological characteristics are still needed to be investigated.
- There are significant works available based on the experimental characterization of MR damper. But a limited work has been done in the area of computational methods to characterize the MR damper using coupled FEA and CFD approach.
- Combining different modes of operations of MR devices and to characterise the MR damper.

2.9 OBJECTIVES

1. To study the rheological properties of different proportion of the MR fluids by using rotational rheometer and also to evaluate optimal volume fraction of suspension particles of MR fluid.
2. To evaluate the dynamic performance of monotube magnetorheological damper through experimental study.
3. Magnetostatic analysis of monotube MR damper using finite element analysis and optimizing the magnetic coil parameter to maximize the magnetic flux density in the fluid flow gap.

4. Computational fluid dynamic (CFD) analysis of monotube damper to evaluate the dynamic performance and to compare analysis results with experimental results.
5. Evaluate the dynamic performance of quarter car semi-active suspension system by adopting suitable control strategy.
6. To implement and evaluate dynamic response of semi-active suspension system comprising MR damper in a three-wheeler vehicle subjected to random road excitation.

2.10 SCOPE

The main scope of this thesis is the characterization of MR fluid and MR damper using computational and experimental methods and also to investigate the optimal design conditions required for MR damper applications. It is also intended to study the feasibility of implementing the MR damper in a semi-active suspension system and study its performance in vehicle models to improve ride comfort and road holding performance, subjected to random road irregularities.

1. Development of a non-parametric model based on the computational approach by surpassing the experimental methods.
2. Comparative study of performance in terms of ride comfort and road holding of a vehicle with conventional passive dampers and a vehicle equipped with MR damper.
3. Implementing the MR damper in three-wheeler vehicle subjected to random road excitation to improve ride comfort and stability.

2.11 SUMMARY

This chapter presented various works on characterization of MR fluid dampers and its applications. Literature was basically classified into MR fluid, MR fluid applications, MR damper and its application in vibration isolation, MR damper models, active vibration control and semi-active vibration control in vehicle suspension system.

CHAPTER 3

METHODOLOGY AND EXPERIMENTAL SETUP

3.1 INTRODUCTION

The advanced technologies involving enhancement of qualitative performance of system and which can be controlled as per the desirability are needed in various applications. Such technologies are evolved by adopting smart materials. The smart materials are those whose physical behavior can be controlled by external stimulus. Magnetorheological fluid is one such materials, which has flexibility to the stimulus. The change in rheological properties due to application of magnetic field can be controlled and it is advantageous to design controllable devices for employing them in various applications. The damping characteristics of a damper are expressed through force versus displacement and force versus velocity curves. These characteristics are obtained either through analytical or experimental methods. This chapter provides the detailed view of methodology of research work and experimental setup used in the research work.

3.2 METHODOLOGY

The characterization of MR fluid and performance evaluation of MR damper in semi-active suspension system are focused in this research work. The methodology involved and steps followed in this research work is presented in figure 3.1. MR fluid samples with different volume fraction of iron particle were prepared and their rheological behavior under external magnetic field were evaluated through experimentation. An optimization process was adopted to identify the optimal proportion of MR fluid for MR damper application. Later, shear mode type monotube MR damper was characterized to evaluate the damping force under different input conditions.

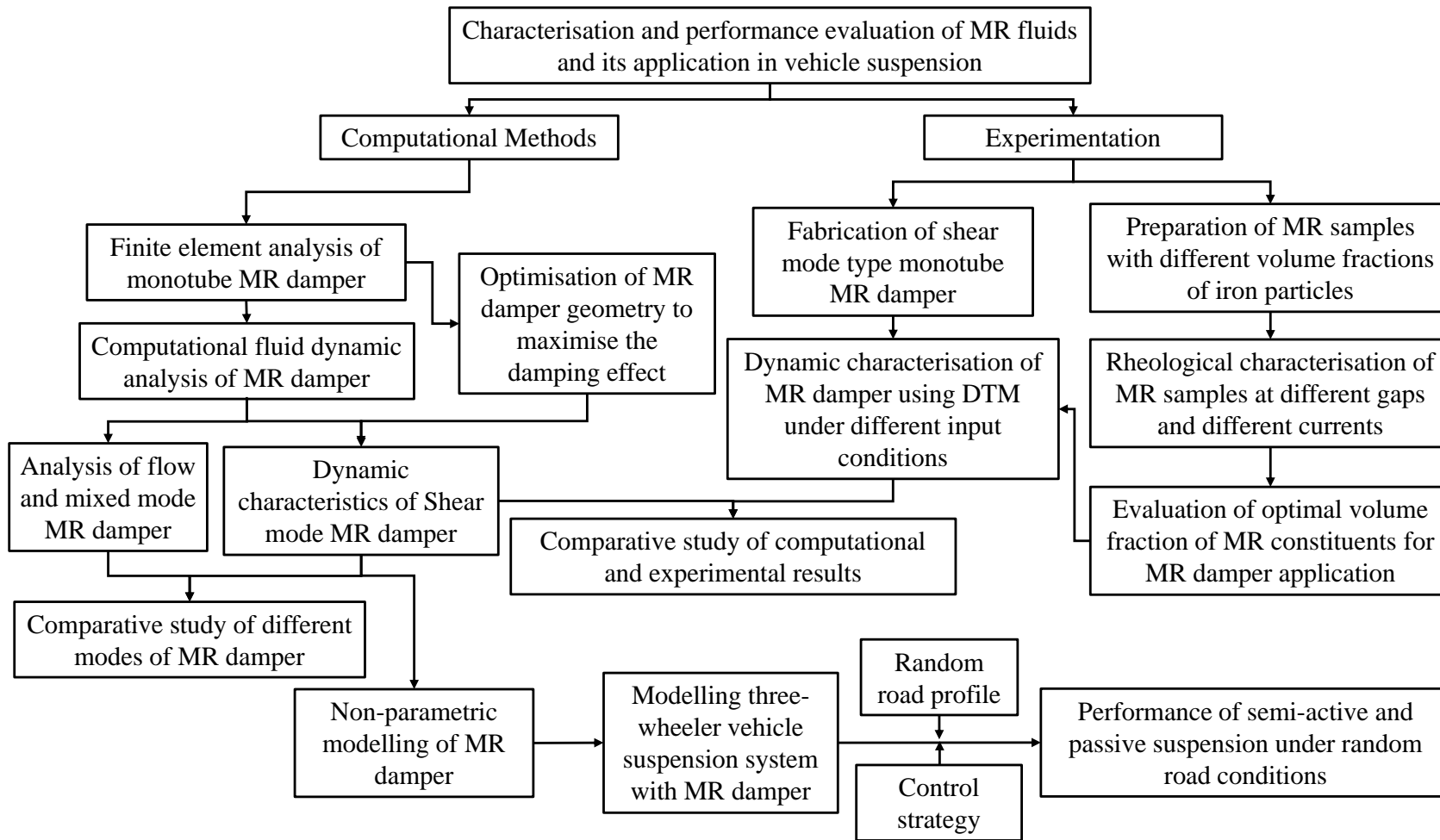


Figure 3.1 Research methodology

Computational fluid dynamics coupled with finite element analysis were carried out to compute the damping force and the results are validated with the experimental results. Further, a nonparametric model was developed to predict the behavior of the MR damper. This model is incorporated in the quarter car vehicle suspension to evaluate the ride comfort and road holding performance under different random road conditions. Then, the performance was compared with those of passive suspension system.

3.2.1 Preparation of MR fluid and Evaluation of optimum volume fraction of iron particles in the MR fluid

The preparation of MR fluid is based on either volume fraction or weight fraction of constituents such as carrier fluid, ferrous particles and additives. The selection of these constituents is crucial since they have significant effect on the rheological properties and performance of the MR fluids. Usual proportion of iron particles in the range of 20-40 % volume fraction. But the optimal proportion for particular application remains unique, hence it is necessary to find the optimal proportion for MR damper application. The constituents are not the sole influencing factors for variation of the rheological properties. Few other parameters such as magnitude of external magnetic flux density and parallel plate shear gap are also influential. The rheological properties can be estimated using a sophisticated rotational type rheometer. By considering all these parameters as variables and the response to these parameters as the objective function, an optimization problem can be formulated to evaluate the optimal proportion of the MR fluid constituents and effect of each parameter on the response. The procedure for preparation, characterization and optimization of the MR fluids is discussed in details in chapter 4.

3.2.2 Dynamic characterization of an MR damper

The characteristics of MR dampers can be studied using force versus displacement, force versus velocity, energy dissipation and equivalent damping coefficients. These parameters are very much necessary to be evaluated to characterize the MR damper under different input conditions. The damping force at different currents and displacement can be obtained using a dynamic test machine (DTM). These curves

provide the complete information about the dynamic behavior of the MR damper and area under these curves gives energy dissipation for particular current and frequency. The dynamic behavior of MR damper is elaborated in chapter 5.

3.2.3 Optimization of an MR damper

The geometric parameters of the electromagnetic coil play an important role in enhancing the performance of an MR damper. These parameters include shear fluid flow gap, number of turns of copper wire, DC current. Effective shear gap length and material used for the components have significant effect. Magnetic flux density and fluid flow gaps highly influence on damping force. Increase in the magnetic flux density leads to increase in the field dependent shear stress which again leads to increase in the resistance to fluid flow. Reduction in the shear gap enhances the damping range. The damping force is directly proportional to length of effective region and inversely proportional to cube of the fluid shear gap. Hence, minimizing the shear gap and maximizing magnetic flux density to obtain the optimal value of the parameters is the prime interest. The design optimization of MR damper is studied in chapter 6.

3.2.4 Coupled FEA and CFD analysis of MR damper

Finite element analysis is coupled with computational fluid dynamic analysis to estimate the characteristics of the monotube MR damper. The magnetic flux density induced in the shear gap of the damper was computed through magnetostatic analysis for various DC current inputs. Due to induced magnetic flux density, the rheological properties of the MR fluid in the shear gap will change and the fluid behaves as non-Newtonian fluid. These changes can be expressed using different fluid models, such as Bingham, Hershel-Bulkley and Casson models. These models are supportive to represent the non-Newtonian nature of fluid in the shear gap while performing CFD analysis. The detailed approach of computational analysis is discussed in chapter 7.

3.2.5 Development of nonparametric model of MR damper and dynamic analysis of vehicle suspension

The non-parametric modelling of MR damper is based on analytical expression, which serve as representative model of the MR damper. These expressions are obtained from the experimental data and device working principle. The most commonly used non-parametric model is a polynomial model. The damping force can be expressed in terms of damper velocity, displacement and acceleration using polynomial models. The order and coefficients of the polynomials can be identified from different methods with a satisfactory similarity of model prediction and actual experimental data. Comparative study was conducted between passive and semi-active suspension system. Development of mathematical modeling of vehicle is conferred in chapter 8.

3.3 EXPERIMENTAL SETUP

3.3.1 Rheological characterization

The behavior of MR fluid when subjected to external magnetic field can be estimated using a sophisticated rheometer. The variation in the rheological properties in steady and dynamic conditions were evaluated under different magnetic flux densities and angular frequencies. The instrument employed for this study was a parallel plate type rotational rheometer incorporated with a magnetorheological device cell. The schematic representation and its corresponding components are detailed in figure 3.2.

3.3.1.1 Measuring tool (PP-20)

The measuring tool is the most important part of the rheometer instrument as shown in figure 3.3. The measuring tool is also called as tool masters, which is having automatic tool recognition and configuration structure. Various rheological properties of the MR fluid sample can be estimated by rotating, oscillating or applying a step function to the measuring system – either by controlling motor torque or position change. The measuring tool is driven by an electric motor to shear the sample and also it measures the torque to calculate yield stress of the sample.

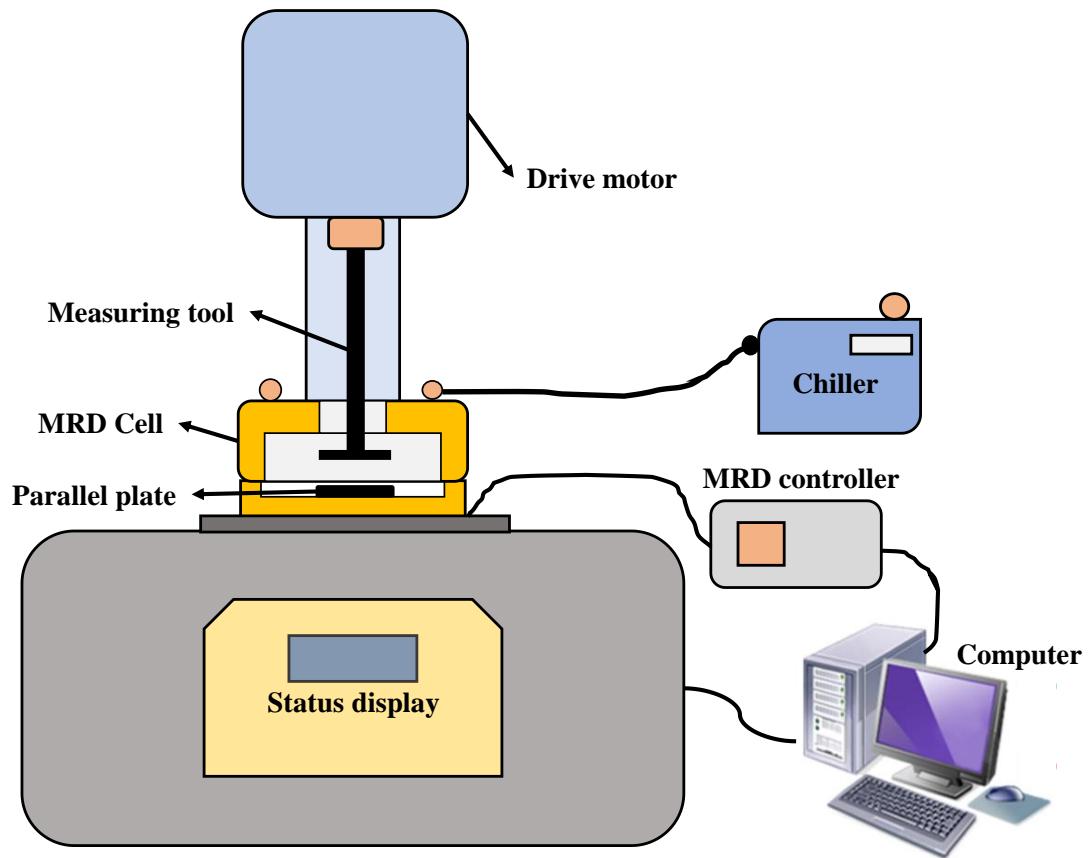


Figure 3.2 Rotational plate type rheometer



Figure 3.3 Measuring tool PP20 (Courtesy: Anton Paar)

3.3.1.2 MRD cell

The Magneto-Rheological Device (MRD) is used to investigate the influence of a magnetic field on magnetorheological fluids (MRF). The applied magnetic flux density of upto 1 Tesla is controlled by a rheometer software and can be adjusted according to requirements. In addition, a Hall effect sensor and temperature sensor allow online measurements of the actual magnetic flux density and temperature. The MRD consists of a liquid-temperature-controlled bottom plate with built-in coils. A magnetic yoke shown in figure 3.4 covers the plate to ensure a homogenous field and perpendicular field lines with respect to the plate. The parallel-plate system is made of non-magnetized metal, preventing radial forces acting on the shaft. The yoke can be temperature-controlled up to 70 °C with the liquid used in the bottom Peltier plate. A high-temperature version for operations at up to 170 °C is available, employing liquid temperature control in the bottom plate using an oil bath and Peltier temperature control of the yoke. The MRD is fully integrated in the rheometer software, which controls the magnetic field and records all important parameters.



Figure 3.4 Magnetorheological device cell

3.3.2 Damper test facility

The damper test facility can be used for estimating the characteristics of MR damper under various input conditions. The main components of the damper test facility are controllable electric motor driven shaker, LVDT, load cell, data acquisition system,

DC power supply and computer system. The schematic diagram of the damper test facility is illustrated in figure 3.5. The detailed functions and features of each component of the test facility are elaborated in the following sub sections.

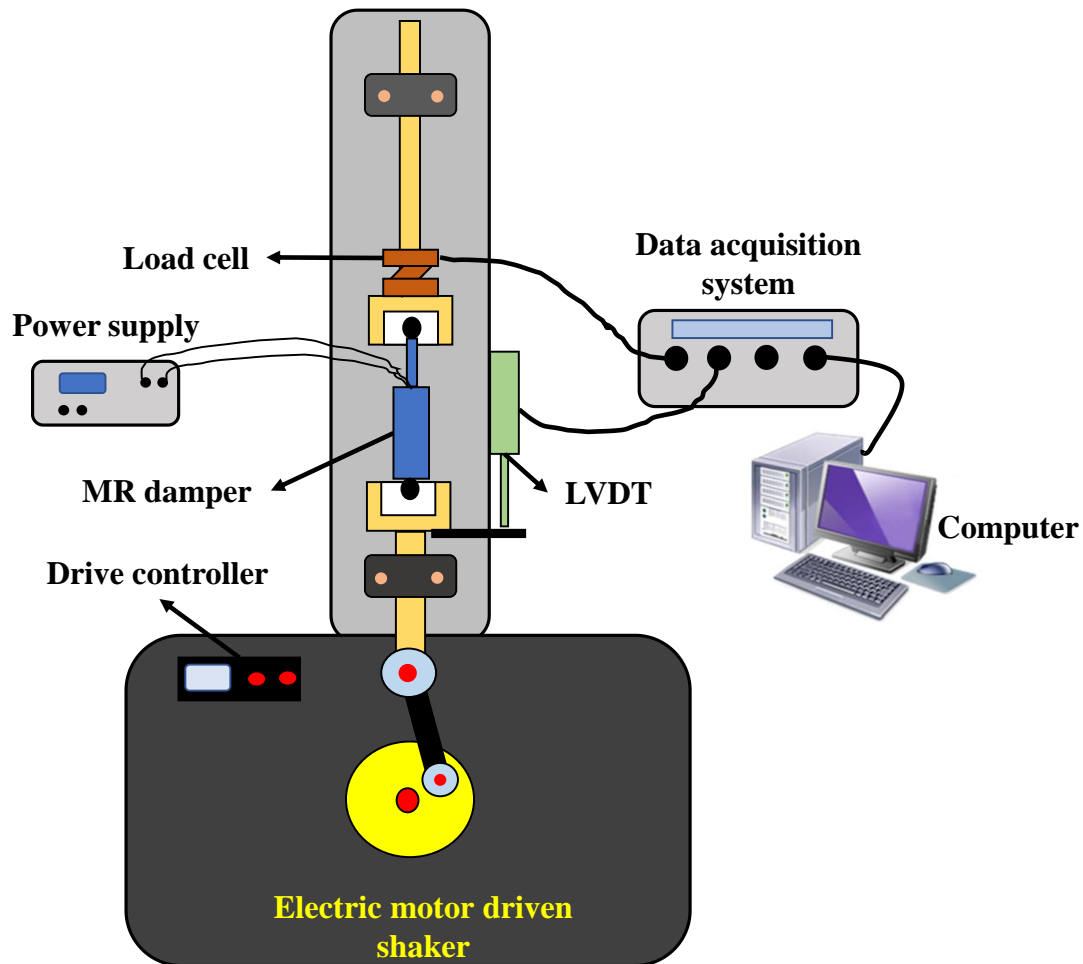


Figure 3.5 Schematic representation of damper testing machine

3.3.2.1 Electric motor driven shaker

The electric motor driven shaker is driven by a variable speed electric motor with cam system to provide time harmonic dynamic force to the MR damper. The mechanical exciter has a maximum force of 500 N with frequency in the range of 0.1 to 10 Hz which is compatible to PC based data acquisition system. Peak to peak stroke/displacement is about 15 mm.

3.3.2.2 DC Power supply

The programmable DC power supply shown in figure 3.6 is used for exciting the electromagnetic coil to induce the magnetic field inside the MR damper. The specifications of the DC power supply are as given in table 3.1



Figure 3.6 Programmable DC power supply

Table 3.1 Specifications of DC power supply (Aplab Ltd.)

Parameter	Specification
Output power	1.2 kW
Output voltage	0-60 V
Output current	0-20 A
Operating temperature	0-50 °C
Relative humidity	< 80%

3.3.2.3 Data acquisition System

The data acquisition system (DAQ) consists of hardware components to acquire the measured signal from the transducers and sensors. The measured output signal from the load cell and LVDT are acquired for signal conditioning and processing in the hardware unit. The processed analog signals are converted into digital signals. These output data are further processed to obtain the actual quantities measured from the sensors.

3.3.2.4 Linear Variable Displacement transducer (LVDT)

An LVDT is used for measuring the displacement of the MR damper. It is connected between a fixed reference point and top end connector of the MR damper. It is a long stroke displacement transducer used to measure the static and dynamic displacement. Figure 3.7 shows the displacement transducer (LVDT) and its specifications are provided in Table 3.2.

Table 3.2 Specification of the displacement transducer (Gefran-LVDT)

Parameter	Specification
Stroke range	10-50 mm
Independent linearity	$\pm 0.1\%$ full scale
Resolution	Infinity
Temperature range	-30°C to 100°C
Max Displacement speed	10 m/s

3.3.2.5 Force transducer

Maxload force transducer is used in the experimental setup and it is located above the upper fixture of damper facility. Force transducer offers a wide selection of force measurement ranges for compression and tension. Figure 3.8 shows the force transducer and specifications are provided in Table 3.3.

Table 3.3 Specifications of the force transducer

Parameter	Specification
Measuring direction	Tension/compression
Measuring range	-100 to 100 Kg
Measuring mode	Direct
Output	2.0 mV/V
Operating temperature range	-50 to 120°C



Figure 3.7 Displacement transducer



Figure 3.8 Force transducer

3.4 SUMMARY

The detailed overview of the research work, methodology adopted are discussed in first section of this chapter. Also, brief explanation about preparation and characterization of MR fluids, dynamic characterization of MR damper through computational and experimental method are included. Later sections describe the rheometer and damper test facility, sensors, actuators, transducers and data acquisition systems used for the experimentation. In the subsequent chapters, above said methods have been applied to study dynamic behavior of MR damper.

CHAPTER 4

PREPARATION AND RHEOLOGICAL CHARACTERIZATION OF MR FLUID

4.1 INTRODUCTION

The magnetorheological fluids are very much responsive to the external magnetic field. The change in its rheological behavior under external field can be evaluated through sophisticated instruments. It is important to know the variation in properties such as shear stress, viscosity, viscoelastic behavior, etc., before employing these fluids in any application. Also, each application requires specific proportion of MR fluid. Hence it is necessary to find the optimal proportion of MR fluid constituent for a particular application. This chapter discusses about the evaluation of MR fluid properties under different magnetic field and determine the optimal proportion of MR fluid for MR damper application.

4.2. SAMPLE PREPARATION

Three samples were prepared with different proportions of carrier fluid and suspension particles. Silicone oil was used as the carrier fluid which has high flash and fire point values. Hence, silicone based MR fluid can be used in applications, where temperature variations are significant. Silicone oil used in this work has a viscosity of 0.340 Pa-s and a density of 0.965 g/cm³. Carbonyl iron powder of approximate mesh size of 6.23 μm, 2.33 g/cm³ density and of spherical shape was used as the magnetisable particles. The iron powder purity is of nearly 99.62 % as per the specification provided by the Chengdu Nuclear 857 New Materials Co., Ltd. A small amount of lithium based grease (1% by volume) was added to each sample as antifriction agent and stabilizer in order to reduce the sedimentation of the particle. Measured quantity of silicone oil was taken in a small vessel and mixed with grease, then stirred till the grease mixed uniformly in silicone oil. Later, measured amount of carbonyl powder was added to the solution and stirred with constant speed of 450

RPM using an electromechanical stirrer for about 6-8 hours and ensure uniformity of particle distribution in the carrier fluid. The details of three samples prepared are tabulated in table 4.1.

Table 4.1 Composition of MR fluid samples

MR Fluid Sample	Composition	Volume fraction (%) of iron powder
Sample 1	Silicone and Carbonyl iron powder	25
Sample 2	Silicone and Carbonyl iron powder	30
Sample 3	Silicone and Carbonyl iron powder	35

4.3 APPARATUS

The rheological characterisation was carried out using Anton Paar rotational type rheometer MCR 302 with parallel plate configuration and magnetorheological device (MRD) cell attachment as shown in figure 4.1. The MRD attachment has capability for applying magnetic flux from 0 T to a maximum of 1 T. The tool used as parallel plate for measurement has a diameter of 20 mm (PP20/MRD/T1/P2). The experimental setup has three main parts, i.e measuring plate, MRD attachment cell and software for user interface. MRD attachment consists of a magnetic yoke, which monitors and maintains the temperature in the parallel plate. The electromagnetic coil is situated at the bottom portion due to which magnetic field lines are flowing from bottom plate to the upper plate. It is to be noted that, cup shape yoke doesn't play any role apart from maintaining the temperature of measuring area. The chiller outlet is attached to the yoke in order to maintain the temperature of sample and measuring plate.

The steady shear flow experiments were conducted at different values of gap between the two parallel plates 'h' at 0.25 mm, 0.5 mm and 1.0 mm. To ensure homogeneity and uniform distribution of iron particles, MR samples were thoroughly mixed before placing in the MRD cell. The required amount of MR sample for each gap is calculated to avoid the delivery of excess amount of sample into the cell. The

measuring plate diameter is of 20 mm and the volume (V) of sample required for the gaps $h = 0.25, 0.5$ and 1 mm are $V = 0.0785, 0.157$ and 0.314 ml respectively. All three samples were subjected to pre-shear for 25 seconds at constant shear rate of 10 s^{-1} after placing in MRD cell to obtain uniformity of the sample. After pre-shear, a magnetic sweep or current sweep is performed by applying current from 0 A to 2 A . The dynamic measurements were also conducted by adopting frequency sweep method. The samples were sheared to determine the critical yield stress and these values were used for evaluating the viscoelastic behaviour under different magnitude of current. The frequency sweep from 10 Hz to 100 Hz is performed at 0.25 A , 0.5 A and 1.0 A .

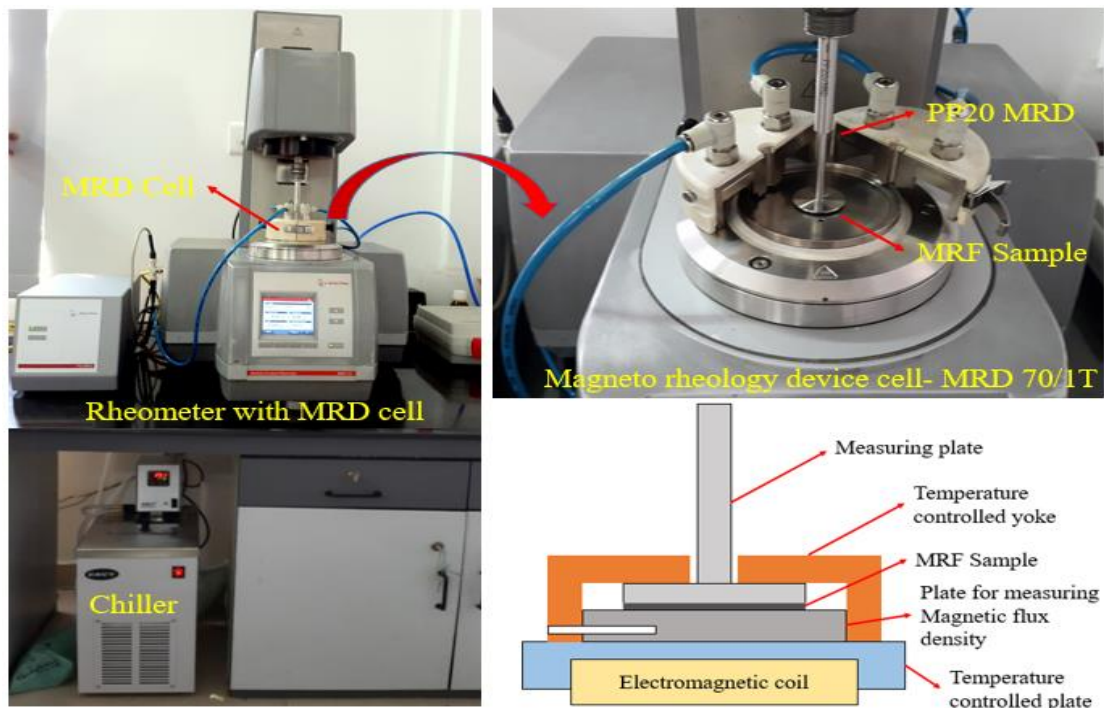


Figure 4.1 Rheometer MCR 302 with MRD Cell (70/1T)

4.4 COMPUTATION OF DAMPING FORCE OF MR DAMPER

Figure 4.2 illustrates the schematic diagram of MR damper model having a fluid flow gap (h) through the piston head. Since there is no relative motion between walls of the annular channel in the piston head, the mechanism of fluid flow is flow mode type. The dimensions of the MR damper are detailed in table 4.2.

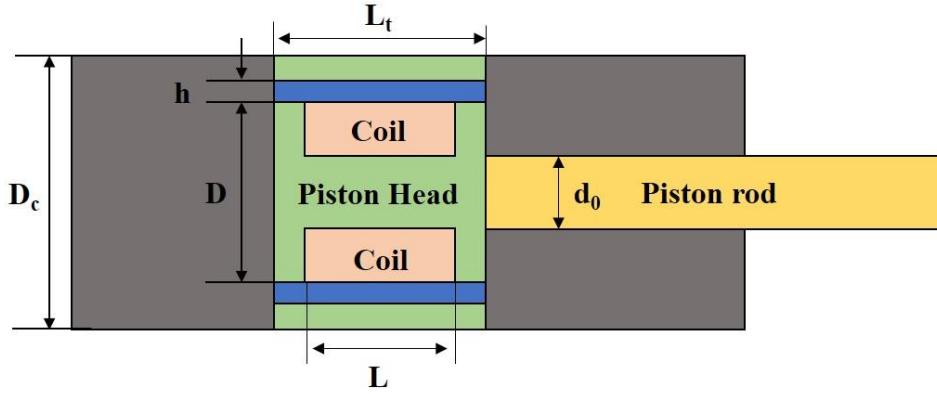


Figure 4.2 MR damper model

Table 4.2 Dimensions of MR damper

Sl. No	Parameter	Dimension (m)
1	Diameter of cylinder (D_c)	0.032
2	Diameter of piston head (D)	0.030
3	Fluid flow gap (h)	0.001, 0.0005, 0.00025
4	Length of piston head (L_t)	0.030
5	Length of effective area at fluid flow gap (L)	0.028
6	Piston rod diameter (d_0)	0.005

Damping force (F_f) developed in the flow mode type of MR damper is expressed as (Jolly et al. 1998, Xu et al. 2013):-

$$F_f = F_{f\mu} + F_{f\tau} = (\Delta P_{f\mu} + \Delta P_{f\tau}) A_{fp} \quad (4.1)$$

$$F_{f\mu} = \Delta P_{f\mu} A_{fp} = \frac{12\mu Q_f L}{h^3 w} A_{fp} \quad (4.2)$$

$$F_{f\tau} = \Delta P_{f\tau} A_p = \frac{c_f \tau_b L_t}{h} A_{fp} * Sgn(\dot{u}) \quad (4.3)$$

$$A_{fp} = A_p = \frac{\pi}{4} [D_2^2 - \{(D_c + h)^2 - D_c^2\} - d_0^2] \quad (4.4)$$

$$w = \pi(D_c + h); c_f = \left(2.07 + \frac{12Q_f\mu}{12Q_f\mu + 0.4w\tau_b h^2} \right) \quad (4.5)$$

$$F_f = \frac{12\mu Q_f L}{g^3 \pi (D_2 + h)} A_{fp} + \left(2.07 + \frac{12Q_f\mu}{12Q_f\mu + 0.4w\tau_b h^2} \right) \frac{c\tau_b L_t}{h} A_{fp} \quad (4.6)$$

where, F_f = Damping force (N), $F_{f\mu}$ = Viscous damping force (N), $F_{f\tau}$ = Damping force due to shear stress (N), Q_f = Volumetric flow rate, τ_y = Field dependent shear stress (Pa), μ = Viscosity (Pa-s), A_{fp} = Area of piston head (m²), h = Fluid flow gap, \dot{u} = Relative velocity (m/s), c_f = Flow rate dependent coefficient, w = circumference (m).

The rheological properties measure through the rheometer are represented as a function of exciting current through polynomial equation (tabulated in table 4.5). These equations are substituted into equation (4.6) to estimate the damping force under different current and fluid flow gaps.

4.5 OPTIMISATION THROUGH PARTICLE SWARM OPTIMISATION (PSO)

In order to obtain optimal proportion of iron particles and parameters that are highly influential for yielding better damping force, different optimisation techniques can be utilised. Among various techniques it was identified from the literature that, particle swarm optimisation techniques can provide better results compared to other techniques (Eberhart et al.1995 and Lee et al. 2007). PSO is a swarm intelligence method and it uses some intelligent agents called particles to attain the upper level of intelligence, which is absolutely impossible to reach by any of the individual particle in the swarm.

The candidate solution of PSO is called as the swarm and this swarms contains intelligent particles. Every particle is a candidate solution to the optimisation problem which needs to be solved. Each particle of the swarm has a position in the search space of optimisation problem. The search space has all the possible solutions and the best possible solution among these are needed to be identified. Each member in the

swarm interacts and learn from some simple rules to find the best solution from optimisation problem.

A particle 'i' has a position $\vec{x}_i(t)$ and moves at a velocity $\vec{v}_i(t)$ in the search space. In addition to velocity, each particle has a memory of its own best position denoted as personal best $\vec{p}_i(t)$ which is best experience of the particle. Also, among all the personal best experiences of each particle, some particle will have common best experience called as global best $\vec{g}_i(t)$. For one iteration of PSO, every position and velocity are updated. When the particle moves, it uses components of personal best, global best and velocity. A new position $\vec{x}_i(t + 1)$ and velocity $\vec{v}_i(t + 1)$ are created by previous velocity, $\vec{p}_i(t)$ and $\vec{g}_i(t)$. Obeying these rules will help to find the best solution of the optimisation problem.

Mathematical model of a particle in PSO to update the position and velocity of the particles are given equations (4.7) and (4.8) respectively.

$$\vec{x}_{ij}(t + 1) = \vec{x}_{ij}(t) + \vec{v}_{ij}(t + 1) \quad (4.7)$$

$$\vec{v}_{ij}(t + 1) = w \left(\vec{v}_{ij}(t) \right) + r_1 \times c_1 \left(\vec{p}_{ij}(t) - \vec{x}_{ij}(t) \right) + r_2 \times c_2 \left(\vec{g}_{ij}(t) - \vec{x}_{ij}(t) \right) \quad (4.8)$$

Velocity = *Inertia term* + *cognitive term* + *social term*

where, i= Particle, j= component, w = Inertia coefficient, c_1, c_2 = Acceleration coefficient and r_1, r_2 = Uniformly distributed decimal number in between 0 to 1.

Equation 4.8 has three components, which are inertia term, cognitive component and social component. These three terms are combined to obtain the new velocity vector and this new velocity vector translates the position of the particle to the new best position in the search space. The PSO parameters used in the MATLAB code are mentioned in table 4.3.

The steps involved in PSO in the present work is as follows,

1. Initialize population of n particle arbitrarily.
2. Evaluate the fitness values.
3. Identify the best fitness value and assign it as the new p-best.

4. Identify the best fitness value among all p-best and consider as the global best.
5. Evaluate the velocity and translate it to new best position using the mathematical model.
6. Monitor the velocity of each particle and restrict the velocity if it surpasses a specified range.
7. Terminate iteration if the minimum error /Maximum iteration reached or else repeat iteration.

Table 4.3 Parameters of PSO

Number of Parameters	3
Number of Particles	100
Number of Iteration	1000
Acceleration Coefficient	
C ₁	1.9
C ₂	2.5
Inertia Coefficient	
w	1

The objective of this optimisation is to maximise shear stress of MR fluid and damping force of MR damper. These C₁, C₂ and w parameters were obtained on trial and error basis till solution reached optimal value.

4.6 DESIGN OF EXPERIMENTS (DOE)

DOE is used in problems involving more than one input parameter affecting the response or output. Different combinations of parameters are identified, which are referred to as design. Different combinations of design points are selected and series of analysis are conducted with identified set of parameters within the ranges specified. The upper and lower bounds of variables are mentioned in Table 4.4. The design of experiments was conducted by considering the central composite design (CCD) scheme. CCD enables to build a second order polynomial for the response variable based on the previously used factorials by incorporating them at axial and centre point

locations. Hence, it is most useful in the sequential experiments and efficient for fitting second-order model. 27 points were generated and were evaluated through DOE (Table 4.7).

Table 4.4 Range of parameters

Parameter	Lower Bound	Upper Bound
Fluid flow gap (mm)	0.25	1
Volume fraction of Particle (%)	25	35
Current (A)	0.5	2

4.7 ANALYSIS OF VARIANCE (ANOVA)

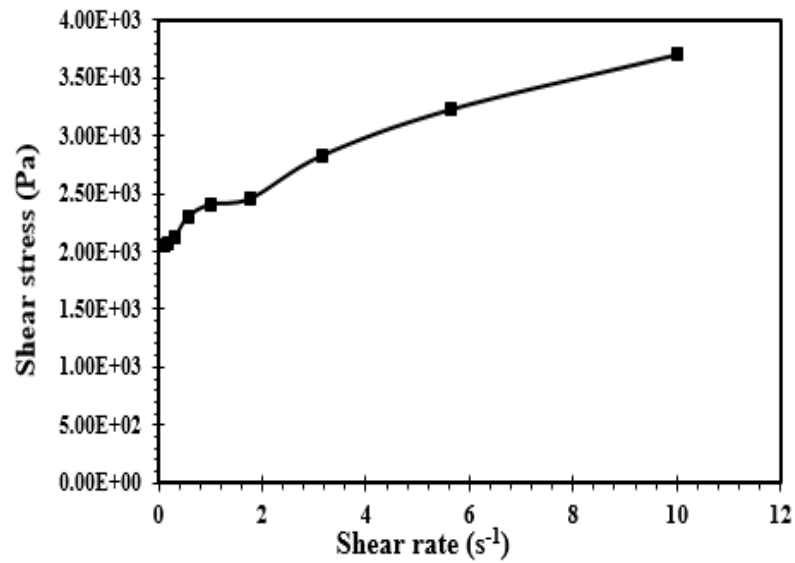
Analysis of variance is a statistical technique, which is employed to separate the total variation. The analysis of variance is used for estimating the interaction between the design parameters and identify the parameters, which have high influence on the responses. Also, the significant and insignificant parameters are identified through ANOVA. There two basic examinations in the ANOVA which are used for verifying the significance of the parameters. They are '*P-Test* (Probability)' and '*F test*'. The significant and insignificant parameters are determined based on the probability of significance known as the *P* value obtained from the ANOVA (Ghodsiyeh et al. 2014). If the *P* value is lesser than 0.05, then the null hypothesis is rejected for the entire population and parameters are significant. And if the *P* value is greater than 0.05, the null hypothesis is not rejected and parameters are insignificant.

4.8 RESULTS AND DISCUSSIONS

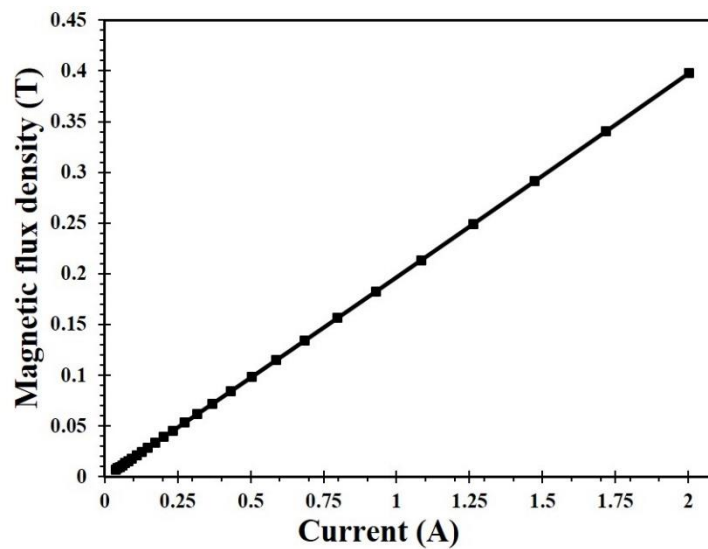
4.8.1 Influence of particle concentration

The steady state shear MR response exhibits thixotropic effect in the cone plate geometry type rheometer, while in parallel plate geometry this property cannot be seen at all or seen rarely (Claracq et al. 2004). Hence, rheometer with plate-plate configuration is used for measurement. Figure 4.3 (a) illustrates the shear stress versus

shear strain behaviour of MR fluid at 1.0 A current and 0.5 mm gap and figure 4.3 (b) depicts induced magnetic flux density versus the applied current.



(a)



(b)

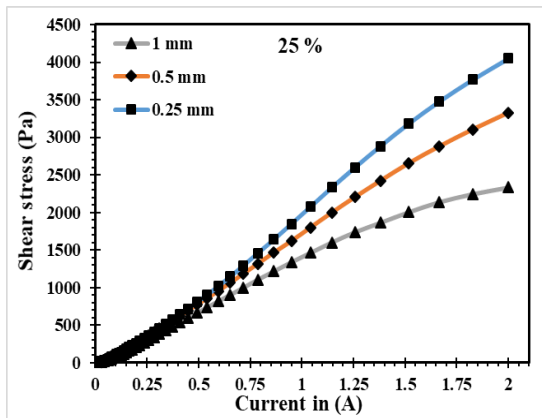
Figure 4.3 (a) Flow curve and (b) Magnetic flux density versus current

The field dependent shear stress is an essential fluid property for estimating the dynamic damping characteristics of MR devices like MR damper. The shear stress of the three MR fluid samples is examined at different gap between the parallel plates

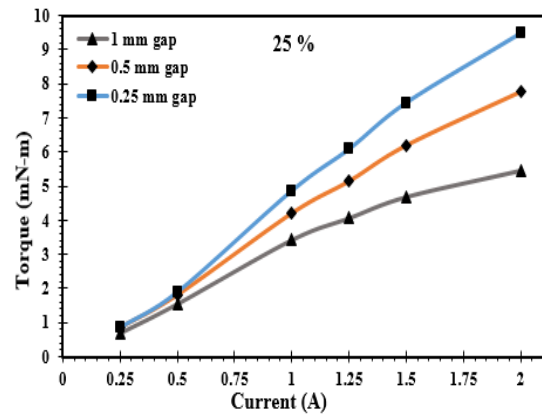
through magnetic sweep. Figures 4.4 (a), 4.4 (c) and 4.4 (e) represent shear stress versus current for the three MRF samples at constant shear rate of 1 s^{-1} and for different plate gaps. It can be clearly observed that the shear stress increases with increase in the applied current. Also, the particle concentration has a significant influence on the rheological properties. MRF ‘sample 3’ with higher concentration of suspension particles has higher shear stress compared to other two samples. The experimental results obtained are in-line with the observations reported by Yang et al. (2009) and Jonkkari et al. (2012).

4.8.2 Influence of parallel plate gap

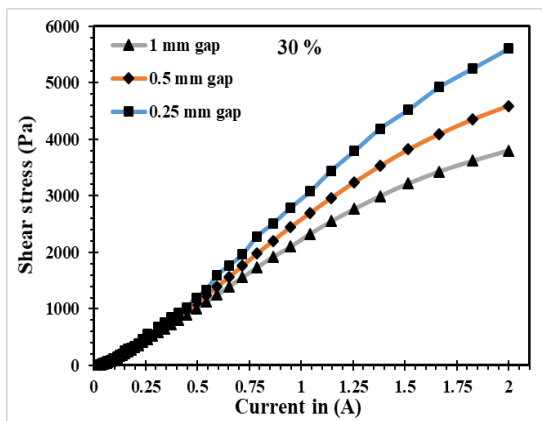
The gap between the parallel plates also has a significant effect on the rheological properties. The effects of the gap were reported by De Vicente et al. (2004) for lower magnetic field strength and lower gaps. The present experiments are conducted for higher values of current and larger gaps for each sample. As illustrated in figures 4.4 (a), 4.4 (b) and 4.4 (c), shear stresses are significantly influenced by the gap between parallel plates. Higher values of shear stress are obtained at smaller gap and vice versa. The maximum shear stress at 0.25 mm gap for 25 %, 30 %, and 35 % samples are 4200 Pa, 5600 Pa, and 8100 Pa respectively. The shear stress is evaluated from torque acting on the measuring tool of the rheometer. The torque felt on the measuring tool increases with the increase of current and it decreases with increase in gap distance. This is due to the higher resistance offered by the magnetically excited fluid to the moving plate. Thus, shear stress is higher at 0.25 mm gap than at 1.0 mm gap. The upper yoke of the MRD cell is used for reducing and maintaining the temperature of the measuring regime and no magnetic flux lines transfer through the yoke. As the gap increases, the magnetic flux at the upper portion is lesser than that at the bottom plate. Due to variation in the magnetic flux, the shear stress is lesser at higher gaps. If the magnetic flux can be applied uniformly throughout the parallel plate gap, the rheological properties would be higher at the higher gap (Jiang and Lu 2002, Chen et al. 2013 and Laun et al. 2011).



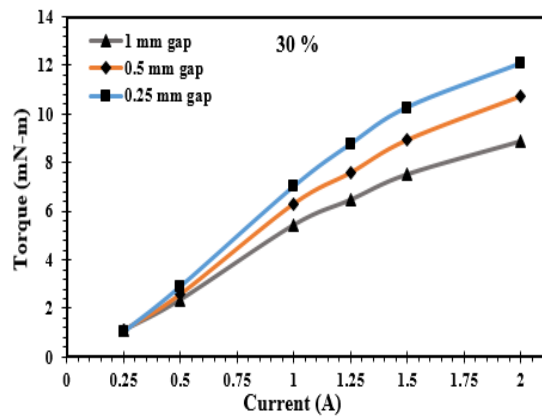
(a)



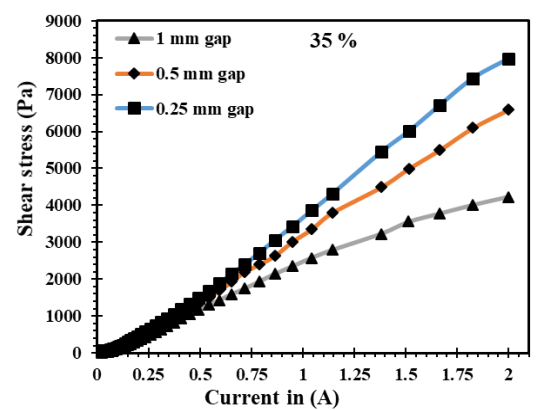
(b)



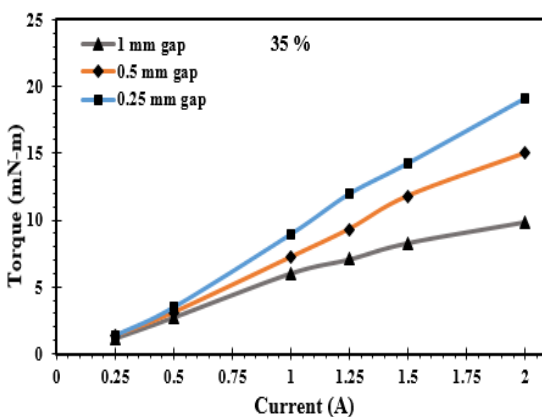
(c)



(d)



(e)



(f)

Figure 4.4 Rheological properties of MR fluid in current sweep for three MR fluid samples. (a), (c), (e) Variation of shear stress and (b), (d), (f) Variation of torque

The magnetic flux density and field intensity induced in the MR fluid in an orifice can be mathematically represented as (Nguyen and Choi, 2009, Parlak et al. 2012),

$$H_{mr} = \frac{N_c I}{2t_d} \quad B = \frac{\mu_0 N_c I}{2t_d / \mu_{rm}} \quad (4.9)$$

where N_c is number of turns of the electromagnetic coil, I is the applied current, t_d is the gap between the plate, μ_0 is the free space permeability and μ_{rm} is the permeability of MR fluid.

From above equations (4.9), it can be observed that magnetic flux density and field intensity are directly proportional to the number of coils and applied current, while they are inversely proportional to the orifice gap. Hence, as the fluid flow gap or orifice gap increases, the magnetic flux density in the gap decreases. Thus, the results obtained from the experimentation of three samples are justified.

4.8.2.1 Polynomial equation

Table 4.5 Polynomial model functions for different MR fluid samples

MRF Sample	Fluid gap	Shear stress as a function of Current
25%	0.25 mm	$\tau_Y = -16.508I^4 - 326.86I^3 + 1129.4I^2 + 1208.8I - 24.453$
	0.5 mm	$\tau_Y = 30.635I^4 - 337.93I^3 + 714.06I^2 + 1359.9I - 41.581$
	1.0 mm	$\tau_Y = 125.15I^4 - 686.19I^3 + 919.59I^2 + 1089I - 32.642$
30%	0.25 mm	$\tau_Y = 283.43I^4 - 1728.4I^3 + 3013.2I^2 + 1433.6I - 33.918$
	0.5 mm	$\tau_Y = 36830.635I^4 - 337.93I^3 + 714.06I^2 + 1359.9I - 41.581$
	1.0 mm	$\tau_Y = 192.58I^4 - 1101.8I^3 + 1600.6I^2 + 1585.1I - 43.899$
35%	0.25 mm	$\tau_Y = 1.9869I^4 - 601.92I^3 + 2088.7I^2 + 2241.5I - 59.374$
	0.5 mm	$\tau_Y = 293.71I^4 - 1605.7I^3 + 2824.9I^2 + 1734.9I - 35.789$
	1.0 mm	$\tau_Y = 342.22I^4 - 1642.3I^3 + 2131.9I^2 + 1715.6I - 59.484$

The polynomial equations shown in table 4.5 are obtained from the experimental results. These models provide a relationship between the shear stress and applied

current. The shear stress versus DC current plots as shown in figure 4.4 are fitted with polynomial equations using the least square method. These models will serve the purpose of evaluating the shear stress and damping force at any arbitrary value of current in the range of 0 - 2A. The 4th order polynomial equation best fits the experimental values during the curve fitting process and the results were more accurate compared to the 3rd order polynomial equations.

Normal stress was calculated from the normal force acting on the measuring tool plate of rheometer. The relation between the normal stress and force is expressed as (Laun et al. 2008)

$$\sigma_n = \frac{2F}{\pi \left(\frac{d}{2}\right)^2} \quad (4.10)$$

where ‘F’ is the normal force and ‘d’ is diameter of parallel plate.

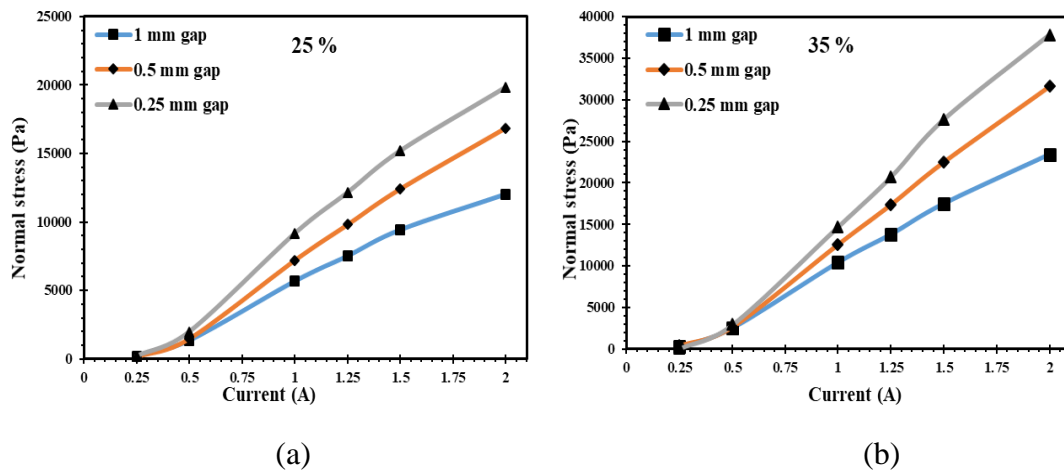


Figure 4.5 Normal stress variation against current for (a) 25 % MRF sample, (b) 35 % MRF sample

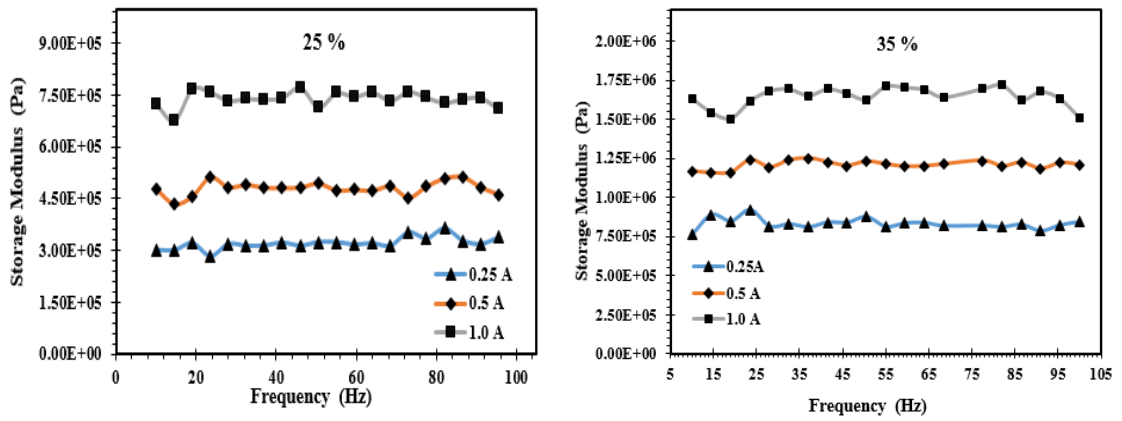
Figure 4.5 shows the variation of normal stress with respect to the changes in applied current, particle concentration and plate gap. An increment in current provides higher value of magnetic flux, which leads to enhance of bonding strength of the iron particles, making the fluid more viscous. Thus, the normal force acting on the parallel plate increases with increase of current, further leading to enhancement of normal stress. Also, from figure 4.5, it can be observed that the normal force tends to decrease with increase of gap for all currents. At 2.0 A current, the normal stress

obtained for 0.25 mm gap is 1.6 times more than that at 1.0 mm gap for both 25 % and 35 % MRF samples. On the other hand, due to increase of particle concentration, the normal stress of 35 % MRF sample is nearly twice that of 25 % sample.

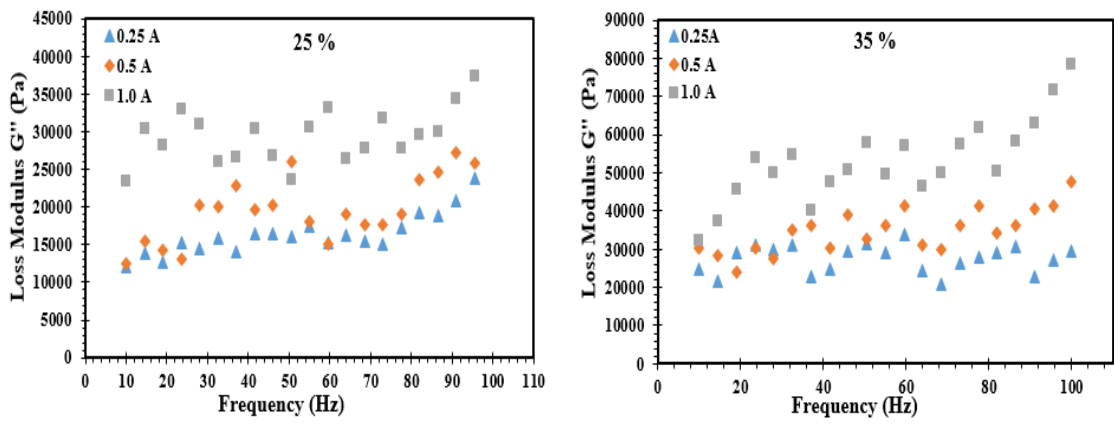
4.8.3 Dynamic characteristics

The viscoelastic behavior of MR fluids can be seen within the pre-yield region of the flow curve. The viscoelastic properties such as storage modulus (G'), loss modulus (G'') and complex viscosity are evaluated by oscillatory frequency sweep from 10 Hz to 100 Hz for different applied current and fixed strain amplitude of $0.001s^{-1}$. The energy storage capability of MR sample is explained based on the storage modulus, where it represents the elastic nature of the fluid. On the other hand, loss modulus signifies the energy dissipation of the MR sample, where the viscous nature of fluid can be examined (de Vicente et al. 2004, Rajamohan 2009). Response of storage modulus, loss modulus and complex viscosity properties of MR samples to the frequency sweep at 0.25 A, 0.5 A and 1.0 A are illustrated in figures 4.6 (a-c). It can be observed from the results that these properties are well responsive to the concentration of particle in the MR samples as well as the applied current. There is a significant shift of values of these properties at minimum and maximum value of current as depicted in figures 4.6 (a-c).

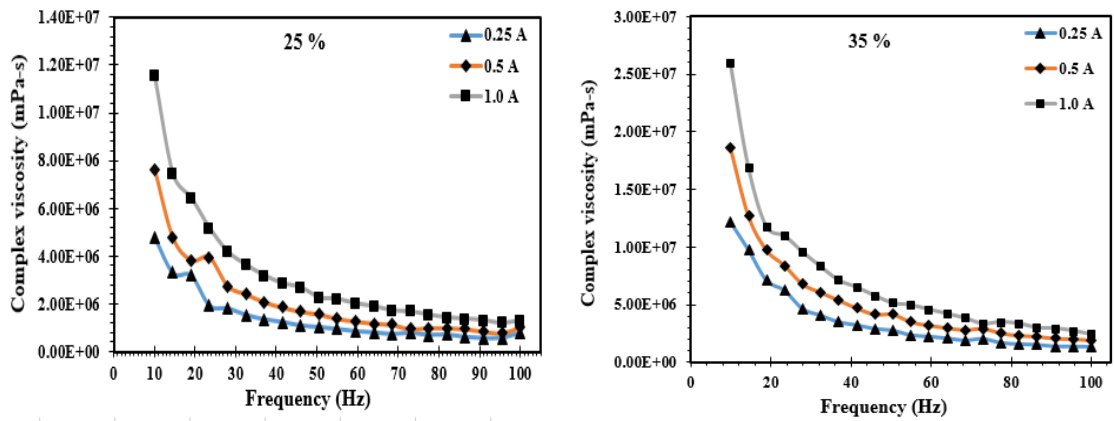
However, variation due to the increment in the frequency are not extensive compared with responses to current and concentration of particles. At 10 Hz frequency, the shift of storage modulus (G') of sample 1 at 1.0 A current is 2.13 times more than that at 0.25 A. Based on concentration of particles, the storage modulus of sample 3 is 2.5 times greater than that of sample 1 at 0.25 A current and 10 Hz frequency. Also, loss modulus (G'') is very much responsive to the current and concentration of particles, which is clearly depicted in figures 4.6 (b). Here the loss modulus is well behaved in response to the frequency as compared to that of storage modulus and a notable increment in loss modulus can be seen with respect to frequency change. The loss modulus in all the cases is lesser than the storage modulus. Hence, the samples under external stimulus field exhibits more semisolid behavior than liquid.



(a)



(b)



(c)

Figure 4.6 Frequency dependency of (a) Storage modulus, (b) Loss modulus and (c) Complex viscosity

Figures 4.6 (c) shows the variation in complex viscosity with respect to frequency and the concentration of iron particles. At lower frequency, the complex viscosity is having higher values and it tends to decay as the frequency increases. Complex viscosity has substantial increment with increase in applied current.

4.8.4 Statistical analysis

The statistical analysis of design points and their respective responses are analyzed through regression analysis with the help of design expert software. The relationship between the design parameters (independent) and responses (dependent variable) are established through regression function. Here, the dependent parameters are damping force and shear stress, while the independent parameters are fluid gap, particle concentration and current. The final established mathematical regression functions are tabulated in table 4.6 and same are used as the objective functions in optimization algorithms. The objective of the optimization is to maximize the damping force and shear stress of the MR fluid and consequently the optimal proportion of the particles in the fluid.

Table 4.6 Regression model/Objective functions

Sl.No	Response	Regression equation
1	Force	$3482.42 - 25266.15 \times (h) + 422.75 \times (P) - 1444.26 \times (C) + 98.95 \times (h) \times (P) - 738.09 \times (h) \times (C) + 26.13 \times (P) \times (C) + 14828.65 \times (h)^2 - 8.83 \times (P)^2 + 612 \times (C)^2$
2	Shear stress	$44468.49 + 2561.72 \times (h) - 3026.73 \times (P) + 108.92 \times (C) - 116.71 \times (h) \times (P) - 1634.89 \times (h) \times (C) + 81.46 \times (P) \times (C) + 934.58 \times (h)^2 + 51.41 \times (P)^2 + 217.35 \times (C)^2$

Table 4.7 Design of Experiments

Run	Gap-h (mm)	Percentage of Particle-P (%)	Current- C (A)	Shear stress (Pa)	Damping force (N)
1	0.5	25	0.25	1111.763875	333.05
2	0.25	30	2	4031.739	4478.831
3	1	25	0.25	1023.11225	51.3081
4	1	30	1	1417.178	118.4935
5	0.25	30	0.25	820.40775	3505.34
6	0.5	35	0.25	1355.530375	385.98
7	0.5	25	2	4594.792	599.8813
8	0.5	30	0.25	776.5626875	375.467
9	1	35	1	2487.936	122.4525
10	1	35	2	4236.436	191.377
11	1	30	0.25	663.899875	64.667
12	0.25	35	2	7994.8564	4978.62
13	0.25	35	0.25	1508.435181	3572.48
14	0.25	35	1	3670.8929	122.4525
15	0.25	25	0.25	1237.850188	3415.641
16	1	25	1	2232.581	86.002
17	0.5	35	1	3212.021	570.063
18	0.25	25	2	5593.718	4127.565
19	0.25	30	1	1970.379	3906.465
20	1	35	0.25	1147.39225	73.32
21	0.5	30	1	1725.095	529.94
22	0.5	30	2	3321.203	717.064
23	1	30	2	2378.758	176.354
24	0.5	25	1	2589.342	438.0816
25	0.25	25	1	2967.913	3684.127
26	0.5	35	2	6587.371	896.74
27	1	25	2	3795.581	118.4935

Table 4.8 Analysis of Variance for shear stress

Source	Sum of Squares	df	Mean Square	F Value	p-value	Remark
Model	2.27	9	0.25	1968.9	< 0.0001	Significant
A-Gap	0.12	1	0.12	943.19	< 0.0001	Significant
B-Particle concentration	0.035	1	0.035	273.21	< 0.0001	Significant
C-DC Current	1.24	1	1.24	9734.71	< 0.0001	Significant
AB- Gap Particle conc.	0.0036	1	0.00356	27.87	< 0.0001	Significant
AC- Gap Current	0.013	1	0.013	98.26	< 0.0001	Significant
BC- Current Particle conc.	0.0017	1	0.0017	13.29	0.002	

Table 4.9 Analysis of Variance for damping force

Source	Sum of Squares	df	Mean Square	F Value	p-value	Remark
Model	11.83	9	1.31	1199.4	< 0.0001	Significant
A-Gap	10.41	1	10.41	9498.82	< 0.0001	Significant
B-Particle concentration	0.066	1	0.066	60.54	< 0.0001	Significant
C-DC Current	0.28	1	0.28	256.17	< 0.0001	Significant
AB- Gap Particle conc.	0.011	1	0.011	10.29	0.0052	
AC- Gap Current	0.056	1	0.056	51.42	< 0.0001	Significant
BC- Current Particle conc.	0.00439	1	0.00139	4	0.0616	

The results in tables 4.8 and 4.9 show that the “P value” are less than 0.05, indicating that the model parameters are significant. It can be observed that, there are three main parameters (gap, current and particle concentration) which are significant. The interaction of between Gap-Particle and Gap-DC current is significant, while the interaction between particle concentration-DC current is not significant. ANOVA for damping force indicated that the interaction between Gap-DC current alone is significant.

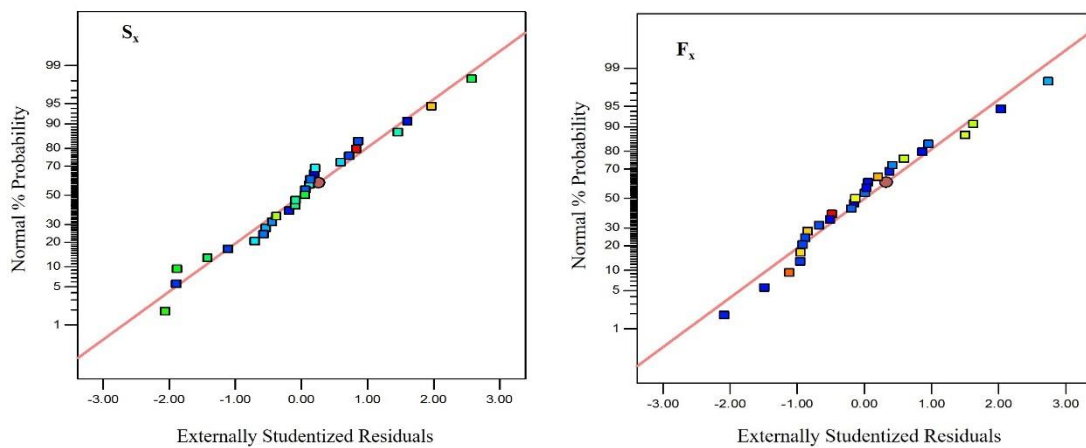


Figure 4.7 Normality plot of residuals

Figure 4.7 illustrates the standard residuals plotted against percentage probability distribution of shear stress and damping force of MR dampers. A normality test was carried out to verify, if the data points are obtained from normally distributed population. From figure 4.7, it can be observed that the residuals data points closely follow the reference normal distribution line. Hence obtained data points are from normally distributed population.

Figure 4.8 illustrates run chart of shear stress and damping force of MR damper. The run chart is a plot, which presents the variation of residuals for each run. This chart displays the number of standard deviation values which falls off from the control limit in a given iteration. The 95% confidence control limits on a run chart are represented by redlines (upper and lower red lines). The point which falls outside the red line is referred to as outliers. Also, it can be observed that there are no outliers in the chart as all points are falling within the limit, which suggests that the responses are stable.

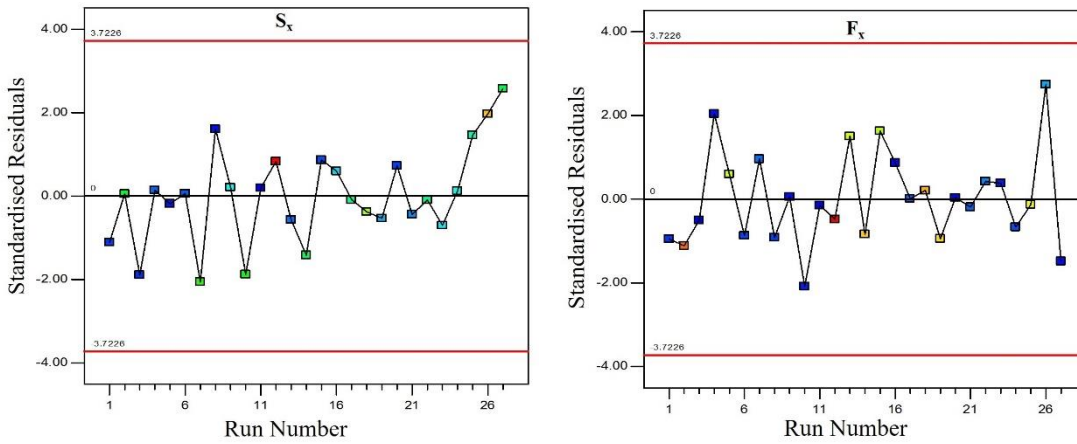


Figure 4.8 Run chart of shear stress and damping force

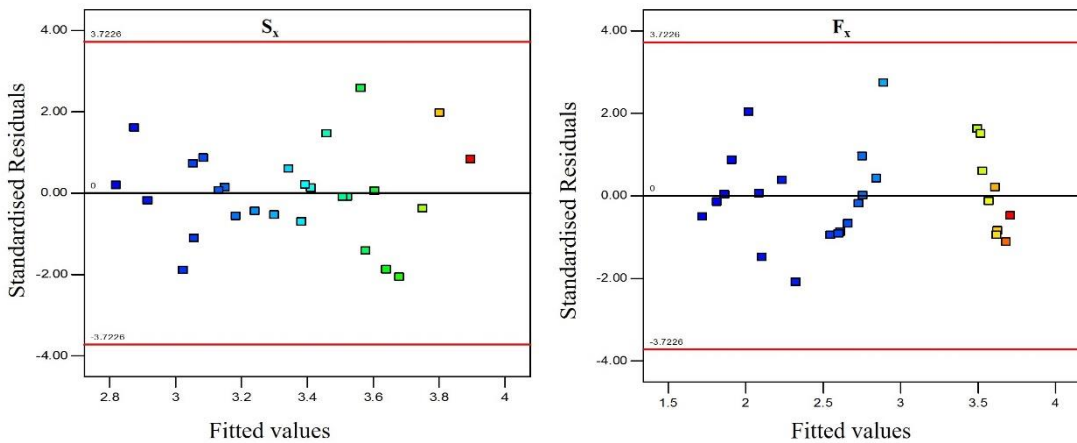


Figure 4.9 Residuals versus fitted value

Figure 4.9 indicates the values of the residuals at the vertical axis plotted against the fitted values of responses (shear stress and damping force). The distribution of residuals at different levels within the analysis does not show any extreme variation from the one end to another. Careful observation of these distribution reveals that the variance of the residuals is similar and consistent at different levels. This allows us to find the equality of variance. Since a similar scatter or distribution can be seen, it is referred to as homoscedasticity.

4.8.5 Response surface method

The response surface method is employed in the optimisation process to carry out the design of experiments. The main purpose of response surface is to point out the significant variable parameters, which are influential on the response output parameter. The variation of response (shear stress and damping force) with the variable parameters such as fluid gap, particle concentration and DC current were plotted in 3D space (figures 4.10 and 4.11). It can be observed that the damping force reduces with increment in fluid gap till 0.75 mm. On further increment the force tends to saturate. However, the damping force tends to increase as the DC current and particle concentration values are increased. Figures 4.12 and figure 4.13 shows the variation of shear stress with the variable parameters. From this 3D surface plot, it can be observed that the shear stress value increases with decrement in the fluid gap and increment in the DC current and particle concentration.

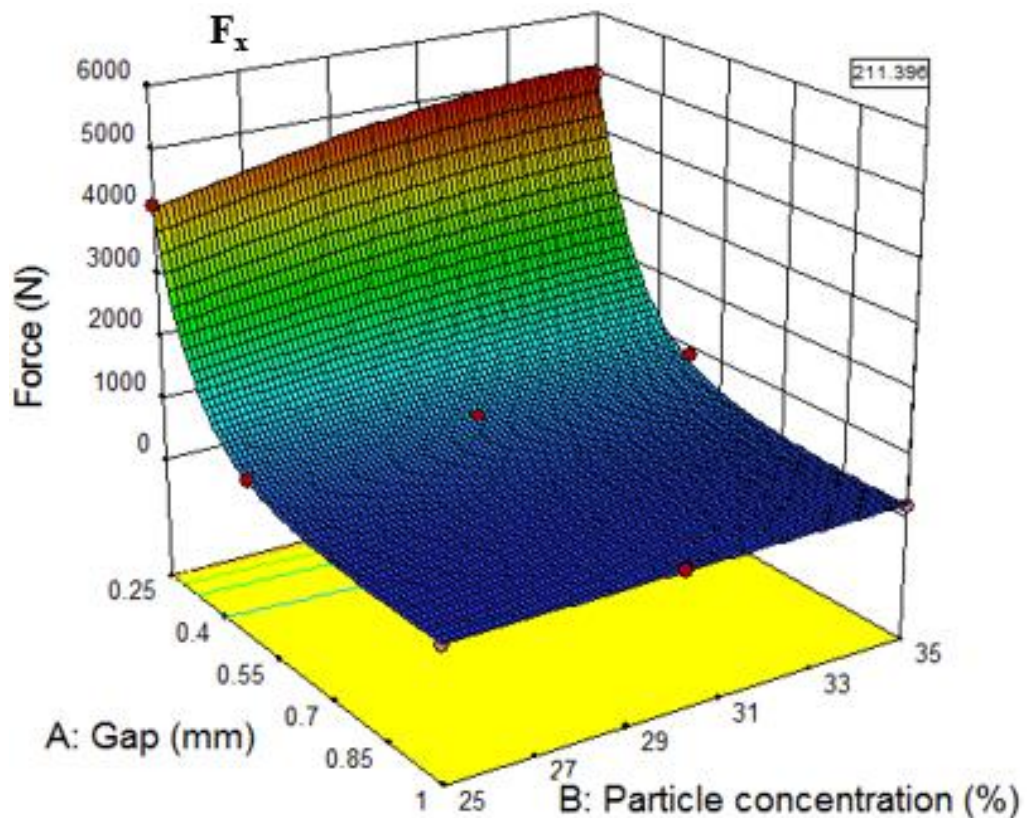


Figure 4.10 3D response surface of damping force versus Gap and particle concentration

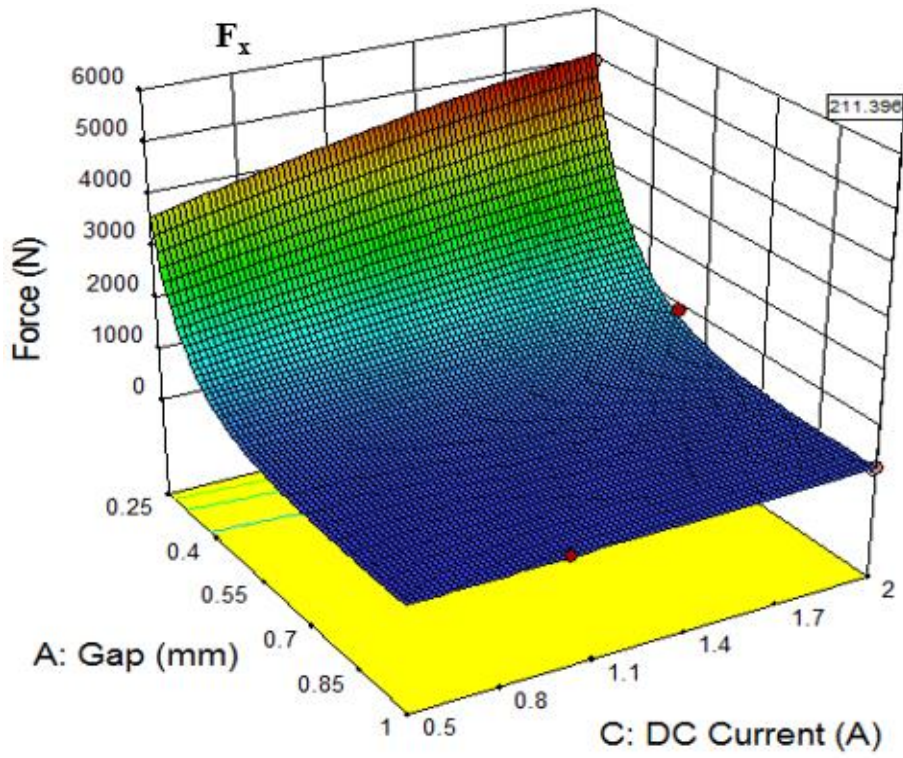


Figure 4.11 3D response surface of damping force versus Gap and DC current

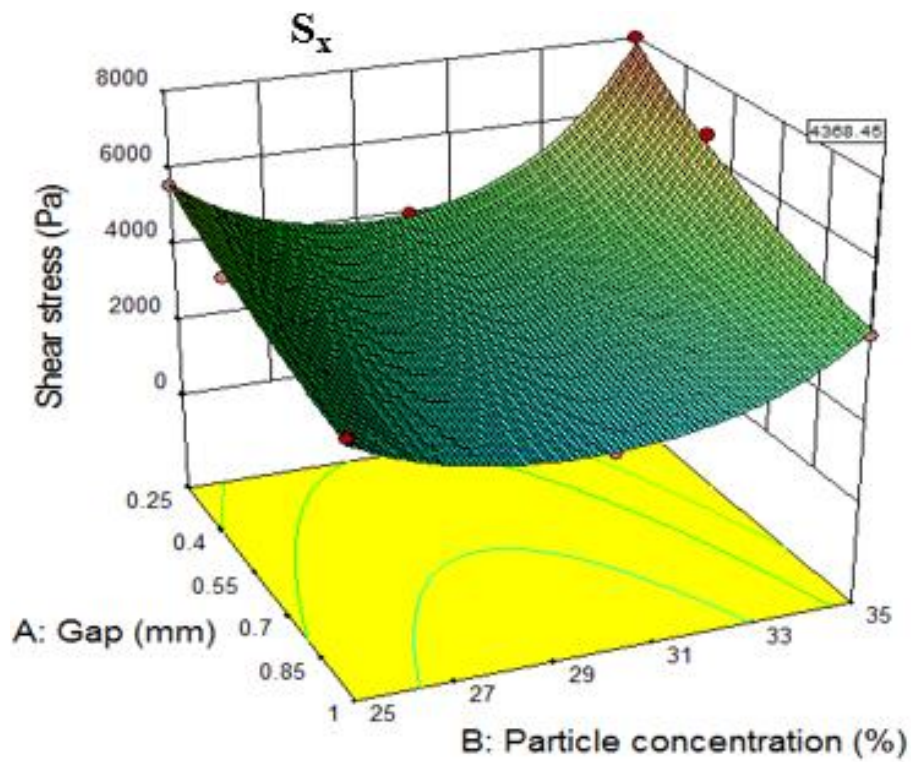


Figure 4.12 3D response surface of Shear stress versus Gap and particle concentration

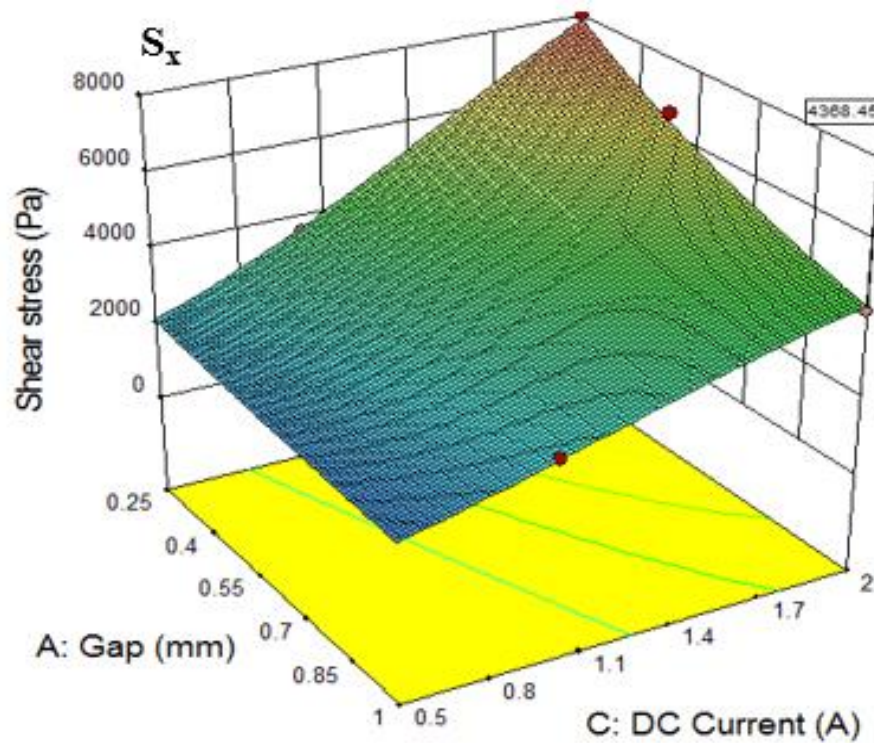


Figure 4.13 3D response surface of Shear stress versus Gap and DC current

Tables 4.10 and Table 4.11 summarize the optimal variable parameters obtained through single objective and multi objective particle swarm optimisation respectively, considering regression equations of table 4.6 as objective functions. The results obtained are within the specified upper and lower bounds. It can be observed that maximum shear stress is obtained with higher level of particle concentration, which is due to increase in number of particle chain formation occurring as a result of external magnetic field. The maximised value of objective function S_x is attained for 34 % of particle concentration in the present study. For the objective function F_x , the maximised value is attained for 31 % of particle concentration. Both objective functions are combined and solved using multi objective PSO. It can be seen that, 33 % particle concentration of particle is optimal value, having influence on both objective functions. Observing both results, it can be concluded that 31 % to 33% of volume fraction of iron particles in MR fluid would be best suited for damper application.

Table 4.10. Summary of optimal variable parameters from single objective PSO

	Gap (mm)	Particle Concentration (%)	Current (A)	Response
Shear Stress (S_x)	0.27	34.6	1.94	6600.1 Pa
Force (F_x)	0.26	30.7	1.96	4061.7 N

Table 4.11. Summary of optimal parameters obtained from multi objective PSO

	Gap (mm)	Particle Concentration (%)	Current (A)	Force (F_x)	Shear stress (S_x)
MPSO	0.26	33	1.8	3718.49 N	5919.04 Pa

4.9 SUMMARY

The characterisation of MR fluid samples which are prepared based on the different volume fractions of carbonyl iron powder is discussed. The rheological properties of MR fluid samples under different magnetic fields and fluid gap are evaluated using rotational type rheometer attached with magnetorheological device cell. Based on the results obtained from the experiments, these fluid properties are used for computing the damping force of MR damper. An optimisation technique was adopted to find out optimal proportion of particle concentration for MR damper application. Different set of experiment runs were formulated using design of experiments and response to each experiment set was evaluated. Analysis of variance was used for verifying the significance of each parameters through statistical analysis and the objective function was obtained as a function of input variable. Later, using single and multi-objective particle optimisation techniques the optimal proportion of iron particles was identified. It was observed that 33 % particle concentration is optimal value having influence on both objective functions.

CHAPTER 5

FABRICATION AND CHARACTERISATION OF MONOTUBE MR DAMPER

5.1 INTRODUCTION

This chapter discusses the MR damper configuration and evaluation of dynamic characteristics of a monotube MR damper through experiments. The damper performance is determined by its energy dissipation capability under random input conditions. The energy dissipation is indicated by the amount of force induced in the damper. Based on the operation modes, MR dampers are categorized into four fundamental types. They are flow mode, shear mode, squeeze mode and pinch mode dampers and each mode serves different purpose and application. Also, the damper performance is depending upon various parameters such as electromagnetic coil parameters, fluid flow gap, dimensions of the piston head, operating frequency, DC current and constituents of MR fluid. Taking all these parameters into consideration, a shear mode type monotube MR damper was developed and its dynamic characteristics are presented in detail.

5.2 SHEAR MODE TYPE MONOTUBE MR DAMPER

5.2.1 MR damper characteristics

5.2.1.1 Controllable damping force

The damper performance is estimated based on two important parameters i.e., controllable force and dynamic range. The total damper resistance force is summation of controllable force and uncontrollable force. Controllable force is due to field dependent shear stress and uncontrollable force which is due to viscosity and friction. The dynamic range is expressed as ratio of damping resistance force and uncontrollable force, which is as follows (Parlak et al. 2012),

$$D = \frac{F}{F_u} = 1 + \frac{F_\tau}{F_\mu + F_f} \quad (5.1)$$

Controllable and uncontrollable force are defined as follows,

$$F_\mu = \left(1 + \frac{whu}{2Q}\right) \frac{12\mu QLA_t}{wh^3} \quad (5.2)$$

$$F_\tau = \left(2.07 + \frac{12Q\mu}{12Q\mu + 0.4wh^2\tau_b}\right) \frac{\tau_b LA_t}{h} \text{sgn}(u) \quad (5.3)$$

where, F_τ is controllable force due to shear stress, F_μ is uncontrollable force due to viscosity, F_f is frictional force, w is circumference of annular gap, h is annular gap, Q is volumetric flow rate, L is annular gap length, μ is viscosity of fluid, A_t is piston head area, τ_b is field dependent yield stress, u is velocity.

5.2.1.2 Effective stiffness

The MR damper stiffness is represented by the slope of the force versus displacement curve. The stiffness of the damper is also associated with amount of magnetic flux density induced in the coil. The dynamic field dependent stiffness transfer function (K_{dyn}) can be evaluated by using equation (5.4).

$$K_{dyn} = \frac{F_{Max} - F_{min}}{X_{max} - X_{min}} \quad (5.4)$$

where,

F_{Max} and F_{min} are the maximum and minimum damping force,

X_{max} and X_{min} are the maximum and minimum excitation displacement

5.2.1.3 Energy dissipation

The energy dissipated (E_d) in the MR damper is equivalent to the area under the force versus displacement curve for a particular cycle.

$$E_d = \int F(t) du \quad (5.5)$$

The damper performance is indicated with values of the dynamic range of the MR damper, which is expressed as the ratio of on-state damping coefficient to the off-state damping coefficient (Snyder et al. 2001).

5.2.1.4 Equivalent damping coefficient

The equivalent damping can be calculated by equating the energy dissipated over a cycle at a certain frequency and equating it to the dissipated energy in the damper under the excitation of magnetic field (nonlinear device). Off state damping force is given by

$$F(t) = C_e v(t) \quad (5.6)$$

where, $v(t)$ is the velocity of the piston.

The equivalent damping coefficient (C_e) is calculated by using following equation

$$C_e = \frac{E_d}{\pi f A^2} \quad (5.7)$$

where A is amplitude and f is frequency

5.2.2 Components of MR damper

Monotube MR damper is a common choice for MR applications mainly due to its simplicity and the fact that it comprises of few components. The main components of MR damper are electromagnetic coil incorporated in the piston head, cylinder, piston rod, rod guide, oil seals and connectors. The piston head inside the cylinder divides its volume into two sections. The shear flow gap between the piston head and cylinder allows the fluid to flow from one chamber to other chamber during the motion.

5.2.3 Material Selection

The material selection for MR damper components is important in developing MR damper. In particular, the material adopted for electromagnetic coil is critical one since the damping force is highly influenced by the magnetic flux density induced in the annular gap. In order to obtain effective magnetic field, an appropriate material has to be identified. The magnetic flux density depends on the electromagnetic coil

parameters such as number of turns of the coil, gauge of the wire and material of the core. As the number of turns increases, the magnetic flux induced will also increase. In case of different materials with similar geometric dimensions of the electromagnetic coil, the magnetic field strength varies with material used for the core. Ferromagnetic material is the most suitable material for the core, as it can be magnetised effectively and these materials include low carbon steel, magnetic iron and various nickel based alloys. The material with high magnetic permeability allows the magnetic flux lines to pass through central core and flux lines can be easily created. Thus, materials with good magnetic permeability offer better magnetic field. Table 5.1 shows some of the ferromagnetic materials and their permeability.

Table 5.1. Magnetic permeability of different materials (Choi et al. 2012)

Material	Permeability, μ (H/m)
Iron (99.8% pure)	6.3×10^{-3}
Carbon Steel	1.26×10^{-4}
Iron (99.95% pure <i>Fe</i> annealed in <i>H</i>)	2.5×10^{-1}
Aluminium	1.256665×10^{-6}
SAE 1018	B-H Curve

5.2.4 Geometric details of monotube MR damper

Figure 5.1 shows the components of the fabricated monotube MR damper. The important part of the damper is the electromagnetic coil incorporated in the piston head. The dimensions of the MR damper are tabulated in the table 5.2. The electromagnetic coil consists of 900 turns of 24 AWG copper wire. The piston head is made of SAE1018 low carbon steel and piston rod, cylinder, guide bush is made up of nonmagnetic steel, so that the flux leakage out of the damper is nullified. The lead wires of the coil are passed through the hole drilled in the piston rod for connecting it to the DC power supply. The guide bush causes the piston head to reciprocate in the cylinder. The bush guide consists of oil seal to avoid the leakage of the fluid during experimentation. The prepared MR fluid samples were stirred to ensure uniform distribution of iron particles in the carrier fluid and then required amount was filled

into the cylinder. The dimensions are considered based on the reverse engineering, where several research papers related to the design of MR damper electromagnetic coil were considered and based on the study these dimensions are obtained.

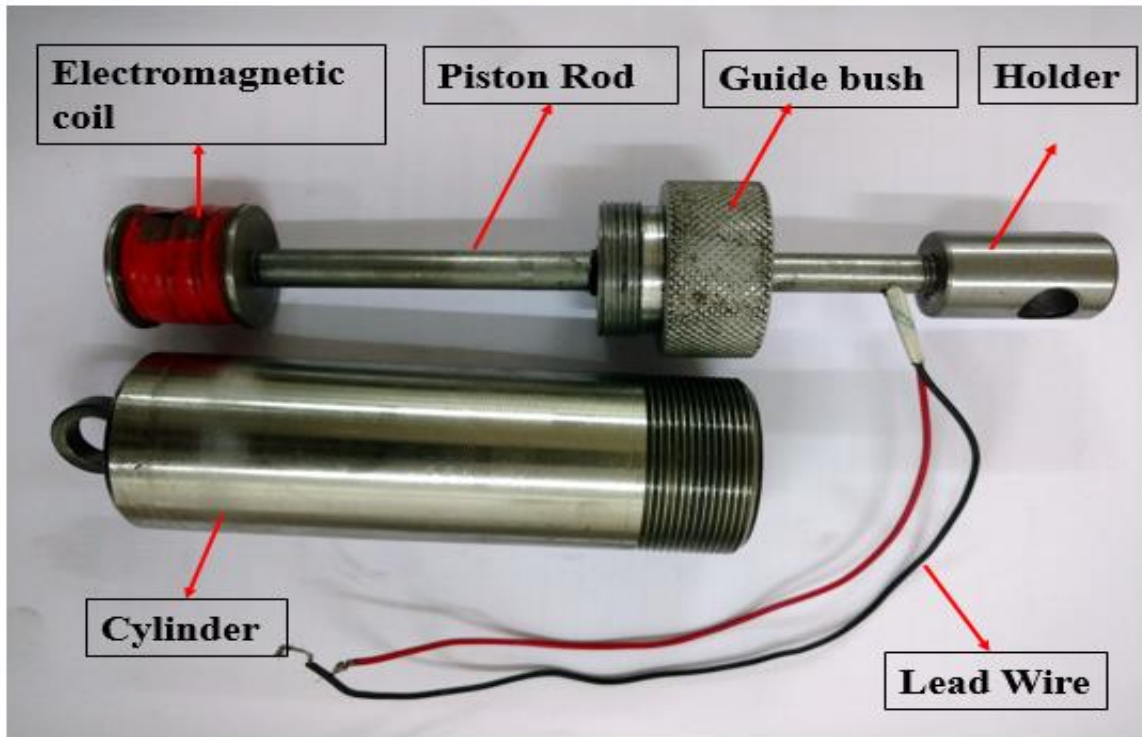


Figure 5.1 Monotube MR Damper

Table 5.2 Dimensions of the MR damper

Sl. No	Parameter	Dimensions in mm
1	Cylinder outer radius	17
2	Core depth	7
3	Piston radius	15
4	Piston length	30
5	Coil housing length	26
6	Flange thickness	2
7	Annular gap	1

5.3 EXPERIMENTAL SETUP

Dynamic behaviour of MR damper was determined experimentally using damper test facility as figure 5.2. This experimental set up is custom built facility for low force range experimental purpose and has been developed in the laboratory. The damper testing facility consists of variable speed motor with cam system, load cell, linear variable differential transformer (LVDT) and data acquisition system.

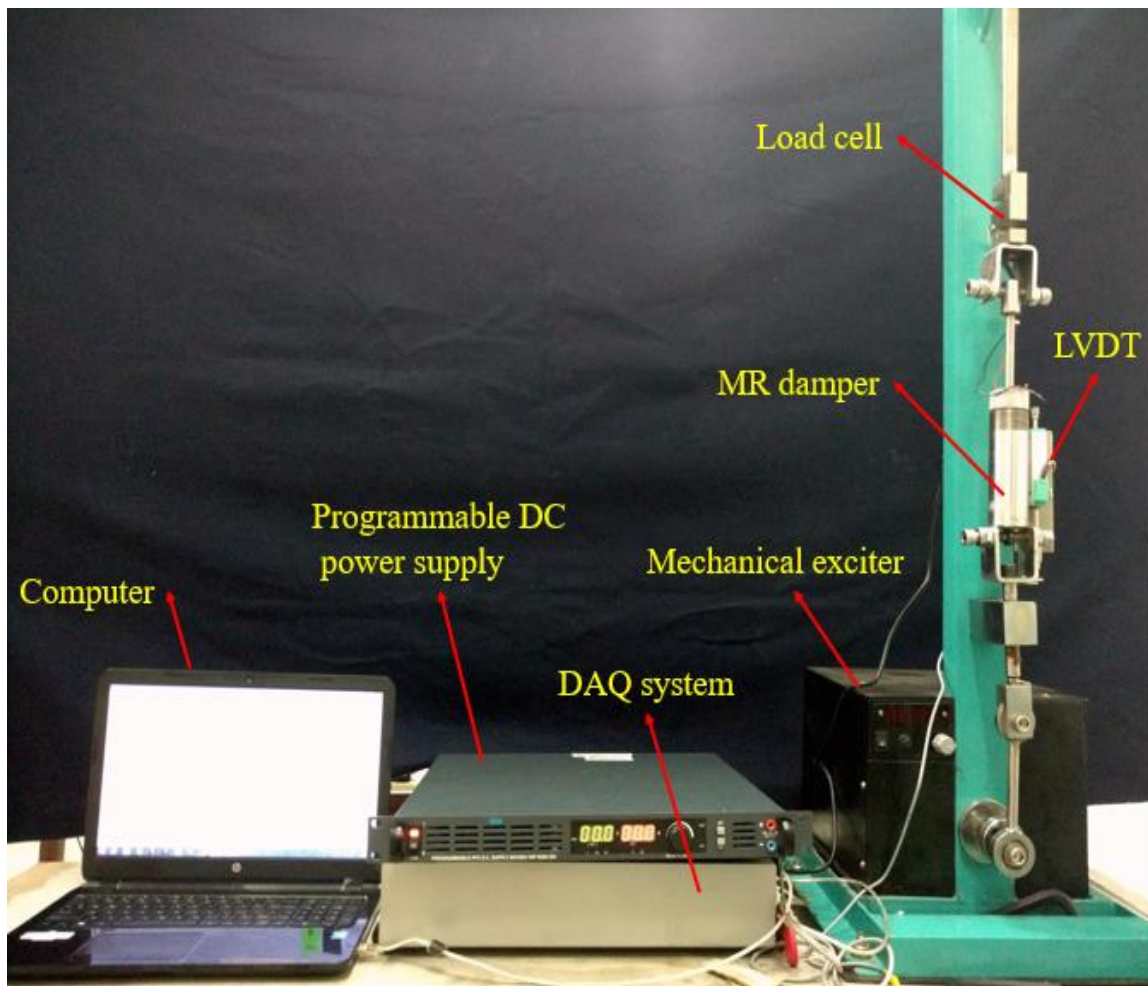


Figure 5.2 Damper testing facility

The variable speed motor with cam system is used to give specified displacement of MR damper at required frequency. The mechanical exciter has a maximum force capacity of 500 N with frequency in the range of 0.1 to 10 Hz. Peak to peak stroke/amplitude is 15 mm. The MR damper tests were carried out at 1.0 Hz, 1.5 Hz

and 2 Hz frequencies under different DC current input. The DC current supply was varied in range of 0.1A to 0.4A with sinusoidal excitation of ± 10 mm stroke length, which was measured by using LVDT. The DC current to the MR damper was controlled by using programmable DC power supply. The load cell located at the top end of MR damper piston rod was used to acquire force induced in the MR damper due to the excitation.

5.4 RESULTS AND DISCUSSIONS

The dynamic characteristics of MR damper are represented by force versus displacement curves. The damping force obtained at a constant displacement of 10 mm for different currents and frequencies are plotted in the figures 5.3 to figure 5.5. It can be observed from the plots that the damping force increases with increase in the magnitude of DC current. Also, there is a considerable variation in damping force with respect to frequency. At a constant frequency of 2 Hz, the maximum damping force for 0.1 A and 0.4 A currents are 92.6 N and 161.2 N respectively, which indicates that damping force at 0.4 A is 1.75 times that at 0.1 A. At constant current of 0.4 A, the damping force at 2 Hz is 1.5 times than that at 1 Hz frequency.

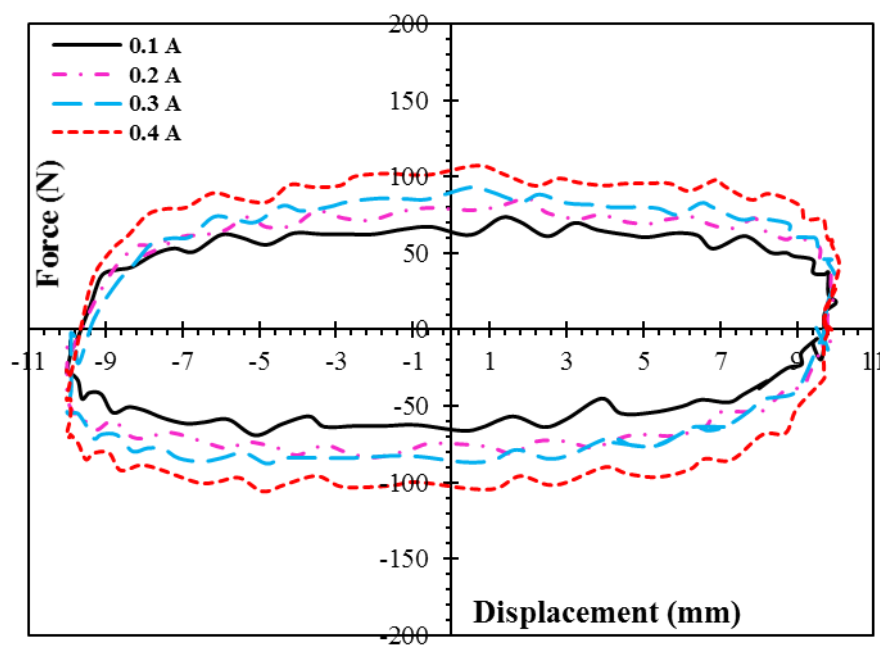


Figure 5.3 Force versus displacement plot at 1 Hz frequency

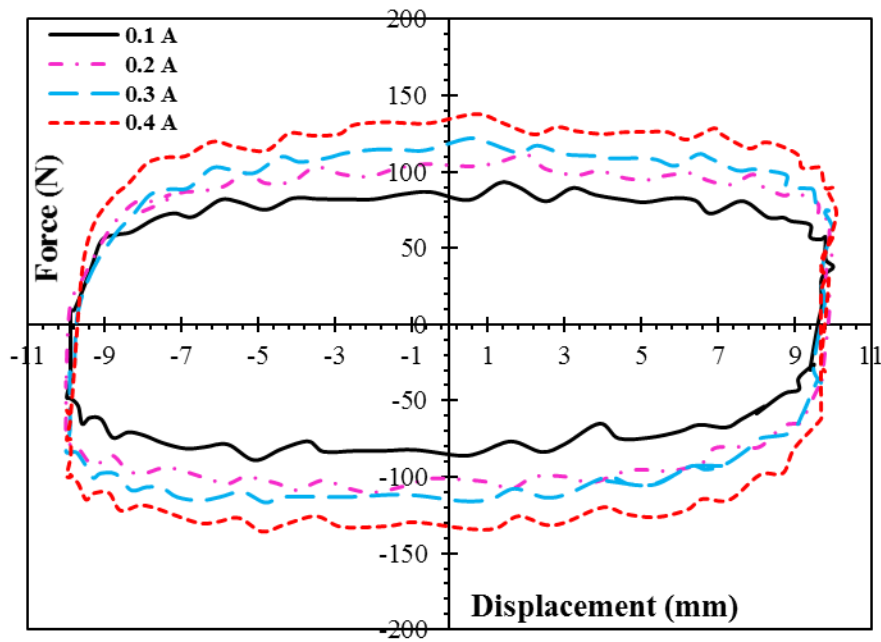


Figure 5.4 Force versus displacement plot at 1.5 Hz frequency

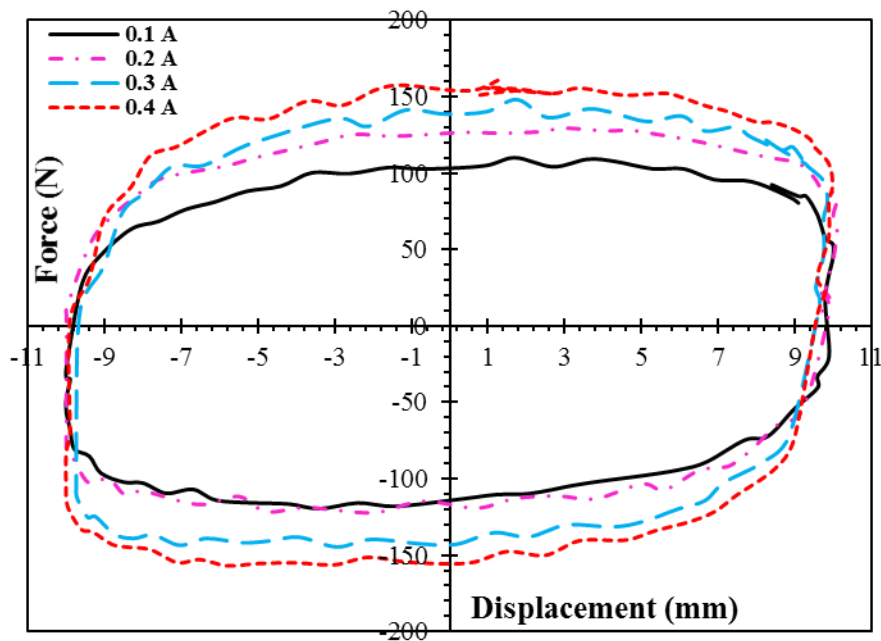
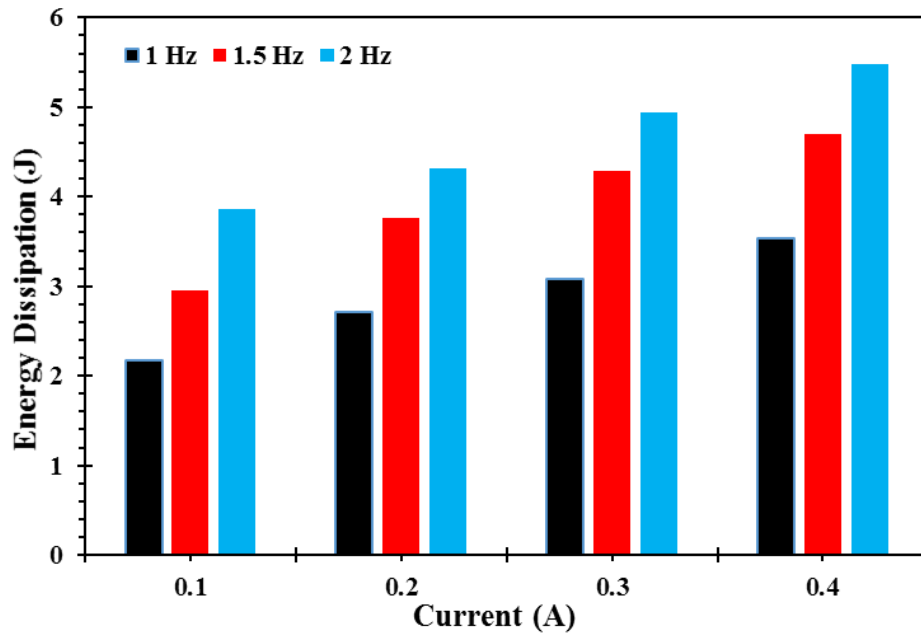


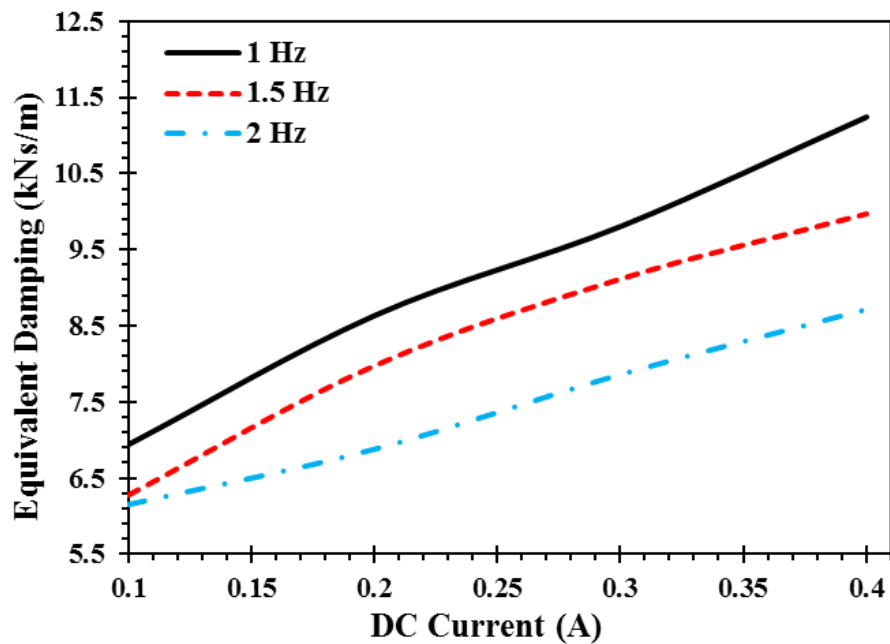
Figure 5.5 Force versus displacement plot at 2 Hz frequency

The area enclosed by the force versus displacement curve represent the energy dissipation of the damper. Figure 5.6 (a) depicts the energy dissipated at different magnitudes of current and frequency. It can be observed that as the current increases,

the amount of energy dissipated from the damper increases and a similar trend is observed in case of frequency. At a frequency of 2 Hz, the energy dissipated at 0.4 A current is 1.5 times greater than that at 0.1 A.



(a)



(b)

Figure 5.6 (a) Energy dissipation of MR damper per stroke and (b) Equivalent damping

The equivalent damping coefficients are computed using equation 5.8. Figure 5.6 (b) illustrates the plot of equivalent damping of the damper at different magnitudes of current. It can be observed from plot that the equivalent damping is directly related to energy dissipated in the damper and inversely related to frequency. Field dependent damping coefficient and the applied current can be related by first order exponential function as given in equation (5.8)

$$C_{eq}(I) = a * \exp(b * I) \quad (5.8)$$

where, I is the applied current, a and b are the coefficients of the equation which are determined by curve fitting method.

5.5 SUMMARY

The dynamic characterization of MR damper through experimental approach is discussed in this chapter. The force induced in the MR damper due to application of external magnetic field is evaluated under different operating frequencies using mechanical damper testing facility. The damping force versus displacement curve shows that maximum damping force can be realized at higher frequency and at higher DC currents. Also, it was observed that the area under these curves are increasing with increase in DC current resulting in higher energy dissipation of the damper. Since the area under the curve represents energy dissipated from the damper, the equivalent damping is considerably more at 1 Hz compared to that at 2 Hz frequency. In case of applied DC currents, the equivalent damping increases with value of applied current.

CHAPTER 6

GEOMETRIC OPTIMIZATION OF MR DAMPER AND STATISTICAL ANALYSIS OF DESIGN PARAMETERS

6.1 INTRODUCTION

In the previous chapter, experimental method employed for characterizing the shear mode type monotube MR damper was discussed. In order to maximize the damper performance of the MR damper and to identify the influential aspects, finite element based geometrical optimization is carried out. This chapter discusses the influence of material properties of MR damper components on its damping characteristics and maximization of the damping force through FEA based optimization. Initially, magnetic and non-magnetic materials are selected for MR damper cylinder and variation in the magnetic flux density induced in the shear flow gap is computed at different input current using magnetostatic analysis. Later, geometrical optimization is carried out to maximize the magnetic flux density induced in the shear flow gap and consequently the damping force. Multi-objective genetic algorithm (MOGA) and screening methods were adopted.

6.2 METHODOLOGY OF OPTIMIZATION

The performance of an MR damper depends on the controllable damper force and dynamic range. These two parameters are highly influenced by DC current supplied to the electromagnetic coil. Optimal value of the design parameters of the damper is considered, while designing the MR damper. Figure 6.1 shows overall optimization methodology. Magnetostatic analysis is carried out for the initial configuration. Design of experiments studies are used to identify the effective design points to construct the response surface and to identify the mutual influence of one parameter with other. Based on the response obtained from DOE, the optimization algorithm is

chosen and appropriate objectives are incorporated. Several candidate points are extracted from the optimization results and these candidate points are examined to choose the best candidate, which can maximise the magnetic flux density at the fluid shear flow gap. Based on the results obtained from the FE analysis and optimization, the force versus velocity curve is evaluated under different velocities.

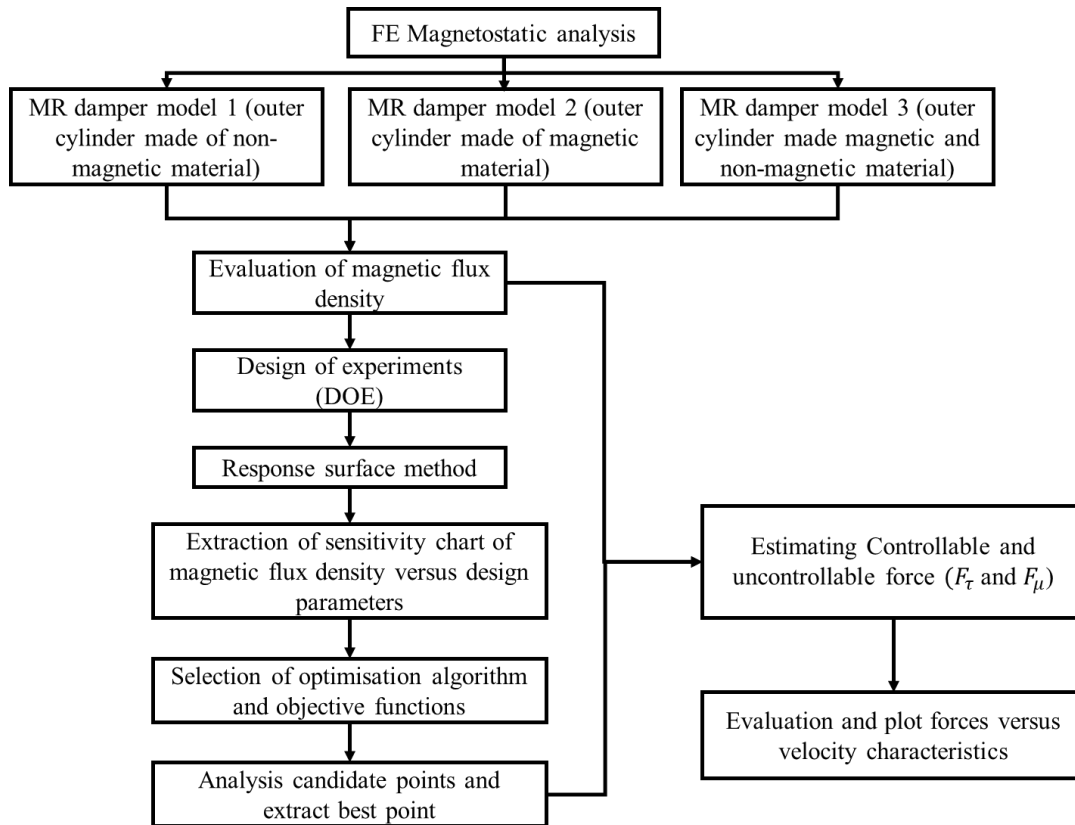


Figure 6.1 Methodology flow chart

6.3 MAGNETOSTATIC ANALYSIS

Magnetic flux density developed in the fluid shear flow gap is evaluated by using finite element analysis. Shear mode type MR damper is considered and three models are chosen, which can be differentiated based on outer cylinder material. The model details are tabulated in table 6.1. A sectional view of MR damper used in the present FEA is illustrated in figure 6.2. The piston is incorporated with 900 turns of copper coil. The boundary conditions applied are shown in figure 6.2 (a) and the dimensions of the MR damper are detailed in figure 6.2 (b).

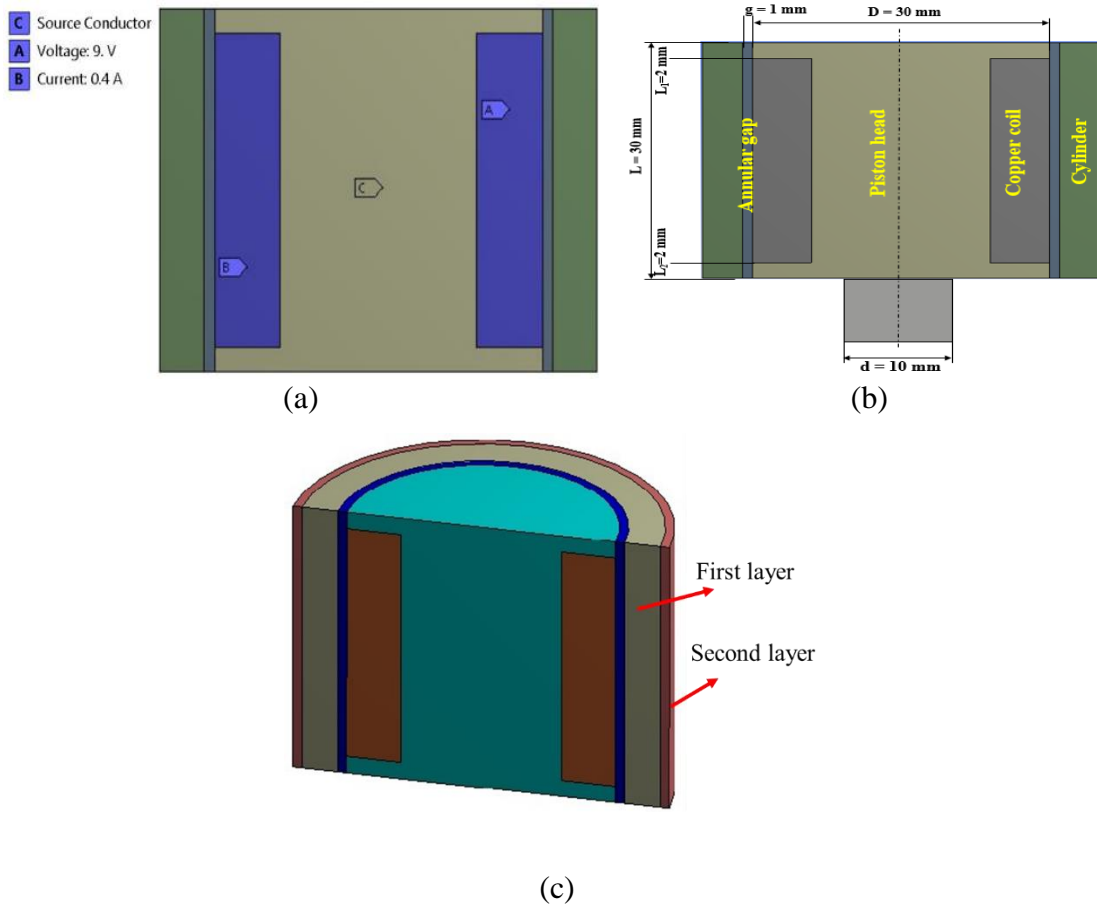


Figure 6.2 Damper model (a) Boundary conditions (b) Dimensions of MR damper model and (c) Model of composite outer cylinder

Table 6.1. Damper model details

Sl.No	Model	Outer cylinder Material	Piston head material
1	Model 1	Non - Magnetic Aluminium	SA1018
2	Model 2	Magnetic - SA1018	SA1018
3	Model 3	SA1018 and Aluminium	SA1018

The source conductor voltage and the DC current flowing across the electromagnetic coil are specified at the symmetric surface of the coil. Direct current ranging from 0.1 A to 1 A is applied in steps of 0.1A. It is assumed that there is zero leakage of flux from the cylinder and also magnetic flux lines are parallel along the symmetric plane. Outer cylinder and piston head are made up of stainless steel and SA1018 respectively, where the stainless steel has least magnetic permeability and SA1018

has relatively large magnetic permeability. Figure 6.3 depicts B-H curve of MR fluid and SA 1018. Corresponding material properties of the MR damper components are provided in table 6.2.

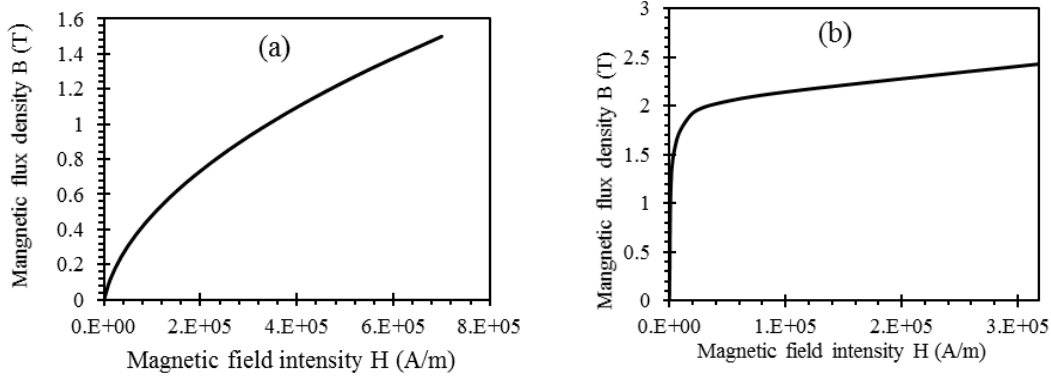


Figure 6.3 B-H Curve of (a) MRF-132 DG (b) SA1018

Table 6.2. Material properties of the MR damper components

Sl.No	Part name	Material	Relative Permeability
1	Cylinder	Aluminium	1
2	MR fluid	MRF-132DG	B-H Curve (Figure 6.3a)
3	Coil	Copper- 30 AWG	1
4	Piston Head	SA1018	B-H Curve (Figure 6.3b)

Magnetic flux density (B) is computed following a two-step procedure. In the first step, current flux density J is calculated for the applied DC current. The calculated current density is further used to evaluate magnetic field intensity (H) developed using Ampere's law and Gauss's law of magnetics.

$$\text{Amperes law} \quad \nabla \times H = J + \frac{dD}{dt} \quad (6.1)$$

$$\text{Gauss's laws} \quad \nabla \cdot D = \rho \quad (6.2)$$

$$\text{Gauss's laws of magnetics} \quad \nabla \cdot B = 0 \quad (6.3)$$

Magnetic flux density can be expressed as, (Nguyen et al. [13])

$$B = \frac{\mu_0 N_c I}{2 \frac{g}{\mu_r}} \quad (6.4)$$

where, ρ = Free electric charge, $J = \frac{I}{A}$ = Current density, D = Electric flux density, I = Current (A), g = fluid flow gap (mm), μ_r = Relative permeability of MR fluid, B = Magnetic flux density, A = Area in m^2 , μ_0 = Magnetic permeability of free space ($\mu_0 = 4\pi \times 10^{-7} \text{ TmA}^{-1}$), N_c = Number of turns in electromagnetic coil

6.4 ESTIMATION OF DAMPING FORCE OF MR DAMPER

Damping force can be estimated based on the magnetic flux density induced at the effective/annular gap of the MR damper. Then, force versus velocity characteristics are evaluated through analytical expressions. The methodology of estimating the force versus velocity is shown in the figure 6.4.

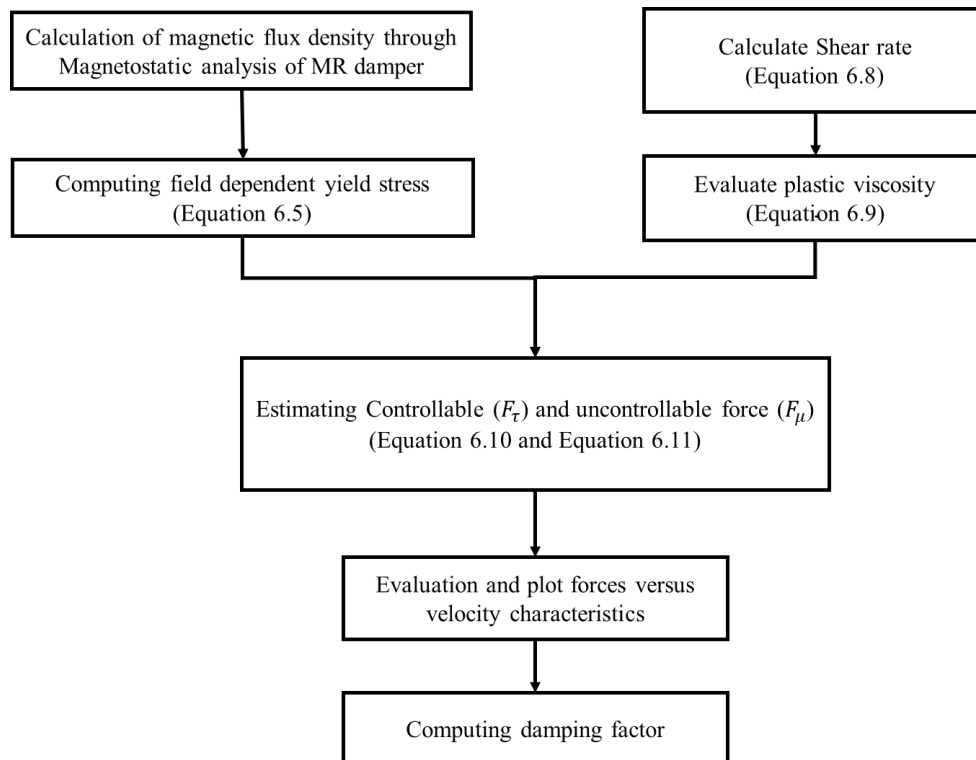


Figure 6.4 Flowchart for damping force estimation

Magnetic flux density obtained from the FE analysis are substituted in equation 6.5 and the magnetic field dependent yield stress of MR fluid is evaluated (Properties are tabulated in table 6.3). (Choi and Han, 2006).

$$\tau_B = 39.7B^4 - 132.4B^3 + 119.1B^2 + 10.3B + 0.1 \quad (6.5)$$

Table 6.3. Properties of MR Fluid- 132 DG (Lord co.)

Sl. No	Properties	Value
1	Viscosity	0.112 ± 0.02 Pas
2	Magnetic permeability	4 H/m
3	Density	2.95-3.15 g/cm ³
4	Operating Temperature	-40 to +130 °C
5	Specific Heat	800 (J/kg K)

The total force induced in the MR damper is equal to summation of controllable F_τ , frictional force F_f and uncontrollable force F_μ (Xu et al. 2013 and Ronge et al. 2011).

$$F = F_\tau + F_\mu + F_f \quad (6.6)$$

$$Q = \dot{u}A_f \quad (6.7)$$

$$\dot{\gamma} = \frac{\text{Velocity}}{2 * \text{fluid flow gap}} \quad (6.8)$$

$$\mu = 0.0006\dot{\gamma}^{-0.6091} \quad (6.9)$$

$$F_\tau = \left(2.07 + \frac{12Q\mu}{12Q\mu + 0.4wg^2\tau_y} \right) \frac{\tau_y LA_p}{g} \text{sgn}(\dot{u}) \quad (6.10)$$

$$F_\mu = \left(1 + \frac{wg\dot{u}}{2Q} \right) \frac{12\mu QL_t A_p}{wg^3} \quad (6.11)$$

$$w = \pi \left(\frac{g}{2} + D + \frac{g}{2} \right) \quad (6.12)$$

$$A_p = \frac{\pi(D^2 - d_0^2)}{4} \quad (6.13)$$

$$K = \frac{F_\tau}{F_{\mu f}} = \frac{\text{Controllable force}}{\text{Uncontrollable force} + \text{frictional force}} = \frac{F_\tau}{F_\mu + F_f} \quad (6.14)$$

where, L = Effective or annular gap length (mm), $L_t = L_1 + L_2$ = Total effective axial pole length (mm), w = Mean circumference of annular gap (mm), D = Diameter of piston head (mm), g = Height of annular gap/ fluid flow gap (mm), μ = Apparent viscosity (Pa-s), τ = Shear strength (Pa), d_0 = Diameter of piston rod (mm), Q = Volumetric flow rate (mm³/s), u = relative velocity (mm/s), K = damping factor, A_f cross section of fluid flow gap.

6.5 OPTIMIZATION OF MONOTUBE MR DAMPER

The parameters which effect the magnetic flux density across the MR fluid in the annular gap are number of turns of the electromagnetic coil, DC current supplied, fluid flow gap width and the flange length of coil. A set with different combination of design points are identified through design of experiments and the effective points are used to construct the response surface and the sensitivity of each design variable is obtained. Based on the sensitivity, objective function is decided.

6.5.1 Design of Experiments

Design of experiment (DOE) is a statistical method, which provides best possible design variables influencing the output of the optimization problem. DOE is used in problems involving more than one input parameter affecting the response or output. Different combinations of parameters are identified, which are referred as design points. Different combinations of design points are selected and series of analysis are conducted with identified set of parameters within the ranges specified. The upper and lower bounds of variables are mentioned in table 6.4.

Table 6.4. Design parameters range and sensitivity

Design parameter	Range	Sensitivity
Fluid flow gap	0.5mm-1.5 mm	Effective
Number of turns	500-1000	Effective
DC current	0.1A-1A	Effective
Flange length	22mm-27mm	Effective
Coil width	4mm-6mm	Not effective

The location of design points is determined and they are incorporated as part of response surface. Based on parameter range and design points, design of experiments is conducted by considering the central composite design (CCD) scheme. The main intention of performing DOE is to find required information with minimum number of design points and such effective points provide better accuracy of the response surface (Celik et al. 2016). The central composite design scheme is used in DOE, which is factorial design consisting one centre point and axial input parameters along the axis.

CCD is used to capture the spontaneous change inside the design space and to provide better response surface fit. If N is the number of input parameters, then a central composite design consists of one centre point, $2 \times N$ axial points located at positive and negative place on the axis of the desired input parameter and $2^{(N-f)}$ factorial points placed on a positive and negative location through diagonal of the input parameters. Figure 6.5 depicts the central composite design.

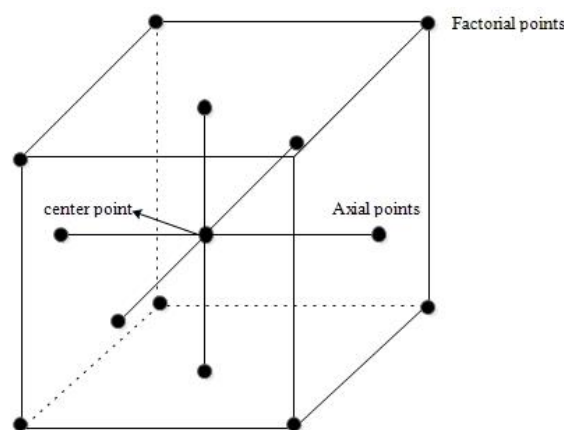


Figure 6.5 Central composite design

6.5.2 Response surface and optimization

Procedure involved in response surface method is based on the combination of statistical and mathematical techniques. The response surfaces describe the output parameters in terms of input parameters and these are constructed from design of experiments, which offers effective approximated values of output parameters. The accuracy of the response surface depends on the complexity of the solution, design

points from DOE and the type of regression model. Standard full second order polynomial model is used for creating the response surface. Regression analysis is a statistical method, where the dependency of one dependent design input point on other quantitative variable point is estimated. Also, the regression analysis determines the interaction between the input parameters and the output parameters by assuming that there is availability of output design points with their corresponding input design points in an n- design points (Myers et al. 2016).

6.6 RESULTS AND DISCUSSIONS

6.6.1 Results of Magnetostatic analysis

Magnetic flux density developed at the annular gap of MR damper model 1, 2 and 3 are computed for current inputs ranging from 0.1 A to 0.4 A in steps of 0.1A. Figure 6.6 (a), (b) and (c) illustrates the magnetic flux induced for *model 1*, *model 2* and *model 3* respectively. The magnetic flux obtained for *model 1* is relatively lower than that for *model 2* and *model 3*. Since the *model 1* damper cylinder is made up of nonmagnetic material, the flow of magnetic flux lines is restricted. But in case of *model 2* and *model 3* MR damper, the cylinder is made up of magnetic material and has higher magnetic permeability offering the magnetic flux to pass through. In case of *model 2* damper, when the electromagnetic coil gets excited, the magnetic effect can attract the magnetisable material on to the outer surface of the cylinder. Hence, it is necessary to isolate the outer surface magnetic cylinder using a nonmagnetic material. A composite cylinder with combination of magnetic and nonmagnetic material is modelled as cylinder for the MR damper *model 3* to analyse the changes in the induced magnetic flux density at the annular gap. The percentage increase in magnetic flux of *model 2* is 61.94 % and 2.61 % more than the *model 1* and *model 3* respectively. Figure 6.6 (d) shows similar 'maximum magnetic flux developed in *model 2* and *model 3* and magnetic flux leakage is reduced to less than 1% on usage of composite cylinder. Hence, it is advisable to use the composite type cylinder (*model 3*). In further work, *model 1* and *model 3* MR damper are considered for the optimization.

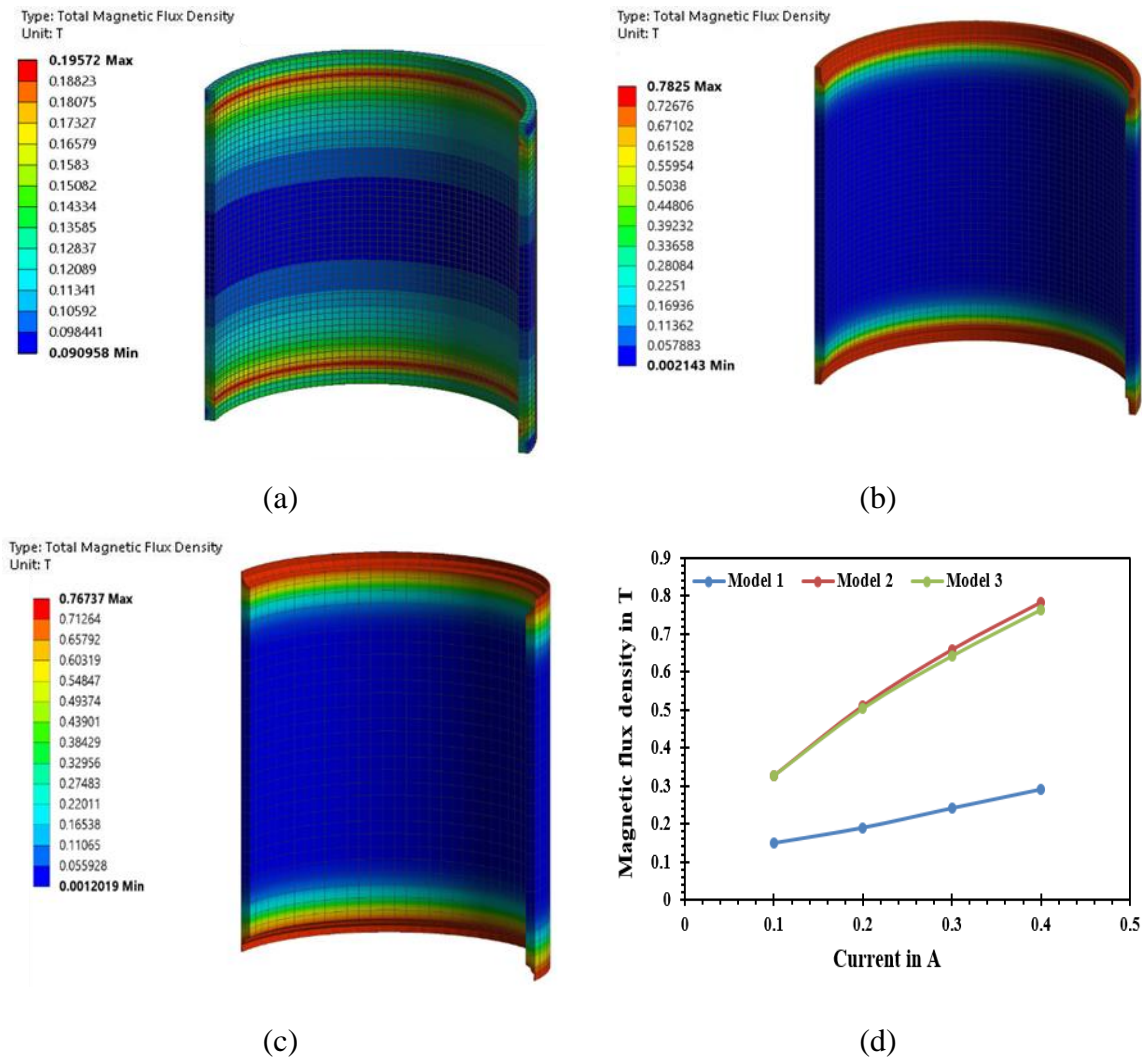
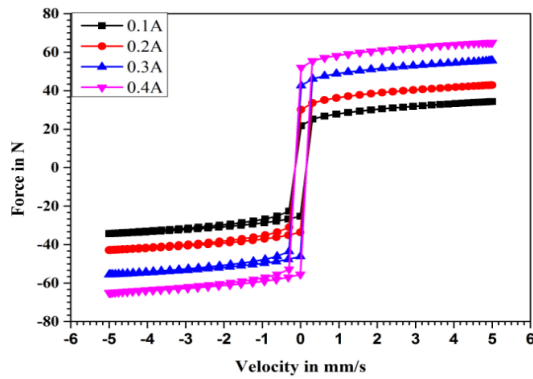


Figure 6.6 Magnetic flux density induced in the annular gap for (a) Damper *model 1* (b) Damper *model 2* (c) Damper *model 3* and (d) Comparison of three models

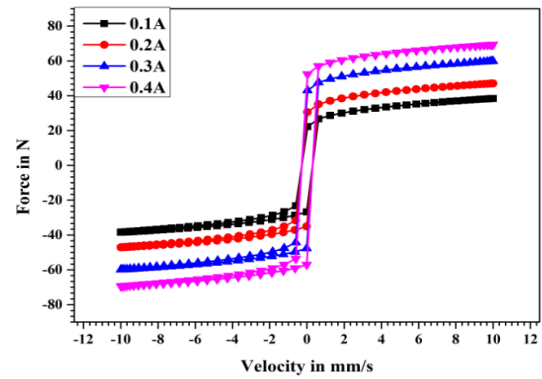
6.6.2 Damping force results

The force induced in the MR damper is calculated for 0.1 A, 0.2 A, 0.3 A, 0.4 A with a velocity of 5 mm/s, 10 mm/s, 15 mm/s and 20 mm/s. Figure 6.7 and Figure 6.8 illustrate the force versus velocity curve at different currents for *model 1* and *model 3* respectively. The maximum force developed in damper increases with velocity and current supplied to the electromagnetic coil of MR damper. The change in the damping force due to increment in velocity is much smaller than force change due to increment in current. It can be seen that the influence of velocity on the damping force is not obvious, while the influence of current is significant. Maximum damping force

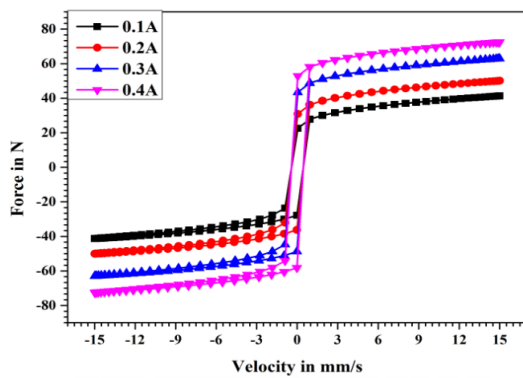
obtained from *model 1* and *model 3* are 75 N and 191 N respectively at velocity of 20 mm/s and for current of 0.4 A.



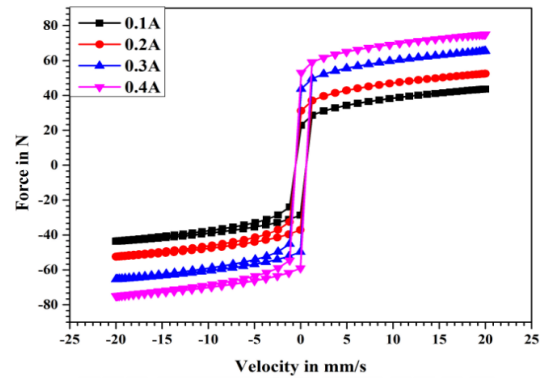
(a)



(b)

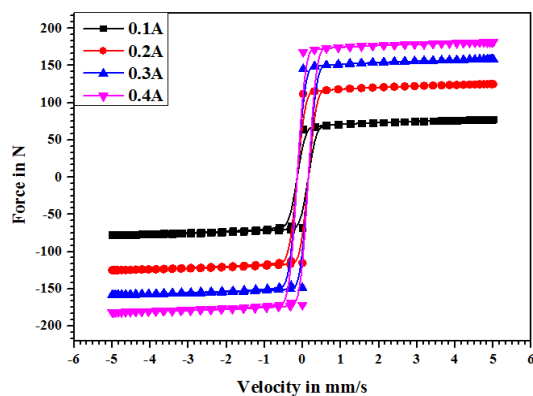


(c)

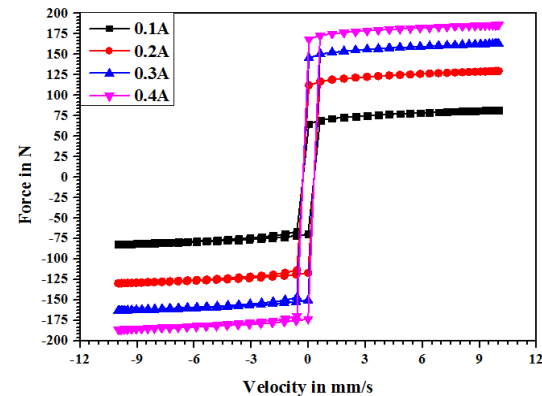


(d)

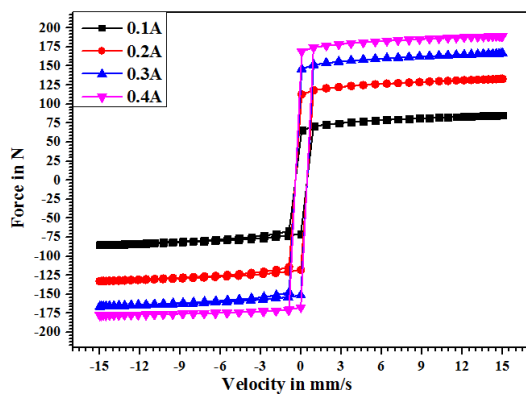
Figure 6.7 Force versus velocity - MR damper *model 1* at velocity, (a) 5mm/s, (b) 10mm/s, (c) 15mm/s and (d) 20mm/s



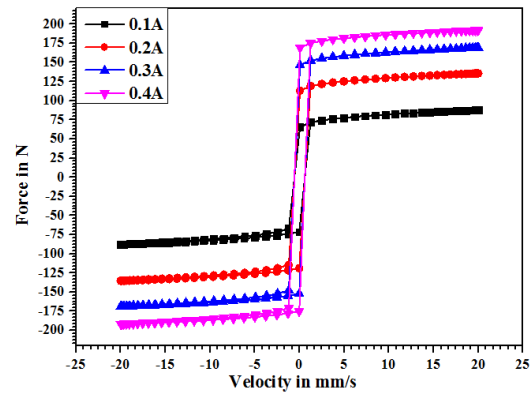
(a)



(b)



(c)



(d)

Figure 6.8 Force versus velocity - MR damper *model 3* at velocity, (a) 5mm/s, (b) 10mm/s, (c) 15mm/s and (d) 20mm/s

6.6.3 Optimization results

CCD offers to construct on previously used factorials by incorporating axial and centre points. Hence, it is more useful in the sequential experiments and is efficient for fitting second order model. There are 27 points generated and are evaluated through DOE (table 6.5).

6.6.3.1 Analysis of variance (ANOVA)

The influence of design parameter on the response and interaction between the parameters need to be determined to analyse the results and to verify, whether the parameters are significant and desirable. Analysis of variance (ANOVA) is employed to identify the significant and insignificant parameters. ANOVA is a mathematical and statistical technique, which separates the components of total variation (Ganji et al. 2016, Ficici et al. 2014). DESIGN EXPERT software is employed for verifying the significance of the model through F test and probability test. A total of 27 sets were simulated and the response were obtained for *model 1* and *model 3* damper and these values are used for analysis of variance. The results obtained from the ANOVA are tabulated in table 6.6 and table 6.7. The significant and insignificant parameters are determined based on the probability of significance known as the P - value obtained from the ANOVA (Ghodsiyeh et al. 2014).

Table 6.5. Design of experiments

Run	Current Magnitude(A)	Number of Turns	coil height(mm)	coil width(mm)	Fluid Flow gap(mm)	Magnetic Flux Density(T)
1	0.55	750	26.00	6.00	1.25	0.161
2	0.10	750	26.00	6.00	1.25	0.036
3	1.00	750	26.00	6.00	1.25	0.258
4	0.55	500	26.00	6.00	1.25	0.116
5	0.55	1000	26.00	6.00	1.25	0.203
6	0.55	750	23.40	6.00	1.25	0.168
7	0.55	750	28.60	6.00	1.25	0.249
8	0.55	750	26.00	5.40	1.25	0.161
9	0.55	750	26.00	6.60	1.25	0.162
10	0.55	750	26.00	6.00	0.50	0.188
11	0.55	750	26.00	6.00	2.00	0.171
12	0.42	679	25.26	5.83	1.46	0.119
13	0.68	679	25.26	5.83	1.04	0.171
14	0.42	821	25.26	5.83	1.04	0.137
15	0.68	821	25.26	5.83	1.46	0.201
16	0.42	679	26.74	5.83	1.04	0.126
17	0.68	679	26.74	5.83	1.46	0.187
18	0.42	821	26.74	5.83	1.46	0.147
19	0.68	821	26.74	5.83	1.04	0.214
20	0.42	679	25.26	6.17	1.04	0.118
21	0.68	679	25.26	6.17	1.46	0.174
22	0.42	821	25.26	6.17	1.46	0.139
23	0.68	821	25.26	6.17	1.04	0.198
24	0.42	679	26.74	6.17	1.46	0.125
25	0.68	679	26.74	6.17	1.04	0.185
26	0.42	821	26.74	6.17	1.04	0.148
27	0.68	821	26.74	6.17	1.46	0.218

Table 6.6. ANOVA table for damper *model 1*

Source	Sum of Squares	df	Mean Square	F Value	p-value Prob > F	
Block	2.59×10^{-5}	1	2.59×10^{-5}			
Model	0.24	15	0.016	105.02	< 0.0001	Significant
A-No.of Turns	0.027	1	0.027	173.54	< 0.0001	Significant
B-coil height	2.24×10^{-4}	1	2.24×10^{-4}	1.47	0.2539	
C-coil width	1.43×10^{-5}	1	1.43×10^{-5}	0.093	0.7663	
D-flow gap	1.26×10^{-5}	1	1.26×10^{-5}	0.082	0.7804	
E-Current	0.2	1	0.2	1324.74	< 0.0001	Significant

Table 6.7. ANOVA table for damper *model 3*

Source	Sum of Squares	df	Mean Square	F Value	p-value Prob > F	
Block	0.22	1	0.22			
Model	1.74	5	0.35	56.53	< 0.0001	Significant
A-No. of Turns	0.092	1	0.092	15	0.0009	Significant
B-coil height	2.20×10^{-3}	1	2.20×10^{-3}	0.36	0.5565	
C-coil width	2.79×10^{-3}	1	2.79×10^{-3}	0.45	0.5085	
D-flow gap	0.27	1	0.27	44.12	< 0.0001	Significant
E-Current	1.37	1	1.37	223.05	< 0.0001	Significant

If the *P-value* is lesser than the 0.05, then the null hypothesis is rejected for the entire population and parameters are significant. But if the *P-value* is greater than 0.05 null hypothesis is not rejected and parameters are insignificant. The results in the table 6.6 and 6.7 shows that the values of "*p-value Prob > F*" is less than 0.05, indicating model terms are significant. In case of *model 1*, A-Number of turns and E- Current magnitude are significant model term, while in case of *model 3* damper, A-Number of turns, D-flow gap and E- current magnitude are significant parameters. Other parameter values, which are greater than 0.10 indicate the model terms are not significant. Also, it is observed from the table 6.6 and table 6.7 that *F* values of the

models are 105.02 and 56.53 respectively, while the p -value of the models in both cases is less than 0.0001 indicating that the models are significant.

Table 6.8 shows the summary of statistics. The ‘adjusted R-squared’ compares the explanatory power of regression models that contain different numbers of predictors. The capability of regression models in predicting the response of the observation can be evaluated through predicted R-Squared value. The R-squared value is used to estimate closeness of the given data to the reference fitted regression line. $R\text{-Squared} = (\text{Explained variation}/\text{Total variation})$. Its value will be fall between 0% to 100 %, if the value is 0 % it refers that none of the variability of the response data around its mean. When it is 100% it refers that all variability of the response data is around its means. Higher the value of R-squared value provides better model fit to the data. Both R-squared and Adj-R-Squared provides information about how many data points fall within the regression equation line. The main difference between them is Adjusted R-squared provides the percentage of variation explained by only the independent variables which have a higher influence on the dependent variable. Adjust-R-squared is an unbiased estimate of the population of R-squared. Predicted R-Squared value provides the information about prediction capability of a regression model for the new set of observations. The higher value of predicted R-squared indicates that model has the greater predictive capability.

It can be seen that, in case of *model 1* the ‘Pred R-Squared’ value is 0.8120 and the ‘Adj R-Squared’ value is 0.9842. While in case of *model 3* ‘Pred R-Squared’ value is 0.8822 and ‘Adj R-Squared’ value is 0.9174. Since in both cases, the difference between them is less than 0.2, they are in reasonable agreement. The ‘Adeq Precision’ measures the signal to noise ratio, if the ratio is greater than 4, then it is desirable. *Model 1* has ratio of 32.405 and *model 3* has a ratio of 27.074, which indicate an adequate signal.

Table 6.8. Summary of statistics

Model	Model 1	Model 3
R-Squared	0.993692	0.9339
Adj R-Squared	0.98423	0.9174
Pred R-Squared	0.8120	0.8822
Adeq Precision	32.40508	27.074

Table 6.9. ANOVA Coefficient Estimate

Parameters	Coefficient Estimate	
	Model 1	Model 3
A-No. of Turns	0.038422	0.071652
B-coil height	0.003531	-0.01106
C-coil width	0.000987	-0.01354
D-flow gap	-0.00093	-0.1336
E-Current	0.106154	0.276319

The effect of parameters on the response is determined based on the coefficient estimate. Higher coefficient value indicates strong influence on the response. The coefficients for the *model 1* and *model 3* obtained from the ANOVA are shown in the table 6.9. Among all the parameters, ‘A-Number of turns’ and ‘E-Current magnitude’ have the strongest effect on the response, because they have a higher value when coefficient compared to other parameters.

6.6.3.2 Normality test

In order to check whether the data points are obtained from the normally distributed population, a normality test has been conducted. Figure 6.9 illustrates the standard residuals plotted against normal percentage probability distribution for *model 1* and *model 3* MR dampers. The straight reference line represents the exact normal distribution and the points distributed are residual data points. It can be observed that residual data points are closely fitting with a straight reference line suggesting that the analysis data does closely follow the normal distribution.

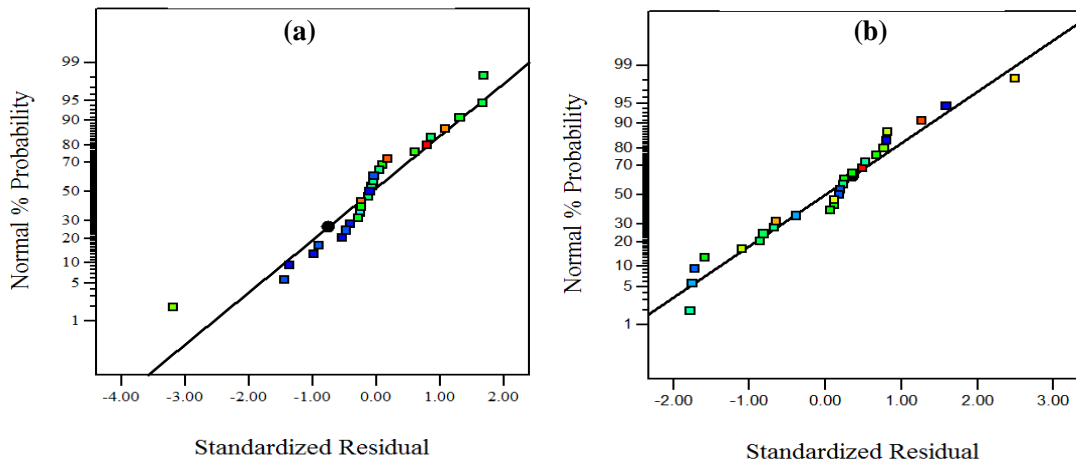


Figure 6.9 Normal plot of (a) Model 1 and (b) Model 3 MR dampers

6.6.3.3 Homoscedasticity

Figure 6.10 indicates the values of the residuals on the vertical axis plotted against the fitted values of response for *model 1* and *model 3* MR dampers. The distribution of residuals at different levels within the analysis does not show any extreme variation from the one end to another. With thorough observation of distribution, the variance of the residuals is similar and consistent at different levels, which allows to find the equality of variance. Since the similar scatter or distribution can be seen it is referred as homoscedasticity.

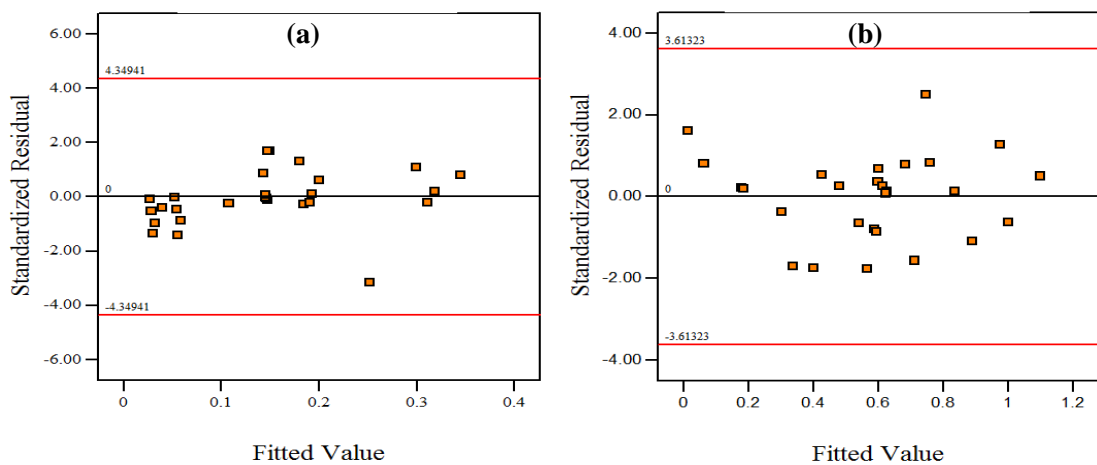


Figure 6.10 Residuals plot of (a) Model 1 and (b) Model 3 MR dampers

6.6.3.4 Run chart

The values of residuals are plotted over the run, which is referred as the run chart. This chart displays number of standard deviations in a given run falling off compared to expected. Figure 6.11 illustrates run chart of *model 1* and *model 3* dampers. The upper and lower red lines refer to 95% confidence control limits on the run chart.

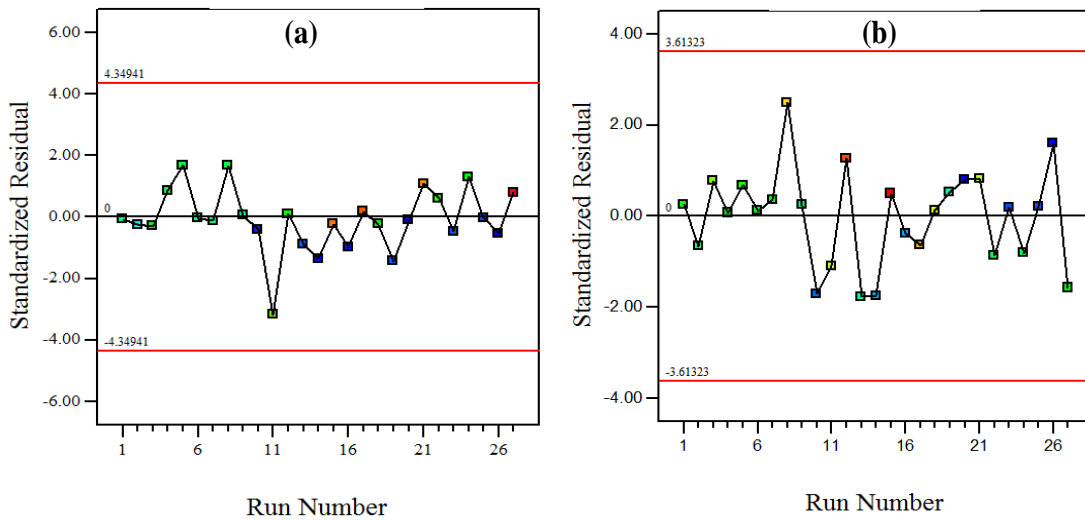


Figure 6.11 Run chart of (a) Model 1 and (b) Model 3 MR dampers

The point which is falling outside the red line are referred as outliers. From figure 6.11 it can be observed that there are no outliers in the chart, all points are falling within the limit, which suggests the responses are stable.

6.6.3.5 Sensitivity and Response surfaces

From the response surface, sensitivity of the design parameters is evaluated. Figure 6.12 illustrate the sensitivity chart obtained from the response surface. Since there are more than two parameters which influences the magnetic flux density, screening optimization algorithm is adopted which is based on the sampling and sorting method. Basically, screening algorithm develops new sample sets and these sets are sorted depending upon the specified objective functions. It is fast and exhaustive approach, which can locate the approximate solution quickly. Further, another method called

multi objective genetic technique is also used for optimization, which supports multi objectives and constraints to evaluate the global optimum points.

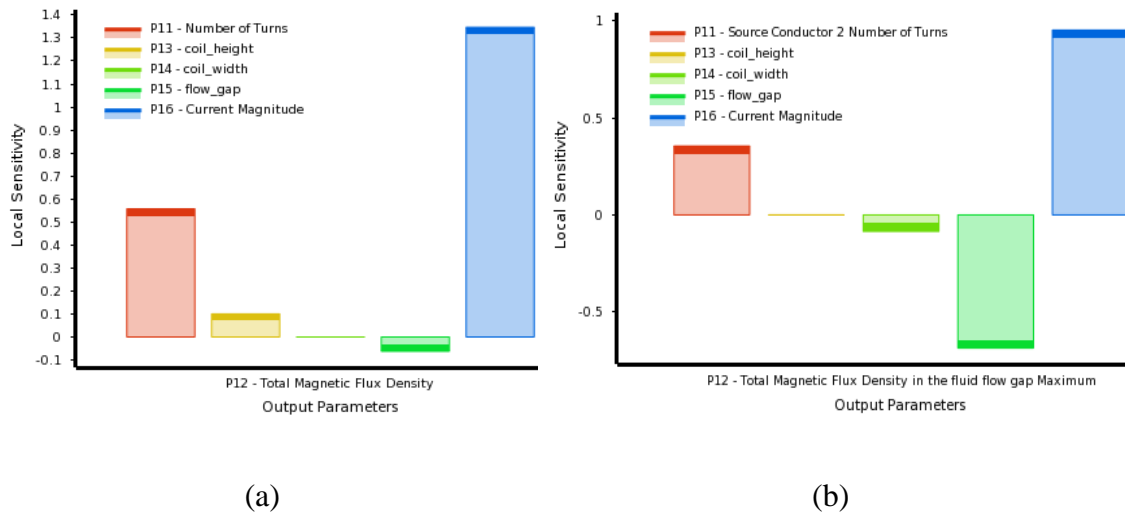


Figure 6.12 Local sensitivity chart for (a) *Model 1* and (b) *Model 3* MR dampers

The magnetostatic analysis is used for calculating the magnetic flux generated along in the annular gap/ fluid flow gap. The dynamic performance of the MR damper depends on the magnetic flux density induced at the effective area gap. The magnetic flux density and magnetic flux lines developed in the annular gap for different damper models is illustrated in the figures 6.6. Magnetic flux density is computed for voltage of 9 V and 1 A current for the initial configuration of the MR damper. A design of experiment with 27 design points are developed and responses are analysed. 3D response surface is generated from analysis of these design points. The sensitivity chart obtained from the response surface shows that the number of coils, DC current and fluid flow gap have more influence on objective function as illustrated in figure 6.12.

Figures 6.13 and 6.14 shows response surface developed based on full second order polynomial method. Design variables which predict the maximum magnetic flux density are evaluated through the screening optimization method and MOGA algorithm. These parameters are identified between the upper and lower range values.

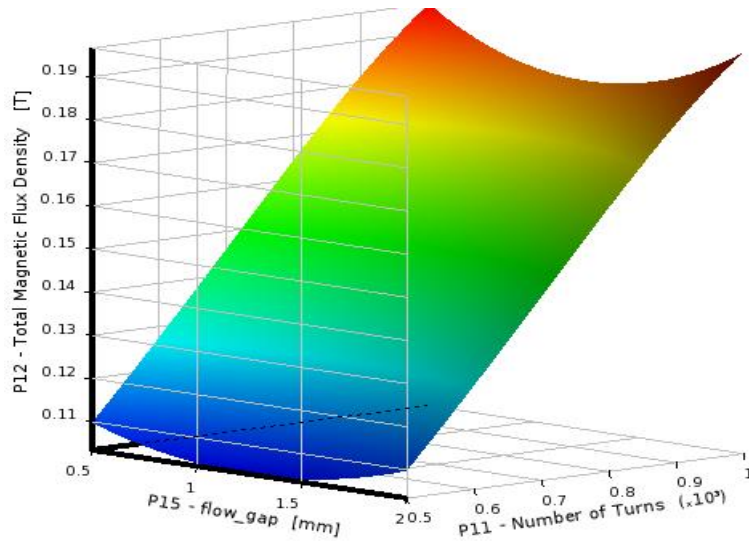


Figure 6.13 3D Response surface of magnetic flux, flow gap and number of turns for *model 1* MR damper

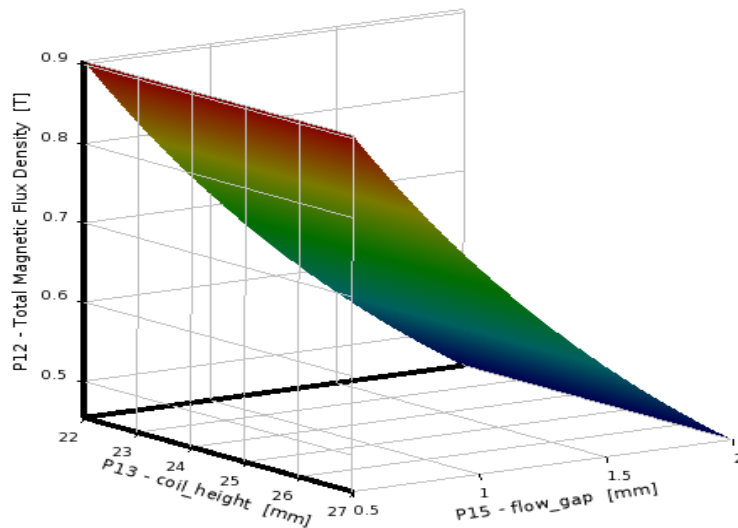


Figure 6.14 3D Response surface of magnetic flux, flow gap and coil height for *model 3* MR damper

Magnetic flux density increases linearly with increase in number of turns in electromagnetic coil for both models (Figure 6.15 (a) and (b)). The magnetic flux density increases linearly with DC current upto 0.8 A for both *model 1* and *model 3* dampers. Further, it tends to saturate beyond this value as shown in the Figures 6.16 (a) and (b). Based on the specified objectives, the optimization suggested three best

candidates for the MR damper *model 1* and *model 3* as given in the table 6.10 and table 6.11 respectively. Among the three candidates, the first candidates, provided the highest magnetic flux density than other two candidates.

The candidate's points obtained from screening optimization and the MOGA algorithm were found to have almost similar values for all the design variables. Three candidate points are identified in each model. The best candidate's points extracted from the screening optimization and MOGA optimization for the *model 1* and *model 3* are tabulated in the tables 6.10 to 6.13.

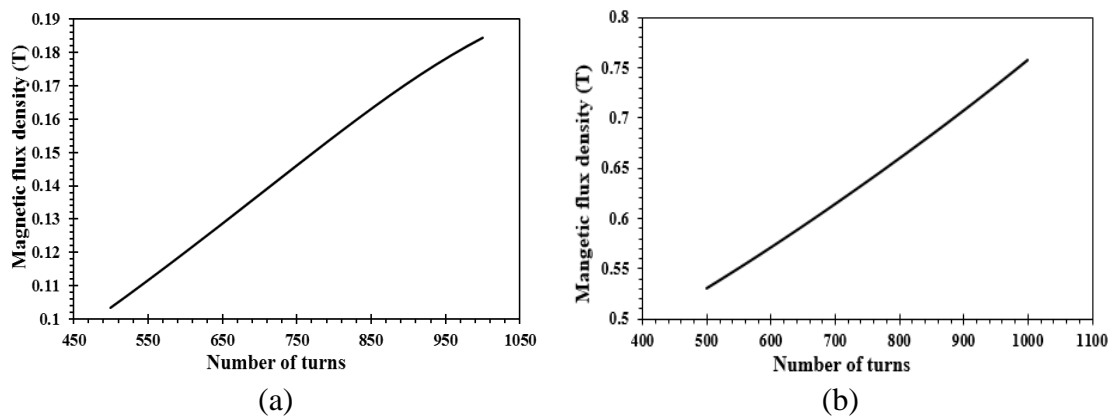


Figure 6.15 (a) Number of turn versus magnetic flux density for *model 1* MR damper
(b) *Model 3* MR damper

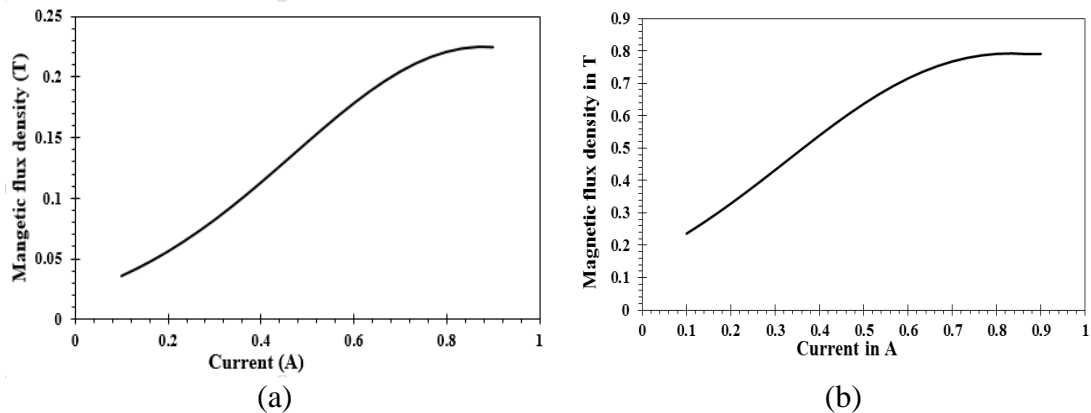


Figure 6.16 Magnetic flux density versus DC current (a) *Model 1* MR damper and (b) *Model 3* MR damper

Table 6.10. Candidate points obtained through optimization using screening algorithm
for *model 1* damper

Candidate point	Fluid flow gap (mm)	Number of turns	DC current (A)	Coil height (mm)	Coil width (mm)	Magnetic flux (T)
Candidate 1	0.50	990	0.98	27.00	4.23	0.31
Candidate 2	0.58	970	0.85	23.94	5.17	0.27
Candidate 3	0.72	980	0.71	22.86	4.99	0.24

Table 6.11. Candidate points obtained through optimization using screening algorithm
for *model 3* damper

Candidate point	Fluid flow gap (mm)	Number of turns	DC current (A)	Coil height (mm)	Coil width (mm)	Magnetic flux (T)
Candidate 1	0.65	960	0.57	26.49	5.89	0.98
Candidate 2	0.52	890	0.76	26.39	4.84	1.103
Candidate 3	0.50	1000	0.71	26.63	4.00	1.241

Table 6.12. Candidate points obtained through optimization using MOGA algorithm
for *model 1* damper

Candidate point	Fluid flow gap (mm)	Number of turns	DC current (A)	Coil height (mm)	Coil width (mm)	Magnetic flux (T)
Candidate 1	0.56	970	0.86	27.00	5.50	0.261
Candidate 2	0.52	995	0.98	26.90	4.40	0.3044
Candidate 3	0.61	950	0.88	26.98	5.10	0.246

Table 6.13. Candidate points obtained through optimization using MOGA algorithm for *model 3* damper

Candidate point	Fluid flow gap (mm)	Number of turns	DC current (A)	Coil height (mm)	Coil width (mm)	Magnetic flux (T)
Candidate 1	0.540	980	0.74	26.13	4.08	1.213
Candidate 2	0.534	950	0.75	22.15	4.03	1.201
Candidate 3	0.560	960	0.78	26.57	4.06	1.212

The desirable candidate point is extracted from three candidates obtained from both screening and MOGA optimization. The best candidate points of MR damper *model 1* and *model 3* extracted are tabulated in the tables 6.14 and table 6.15 respectively.

Table 6.14. Optimized design parameters based on MOGA and screening method for *Model 1* damper

Method	Fluid flow gap (mm)	Number of turns	DC current (A)	Coil height (mm)	Coil width (mm)	Magnetic flux density (T)
MOGA	0.52	995	0.98	26.9	4.40	0.3044
Screening	0.50	990	0.98	27	4.23	0.3071

Table 6.15. Optimized design parameters based on MOGA and screening method for *Model 3* damper

Method	Fluid flow gap (mm)	Number of turns	DC current (A)	Coil height (mm)	Coil width (mm)	Magnetic flux density (T)
MOGA	0.54	980	0.74	26.13	4.08	1.213
Screening	0.50	1000	0.71	26.63	4.00	1.241

The damping force is calculated for the optimum values of the design parameters obtained from above optimization procedure. Figure 6.17 illustrates the force versus velocity behaviour for optimized values of *model 1* and *model 3* MR dampers. It can be observed that damping force developed for the *model 3* is much higher than that of

model 1 MR damper. The damping force change in *model 3* is 2.79 times more than the *model 1* at the velocity of 20 mm/s.

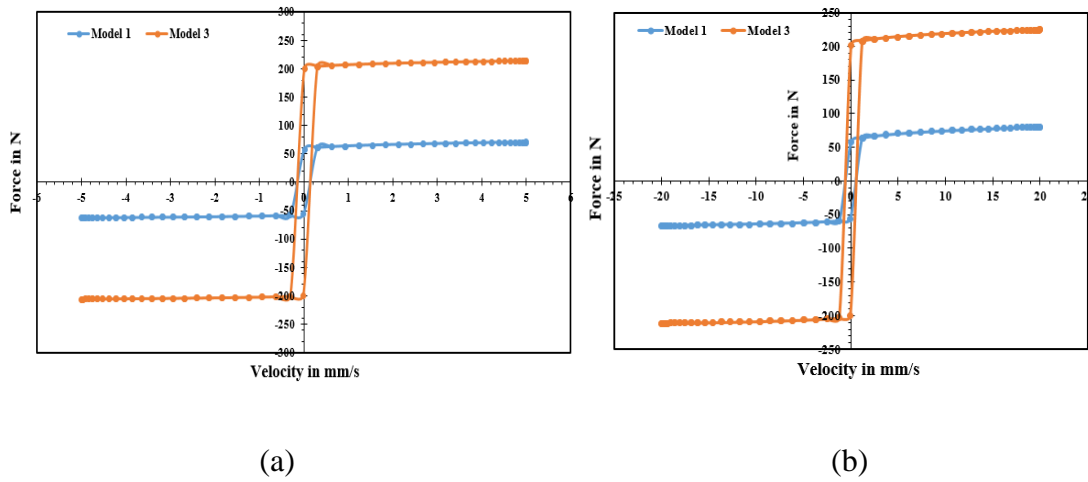


Figure 6.17 Force versus velocity curve for optimized MR damper

6.7 SUMMARY

In this chapter, the influence of material properties of MR damper components on the induced magnetic flux density and geometrical parameters on the damping force were presented. Three different cases were considered based on the magnetic and nonmagnetic materials used for cylinder. The magnetic flux density induced in shear flow gap for each case is computed through magnetostatic analysis. The design parameters such as shear flow gap, flange length, number of turns of coils and DC currents were used as the variables. Through central composite design, a set of DOEs were formulated and response of each run of the DOE is evaluated through FE analysis. The significance of design variables and interaction of each variable was estimated through analysis of variance. Based on the DOE results, multi-objective genetic algorithm and screening optimization techniques were employed to maximize the magnetic flux density and to identify the optimal values of the design variables. Using the analytical method, damping force of each model was computed for the obtained optimal values of the design variables and found that the *model 3* MR damper has 2.7 times greater damping force compared to *model 1*.

CHAPTER 7

COMPUTATIONAL FLUID DYNAMIC ANALYSIS OF MR DAMPER

7.1 INTRODUCTION

In this chapter, computational methods are used for characterising the monotube MR damper under different input conditions and the results are elaborated. The predicted characteristics of the MR damper through the computational analysis are validated with the experimental results. Computational analysis is accomplished through two steps. Initially, magnetic flux density induced in the shear flow gap is estimated through magnetostatic analysis. Changes in the rheological properties due to induced magnetic flux density is evaluated and are used in CFD analysis to estimate the damping force. The effect of frequency, fluid flow gap length on the damping characteristics are estimated. Utilising the validated CFD analysis method, three modes of operation are considered to make comparative study about the performance of each mode. The three modes are shear mode, flow mode and mixed mode.

7.2 COMPUTATIONAL ANALYSIS

The computational approach is employed for characterising the MR damper under different input conditions. By coupling FEA and CFD analysis, damping force of the MR damper can be estimated. The procedure adopted for computational analysis is illustrated in figure 7.1. Initially, shear mode type of MR damper is considered for analysis to evaluate the damping force and the credibility of the obtained results are validated with the experimental results. Using validated model, the influence of frequency and fluid flow gap length are estimated under different currents. Later, same approach is extended for evaluating the performance of the flow mode and combined shear-flow mode dampers. The comparison of dynamic characteristics of all three models is studied and elaborated.

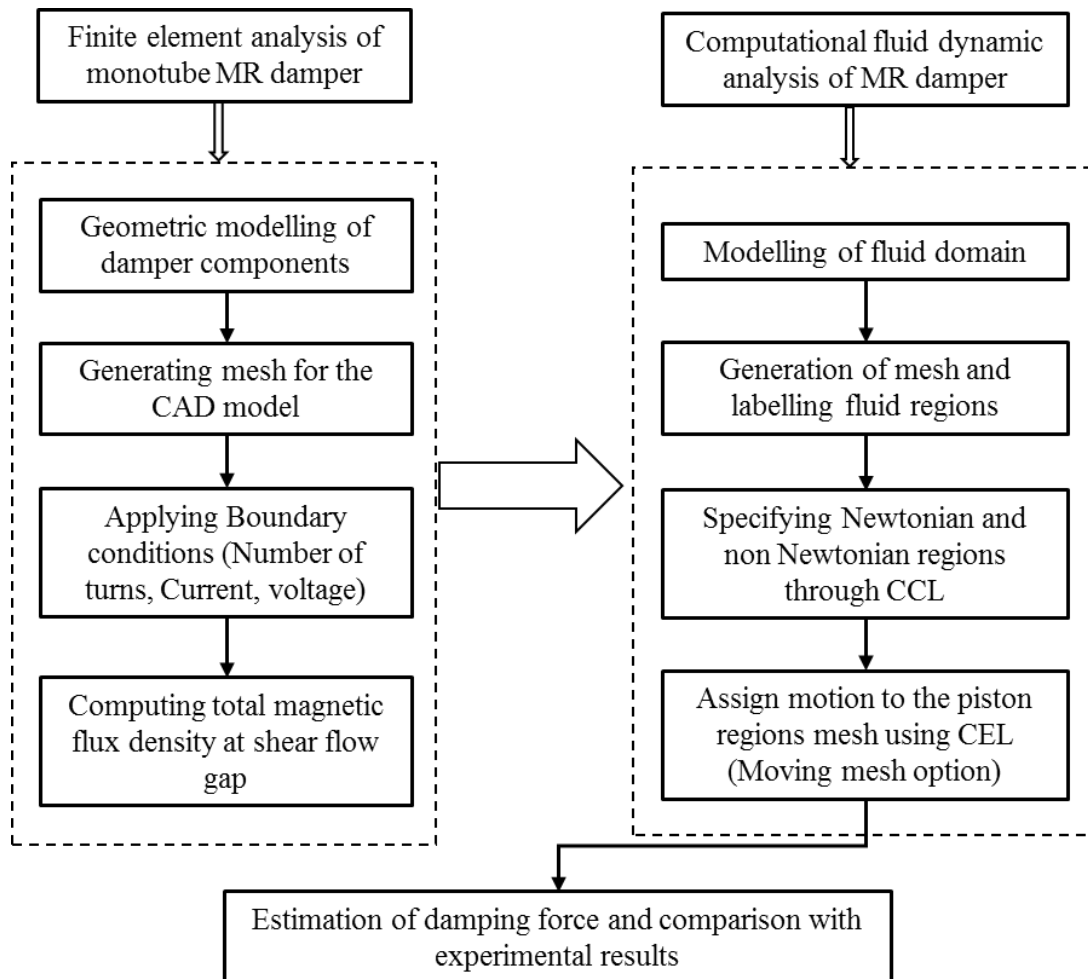


Figure 7.1 Procedure of Computational method

7.2.1 Magnetostatic analysis of monotube MR damper

The damping characteristics of MR damper depends upon the magnetic flux induced at the effective area/fluid flow gap. A higher magnetic flux at the annular gap or fluid flow gap improves the performance of the damper. Magnetic flux density in fluid flow gap can be obtained by finite element method. Finite Element Method Magnetic (FEMM) software was employed for computing the magnetic flux induced at electromagnetic coil in the piston head. The parameters which influence the amount of magnetic flux generation are selection of materials, polarity of the coil, fluid flow gap, diameter of piston head, rod and thickness of the hub. The dimensions of the MR damper and material used for the components are tabulated in table 7.1 and table 7.2 respectively. The 2-D models of the MR dampers for FEA analysis is illustrated in

figure 7.2. The mesh consists of 4313 triangular elements. The piston head is wound with 30 AWG copper coil with 300 turns. The magnetic flux developed is computed for DC current ranging from 0.1 A to 0.5 A with an increment of 0.1A. It is assumed that there is zero leakage of flux from the cylinder. Current density (J) for the applied current can be calculated by using Kirchhoff's law as,

$$J = \frac{N_c I}{A} \quad (7.1)$$

where, N_c = Number of turns in the coil, I = Applied current (A), A = Coil Area in m^2

Table 7.1. Dimensions of the monotube damper

Sl. No	Parameter	Dimensions in mm		
		Shear mode (<i>Model-Shear</i>)	Flow mode (<i>Model-Flow</i>)	Mixed mode (<i>Model-Mixed</i>)
1	Cylinder outer diameter (D_0)	34	34	34
2	Core depth (C_w)	7	7	7
3	Piston Diameter (P_t)	30	20	30
4	Piston length (L)	30	30	30
5	Coil housing length (C_l)	26	26	26
6	Flange thickness (W_1 and W_2)	2	2	2
7	Annular gap (A_g)	1	1	1

Outer cylinder and piston head are made of stainless steel and SAE1018 steel respectively, where the stainless steel has least magnetic permeability and SAE steel has higher magnetic permeability, which are important material properties to be defined in the analysis. The material properties of the damper components are given in table 7.2. The maximum magnetic flux density is calculated in the annular gap, where the MR fluid gets excited. The calculated magnetic flux is used to find the dynamic viscosity of the fluid equation and the magnetic field dependent yield stress (τ_B), which is obtained by using the equation (7.2) (Choi and Han, 2012),

$$\tau_B = 39.7B^4 - 132.4B^3 + 119.1B^2 + 10.3B + 0.1 \quad (7.2)$$

where, τ_B = Field dependent yield stress (Pa), B = Magnetic flux density (T)

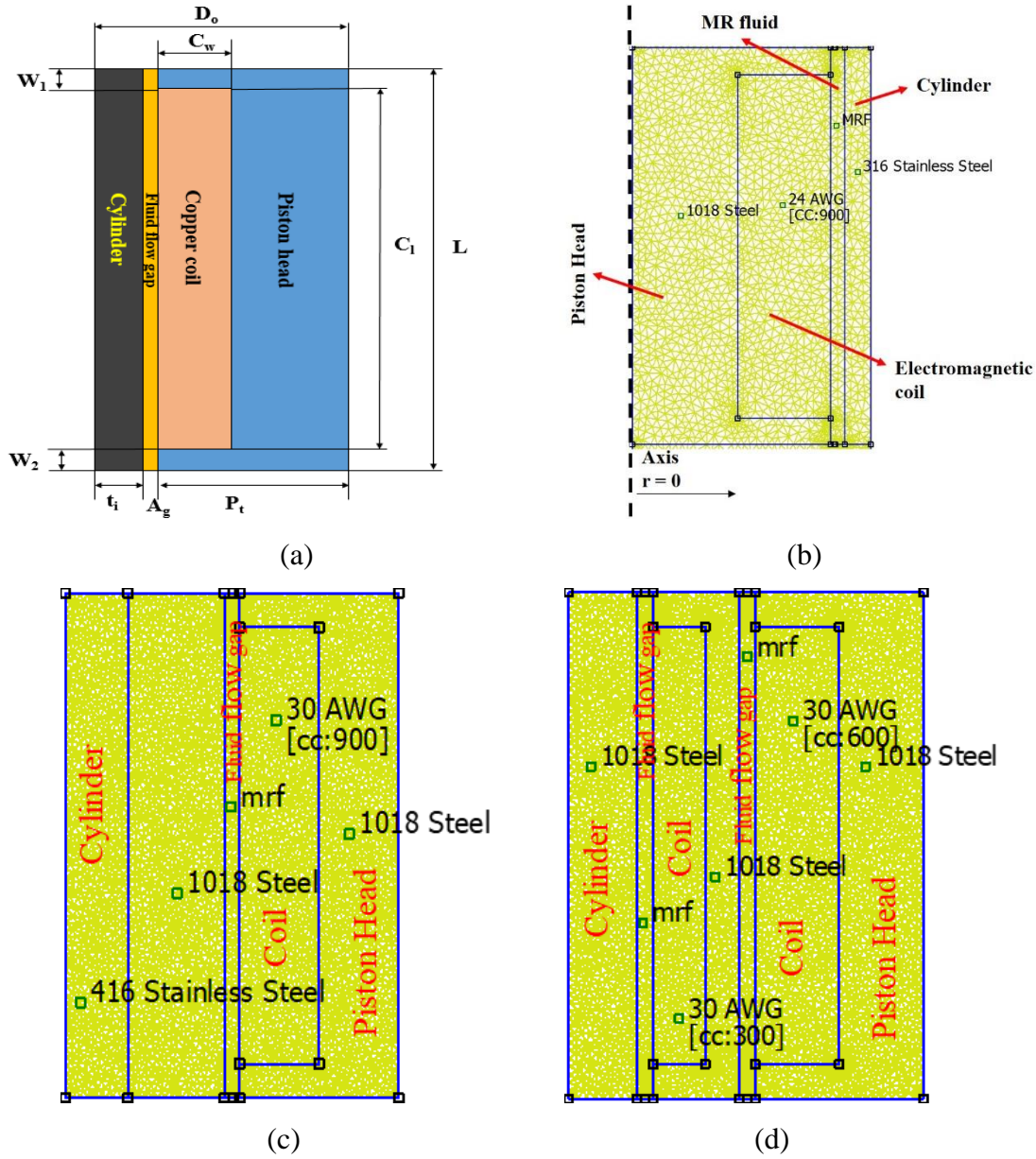


Figure 7.2 Monotube damper model (a) Dimensions and (b), (c), (d) mesh of *Model-shear*, *Model-flow* and *Model-mixed* MR damper respectively

Table 7.2 Material Properties of the MR damper components

Sl.No	Part name	Material	Relative Permeability
1	Cylinder	Steel	2000
2	MR fluid	MRF-132DG	B-H Curve (Figure 6.3a)
3	Coil	Copper- 30 AWG	1
4	Piston Head	SA1018	B-H Curve (Figure 6.3b)

7.2.2 CFD analysis of MR Damper

The region inside the MR damper occupied by MR fluid is considered for computational analysis and the same is modelled in ANSYS design modeller. Figure 7.3 shows the CFD model created for CFD analysis. Table 7.4 provides details about CFD model boundary conditions. The motion of the piston in the cylinder is achieved by command expression language (CEL). There are two regions in the MR damper, first one is Newtonian region, which is not under the influence of magnetic field. The second region is a non-Newtonian region in the fluid flow gap, where fluid gets magnetically excited leading to change in the rheological properties. These two regions are specified through the material properties in the pre-processor with the help of command language (CCL). The non-Newtonian region behaviour is well represented by Bingham model, which is incorporated in the simulation and is achieved by writing the CEL expression. CFD analysis setting details are given in table 7.3.

Table 7.3 CFD analysis details

Parameter	Value
Analysis type	Transient
Analysis time	1 s, 0.7 s, 0.5 s, 0.42 s, 0.3 s
Time steps	0.005 s
Stroke length	10 mm
Frequency	1, 1.5, 2, 2.5 and 3Hz
Number of elements	2, 11,907
Number of nodes	1, 09,562

Table 7.4 Boundary conditions of CFD analysis

Boundary Conditions	Location
No-slip Boundary	Outer surfaces of the cylinder and Piston rod
	Top and bottom surface of the cylinder
Wall with specified distance	Piston head walls

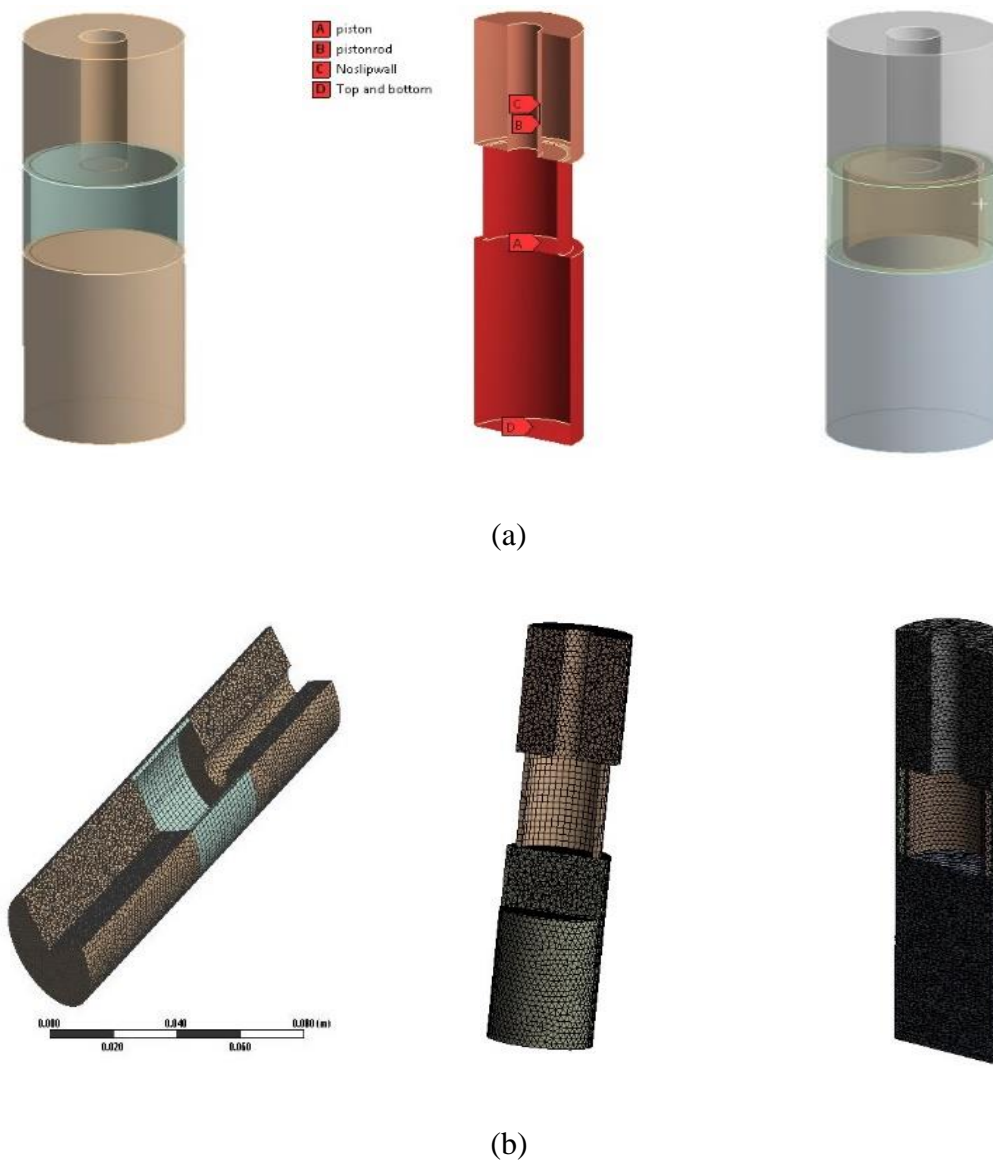


Figure 7.3 Computational Fluid domain (a) Model and Boundaries, (b) Meshed model

The well-known Maxwell's equations are used in FE analysis and Navier–Stokes equations are used in CFD modelling. The interaction between these two equations are achieved through field dependent shear stress, which further influences the dynamic viscosity. The MR fluid flow in the MR damper is governed by Navier-Stokes equations (7.3) and (7.4) (Anderson, 1995, Sahin, 2003). The Maxwell equations are first solved to obtain the magnetic field and results are used as the input to the fluid dynamic problem by considering field dependent shear stress and dynamic viscosity. The non-depersonalized continuity and Navier-Stokes equations are given by,

Continuity equation:

$$\nabla \cdot U = 0 \quad (7.3)$$

Momentum equation:

$$\rho \frac{\partial U}{\partial t} + (U \cdot \nabla) \cdot U + \nabla P = \frac{\mu}{\rho} (\nabla^2 U) \quad (7.4)$$

Interaction between the Naiver–Stokes momentum (7.4) and Maxwell's equations is through dynamic viscosity, which can be expressed as

$$\rho \frac{\partial U}{\partial t} + \rho (U \cdot \nabla) \cdot U + \nabla P = \mu_m (\dot{\gamma}, \tau_b) (\nabla^2 U) \quad (7.5)$$

where, U is the velocity (m/s), μ_m is the dynamic viscosity (Pa-s), p is the static pressure (Pa), ρ is the fluid density (kg/m³) and $\dot{\gamma}$ is shear rate (1/s).

The shear stress transport (SST) k - ω model is used as the turbulence model (Menter, 1992, Arun and Tulapurkara, 2005). The sinusoidal motion of piston in the cylinder is achieved by writing sine function with the help of CEL and moving mesh option provides privilege for the motion of the piston. Newtonian and magnetized non-Newtonian region (shear flow gap) are specified by writing CFX command language (CCL), when the piston is under motion in the same computational domain. The magnetic dependent yield stress for the MR fluid is obtained using the curve fit equation (7.2) by substituting magnetic flux density. The predicted yield stress is substituted in the Bingham model to calculate the dynamic viscosity. The Bingham model is used to express the non-Newtonian region in the shear flow gap near the piston. Non-

Newtonian region is specified in terms of the variable dynamic viscosity and it can be obtained by using Bingham plastic model as shown in equation (7.6) (Wereley et al. 1998).

$$\mu_m = \frac{\tau_b}{\gamma} + \mu \quad \gamma \geq \gamma_c \quad (7.6a)$$

$$\mu_m = \mu_n \quad \gamma \leq \gamma_c \quad (7.6b)$$

where μ_m = Dynamic viscosity (Pa-s), τ_b = Magnetic dependent yield stress (Pa), γ = Shear strain rate (1/s), γ_c = Critical shear strain rate, μ_n = High viscosity (solid type)

In Bingham fluid model, fluid is (solid type) highly viscous in the region of pre-yield, where the shear strain rate is lesser than the critical shear strain rate. Observation showed that fluid started yielding as shear rate increased. When the shear strain rate meets critical value, viscosity of the fluid increases and fluid reaches plastic stage as shown in figure 7.5 (Susan-Resiga et al. 2009). Displacement (x) is specified by using equation (7.7) and force is calculated by integrating the entire pressure applied on the entire surface area of the piston head.

$$x = X_m \cos(\omega t_s) \quad (7.7)$$

where, X_m = Maximum displacement, t_s = Time step ω = Angular velocity = $2\pi f$, f = Frequency (Hz)

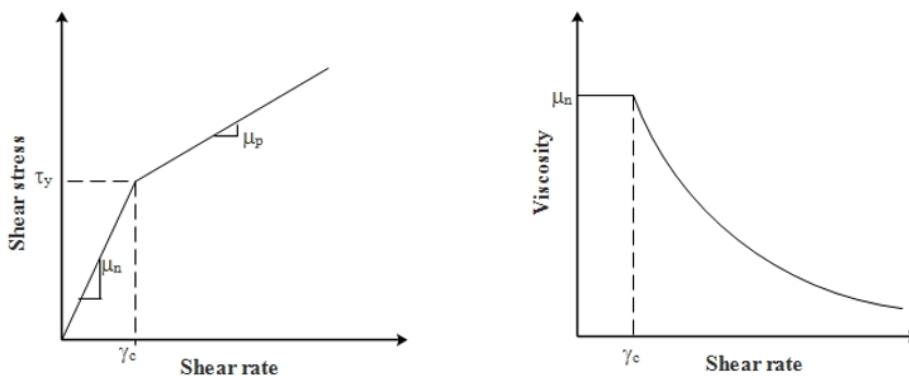


Figure 7.4 Bingham Model (Parlak et al. 2012)

Table 7.5 Mesh dependency check

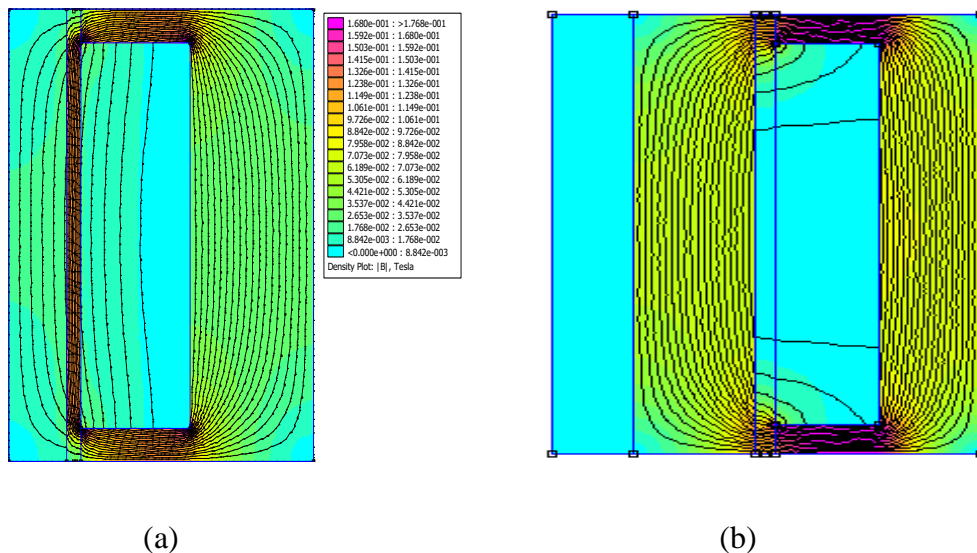
Mesh size	Number of elements	Average velocity (m/s ²)	Percentage change in velocity
Coarse	47,021	0.282	-
Medium	90,234	0.332	17.90
Fine	2,11,907	0.354	6.53

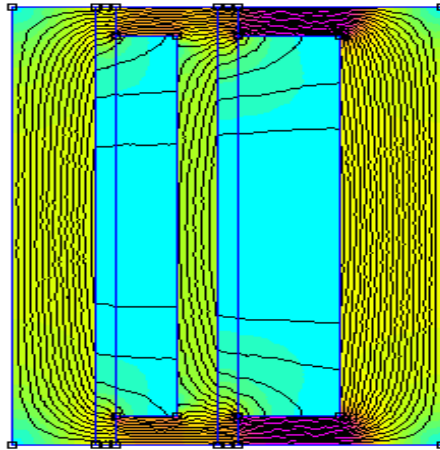
The convergence is verified by conducting sensitivity check and monitoring residual RMS error values (10×10^{-5}). Mesh dependency check is conducted for various mesh sizes in order to identify the appropriate mesh size. The details of the mesh dependency check are tabulated in table 7.5. The mesh dependency check was conducted and it was found that the percentage change in the velocity is significantly small (Table 7.5). Hence, fine mesh size was used for all the CFD analysis.

7.3 RESULTS AND DISCUSSION

7.3.1 Magnetostatic analysis results

The magnetostatic analysis is used for calculating the magnetic flux generated along the fluid flow gap. The magnetic flux lines and contour of magnetic flux density developed at the annular gap is illustrated in figures 7.5 (a) and (b) respectively.





(c)

Figure 7.5 Contours and magnetic flux lines induced for (a) Model-Shear, (b) Model-Flow and (c) Model-Mixed

The magnetic flux is computed for 0.1A to 0.5A current in steps of 0.1A. The induced magnetic flux for the respective current throughout the effective flow gap is depicted in figure 7.6.

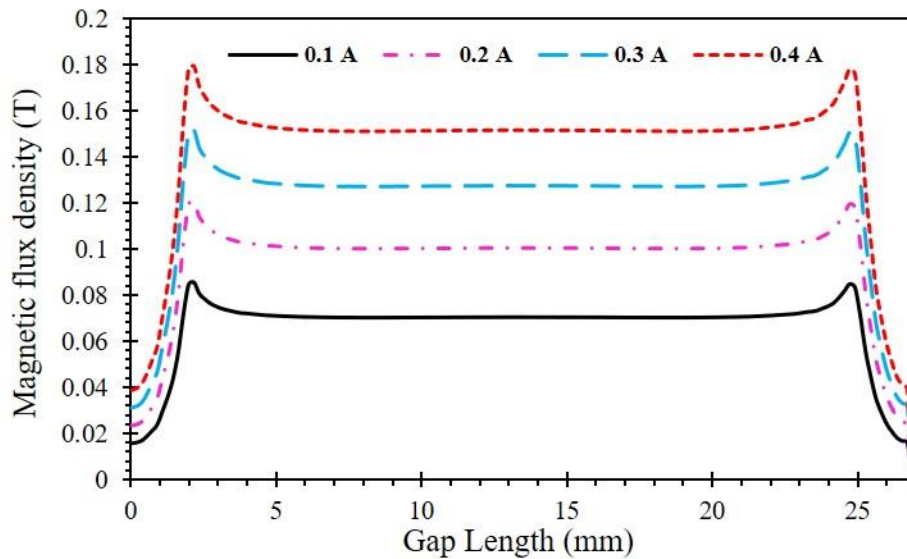


Figure 7.6 Magnetic flux density in the shear flow region of monotube MR damper for applied currents

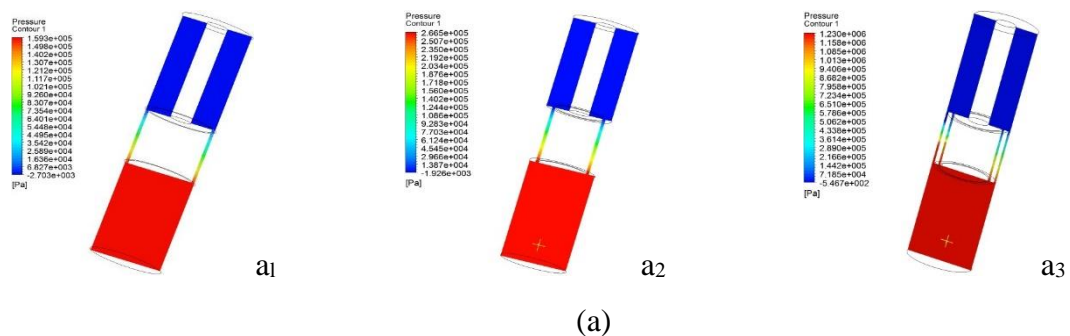
The yield stress of the MR fluid is dependent on the amount of magnetic flux developed. Field dependent yield stress values increases as the magnetic flux density increases. The magnetic dependent yield stress is calculated using the equation (7.2). The maximum magnetic flux density induced for the higher value of DC current is higher at the web of the piston head, which is due to higher value of magnetic permeability of the piston head material (SA1018) than the MR fluid. The respective change in the yield shear stress of the MR fluid with the magnetic flux is illustrated in table 7.6.

Table 7.6 Magnetostatic analysis results of Monotube MR damper

DC Current (A)	0.5	0.4	0.3	0.2	0.1
Magnetic flux density (T)	0.155	0.14	0.126	0.11	0.094
Yield stress (Pa)- τ_B	4087	3528	3033	2503	2012

7.3.2 CFD analysis results

The computational fluid dynamic analysis was conducted to predict the dynamic behaviour of MR damper under different input conditions. The force versus displacement curve was evaluated for different DC currents. The analysis was carried out for frequencies from 0.5 Hz to 3 Hz at constant piston displacement/ stroke length of 10 mm. Figure 7.7 (a) and (b) depicts the pressure variation and velocity stream lines at the plane when the piston is under downward motion. Figure 7.8 (a) and (b) shows pressure variation and velocity stream lines at the plane, when the piston is under upward motion.



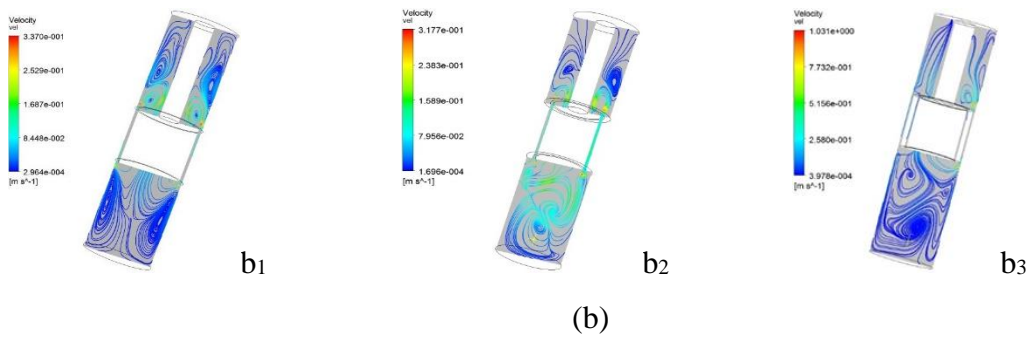


Figure 7.7. Contours under downward motion (a₁, a₂, a₃) Pressure contours (b₁, b₂, b₃)

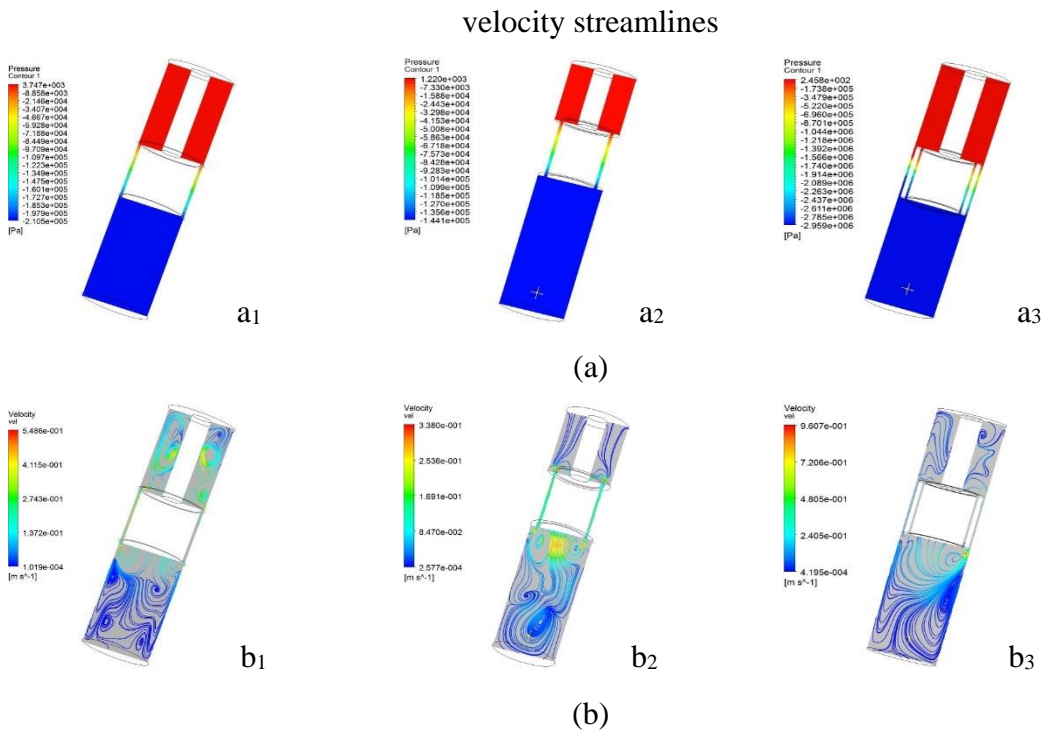


Figure 7.8 Contours under upward motion (a₁, a₂, a₃) Pressure contours (b₁, b₂, b₃) velocity streamlines respectively

7.3.3 Validating the CFD results with experimental results of monotube MR damper

The force versus displacement curves obtained from computational fluid dynamic results were compared with experimental ones. The computed analysis forces were in good agreement with the measured values. The force versus displacement curves were obtained for 1.5 and 2 Hz frequencies. Figure 7.9 and 7.10 shows the comparison of force versus displacement curve obtained for 1.5 Hz and 2 Hz frequencies respectively. The flow of fluid in this damper is of shear mode type. When the fluid gets excited due

to magnetic field, the ferrous particle gets polarised to form a chain like structure. The particle chains are broken and reformed, when the piston is under motion. These chain structures oppose the fluid flow in the annular gap and the chain become stronger under higher magnetic flux. Hence, the force developed in the damper is more at the higher values of magnetic flux developed due to DC current applied. The force induced in the damper represents its dynamic performance.

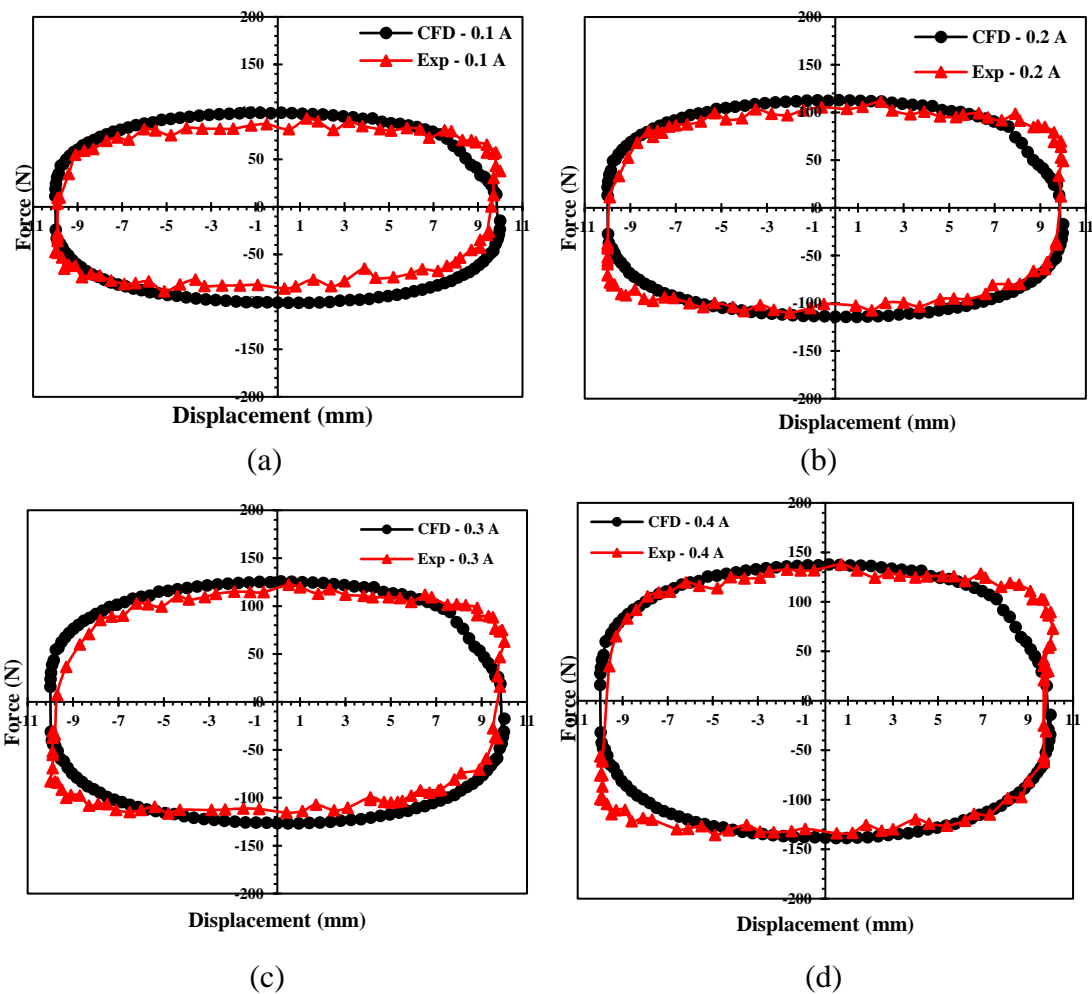


Figure 7.9 Force v/s Displacement plot for MR damper at 1.5 Hz frequency for different currents (a) 0.1 A, (b) 0.2 A, (c) 0.3 A and (d) 0.4 A

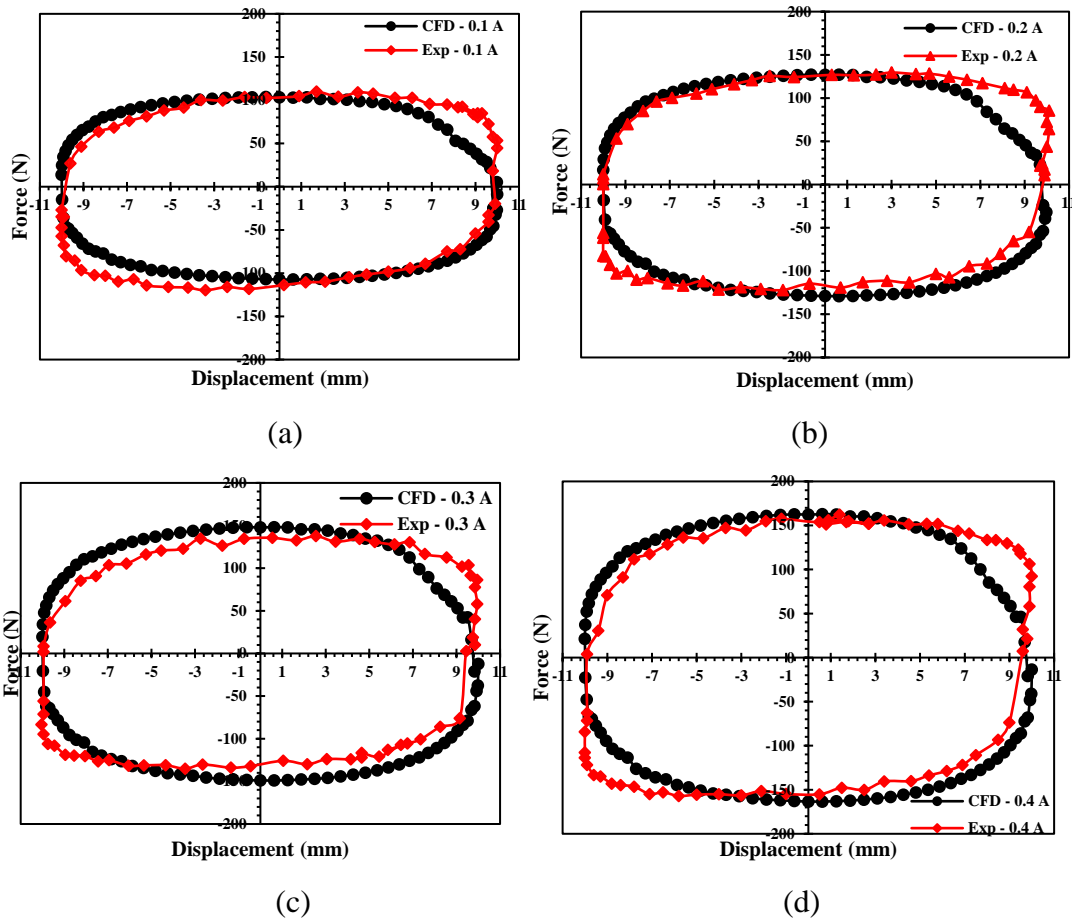
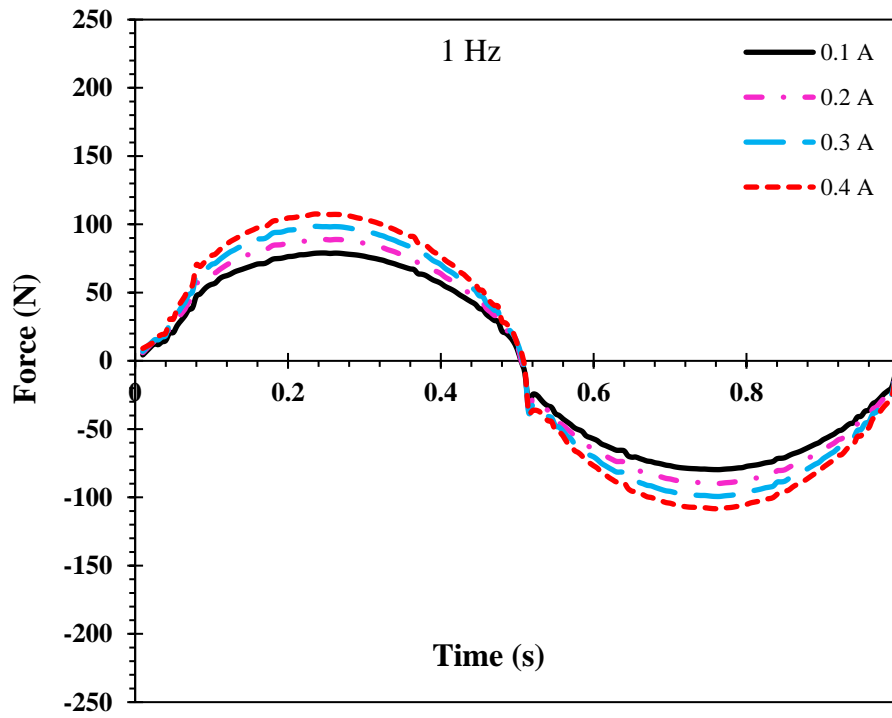


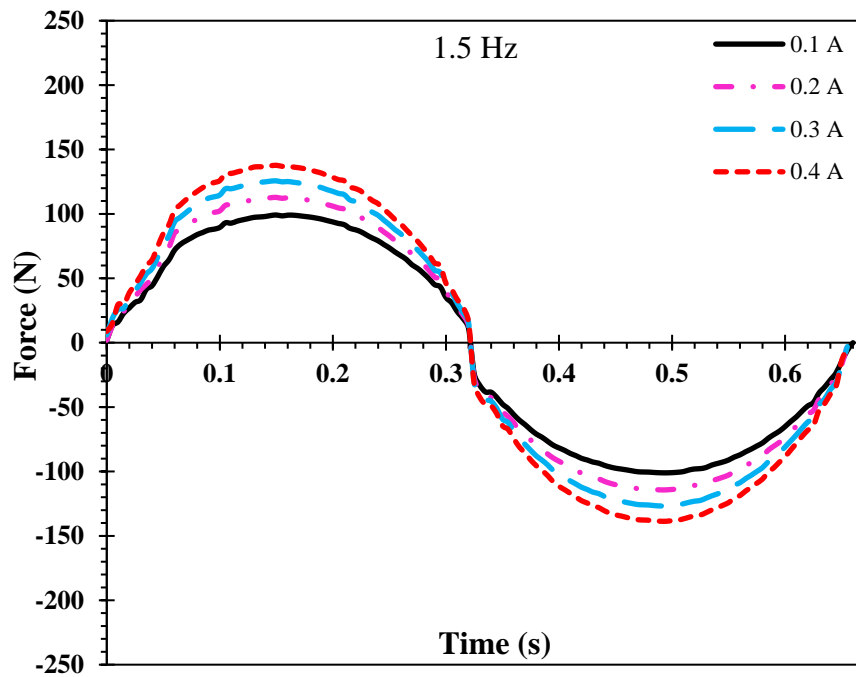
Figure 7.10 Force v/s Displacement plot for MR damper for 2 Hz frequency (a) 0.1 A, (b) 0.2 A, (c) 0.3 A and (d) 0.4 A

7.3.4 Influence of the frequency on damping force (using CFD analysis)

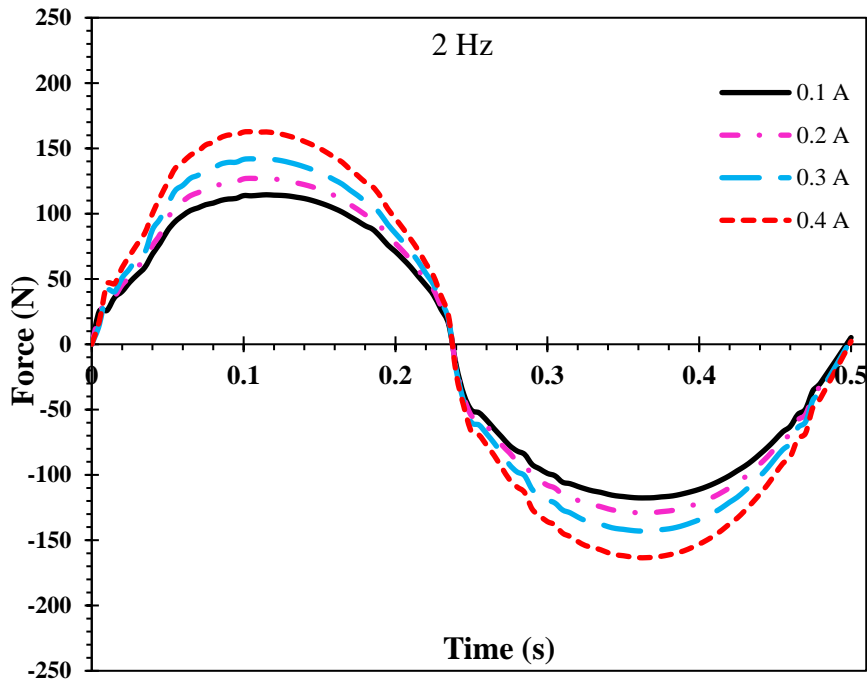
Damping force versus time domain were estimated and plotted for 1 Hz to 3 Hz frequencies in steps of 0.5 Hz as shown in figure 7.11 (a) to (e). The force increases with DC current as well as frequency of operation. The maximum force induced in the damper is 190.25 N at 0.4 A DC current and 3 Hz frequency, while the maximum force for 0.1A DC current is 110.2 N. From results of analysis, it is clear that obtained damping forces at 2.5 Hz and 3 Hz frequency are very close to each other for all values of DC current. It was noted that the change of damping force decreased considerably at higher frequencies.



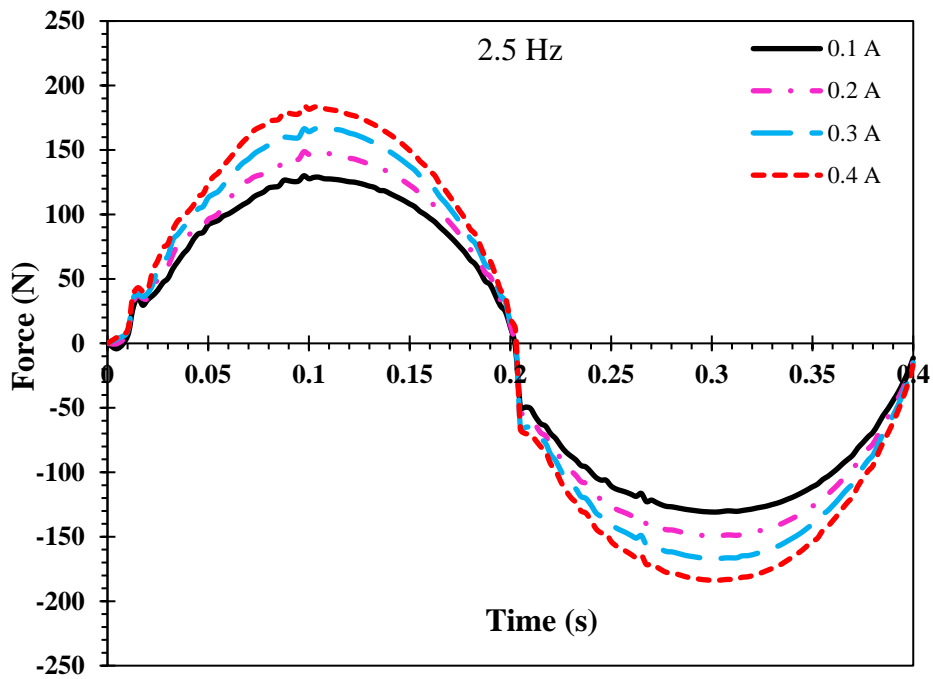
(a)



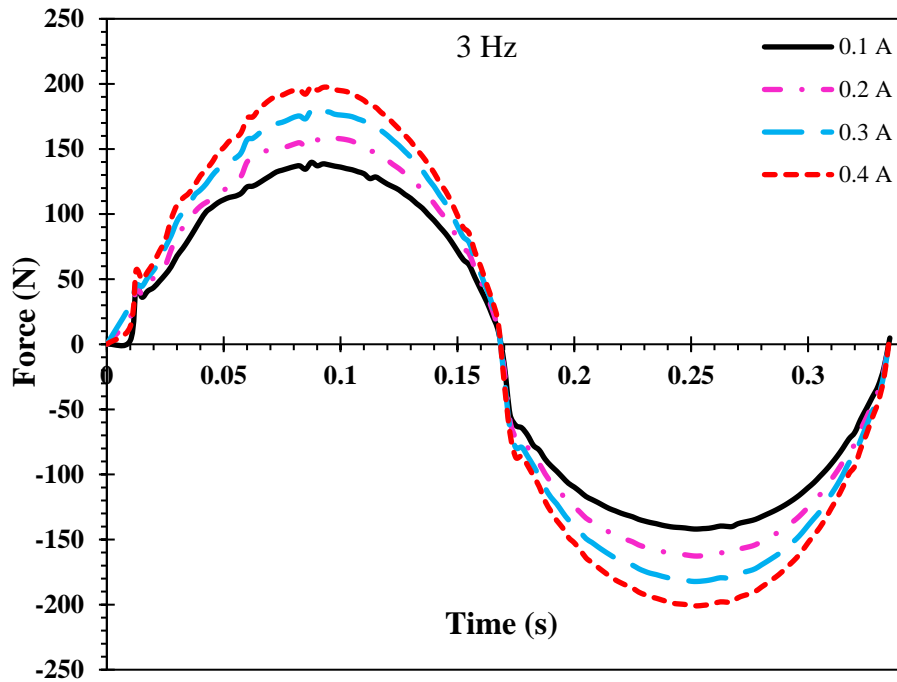
(b)



(c)



(d)



(e)

Figure 7.11 Force versus time history curve of monotube MR damper at (a) 1 Hz, (b) 1.5 Hz, (c) 2 Hz (d) 2.5 Hz and (e) 3 Hz frequency

7.3.5 Influence of effective gap length on damping force (using CFD analysis)

The effective area in the damper where MR fluid is subjected to magnetic field is fluid flow gap between piston head and cylinder. The effect of fluid flow gap was investigated by varying the length from 15 mm to 35 mm in steps of 5 mm using CFD analysis. With increase in the length of the annular gap, the fluid exposure to the magnetic field is more. Due to this, the particle chain formation and the resistance to the fluid flow increases. Hence, the force developed in the damper increases with the effective area/length, as shown in figure 7.12. A higher dynamic range can be seen at 35 mm length of annular gap. On comparison, it was observed that the force developed for 35 mm length provided 1.72 times the force induced for 15 mm length of annular gap.

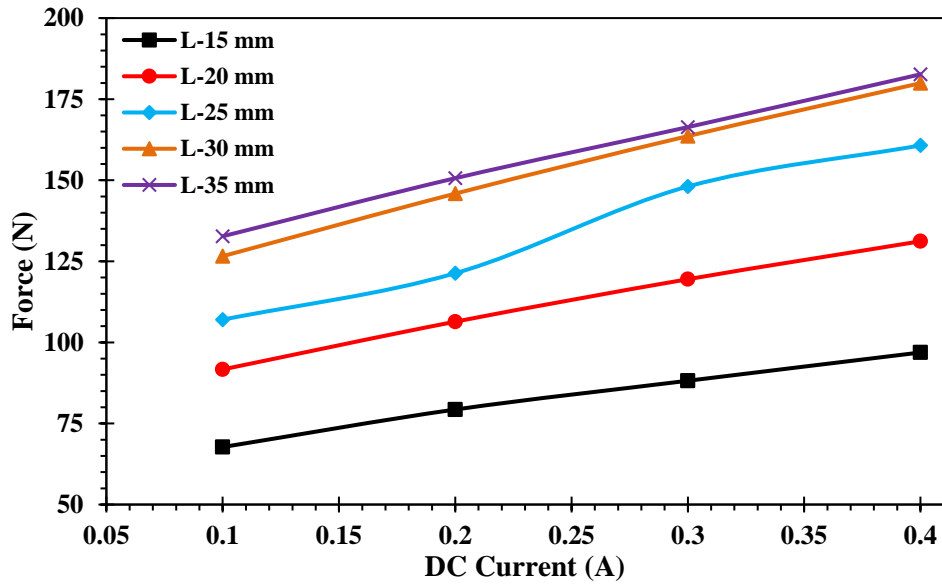
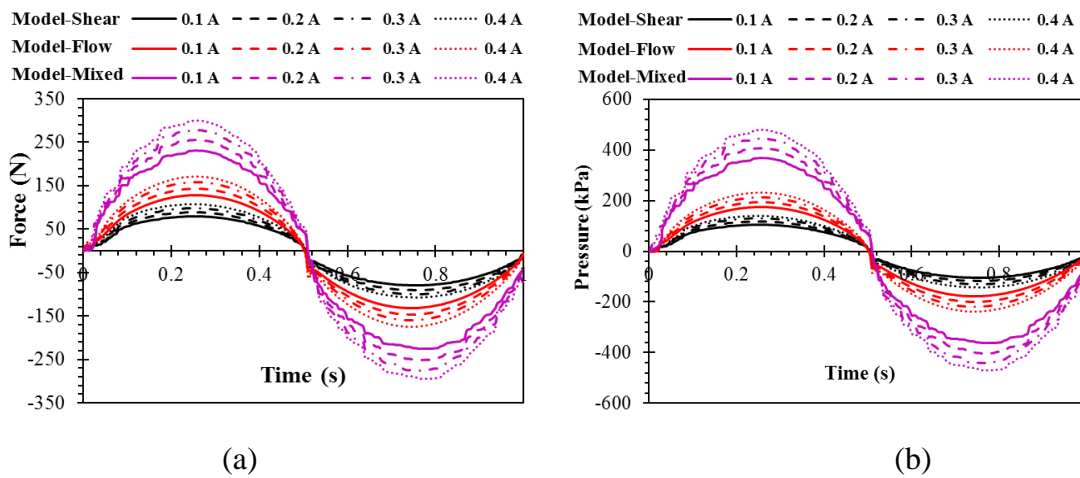


Figure 7.12 Effect of fluid flow gap length

7.3.6 Comparison of modes of MR damper

The pressure created in the MR damper cylinder is estimated for each of the proposed model under lower current ranges. Figures 7.13 (b), (d) and (f) shows variation of pressure with respect to time domain while piston is under sinusoidal movement inside the cylinder at 1 Hz, 2 Hz and 3 Hz frequency respectively.



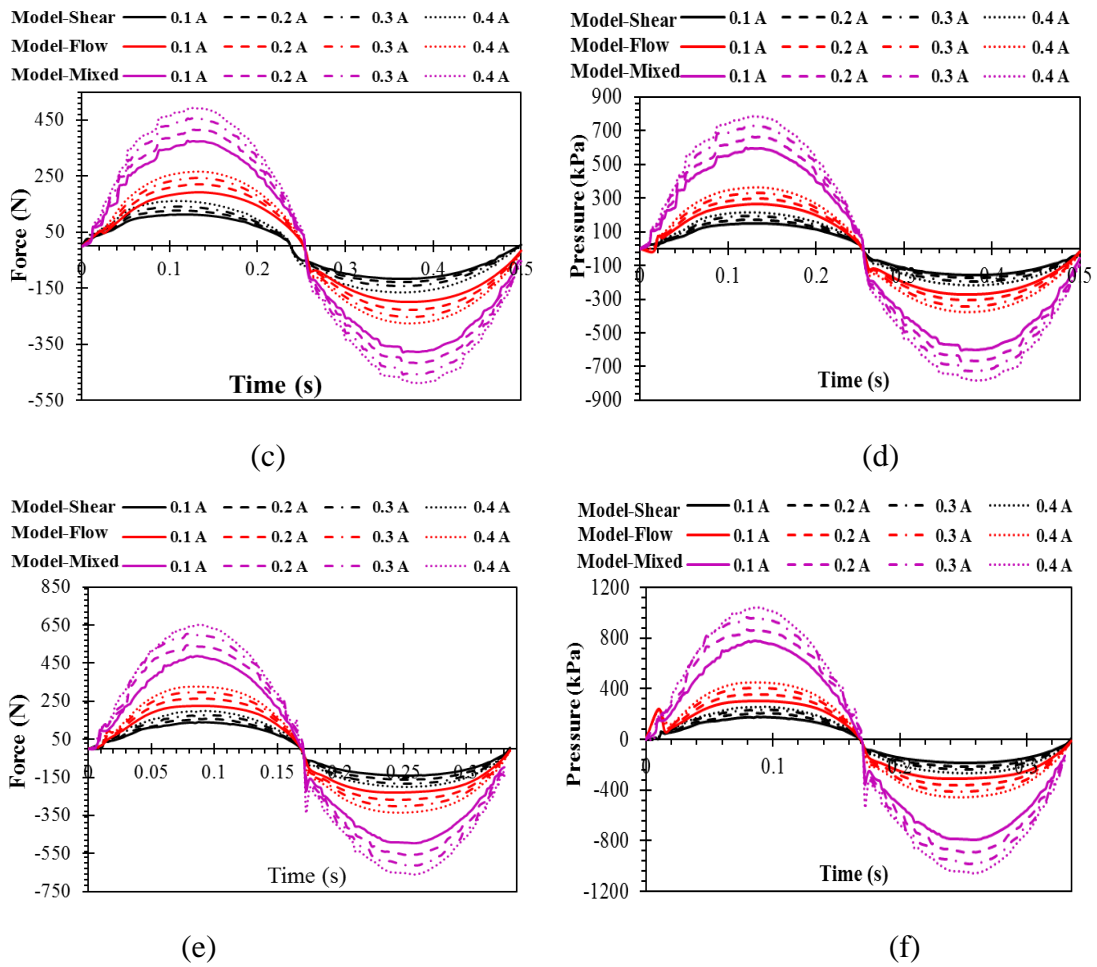


Figure 7.13 Force and Pressure variation with respect to time in cylinder of MR damper (a, b) 1 Hz, (c, d) 2 Hz and (e, f) 3 Hz for all three models

The pressure in the cylinder chamber is dependent on the yield stress induced due to magnetic flux in the annular flow gap. The change in rheological properties of MR fluid under magnetic field offers resistance to flow of fluid through the annular gap, resulting in increase of pressure. As illustrated in figure 7.13, the pressure generated for 0.4 A current is higher than for 0.1 A in all three models. Figure 7.13 (a), (c) and (e) depict the force developed with time for different frequencies and currents. It can be observed that the force induced in the negative cycle with a sinusoidal motion of piston is slightly more than the force induced in positive cycle. Since the force induced in the damper is a product of area of piston head and the pressure, area of piston head exposed to the pressure under the negative cycle is more than that in the positive cycle. The force and

pressure developed in the cylinder chamber of *model-mixed* are significantly higher than the other two models.

Figure 7.14 (a), (b), and (c) are equivalent damping plots for *Model-Shear*, *Model-Flow* and *Model-Mixed* dampers respectively. It can be seen that, '*Model-Mixed*' equivalent damping force is much higher than that of other two models. However, the equivalent damping increases with current applied and decreases as the frequency increases in each case. The equivalent damping is depending on the energy dissipated in the damper for that particular input and it is directly proportional to it (equation 7.8).

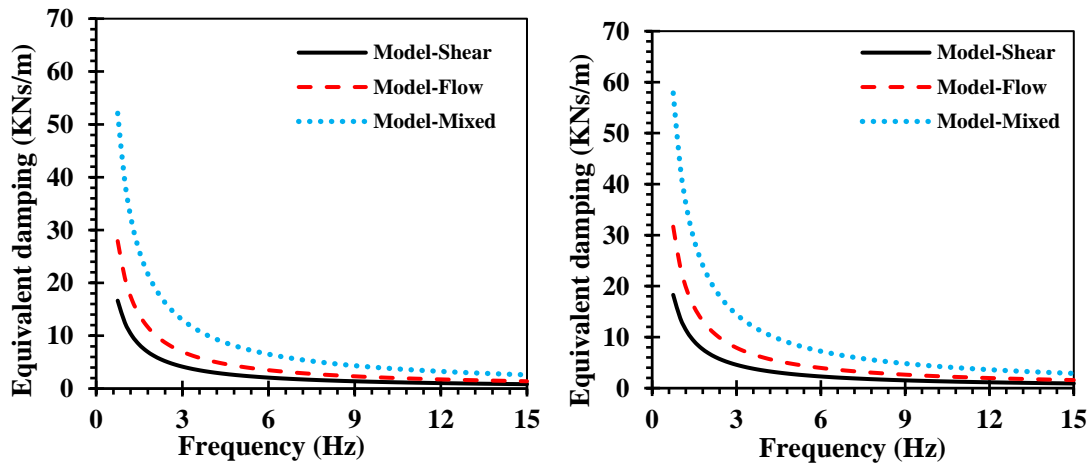
The on-state equivalent damping (C_e) is represented as (Snyder et al. 2001),

$$C_e = \frac{E_d}{\pi f A^2} \quad (7.8)$$

$$E_d = \int F(t) du \quad (7.9)$$

where A = amplitude of displacement, f = frequency, F = damping force, E_d = Energy dissipation, u = displacement.

The energy dissipation in '*Model-Mixed*' is 2.95 times more than that of *Model-Shear* and 1.78 times that of '*Model-Flow*' at 0.4 A current. Since *Model-Mixed* has higher energy dissipation, the equivalent damping is highest for *Model-Mixed*. The energy dissipation of three models at different currents is illustrated in figure 7.14 (e)



(a)

(b)

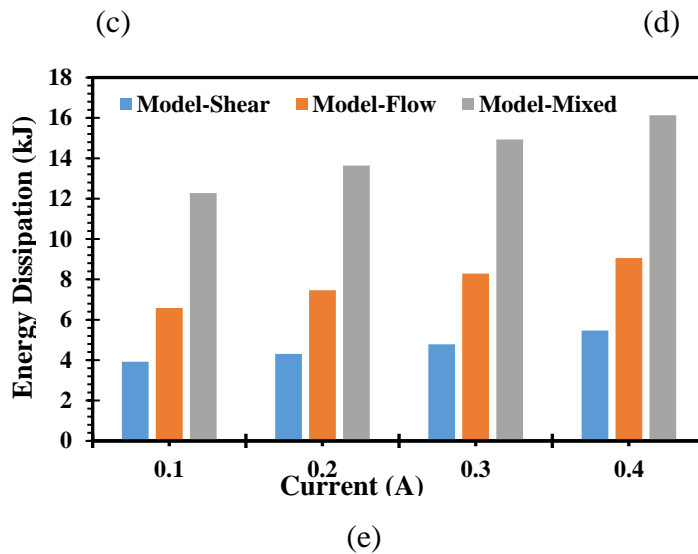
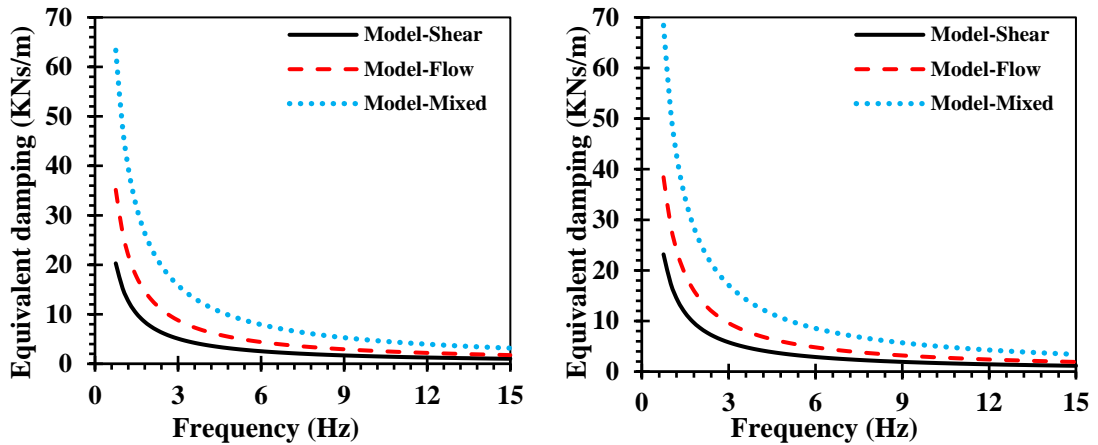


Figure 7.14 Equivalent damping for (a) 0.1 A, (b) 0.2 A, (c) 0.3 A, (d) 0.4 A and (e) Energy dissipation for three damper models

7.4 SUMMARY

The characterization of shear mode type monotube MR damper through computational approach was discussed and elaborated. A coupled FEA and CFD analysis was used for estimating the magnetic flux density and damping force for different currents. The characteristics such as damping force versus displacement, equivalent damping, energy dissipation was also estimated. The credibility of the shear mode monotube MR damper analysis results were validated with experimental results and found good agreement. Later, performance of flow and mixed mode MR dampers was carried out and compared the variations in the damping characteristics under different inputs with shear mode

damper. The mixed mode damper was realized by combining the flow and shear mode operations. Results showed that combination of two modes of operation could enhance the damping force to a significant level.

CHAPTER 8

DYNAMIC ANALYSIS OF A VEHICLE WITH SEMI-ACTIVE SUSPENSIONS SYSTEM

8.1 INTRODUCTION

In the previous chapter, characteristics curves of shear mode monotube MR damper were evaluated under different input currents using computational and experimental methods. In this chapter, by utilizing these characteristic curves, non-parametric models representing the hysteresis behavior of MR damper are developed. These models are incorporated into quarter car and three-wheeler passenger vehicle as semi-active suspensions. The dynamic behavior of quarter car and three-wheeler semi-active suspension system subjected to random road profile is evaluated. The road holding and ride comforts of passive and semi-active suspensions systems are also compared.

8.2 NON-PARAMETRIC MODELLING OF MR DAMPER

The non-parametric approach can be employed to formulate a representative model of MR damper which could exhibit the exact behavior. In this work, a non-parametric polynomial equation is formulated using the computational results of the MR damper. The damping characteristic is evaluated through coupled FE and CFD analysis. The obtained results are validated with experimental results. Later, the using least square curve fitting method, a polynomial equation and its coefficients are evaluated. This mathematical equation builds a relationship between the damping force and the applied current. The passive damper in quarter car suspension is replaced with this non-parametric model to estimate the dynamic performance the vehicle under random road excitation. Also, ride comfort and road holding of the three-wheeler vehicle with this MR damper was evaluated. The methodology of non-parametric modeling is as shown in figure 8.1.

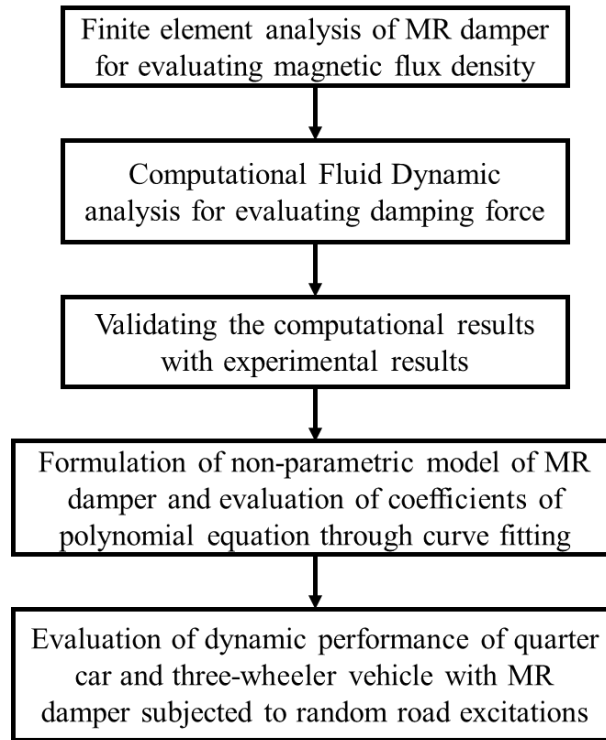


Figure 8.1 Non-parametric modelling flow chart

A non-parametric force model was developed from the results obtained from the CFD analysis. The least square curve fit function was used for extracting the force model, as a function of DC current. The polynomial model was used to express force as the function of current (I) applied to MR damper (F_d). Damper force curve is fitted by polynomial with sinusoidal displacement function, ($x= a.\cos(2\pi ft)$)

$$F_d = \sum_{i=0}^n (c_i I^i) x \quad (8.1)$$

where, n is the order of polynomial and third order polynomial function was considered to establish a relation between the damping force and applied current as given in equation 8.2.

$$F_d (I) = (c_1 I^3 + c_2 I^2 + c_3 I + c_4) \quad (8.2)$$

where, I is the applied current in ‘A’ and the coefficients of the force model are obtained from least square curve fit method using MATLAB. The obtained values are given in table 8.1.

Table 8.1 Coefficient of polynomial equation

Parameters	Value	
	Shear mode	Mixed mode
c_1	150	175.3
c_2	- 22.5	- 263.4
c_3	407.15	277.3
c_4	336.2	68.17

8.2.1 Random road profile model

When a vehicle travels at a constant velocity, the road roughness is viewed as stationary process in spatial domain. The power spectral density (PSD) of road roughness in spatial domain can be expressed as (He et al. 2008),

$$G_q(\Omega) = G_q(\Omega_0) \left(\frac{\Omega}{\Omega_0} \right)^{-2} \quad (8.3)$$

where, $G_q(\Omega)$ is the spatial power spectral density, $G_q(\Omega_0)$ is coefficient of road roughness, Ω is spatial angular frequency and Ω_0 is the reference spatial angular frequency.

The power spectral density (PSD) corresponding to the road excitation being the response of the first order linear filter to white noise excitation and road roughness is given by (He at al. 2008),

$$\dot{Z}_r(t) + 2\pi un_0 Z_r(t) = \sqrt{G_q(\Omega_0)u} w(t) \quad (8.4)$$

where, $Z_r(t)$ is road roughness amplitude, u is the vehicle forward velocity, $w(t)$ is the white noise signal whose power spectral density is unity, and n_0 is reference spatial angular frequency.

Based on the pavement roughness, International Organization for Standardization (ISO-8606) classified roads into 8 classes, indicated by letters A-H. Among those A-E classes are for hard surface road and its roughness values are given in Table 8.2 (Tyan et al. 2009, Barbosa, 2011).

Table 8.2 Road roughness detail

Degree of road roughness $G_q(\Omega_0)$ ($10^{-6}\text{m}^2/(\text{rad/m})$)	
Road classes	Geometric mean
A (very good road)	16
B (Good road)	64
C (Average road)	256
D (Poor road)	1024
E (Very poor road)	4096

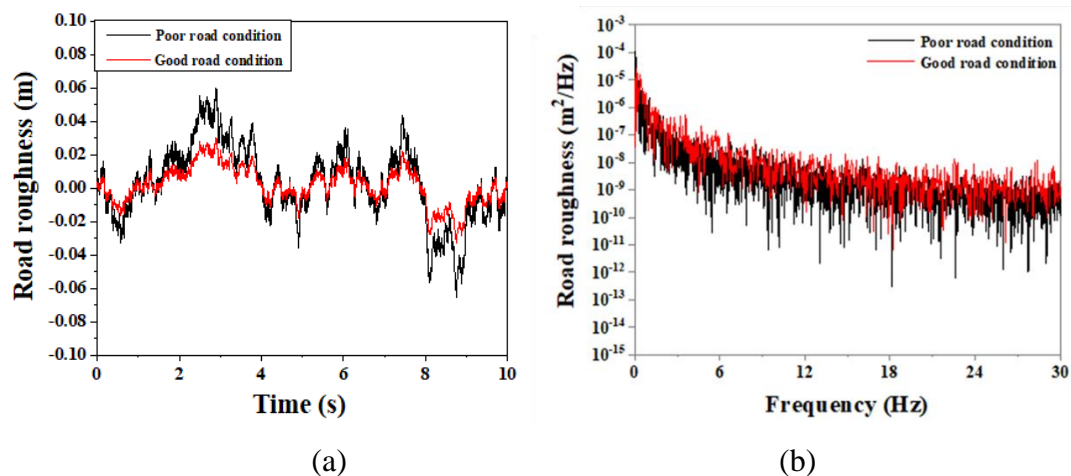


Figure 8.2 Random road roughness profile in (a) Time domain and (b) PSD

In this research work, poor and good road conditions (B and D-level road) were considered to evaluate the performance of vehicle models. Figure 8.2 shows the random

road roughness profile in time domain and its PSD, when vehicle speed is at 25 m/s on B and D level road.

8.2.2 Performance indices

Performance indices help to evaluate the quality of the suspension system and these can be estimated by considering ride comfort and road holding capabilities of the suspension system. Ride comfort is strongly related to the acceleration of the vehicle body and road holding is directly related to the variation of vertical tyre force. The performance index for ride comfort and road holding are formulated as follows (Jonasson and Roos, 2008).

$$P_{\text{comfort}} = \frac{|\ddot{x}_{\text{semi-active}}|_{\text{RMS}}}{|\ddot{x}_{\text{Passive}}|_{\text{RMS}}} \quad (8.5)$$

$$P_{\text{Road holding}} = \frac{|F_{t, \text{semi-active}}|_{\text{RMS}}}{|F_{t, \text{Passive}}|_{\text{RMS}}} \quad (8.6)$$

where, F_t is vertical tyre force and \ddot{x} is sprung mass acceleration.

If the performance index $P_{\text{comfort}}/P_{\text{Road holding}} < 1$, then the performance of semi-active suspension system is considered to be of superior quality when compared to passive suspension system.

8.3 MATHEMATICAL MODELING OF VEHICLE

The performance of MR damper used as a semi-active suspension element with suitable control strategy has been analyzed using a mathematical modelling of vehicles such as quarter car and three-wheeler vehicle model subjected to stationary random road excitation.

8.3.1 Semi-active control strategies

The performance of semi-active suspension system is based on the type of control strategy used. The main aim of semi-active control strategy is to minimize the acceleration of vehicle body and tire deflection in order to provide safety and ride

comfort against road disturbance. Proportional Integral Derivative (PID) control strategy is used for analysis of the dynamic performance of the MR damper incorporated in the three-wheeler vehicle model in mitigating the vibration and enhancement of road holding and ride comfort. And, fuzzy logic controller is employed for dynamic analysis of quarter car vehicle suspension system.

8.3.1.1 Fuzzy logic control strategy

The control structure for quarter car model with fuzzy logic controller is as shown in Figure 8.3. Fuzzy logic control algorithm is mostly used in the control of automotive instruments and machines. The fuzzy logic control algorithm is adaptive in nature as they provide robust performance under variation in parameter and load disturbance effect. Fuzzy controller is based on conditional statements and its control rules are defined based on human experience. Fuzzy controllers are widely used in the automotive industry. Automatic transmissions, anti-braking system, (ABS) and cruise control systems are frequently based on this paradigm of control theory. The idea of fuzzy control is to operate on rules which are human-readable and this represents a human's heuristic knowledge about how to control a process (Slaski and Maciejewski 2011).

Table 8.3 Fuzzy rules

Relative Velocity, ($\dot{x}_1 - \dot{x}_2$)	Sprung Mass Velocity, \dot{x}_1				
	NL	NM	S	PM	PL
NL	PL	PL	PL	PM	S
NM	PL	PL	PM	S	NM
S	PL	PM	S	NM	NL
PM	PM	S	NM	NL	NL
PL	S	NM	NL	NL	NL

Design of fuzzy logic controller consists of the following three steps (Stribrsky et al. 2003). First is fuzzification stage, which changes input values (crisp) into fuzzy values. The input must always be a numerical value and has to be fuzzified. For the input and

output variables a triangular membership functions are employed. Fuzzy inference is the second step which processes the input data with the rule base to produce fuzzy outputs. 25 rules are used in this study.

Table 8.3 shows the proposed rules for controller. Final step is defuzzification, where the defuzzifier is responsible for the conversion of fuzzy inference input to a crisp set of output values. Centroid method was used for defuzzification stage. Figure 8.3 shows the application of fuzzy logic controller in semi-active quarter car model with MR damper. Two input variables are taken for the controller.

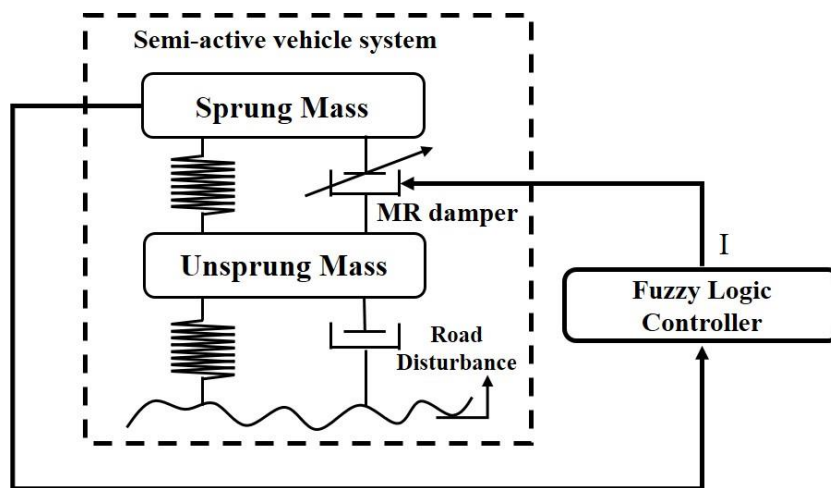
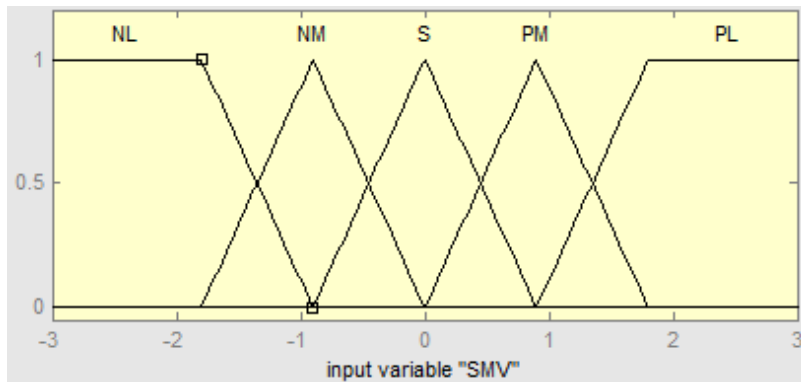


Figure 8.3 Control structure for quarter car model with fuzzy logic controller

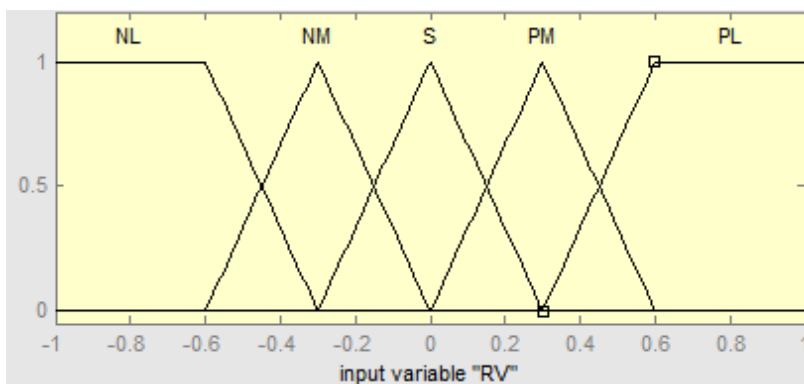
For fuzzy logic controller, the input variables are relative velocity between sprung and unsprung mass and sprung mass velocity. The linguistic variables are used to denote the inputs and output, in the form of fuzzy sets. They are “Negative Large” (NL), “Negative Medium” (NM), “Small” (S), “Positive Medium” (PM) and “Positive Large” (PL). The input range selected for relative velocity between sprung mass and unsprung mass is [-3 to 3] and the input range selected for sprung mass velocity is [-1 to 1]. Similarly, output range selected for current is [-0.5 to 0.5]. These ranges are indicated in figure 8.4 with their respective membership functions. There are 25 rules in the rule base as shown in Table 8.3. The general form of the rules of the fuzzy logic controller is given below.

$$\text{IF } (\dot{x}_s - \dot{x}_u) \text{ AND } (\dot{x}_s) \text{ AND } (\ddot{x}_s) \text{ THEN } (I)$$

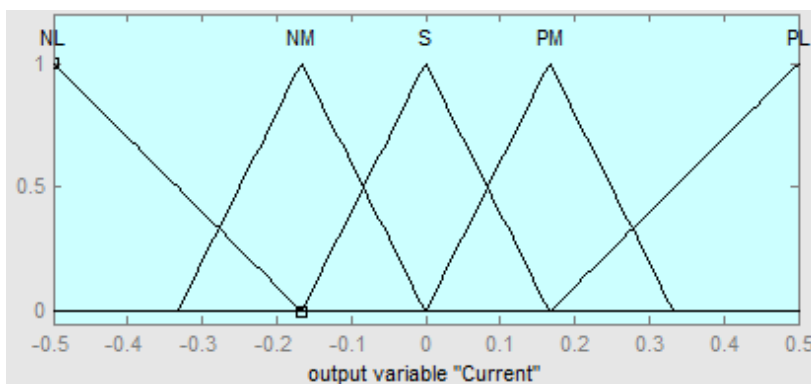
where, \dot{x}_s is the sprung mass velocity, \dot{x}_u is unsprung mass velocity, \ddot{x}_s is sprung mass acceleration and I is the current output from controller to the MR damper.



(a)



(b)



(c)

Figure 8.4 Fuzzy membership functions (a, b) Input membership and (c) Output membership

8.3.1.2 Proportional-Integral-Derivative (PID) control strategy

PID controller is used to increase the ride comfort and road holding performance of the three-wheeler car model. The PID controller consists of three different parameters such as proportional (P), integral (I) and derivative (D), which are used to decrease the rise time, eliminate the steady state error, decrease the settling time and overshoot of the system. PID controller is a closed loop feedback control system which is used to minimize the error value between a measured process variable and a desired set point (Gaur and Sheilza, 2013). The PID control strategy is given in equation (8.7).

$$u(t) = K(p)e(t) + K(i) \int_0^t e(t)dt + K(d) \frac{de(t)}{dt} \quad (8.7)$$

where, $u(t)$ is control signal, $K(p)$ is proportional co-efficient, $K(i)$ is integral co-efficient, $K(d)$ is derivative co-efficient and $e(t)$ is error signal.

The relative displacement between sprung and unsprung masses is given as input to the PID controller. The control structure for three-wheeler car model with PID controller is as shown in Figure 8.5.

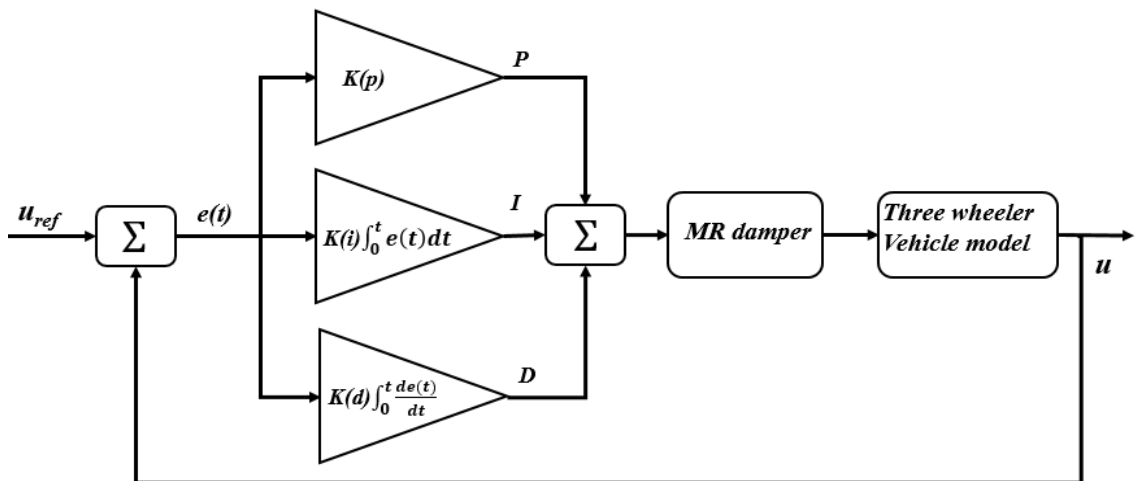


Figure 8.5 Control structure for three-wheeler car model with PID controller

In PID controller, better control action on the system can be achieved by tuning the parameters of the controller. Parameters of the PID controller are dependent on

each other. If one of the parameters value changes, it affects the other two parameters. The manual tuning method is adapted for getting optimal parameters of PID controller which are given in Table 8.4.

Table 8.4 Optimal parameter of PID controller

Parameters	$K(p)$	$K(i)$	$K(d)$
Value	10	0.05	15

8.3.2 Dynamic analysis of quarter car model

The vertical vibration of a vehicle represented by a quarter car model consists of sprung and unsprung masses. Two-degrees of freedom quarter car model was considered for non-parametric modelling under vertical motion as illustrated in figure 8.6. The parameters involved in the analysis are sprung mass (M_1) which represents 1/4 of the body of the vehicle, the unsprung mass (M_2) which represents one wheel of the vehicle, stiffness of suspension system (K_1), stiffness of tyre (K_2), damping coefficient of suspension system (C_1), damping coefficient of tyre (C_2) and variable damper force (F_d). The vertical motions are displacement of sprung mass (x_1), displacement of unsprung mass (x_2) and road disturbance (x_r). Table 3.3 provides the parameters of suspension system used in the quarter car model (Ansar et al. 2014).

Following are the equations of motion for quarter car model with passive suspension

Sprung mass bounce

$$M_1 \ddot{x}_1 + K_1(x_1 - x_2) + C_1(\dot{x}_1 - \dot{x}_2) = 0 \quad (8.8)$$

Unsprung mass bounce

$$M_2 \ddot{x}_2 + C_1(\dot{x}_1 - \dot{x}_2) + C_2(\dot{x}_2 - \dot{x}_r) + K_1(x_2 - x_1) + K_2(x_2 - x_r) = 0 \quad (8.9)$$

The equations of motion for semi-active suspension system can be obtained using Newton's second law of motion, as described below.

Unsprung mass bounce,

$$M_2\ddot{x}_2 + C_2(\dot{x}_2 - \dot{x}_r) + K_2(x_2 - x_r) - K_1(x_1 - x_2) - F_d = 0 \quad (8.10)$$

Sprung mass bounce,

$$M_1\ddot{x}_1 + K_1(x_1 - x_2) - F_d = 0 \quad (8.11)$$

where, \ddot{x}_1 = Acceleration of sprung mass, F_d = Damping force, \ddot{x}_2 = Acceleration of unsprung mass, \dot{x}_2 = Velocity of unsprung mass, \dot{x}_r = velocity of road disturbance

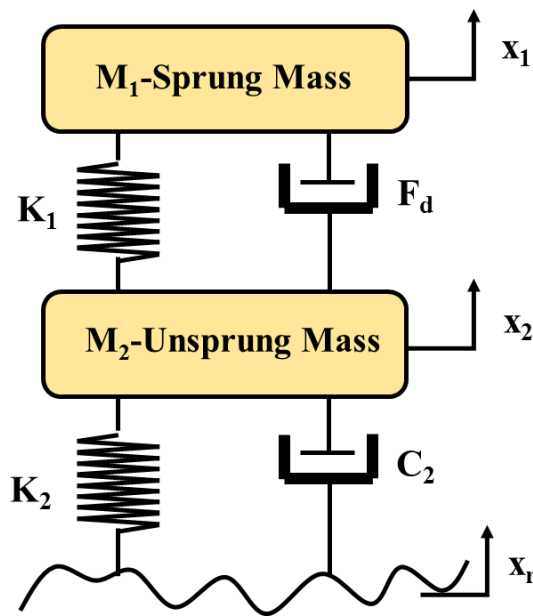


Figure 8.6 Quarter car model with semi-active suspension

The above equation can be written in the form of state space variables given by

$$\begin{cases} \dot{x} = Ax + Bu \\ y = Cx + Du \end{cases} \quad (8.12)$$

where,

$$x = [x_1 \quad x_2 \quad \dot{x}_1 \quad \dot{x}_2]^T \quad u = [F_d \quad x_r \quad \dot{x}_r]^T$$

$$A = \begin{bmatrix} 0 & 0 & 1 & 0 \\ 0 & 0 & 0 & 1 \\ -\frac{K_1}{M_1} & \frac{K_1}{M_1} & 0 & 0 \\ \frac{K_1}{M_2} & -\left(\frac{K_1+K_2}{M_2}\right) & 0 & \frac{-C_2}{M_2} \end{bmatrix} \quad B = \begin{bmatrix} 0 & 0 & 0 \\ 0 & 0 & 0 \\ -\frac{1}{M_1} & 0 & 0 \\ \frac{1}{M_2} & \frac{K_1}{M_2} & \frac{C_2}{M_2} \end{bmatrix}$$

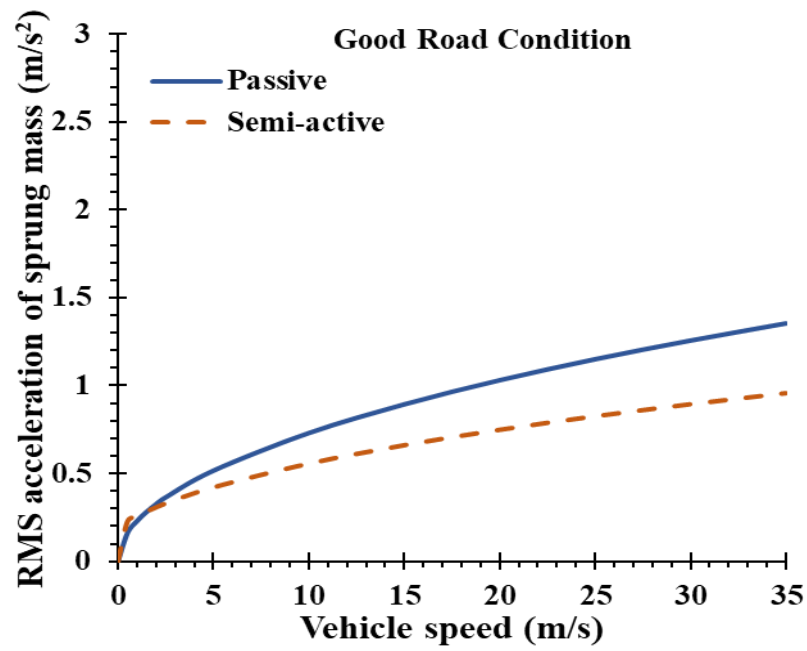
$$C = [1 \quad -1 \quad 0 \quad 0] \quad D = [0 \quad 0 \quad 0]$$

Table 8.5 Parameters of quarter car suspension system (Ansar et al. 2014).

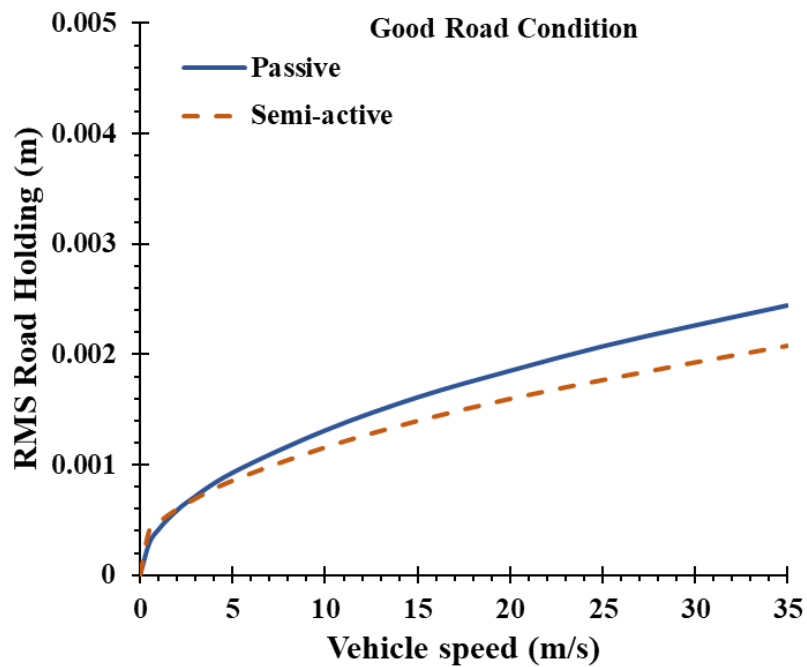
Parameters	Value
Sprung mass (M ₁)	535 kg
Unsprung mass (M ₂)	40 kg
Spring stiffness (K ₁)	96000 N/m
Tire stiffness (K ₂)	350000 N/m
Suspension damping coefficient (C ₁)	3002.3 N. s/m
Tire damping coefficient (C ₂)	300 N.s/m

8.3.2.1 Dynamic response analysis of quarter car model subjected to random road

The performance evaluation of a vehicle with MR damper and passive suspensions subjected to different random road profile were carried out under different velocities. The RMS acceleration and relative displacement between sprung and unsprung masses are indicators of the ride comfort and road holding of a vehicle respectively. Hence, evaluations of ride comfort and road holding ability of the vehicle suspension are performed. Figures 8.7 (a) and (b) show the root mean square (RMS) acceleration of sprung mass versus velocity and RMS road holding versus velocity of a vehicle respectively for passive and MR damper suspension system under good road (Class B) condition. Figures 8.8 (a) and (b) depict the RMS acceleration and road holding versus velocity under poor road (Class D) condition. In case of good road condition, it was observed that the MR damper suspension had 29 % reduction in sprung mass acceleration and 14.81 % reduction in RMS road holding compared to that of vehicle with passive suspension system.

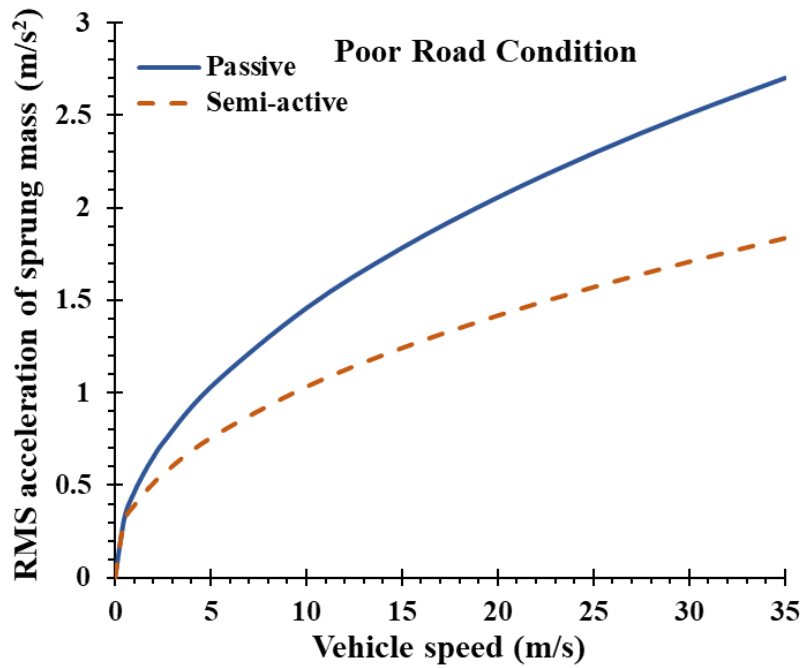


(a)

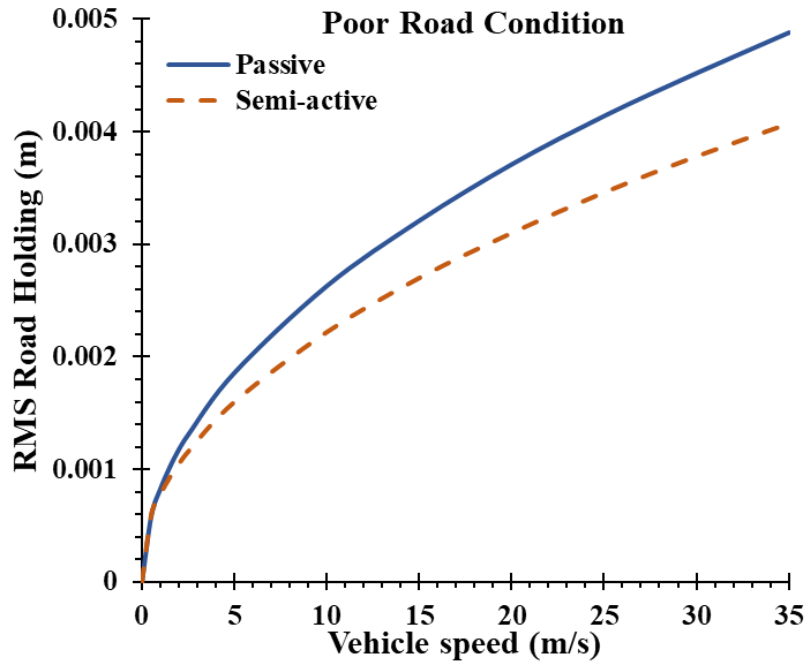


(b)

Figure 8.7 Response of vehicle with MR damper for good road condition, (a) Root mean square acceleration v/s velocity (b) Relative displacement v/s Velocity



(a)



(b)

Figure 8.8 Response of vehicle with MR damper for poor road condition, (a) Root mean square acceleration v/s velocity (b) Relative displacement v/s Velocity

In case of poor road conditions, there was 32.21% reduction in RMS acceleration of semi-active suspension system compared to passive suspension, as observed in Figure 8.8 (a). It was also observed that the RMS road holding (relative displacement of road and unsprung displacement) of semi-active suspension was 16.45% less than the passive suspension as shown in Figure 8.8 (b).

Dynamic analysis has been carried out by using quarter car model with passive and semi-active suspension system subjected to good and poor random road irregularities. The acceleration response in time domain and its spectrum of the passive and semi-active quarter car suspension system at constant speed of 35 m/s are illustrated in Figures 8.9 and Figure 8.10 respectively. It can be seen from the figures that; resonant frequency of the quarter car system occurs below 2 Hz. Observation shows that the semi-active suspension system subjected to good random road condition reduces around 46% of vibration amplitude at resonant frequency of vehicle than passive suspension system. When it is subjected to poor random road condition, semi-active suspension showed 59 % reduction in vibration.

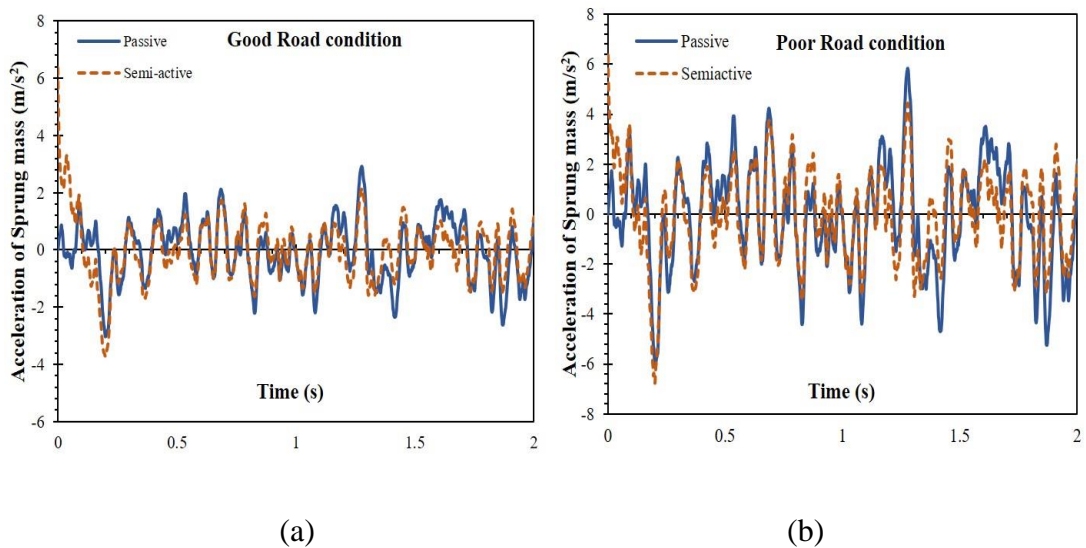


Figure 8.9 Sprung mass acceleration response in time domain

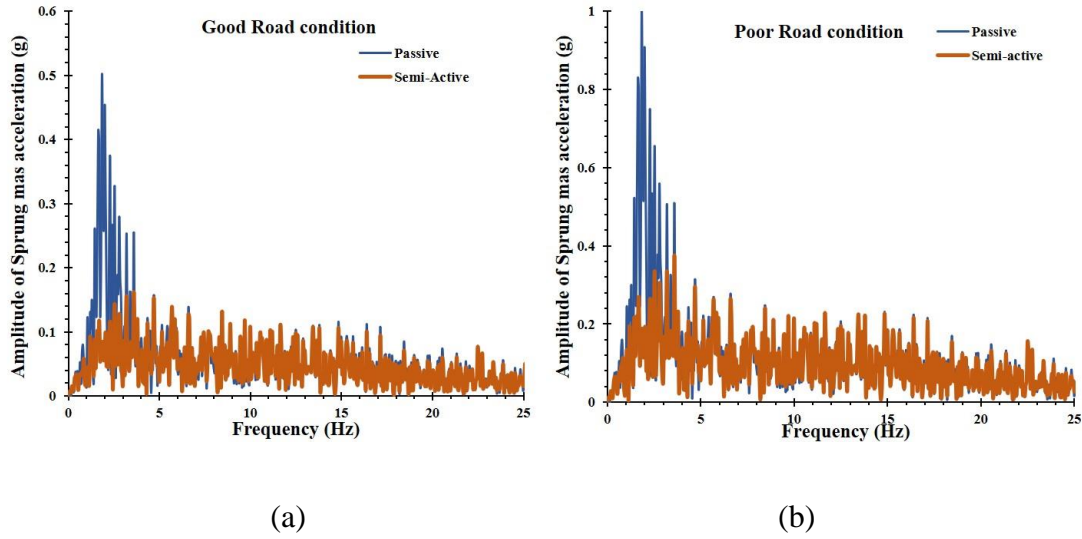


Figure 8.10 Sprung mass acceleration response in frequency domain

8.3.3 Dynamic analysis of three-wheeler passenger vehicle

The three-wheeler passenger vehicle model has been formulated with six degrees of freedom, which includes three vertical movements in the direction of z axes and three rotational movements about three axes (yaw, pitch and roll). The schematic diagram of three-wheeler model is as illustrated in figure 8.11. The body mass is concentrated at the centre of gravity (CG) and coordinate reference for motion of the system coincides with CG. The angular movements are represented as the Euler angles U , α , and β and are used to describe the orientation of body centred frame. These angular motions signify bounce, pitch and roll. Deflection of each wheel of the vehicle are expressed as (Gawade et al. 2005),

$$U_{ba} = U - l_3 \sin \beta - U_{ta} \quad (8.13a)$$

$$U_{bb} = U + l_4 \sin \beta + l_2 \sin \alpha - U_{tb} \quad (8.13b)$$

$$U_{bc} = U + l_4 \sin \beta - l_1 \sin \alpha - U_{tc} \quad (8.13c)$$

Sprung mass bounce

$$M_s \ddot{U} + K_{a1}(U - l_3\beta - U_{ta}) + K_{b1}(U + l_4\beta + l_2\alpha - U_{tb}) + K_{c1}(U + l_4\beta - l_1\alpha - U_{tc}) + F_1 + F_2 + F_3 = 0 \quad (8.14)$$

Sprung mass pitch,

$$I_x \ddot{\beta} + K_{b1}l_1(U + l_4\beta + l_2\alpha - U_{tb}) - K_{c1}l_2(U + l_4\beta - l_1\alpha - U_{tc}) + l_1F_1 + l_2F_2 = 0 \quad (8.15)$$

Sprung mass roll

$$I_y \ddot{\alpha} + K_{b1}l_4(U + l_4\beta + l_2\alpha - U_{tb}) + K_{c1}l_4(U + l_4\beta - l_1\alpha - U_{tc}) - K_{a1}l_3(U - l_3\beta - U_{ta}) - l_3F_1 + l_4F_2 + l_4F_1 = 0 \quad (8.16)$$

The bounce exerted at the three wheels of the vehicle are

$$M_a \ddot{U}_{ta} - K_{a1}(U - l_3\beta - U_{ta}) + K_{a2}(U_{ta} - Z_1) + C_a(\dot{U}_{ta} - \dot{Z}_1) - F_1 = 0 \quad (8.17)$$

$$M_b \ddot{U}_{tb} - K_{b1}(U + l_4\beta + l_2\alpha - U_{tb}) + K_{b2}(U_{tb} - Z_2) + C_b(\dot{U}_{tb} - \dot{Z}_2) - F_2 = 0 \quad (8.18)$$

$$M_c \ddot{U}_{tc} - K_{c1}(U + l_4\beta - l_1\alpha - U_{tc}) + K_{c2}(U_{tc} - Z_3) + C_c(\dot{U}_{tc} - \dot{Z}_3) - F_3 = 0 \quad (8.19)$$

where, U = Sprung mass displacement (Bounce), β = Sprung mass displacement (Pitch), α = Sprung mass displacement (Roll), U_{ta} = Bounce displacement of front wheel, U_{tb} = Bounce displacement of the rear left wheel, U_{tc} = Bounce displacement of rear right wheel, Z_1 = Road amplitude at front wheel, Z_2 = Road amplitude at rear left wheel, Z_3 = Road amplitude at rear right wheel, U_{bb} = Vertical displacement of the rear left corner, U_{bc} = Vertical displacement of rear right corner, U_{ba} = Vertical displacement of front corner.

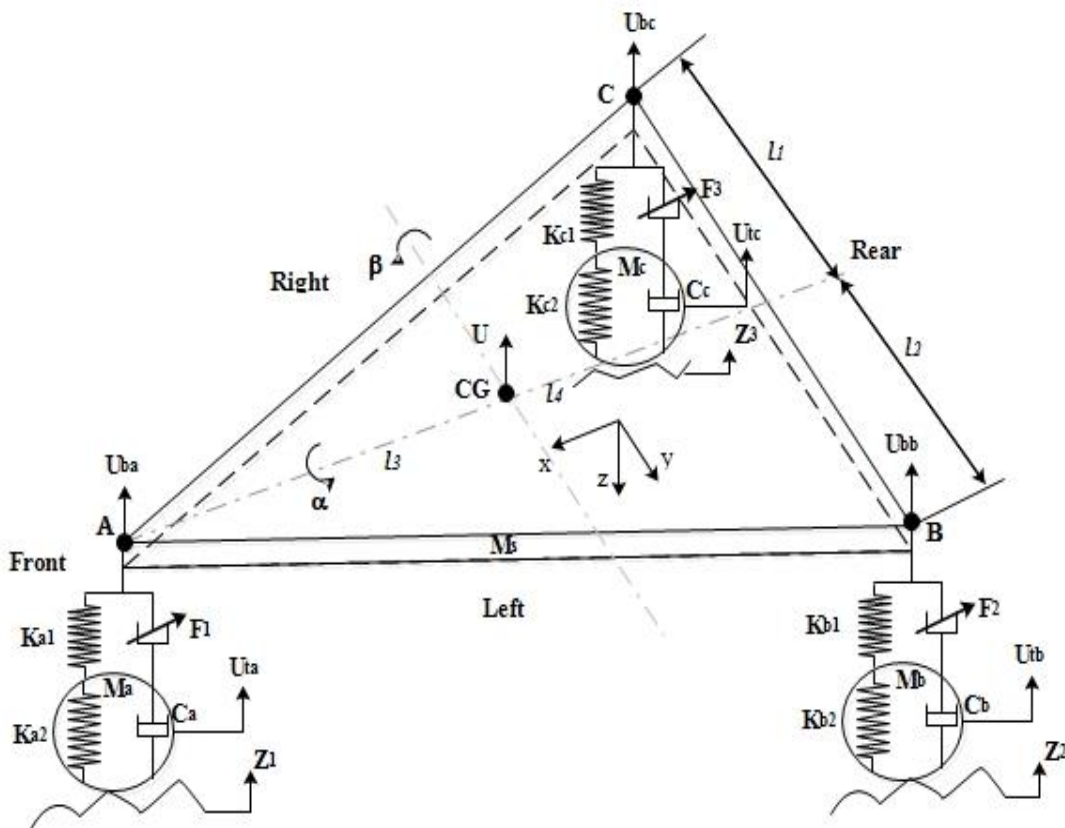


Figure 8.11 Three-wheeler vehicle model

Table 8.6 Parameter values of the three-wheeler (Gawade et al. 2005),

Parameter		Value
M_s	Sprung Mass of the vehicle	492 kg
M_a	Mass of the front wheel	8.5 kg
M_b	The mass of the rear left wheel	9 kg
M_c	Mass of rear right wheel	9 kg
I_x	Rolling moment of inertia	182.2 kg.m ²
I_y	Pitch moment of inertia	170 kg.m ²
K_{a1}	Front spring stiffness	32700 N/m
K_{b1}	Rear left spring stiffness	50400 N/m
K_{c1}	Rear right spring stiffness	50400 N/m
C_c	Rear right wheel damping	436 N.s/m
l_1	Lateral distance of the rear left wheel from CG	0.5750 m

l_2	Lateral distance of rear right wheel from CG	0.5750 m
l_3	Longitudinal distance of front wheel from CG	1.4960 m
l_4	Longitudinal distance of rear axle from CG	0.5040 m
K_{a2}	Front Wheel stiffness	238260 N/m
K_{b2}	Rear left Wheel stiffness	250490 N/m
K_{c2}	Rear right Wheel stiffness	250490 N/m
C_a	Front wheel coefficient of damping	557 N.s/m
C_b	Rear left wheel coefficient of damping	436 N.s/m

Road holding of the vehicle is associated with the stability of the vehicle under road disturbance. The unsprung mass road holding response under different velocities is plotted in figure 8.12 (a). The RMS road holding of the rear wheels of the vehicle is considerably lesser than the front wheel. The root mean square (RMS) acceleration of the unsprung mass versus velocity of bounce, pitch and roll motions of the three-wheeler vehicle is illustrated in figure 8.12 (b). The RMS acceleration of bounce is significantly higher than the pitch and roll motion, while the other two motions have nearly same response. From the simulation results, it can be seen that the overall road holding response of the three-wheeler vehicle is effective.

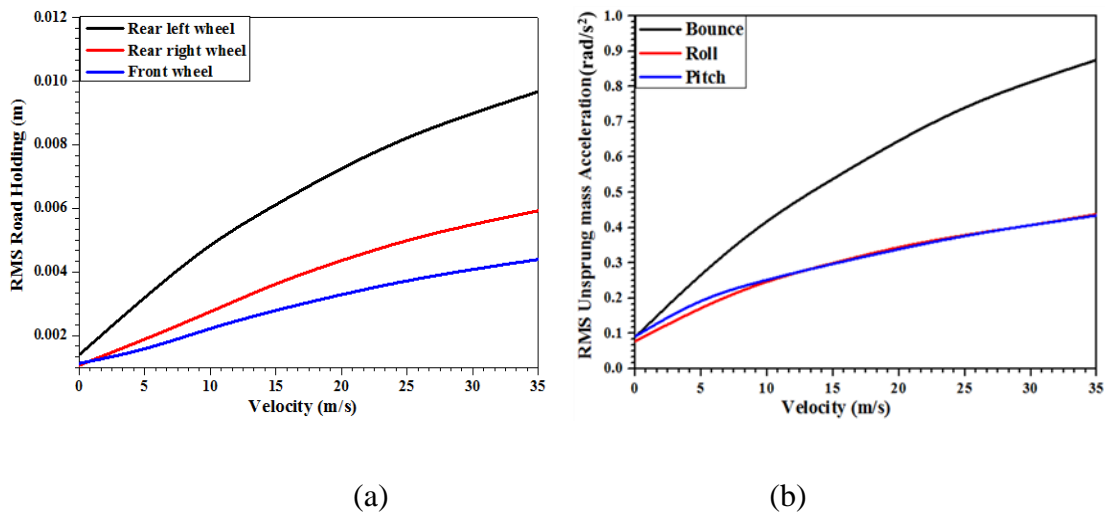
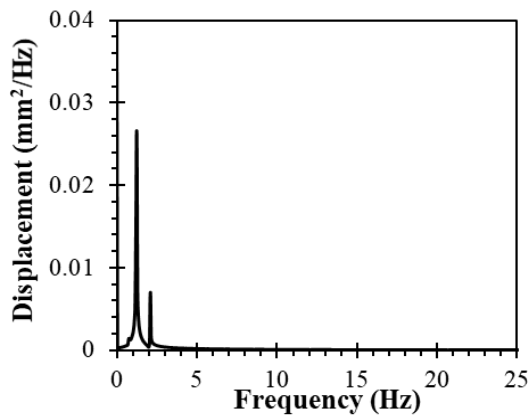
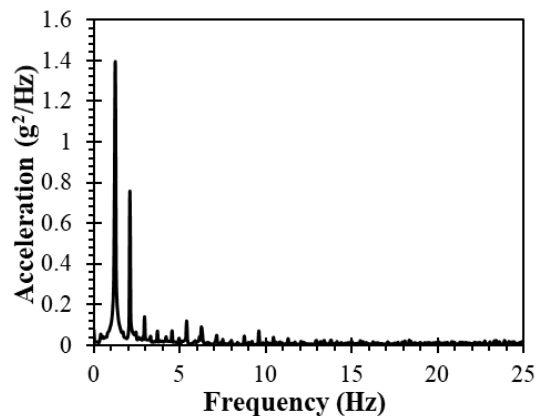


Figure 8.12 (a) RMS Road holding versus velocity and (b) Unsprung mass RMS acceleration

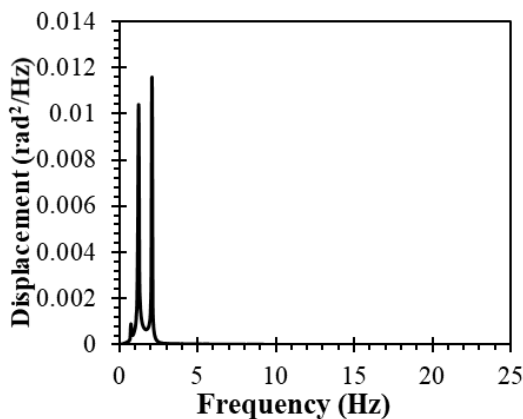
The ride comfort is affected by various factors such as body pitch, bounce and roll under different road input conditions. These responses of the vehicle under random road input are evaluated using Simulink. Acceleration and displacement (bounce, pitch and roll) in the frequency domain of sprung mass are plotted in figures 8.13 (a-f). The results reveal that maximum sprung mass acceleration of bounce is at 1.7 Hz and peak displacement is at 1.6 Hz. The sprung mass bounce, pitch and roll displacement are within 2Hz frequency which is within comfort zone of the passenger. Peak acceleration of the roll is considerably lesser compared to bounce and pitch motion. Even though a small increase in acceleration and displacement of each motion can be seen between 2-3 Hz, the frequency is within the comfortable range.



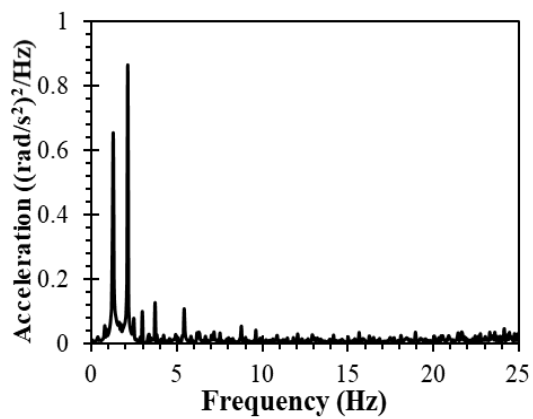
(a)



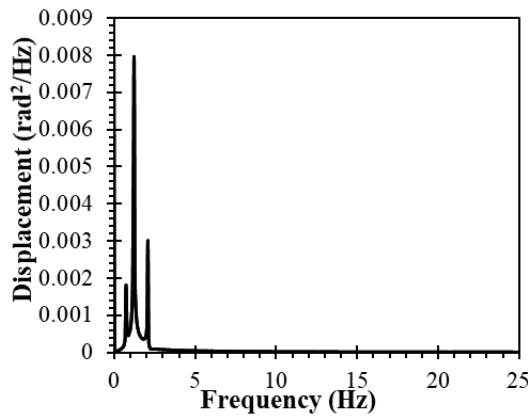
(b)



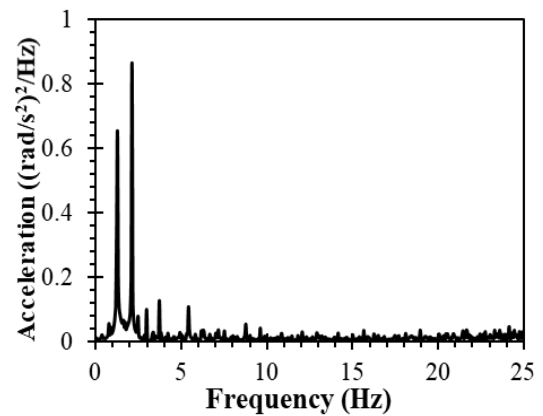
(c)



(d)



(e)



(f)

Figure 8.13 Sprung mass displacement and acceleration in frequency domain for (a, b) Bounce (c, d) Pitch and (e, f) Roll motion of the vehicle

8.4 SUMMARY

A non-parametric representative model exhibiting the hysteretic behavior of MR damper was developed from validated computational results. The dynamic response analysis of a vehicle with passive and semi-active suspension system was studied by using quarter car and further in a three-wheeler vehicle (where semi-active suspension was implemented), under random road excitations. The results of quarter car vehicle with nonparametric MR based suspension system were compared with passive suspension system. It showed that the quarter vehicle with non-parametric based MR suspension system provides good vibration isolation for semi-active suspension than passive suspension system.

CHAPTER 9

SUMMARY AND CONCLUSIONS

9.1 SUMMARY

This research work started with the characterisation of MR fluid samples which were prepared based on the different volume fractions of carbonyl iron powder. The rheological properties of MR fluid samples under different magnetic fields and fluid gap were evaluated using rotational type rheometer attached with magnetorheological device cell. Based on the results obtained from the experiments, these fluid properties were used for computing the damping force of MR damper. An optimisation technique was adopted to find out optimal proportion of particle concentration for MR damper application. Different set of experiment runs were formulated using design of experiments and response to each experiment set was evaluated. Using single and multi-objective particle swarm optimisation techniques, the optimal proportion of iron particles was identified.

The force induced in the MR damper due application of external magnetic field was evaluated under different operating frequencies using mechanical damper test facility. The damping force versus displacement curve showed that maximum damping force can be realized at higher frequency and DC currents. Also, it was observed that the area under these curves was increasing with increase in DC current resulting in higher energy dissipation of the damper. Later, the influence of material properties of MR damper components on the induced magnetic flux density and geometrical parameters on the damping force was evaluated. Three different cases were considered based on the magnetic and nonmagnetic materials used for cylinder. The magnetic flux density induced in shear flow gap for each case was computed through magnetostatic analysis. The design parameters such as shear flow gap, flange length, number of turns of coils and DC currents were used as the variables. The multi-objective genetic algorithm and screening optimization techniques were

employed to maximize the magnetic flux density and to identify the optimal values of the design variables.

A coupled FEA and CFD analysis was used for estimating the magnetic flux density and damping force for different currents. The characteristics such as damping force versus displacement, equivalent damping and energy dissipation were also estimated. The credibility of the shear mode monotube MR damper analysis results were validated with experimental results. Later, performance of flow and mixed mode MR dampers was carried out and the variations in the damping characteristics under different inputs with shear mode damper were compared. The mixed mode damper was realized by combining the flow and shear mode operations.

Performance of developed MR damper model was analyzed by incorporating it into the vehicle model as suspension element. Dynamic response analysis of vehicle was studied by using mathematical models of quarter car model and three-wheeler model subjected to the random road irregularities. The comparative studies were conducted between quarter car passive and MR based suspension system.

9.2 CONTRIBUTIONS

- Evaluated optimal volume fraction of particle in the MR fluid samples for MR damper application using particle swarm optimization technique. Also, effect of fluid flow gap on the shear stress of MR fluid was investigated.
- Presented the importance of material selection for the MR damper components for achieving the maximum damping effect and it was found that by employing materials with higher magnetic permeability, higher magnetic flux density and eventually damping force can be achieved.
- Developed coupled FEA and CFD analysis method to characterize the MR damper under different input conditions and formulated a non-parametric model based on the coupled analysis.
- Formulated mathematical model of quarter car and three-wheeler vehicle model with passive and semi-active suspension system. The developed novel non-parametric model was used as an MR damper in semi-active suspension

system and studied the performance of the vehicle in terms of ride comfort and road holding of vehicle under poor and good road conditions.

9.3 CONCLUSIONS

- MR fluid samples were prepared and characterized through experiments under different plate gaps and currents. From rheological characterization of MR fluid, it was found that fluid gap has a significant effect on the shear stress. Steady state results revealed that shear stress became greater for 35 % volume fraction of particles at 0.25 mm plate gap when applied with 2.0 A current and the magnitude of maximum shear stress was observed to be 8100 Pa. It was also found that shear stress at 0.25 mm gap was 1.92 times greater than that of 1 mm gap for 35 % volume fraction.
- Viscoelastic properties measured from oscillatory test in a rheometer through frequency sweep revealed that the storage modulus of MR samples was highly influenced by magnetic flux density and concentration of iron particles when compared to loss modulus. At a current of 2 A, the storage modulus of 35% volume fraction was 2.2 times greater than that of 25% volume fraction MR fluid. Also, under same conditions, the loss modulus of 35% volume fraction was 2 times greater than that of 25% volume fraction MR fluid. Hence, it can be concluded that elastic behavior of the MR samples dominates the viscous behavior under the application of magnetic fields.
- Response surface methodology was used to study the nature of output parameters for the given input design variables. Further, an optimization study using PSO was carried out to determine the optimal volume fraction of iron particles to maximize the shear stress and damping force of MR damper. From the results of single objective and multi-objective PSO analyses, it can be concluded that 31 to 33% is the optimal particle volume fractions for the desired output.
- Shear mode type monotube MR damper was designed and evaluation of damping characteristics such as force versus displacement, energy dissipation

and equivalent damping was carried out. An observation showed that damping force was 1.75 times greater for constant frequency of 2 Hz with 0.4 A current when compared to 0.1 A. Also at a maximum current of 0.4 A damping force at 2 Hz was 1.5 times greater than that at 1 Hz. Energy dissipation was found to be increasing with current and frequency. Maximum energy dissipation was found at 2 Hz and 0.4 A current which was 1.5 times greater than at 0.1 A with same frequency.

- Magnetic, non-magnetic and combination of these materials (composite cylinder) were considered for cylinder material to study their influence on the performance of the MR damper. The damping force of composite cylinder MR damper was found to be 2.55 times than that of MR damper with nonmagnetic cylinder.
- To maximize the damping force of MR damper, an FEA based geometric optimization was carried out. Using central composite design, a set of 27 experiments (DOE) were generated and response for each experiment was computed using magnetostatic analysis. Using ANOVA, it was found that number of turns, DC current and flow gap have significant effect on the response. The optimal design parameters were identified using screening and MOGA optimization techniques. From the optimized results, it was found that the composite cylinder MR damper provided 2.79 times more damping force than the nonmagnetic cylinder MR damper at the velocity of 20 mm/s.
- Coupled FEA and CFD analysis were performed for estimating the magnetic flux density and damping force for different currents of shear mode MR damper and were validated with experimental results. Later, performance of flow and mixed mode MR dampers was carried out and the variations in the damping characteristics under different inputs with shear mode damper were compared. Observation from the results showed that mixed mode damper had better damping characteristics than the other two models for different current inputs. The maximum damping force at 2 Hz frequency for mixed mode, flow mode and shear mode were 490 N, 270 N and 160 N respectively. Also, energy dissipation in the mixed mode is approximately three times greater than

that of shear mode and twice than that of flow mode, based on the obtained results and observations.

- Under good random road conditions, semi active suspension showed 29 % reduction in sprung mass RMS acceleration of the vehicle and 14.81 % reduction in RMS road holding when compared to that of vehicle with passive suspension system. Under poor random road conditions, there was 32.21% reduction in RMS acceleration and 16.45% reduction in RMS road holding of semi-active suspension system when compared to that of passive suspension.

9.4 SCOPE OF FUTURE WORK

- In the present study, the parallel plate gap effect was studied for MR fluid with standard components such as silicone oil, carbonyl iron powder and grease as additive. Future work can be extended for MR fluid samples with different components and compositions.
- Current investigations were limited to experimental characterization of shear mode type MR damper. Further, a lot of scope exists on design and characterization of MR dampers operating under different modes of operations and also performance studies can be made by combining the all basic modes of operation of MR devices.
- The shear effect on MR fluid can be studied in microscopic level through coupling CFD and discrete element method (DEM).
- Current research work was focused on dynamic analysis of vehicle through numerical analysis. Further the validation of obtained response can be done through experimentations.
- Investigations can be carried out in preparing MR fluid with an arrangement to prevent settling of particles.

REFERENCES

- Agrawal, A., Kulkarni, P., Vieira, S. L. and Naganathan, N. G. (2001). "An Overview of Magneto- and Electro-Rheological Fluids and their Applications in Fluid Power Systems." *Int. J. Fluid Power*, 2 (2), 5–41.
- Ahamed, R., Rashid, M. M., Ferdaus, M. M. and Yusof, H. M. (2016). "Design and modeling of energy generated magneto rheological damper." *Korea Aust. Rheol. J.*, 28 (1), 67–74.
- Ahmadian, M. and Norris, J. A. (2008). "Experimental analysis of magnetorheological dampers when subjected to impact and shock loading." *Commun. Nonlinear Sci. Numer. Simul.*, 13 (9), 1978–1985.
- Ahmadian, M. and Poynor, J. C. (2001). "An evaluation of magneto rheological dampers for controlling gun recoil dynamics." *Shock Vib.*, 8 (3–4), 147–155.
- Ali, S. F. and Ramaswamy, A. (2009). "Hybrid structural control using magnetorheological dampers for base isolated structures." *Smart Mater. Struct.*, 18(5), 055011.
- Amato, F. J. D. and Viassolo, D. E. (2000). "Fuzzy control for active suspensions." *Mechatronics*, 10 (8), 897–920.
- Anakwa, W.K.N., Thomas, D.R., Jones, S.C., Bush, J., Green, D., Anglin, G.W., Rio, R., Sheng, J., Garrett, S. and Chen, L. (2002). "Development and Control of a Prototype Pneumatic Active Suspension System." *ASEE Annu. Conf. Proc.*, 45: 43-49.
- Anderson and John, D. J. (1995). *Computational Fluid Dynamics, The Basics with Applications*. McGraw - Hill Inc, New York.
- Ang, W. L., Li, W. H. and Du, H. (2004). "Experimental and modelling approaches of a MR damper performance under harmonic loading." *J. Inst. Eng.*, 44, 1–14.

Ansar, M., Sudhindra, J. and Deepak, U. (2014). "Performance Analysis of Skyhook, ground hook and hybrid control strategies on semi active suspension system." *Int. J. Current Eng. Techn.*, 3, 265-269.

Arun, M. and Tulapurkara, E. G. (2005). "Computation of turbulent flow inside an enclosure with central partition." *Prog Comput Fluid Dyn, an Int J.*, 5(8), 455-465.

Ashfak, A., Saheed, A., Rasheed, K. A., and Jaleel, J. A. (2011). "Design, fabrication and evaluation of MR damper." *Int. J. Aerosp. Mech. Eng.*, 1, 27-33.

Avinash, B., Sundar, S. S. and Gangadharan, K. V. (2014). "Experimental study of damping characteristics of air, silicon oil, magneto rheological fluid on twin tube damper." *Proc. Mater. Sci.*, 5, 2258-2262.

Avraam, M. and Preumont, A. (2009). "MR-fluid brake design and its application to a portable muscular device." Ph.D, *Thesis*, Universite Libre de Bruxelles.

Barber, D. E. and Carlson, J. D. (2010). "Performance characteristics of prototype MR engine mounts containing glycol MR fluids." *J. Intell. Material Syst. Struct*, 21(15), 1509-1516.

Barbosa, R. S. (2011). "Vehicle dynamic response due to pavement roughness." *J. Braz. Soc. Mech. Sci. Eng.*, 33(3), 302-307.

Bell, R. C., Miller, E. D., Karli, J. O., Vavreck, A. N. and Zimmerman, D. T. (2007). "Influence of particle shape on the properties of magnetorheological fluids." *Int. J. Mod. Phys. B.*, 21(28-29), 5018-5025.

Black, T. and Carlson, J.D. (2006). "*Synthetic Mineral Oils and Bio-Based Lubricants, Chemistry and Technology*, CRC Taylor and Francis, Boca Raton New York London.

Bompos, D. A. and Nikolakopoulos, P. G. (2011). "CFD simulation of magnetorheological fluid journal bearings." *Simulat. Model. Pract. Theor.*, 19(4), 1035-1060.

Bompos, D. A. and Nikolakopoulos, P. G. (2016). “Experimental and Analytical Investigations of Dynamic Characteristics of Magnetorheological and Nano magnetorheological Fluid Film Journal Bearing.” *J Vib Acoust*, 138(3), 031012.

Bompos, D. A. and Nikolakopoulos, P. G. (2016). “Rotordynamic analysis of a shaft using magnetorheological and nanomagnetorheological fluid journal bearings.” *Tribo. Trans.*, 59(1), 108-118.

Böse, H., Gerlach, T. and Ehrlich, J. (2013). “Magnetorheological torque transmission devices with permanent magnets.” *J. Phy. Conf. Series*, 412 (1), 012050.

Bouc, R. (1971). “Mathematical model for hysteresis Acustica.” 24, 16–25.

Bucchi, F., Forte, P., Frenzo, F., Musolino, A. and Rizzo, R. (2014). “A fail-safe magnetorheological clutch excited by permanent magnets for the disengagement of automotive auxiliaries.” *J. Intell. Material Syst. Struct*, 25(16), 2102-2114.

Bullough, W. A., Ellam, D. J., Wong, A. P. and Tozer, R. C. (2008). “Computational fluid dynamics in the flow of ERF/MRF in the control devices and of oil through piezo-hydraulic valves.” *Comput. Struct*, 86, 266-208.

Burson, K. (2006). “Lord MR damping solutions for automotive applications.” *Proc. Veh. Dyn. Expo*.

Carlson, J.D. (2009). *Smart Materials*.” CRC Press, chapter 17: Magnetorheological Fluids, pages 17.1–17.8.

Carlson, J.D. and Jolly, M.R. (2000). “MR fluid, foam and elastomer devices.” *Mechatronics*, 10, 555–569.

Case, D., Taheri, B., and Richer, E. (2016). “Multiphysics modeling of magnetorheological dampers.” *Int. J. Multiphysics*, 7(1).

Celik, H. K., Rennie, A. E. and Akinici, I. (2017). “Design and structural optimisation of a tractor mounted telescopic boom crane.” *J. Braz. Soc. Mech. Sci. Eng.*, 39(3), 909-924.

Charles, S. W. (2002) “The Preparation of Magnetic Fluids.” Lecture notes in physics-new york then berlin, 3–18.

Chen, D. W., Gu, H. B. and Wu, H. (2010). “Application of magneto-rheological (MR) damper in landing gear shimmy.” *Int. Symp. Systems and Control in Aeronautics and Astronautics*, 1212-1216.

Chen, K., Tian, Y., Shan, L., Zhang, X. and Meng, Y. (2013). “The rheological properties of magnetic field excited magnetic powders sheared between two parallel plates.” *Smart Mater. Struct*, 22(11), 115036.

Chen, P., Bai, X. X., Qian, L. J., and Choi, S. B. (2016). “A magneto-rheological fluid mount featuring squeeze mode: analysis and testing.” *Smart Mater. Struct*, 25(5), 055002.

Chen, Y. (2009). “Skyhook surface sliding mode control on semi-active vehicle suspension system for ride comfort enhancement.” *Engineering*, 1(01), 23.

Chin, B. D., Park, J. H., Kwon, M. H. and Park, O.O. (2001). “Rheological properties and dispersion stability of magnetorheological (MR) suspensions.” *Rheo. Acta*, 40, 211–219.

Chiriac, H. and Stoian, G. (2009). “Influence of the particle size and size distribution on the magnetorheological fluids properties.” *IEEE Trans. Magn.*, 45 (10), 4049–4051.

Choi, S. B., and Han, Y. M. (2012). “Magnetorheological fluid technology: applications in vehicle systems. *CRC press, US*.

Choi, Y. T., Cho, J. U., Choi, S. B., and Wereley, N. M. (2005). “Constitutive models of electrorheological and magnetorheological fluids using viscometers.” *Smart Mater. Struct*, 14(5), 1025.

Choi, Y. T., Wereley, N. M., and Jeon, Y. S. (2005). “Semi-active vibration isolation using magnetorheological isolators.” *Journal of Aircraft*, 42(5), 1244-1251.

- Claracq, J., Sarrazin, J. and Montfort, J. P. (2004). "Viscoelastic properties of magnetorheological fluids." *Rheo. Acta*, 43(1), 38-49.
- Claracq, J., Sarrazin, J. and Montfort, J. P. (2004). "Viscoelastic properties of magnetorheological fluids." *Rheo. Acta*, 43(1), 38-49.
- Costa, E. and Branco, P. C. (2009). "Continuum electromechanics of a magnetorheological damper including the friction force effects between the MR fluid and device walls: analytical modelling and experimental validation." *Sens. Actuators, A: Phys.*, 155(1), 82-88.
- Cronje, J.M., Heyns, P.S., Theron, N.J. and Loveday, P.W. (2005). "Development of a variable stiffness and damping tunable vibration isolator." *J. Vib. Control*, 11, 381-396.
- Dahl, P. R. (1976). "Solid friction damping of mechanical vibrations." *AIAA J.*, 14 1675–82.
- De Gans, B. J., Duin, N.J., Van den Ende, D. and Mellema, J. (2000). "The influence of particle size on the magnetorheological properties of an inverse ferrofluid." *J. Chem. Phys.*, 113(5), 2032-2042.
- De Vicente, J., López-López, M. T., Durán, J. D. and González-Caballero, F. (2004). "Shear flow behaviour of confined magnetorheological fluids at low magnetic field strengths." *Rheo acta*, 44(1), 94-103.
- De Wit, C. C., Olsson, H., Astrom, K. J. and Lischinsky, P. (1995). "A new model for control of systems with friction." *IEEE Trans. Autom. Control*, 40, 419–25.
- Diudea, M., Hodor, V., Bălan, R. and Bara, M. "CFD prediction of the flow inside the damper by the use of LES model." *Bulletin of the Transilvania University of Braşov*.
- Djavareshkian, M. H., Esmaeli, A. and Safarzadeh, H. (2015). "Optimal design of magnetorheological fluid damper based on response surface method." *Int. J. Eng.*, 28.
- Dominguez, A., Sedaghati, R. and Stiharu, I. (2006). "A new dynamic hysteresis model for magnetorheological dampers. Smart materials and structures." 15(5), 1179.

- Dutta, S. and Chakraborty, G. (2014). "Performance analysis of nonlinear vibration isolator with magneto-rheological damper." *J. Sound Vib.*, 333(20), 5097-5114.
- Dyke, S. J., Spencer, Jr, B. F., Sain, M. K. and Carlson, J. D. (1998). "An experimental study of MR dampers for seismic protection." *Smart Mater. Struct*, 7(5), 693.
- Eberhart, R. and Kennedy, J. (1995). "A new optimizer using particle swarm theory. IEEE Trans. Energy Convers.,27(1), 39–43.
- Ehrgott, R.C. and Masri, S.F. (1992). "Modeling the oscillatory dynamic behavior of electrorheological materials in shear." *Smart Mater. Struct*, 1, 275–285.
- Elahinia, M., Ciocanel, C. and Wang, S. (2013). "MR-and ER-based semi-active engine mounts." *Smart Mater. Res.*, 21.
- Eshaghi, M., Rakheja, S. and Sedaghati, R. (2015). "An accurate technique for pre-yield characterization of MR fluids." *Smart Mater. Struct*, 24(6), 065018.
- Eski, I. and Yıldırım, Ş. (2009). "Vibration control of vehicle active suspension system using a new robust neural network control system." *Simul. Model. Pract. Th.*, 17(5), 778-793.
- Esteki, K., Bagchi, A. and Sedaghati, R. (2014). "Dynamic analysis of electro-and magneto-rheological fluid dampers using duct flow models." *Smart Mater. Struct.*, 23(3), 035016.
- Fang, F.F., Kim, J.H. and Choi, H.J. (2009). "Synthesis of core-shell structured PS/Fe₃O₄ microbeads and their magnetorheology." *Polymer*, 50 (10), 2290–2293.
- Fatch, M.M. and Alavi, S.S. (2009). "Impedance control of an active suspension system." *Mechatronics*, 19(1), 134-140.
- Ferdaus, M. M., Rashid, M. M., Hasan, M. H. and Rahman, M. A. (2014). "Optimal design of Magneto-Rheological damper comparing different configurations by finite element analysis." *J. Mech. Sci. Technol.*, 28(9), 3667-3677.

- Ficici, F., Durat, M. and Kapsiz, M. (2014). "Optimization of tribological parameters for a brake pad using Taguchi design method." *J. Braz. Soc. Mech. Sci. Eng.*, 36(3), 653-659.
- Forte, P., Paternò, M. and Rustighi, E. (2004). "A magnetorheological fluid damper for rotor applications." *Int. J. Rotating Mach.*, 10(3), 175-182.
- Gamota, D. R. and Filisko, F. E. (1991). "Dynamic mechanical studies of electrorheological materials: moderate frequencies." *J. Rheo.*, 35(3), 399-425.
- Ganji, P. R., Chintala, K. P., Raju, V. K. and Surapaneni, S. R. (2016). "Parametric study and optimization using RSM of DI diesel engine for lower emissions." *J. Braz. Soc. Mech. Sci. Eng.*, 39(3), 671-680.
- Gaur, S. (2013). "Vibration Control of Bus Suspension System using PI and PID Controller." *Int. J. Adv. Eng. Sci.*, 3(3), 94-99.
- Gavin, H., Hoagg, J. and Dobossy, M. (2001). "Optimal design of MR dampers." *Proc. US-Japan Work. Smart Struct. Improv. Seism. Perform. Urban Reg.*, 14, 225-236.
- Gawade, T. R., Mukherjee, S. and Mohan, D. (2005). "Six-degree-of-freedom three-wheeled-vehicle model validation." *Proc. Inst. Mech. Eng. D J. Automob. Eng.*, 219 (4), 487-498.
- Gedik, E., Kurt, H. and Recebli, Z. (2013). "CFD simulation of magnetohydrodynamic flow of a liquid-metal galinstan fluid in circular pipes." *Comp. Model.*, 9, 23-33.
- Gedik, E., Kurt, H., Recebli, Z. and Balan, C. (2012). "Two-dimensional CFD simulation of magnetorheological fluid between two fixed parallel plates applied external magnetic field." *Comput. Fluids*, 63, 128-134.
- Genc, S. and Phulé, P. P. (2002). "Rheological properties of magnetorheological fluids." *Smart Mater. Struct.*, 11(1), 140.

Gertzos, K. P., Nikolakopoulos, P. G. and Papadopoulos, C. A. (2008). “CFD analysis of journal bearing hydrodynamic lubrication by Bingham lubricant.” *Tribo. Int.*, 41(12), 1190-1204.

Ghodsiyeh, D., Golshan, A. and Izman, S. (2014). “Multi-objective process optimization of wire electrical discharge machining based on response surface methodology.” *J. Braz. Soc. Mech. Sci. Eng.*, 36(2), 301–313.

Ghodsiyeh, D., Golshan, A. and Izman, S. (2014). “Multi-objective process optimization of wire electrical discharge machining based on response surface methodology.” *J. Braz. Soc. Mech. Sci. Eng.*, 36(2), 301-313.

Gołdasz, J, and Sapiński, B. (2011). “Modeling of magnetorheological mounts in various operation modes.” *Acta Mech. Auto.*, 5, 29-40.

Goncalves, F. D. and Carlson, J. D. (2009). “An alternate operation mode for MR fluids—magnetic gradient pinch.” *J. Physics Conf. Series*, 149, (1), 012050.

Goncalves, F.D., Koo, J.H. and Ahmadian, M. (2006). “A review of the state of the art in magnetorheological fluid technologies - part i: MR fluid and MR fluid models.” *Shock Vib. Dig*, 38, 203–219.

Gravatt, J. W. (2003). “Magneto-rheological dampers for super-sport motorcycle applications. *Master's Thesis, Virginia Tech.*

Grunwald, A. and Olabi, A.G. (2008). “Design of magneto-rheological (MR) valve.” *Sens. Actuators. A.*, 148, 211–223.

Gudmundsson, K. H., Jonsdottir, F. and Thorsteinsson, F. (2010). “A geometrical optimization of a magneto-rheological rotary brake in a prosthetic knee.” *Smart Mater. Struct.*,19(3), 035023.

Guo, C., Gong, X., Xuan, S., Zhang, Y. and Jiang, W. (2012). “An experimental investigation on the normal force behaviour of magnetorheological suspensions.” *Korea Aust. Rheol. J.*, 24(3), 171-180.

- Guo, S., Yang, S. and Pan, C. (2006). “Dynamic modeling of magnetorheological damper behaviors.” *J. Intell. Mater. Syst. Struct.*, 17, 3–14.
- He, L., Qin, G., Zhang, Y. and Chen, L. (2008). “Non-stationary random vibration analysis of vehicle with fractional damping.” *Int. Conf. Intell. Comput. Technol. Autom.*, 2, 150-157.
- Hesselbach, J. A. K. C. and Abel-Keilhack, C. (2003). “Active hydrostatic bearing with magnetorheological fluid.” *J. Appl. Phys.*, 93(10), 8441-8443.
- Hrovat, D. (1993). “Applications of optimal control to advanced automotive suspension design.” *J. Dyn. Sys. Meas. Control.*, 115(2B), 328-342.
- Hu, G., Xie, Z. and Li, W. (2015). “Optimal design of a double coil magnetorheological fluid damper with various piston profiles.” *11th World Congr. Struct. Multidiscip. Optim.*, 268–273.
- Hu, W. and Wereley, N. M. (2005). “Magnetorheological fluid and elastomeric lag damper for helicopter stability augmentation.” *Int. J. Modern Physics B*, 19(9), 1471-1477.
- Hu, W. and Wereley, N. M. (2008). “Hybrid magnetorheological fluid-elastomeric lag dampers for helicopter stability augmentation.” *Smart Mater. Struct.*, 17, 045021.
- Huang, Y., Liu, X. and Chen, B. (2006). “Autoregressive trispectral characteristics of magnetorheological damping device.” *IEEE Int. Conf. Intell. Robot. Syst.*, 5878-5882.
- Ikhouane, F. and Dyke, S. J. (2007). “Modeling and identification of a shear mode magnetorheological damper.” *Smart Mater. Struct.*, 16, 605–616.
- Imaduddin, F., Mazlan, S. A., and Zamzuri, H. (2013). “A design and modelling review of rotary magnetorheological damper.” *Mater. Des.*, 51, 575-591.
- Jahromi, A.F. and Zabihollah, A. (2010). “Linear quadratic regulator and fuzzy controller application in full-car model of suspension system with magnetorheological shock absorber.” *Int. Conf. Mech. Embed. Syst. App.*, 522-528.

Jan, T. (2003). "Combining analytic models with neural networks." *Proc. Sign. Procs. Info. Tech.*, 605-608.

Jang, I. B., Kim, H. B., Lee, J. Y., You, J. L., Choi, H. J., and Jhon, M. S. (2005). "Role of organic coating on carbonyl iron suspended particles in magnetorheological fluids." *J. Appl. Phys.*, 97(10), 912.

Jeon, D., Park, C. and Park, K. (1999). "Vibration suppression by controlling an MR damper." *Int. J. Modern Phys B*, 13(16), 2221-2228.

Jha, S., and Jain, V. K. (2009). "Rheological characterization of magnetorheological polishing fluid for MRAFF." *Int. J. Adv. Manuf. Technol.*, 42(7), 656-668.

Jiang, W., Zhang, Y., Xuan, S., Guo, C. and Gong, X. (2011). "Dimorphic magnetorheological fluid with improved rheological properties." *J. Magn. Magn. Mater.*, 323, 3246–3250.

Jiang, Z. and Lu K, (2002). "A single-chain model for quasi-static shear stress-strain properties of magnetorheological fluids." *Int. J. Modern Phys B*, 16(18), 2739-2744.

Jimenez, R. and Alvarez, L. (2002). "Real time identification of structures with magnetorheological dampers." *Proc. 41st IEEE Conf. on Decision and Control*, 1, 1017–22.

Jimenez, R. and Alvarez-Icaza, L. (2005). "LuGre friction model for a magnetorheological damper." *Struct. Control Health Monit.*, 12, 91–116.

Jin, G., Sain, M. K. and Spencer, B. E. (2005). "Nonlinear blackbox modeling of MR-dampers for civil structural control." *IEEE Trans. Control Syst. Technol.*, 13(3), 345-355.

Jin, G., Sain, M. K. and Spencer, B. F. (2002). "Modeling MR-dampers: the ridgenet estimation approach." *Proc. 2002 Am. Control Conf.*, 3, 2457-2462.

Jolly, M.R., Bender, J.W. and Carlson, J.D. (1999). "Properties and applications of commercial magnetorheological fluids." *J. Intell. Mater. Syst. Struct.*, 10(1), 5-13.

- Jonasson, M. and Roos, F. (2008). "Design and evaluation of an active electromechanical wheel suspension system." *Mechatronics*, 18(4), 218-230.
- Jonkkari, I., Kostamo, E., Kostamo, J., Syrjala, S. and Pietola, M. (2012). "Effect of the plate surface characteristics and gap height on yield stresses of a magnetorheological fluid." *Smart Mater. Struct.*, 21(7), 075030.
- Kamath, G. M. and Wereley, N. M. (1997). "Nonlinear viscoelastic-plastic mechanisms-based model of an electrorheological damper." *J. Guid. Control. Dyn.*, 20(6), 1125-1132.
- Karkoub, M.A. and Zribi, M. (2006). "Active/semi-active suspension control using magnetorheological actuators." *Int. J. Sys. Sci.*, 37(1), 35-44.
- Kasprzyk, J. and Krauze, P. (2014). "Vibration control for a half-car model with adaptation of the magnetorheological damper model." *Proc. Int. Conf. Model. Identification and Cont.*, 243-248.
- Kciuk, M. and Turczyn, R. (2006). "Properties and application of magnetorheological fluids." *J. Achiev. Mater.*, 18(1-2), 127-130.
- Khiavi, A. M., Mirzaei, M. and Hajimohammadi, S. (2013). "A new optimal control law for semi-active suspension system considering nonlinear magneto-rheological damper model." *J. Vib. Control*, 20(14), 2221-2233.
- Kim, J. H., and Oh, J. H. (2001). "Development of an above knee prosthesis using MR damper and leg simulator. In Robotics and Automation." *Proc. IEEE Int. Conf. Robotics and Automation*, 4, 3686-3691.
- Kim, K., Lee, C., Koo, J. (2008). "Design and modelling of semi-active squeeze film dampers using magneto-rheological fluids." *Smart Mater. Struct.*, 17,1-12.
- Klingenberg, D. J. (2001). Magnetorheology: Applications and challenges. *AIChE Journal*, 47(2), 246-249.

- Koga, K. and Sano, A. (2006). "Query-based approach to prediction of MR damper force with application to vibration control. *American Control Conf.*, 7.
- Kulkarni, P., Ciocanel, C., Vieira, S. L. and Naganathan, N. (2003). "Study of the behavior of MR fluids in squeeze, torsional and valve modes." *J. Intell. Mater. Syst. Struct.*, 14(2), 99-104.
- Kwok, N. M., Ha, Q. P., Nguyen, M. T., Li, J. and Samali, B. (2007). Bouc–Wen model parameter identification for a MR fluid damper using computationally efficient GA." *ISA Trans.*, 46, 167–79.
- Kwok, N. M., Ha, Q. P., Nguyen, T. H., Li, J. and Samali, B. (2006). "A novel hysteretic model for magnetorheological fluid dampers and parameter identification using particle swarm optimization." *Sensor Acuat. A*, 132, 441–51.
- Lai, C. Y. and Liao, W. H. (2002). "Vibration control of a suspension system via a magnetorheological fluid damper." *Modal Analysis*, 8(4), 527-547.
- Lam, H.F., Lai, C.Y. and Liao, W.H. (2002). "Automobile Suspension Systems with MR Fluid Dampers." *Technical Report*.
- Laukiavich, C. A., Braun, M. J., and Chandy, A. J. (2014). "A comparison between the performance of ferro-and magnetorheological fluids in a hydrodynamic bearing." *Proc. Inst. Mech. Eng. J J. Eng. Tribol*, 228(6), 649-666.
- Laun, H. M., Gabriel, C., and Schmidt, G. (2008). "Primary and secondary normal stress differences of a magnetorheological fluid (MRF) up to magnetic flux densities of 1T." *J. Nonnewton Fluid Mech*, 148(1), 47-56.
- Laun, H. M., Gabriel, C., Kieburg, C. (2011). "Wall material and roughness effects on transmittable shear stresses of magnetorheological fluids in plate–plate magnetorheometry." *Rheo. acta*, 50(2), 141-157.
- Lee, T. S., Lin, Y. J. and Ting, O. (2007). "An investigation of grinding process optimization via evolutionary algorithms." *IEEE Proc. Swarm Intel. Symp.*, 176–181.

- Li, W. H., Chen, G. and Yeo, S.H. (1999). “Viscoelastic properties of MR fluids.” *Smart Mater. Struct.*, 8(4), 460.
- Li, W. H., Wang, X. Y., Zhang, X. Z. and Zhou, Y. (2009). “Development and analysis of a variable stiffness damper using an MR bladder.” *Smart Mater. Struct.*, 18(7), 074007.
- Lim, S. T., Cho, M. S., Jang, I. B. and Choi, H. J. (2004). “Magnetorheological characterization of carbonyl iron based suspension stabilized by fumed silica.” *J. Magn. Magn. Mater.*, 282, 170-173.
- Liu, X., Gao, X., Li, F., Yu, H. and Ye, D. (2015). “Shear performance of a metal foam magnetorheological fluid damper.” *IEEE Trans. Magn.*, 51(1), 1-7.
- Liu, Y., Matsuhisa, H., Utsuno, H. and Park, J. G. (2006). “Vibration control by a variable damping and stiffness system with magnetorheological dampers.” *JSME Int. J. Ser. C*, 49(2), 411-417.
- López-López, M. T., De Vicente, J., Bossis, G., González-Caballero, F. and Durán, J. D. G. (2005). “Preparation of stable magnetorheological fluids based on extremely bimodal iron–magnetite suspensions.” *J. Mater. Res.*, 20(4), 874-881.
- López-López, M. T., Zugaldia, A., González-Caballero, F. and Durán, J. D. G. (2006). “Sedimentation and redispersion phenomena in iron-based magnetorheological fluids.” *J. Rheol.*, 50(4), 543-560.
- Lopez-Lopez, M.T., Kuzhir, P., Caballero-Hernandez, J., Rodriguez-Arco, L., Duran, J.D.G. and Bossis, G. (2012). “Yield stress in magnetorheological suspensions near the limit of maximum-packing fraction.” *J. Rheol.*, 56 (5), 1209–1224.
- Ma, X. Q., Rakheja, S. and Su, C. Y. (2006). “Relative assessments of current dependent models for magneto-rheological fluid dampers.” *Proc. IEEE Int. Conf. on Networking, Sensing and Control*, 510, 5.
- Mangal, S. K. and Kumar, A. (2014). “Experimental and Numerical Studies of Magnetorheological (MR) Damper.” *Chin. J. Chem. Eng.*,

Masri, S.F. and Caughey, T.K. (1979). "A nonparametric identification technique for nonlinear dynamic problems." *J. Appl. Mech.*, 46(2), 433–447.

McLaughlin, G., Hu, W. and Wereley, N. M. (2014). "Advanced magnetorheological damper with a spiral channel bypass valve." *J. Appl. Phys.*, 115(17), 17B532.

Mehdi, A. and Young Y. (1999). "Performance Analysis of Magneto-Rheological Mounts," *J. Compos. Mater.*, 33(10), 928–940.

Menter, F. R. (1992). "Performance of popular turbulence model for attached and separated adverse pressure gradient flows." *AIAA J.*, 30(8), 2066-2072.

Myers, R. H., Montgomery, D. and Anderson-Cook, C. M. (2016). Response surface methodology: process and product optimization using designed experiments. *John Wiley & Sons, New Jersey, Canada.*

Narendra, K. S. and Parthasarathy, K. (1990). "Identification and control of dynamical systems using neural networks." *IEEE Transactions on neural networks*, 1(1), 4-27.

Ngatu, G. T. and Wereley, N. M. (2007). "Viscometric and sedimentation characterization of bidisperse magnetorheological fluids." *IEEE Transactions on Magnetics*, 43(6), 2474-2476.

Nguyen, Q. H. and Choi, S. B. (2008). "Optimal design of a vehicle magnetorheological damper considering the damping force and dynamic range." *Smart Mater. Struct.*, 18(1), 015013.

Nguyen, Q. H. and Choi, S. B. (2009). "Optimal design of MR shock absorber and application to vehicle suspension." *Smart Mater. Struct.*, 18(3), 035012.

Nguyen, Q. H. and Choi, S. B. (2009). "Optimal design of MR shock absorber and application to vehicle suspension." *Smart Mater. Struct.*, 18(3), 035012.

Nguyen, Q. H., Choi, S. B., and Woo, J. K. (2014). "Optimal design of magnetorheological fluid-based dampers for front-loaded washing machines." *Proc. Inst. Mech. Eng. C. J. Mech. Eng. Sci.*, 228(2), 294-306.

- Nguyen, Q. H., Choi, S. B., Lee, Y. S. and Han, M. S. (2009). "An analytical method for optimal design of MR valve structures." *Smart Mater. Struct.*, 18(9), 095032.
- Nguyen, S.D., Nguyen, Q.H. and Choi, S.B. (2015). "A hybrid clustering based fuzzy structure for vibration control - Part 2: An application to semi-active vehicle seat-suspension system." *Mech. Syst. Signal Process.*, 56, 288-301.
- Olabi, G. and Grunwald, A. (2007). "Design and application of magneto-rheological fluid." *Mater. Des.*, 28(10), 2658–2664.
- Omidbeygi, F. and Hashemabadi, S. H. (2013). "Exact solution and CFD simulation of magnetorheological fluid purely tangential flow within an eccentric annulus." *Int. J. Mech. Sci.*, 75, 26-33.
- Paksoy, M., Guclu, R. and Cetin, S. (2014). "Semiactive self-tuning fuzzy logic control of full vehicle model with MR damper." *Adv. Mech. Eng.*, 6, 816813.
- Pang, L., Kamath, G. M. and Wereley, N. M. (1998). "Analysis and testing of a linear stroke magnetorheological damper." *AIAA Struct. Dyna. Mater. Conf.*, 4, 2841-2856.
- Park, E. J., da Luz, L. F. and Suleman, A. (2008). "Multidisciplinary design optimization of an automotive magnetorheological brake design." *Comput Struct*, 86(3), 207-216.
- Parlak, Z. and Engin, T. (2012). "Time-dependent CFD and quasi-static analysis of magnetorheological fluid dampers with experimental validation." *Int. J. Mech. Sci.*, 64(1), 22-31.
- Parlak, Z., Engin, T. and Çallı, İ. (2012). "Optimal design of MR damper via finite element analyses of fluid dynamic and magnetic field." *Mechtrics*, 22, (6), 890–903.
- Parlak, Z., Engin, T. and Şahin, İ. (2013). "Optimal magnetorheological damper configuration using the Taguchi experimental design method." *J. Mech. Des.*, 135(8), 081008.

Parlak, Z., Engin, T., Ari, V., Sahin, I. and Calli, I. (2010). "Geometrical optimisation of vehicle shock dampers with magnetorheological fluid." *Int. J. Veh. Des.*, 54(4), 371-392.

Paul, P. S. and Varadarajan, A. S. (2012). "Effect of magneto rheological damper on tool vibration during hard turning." *Front. Mech. Eng.*, 7(4), 410-416.

Paul, P. S., Varadarajan, A. S., Vasanth, X. A. and Lawrance, G. (2014). "Effect of magnetic field on damping ability of magnetorheological damper during hard turning." *Arch. Civ. Mech. Eng.*, 14(3), 433-443.

Phillips, R. W. (1969). "Engineering applications of fluids with a variable yield stress." PhD Thesis. Berkeley: University of California.

Phulé, P. P. and Ginder, J.M. (1999). "Synthesis and properties of novel magnetorheological fluids having improved stability and redispersibility." *Int. J. Mod. Phys. B*, 13,2019-2027.

Porsche adopts magneto rheological engine mounts for new 911 Turbo - SAE International, <http://articles.sae.org/7259/> (Assessed on 25-07-2017).

Potter, J. N., Neild, S. A. and Wagg, D. J. (2011). "Quasi-active suspension design using magnetorheological dampers." *J. Sound Vibration.*, 330(10), 2201-2219.

Prabakar, R.S., Sujatha, C. and Narayanan, S. (2009). "Optimal semi-active preview control response of a half car vehicle model with magnetorheological damper." *J. Sound Vibration.*, 326(3), 400-420.

Priyandoko, G., Mailah, M. and Jamaluddin, H. (2009). "Vehicle active suspension system using skyhook adaptive neuro active force control." *Mech Syst Signal Process.*, 23(3), 855-868.

Pu, H. and Jiang, F. (2005). "Towards high sedimentation stability: magnetorheological fluids based on CNT/Fe₃O₄ nanocomposites." *Nanotechnology*, 16(9), 1486.

- Rabinow, J., (1948). "The magnetic fluid clutches." *Am. Inst Elect Engi Trans*, 67 (2), 1308–1315.
- Rajamohan, V., Sedaghati, R. and Rakheja, S. (2009). "Vibration analysis of a multi-layer beam containing magnetorheological fluid." *Smart Mater. Struct.*, 19(1), 015013.
- Rao, L. G. and Narayanan, S. (2009). "Sky-hook control of nonlinear quarter car model traversing rough road matching performance of LQR control." *J. Sound Vibration.*, 323(3), 515-529.
- Ronge, B. P., Kajale, S. R. and Pawar, P. M. (2011). "*Theoretical and Experimental Analysis of MR Fluid Dampers.*" LAP Lambert Academic publishing, Germany.
- Rosenfeld, N. C. and Wereley, N. M. (2004). "Volume-constrained optimization of magnetorheological and electrorheological valves and dampers." *Smart Mater. Struct.*, 13(6), 1303.
- Rossi, C. and Lucente, G. (2004). "H ∞ control of automotive semi-active suspensions." *In Proceedings of the 1st IFAC Symposium on Advances in Automotive Control.*
- Sahasrabudhe, S. S. and Nagarajaiah, S. (2005). "Semi-active control of sliding isolated bridges using MR dampers: an experimental and numerical study." *Earthquake Eng. Struct. Dynam.*, 34(8), 965-983.
- Sahin, M. (2003). "Solution of the incompressible unsteady Navier–Stokes equations only in terms of the velocity components." *Int J Comput Fluid Dyn*, 17(3), 199-203.
- Sakai, C., Ohmori, H. and Sano, A. (2003). "Modeling of MR damper with hysteresis for adaptive vibration control." *Proc. 42nd IEEE Conf. on Decision and Control*, 4, 3840-3845.
- Salloom, M. Y. and Samad, Z. (2011). "Finite element modeling and simulation of proposed design magneto-rheological valve." *Int. J. Adv. Manuf. Technol.*, 54(5), 421-429.

Samali, B., Widjaja, J., Li, J. and Reizes, J. (2003). "Magneto-rheological shear dampers: Quasi-static modelling and simulation." *Proc. 10th Asia-Pacific Vibration Conf.*, 598-603.

Sapiński, B. (2003). "Non-parametric representations of MR linear damper behaviour." *IUTAM Symposium on Dynamics of Advanced Mater. Smart Struct.*, 347-356.

Schurter, K. C. and Roschke, P. N. (2000). "Fuzzy modeling of a magnetorheological damper using ANFIS." *Ninth IEEE Int. Conf. Fuzzy Syst. FUZZ- IEEE*, 1, 122-127.

Schurter, K. C. and Roschke, P. N. (2001). "Neuro-fuzzy control of structures using acceleration feedback." *Smart Mater. Struct.*, 10(4).

Shah, K., Seong, M. S., Upadhyay, R. V. and Choi, S. B. (2013). "A low sedimentation magnetorheological fluid based on plate-like iron particles, and verification using a damper test." *Smart Mater. Struct.*, 23(2), 027001.

Shams, M., Ebrahimi, R., Raoufi, A. and Jafari, B. J. (2007). "CFD-FEA analysis of hydraulic shock absorber valve behaviour." *Int. J. Automot. Technol.*, 8(5), 615-622.

Sharkawy, A.B. (2005). "Fuzzy and adaptive fuzzy control for the automobiles active suspension system." *Vehicle system dynamics*, 43(11), 795-806.

Shivaram, A. C. and Gangadharan, K. V. (2007). "Statistical modeling of a magneto-rheological fluid damper using the design of experiments approach." *Smart Mater. Struct.*, 16(4), 1310.

Sidpara, A., Das, M. and Jain, V. K. (2009). "Rheological characterization of magnetorheological finishing fluid." *Mater. Manuf. Proces.*, 24(12), 1467-1478.

Sims, N. D., Peel, D. J., Stanway, R., Johnson, A. R. and Bullough, W. A. (2000). "The electrorheological long-stroke damper: a new modelling technique with experimental validation." *J. Sound Vib.*, 229(2), 207-227.

- Slaski, G. and Maciejewski, M. (2011). "Skyhook and fuzzy logic controller of a semi active vehicle suspension." *Prace Naukowe Politechniki Warszawskiej, Transport*, 97-111.
- Snyder, R. A, Kamath, G. M and Wereley, N. M. (2001). "Characterization and analysis of magnetorheological damper behaviour under sinusoidal loading." *AIAA journal*, 39(7), 1240-1253.
- Song, X., Ahmadian, M. and Southward, S. C. (2005). "Modelling magnetorheological dampers with application of nonparametric approach." *J. Intell. Material Syst. Struct.*, 16(5), 421-432.
- Song, X., Ahmadian, M., Southward, S. and Miller, L. (2007). "Parametric study of nonlinear adaptive control algorithm with magneto-rheological suspension systems." *Commun. Nonlinear Sci. Numer. Simul.*, 12(4), 584-607.
- Spencer Jr, B. F., Dyke, S. J., Sain, M. K. and Carlson, J. (1997). "Phenomenological model for magnetorheological dampers." *J. Eng. Mechan.*, 123(3), 230-238.
- Spencer Jr, B. F., Yang, G., Carlson, J. D. and Sain, M. K. (1998). "Smart dampers for seismic protection of structures: a full-scale study." *Second World Conf. Structural Control*, 417-426.
- Stanway, R. S. J. L., Sproston, J. L. and Stevens, N. G. (1987). "Non-linear modelling of an electro-rheological vibration damper." *J. Electrostatics*, 20(2), 167-184.
- Sternberg, A., Zemp, R. and de la Llera, J. C. (2014). "Multiphysics behavior of a magneto-rheological damper and experimental validation." *Eng. Struct.*, 69, 194-205.
- Stribrsky, A., Hyniová, K., Honců, J. and Kruczek, A. (2003). "Using fuzzy logic to control active suspension system of one-half-car model." *Acta Montan. Slovaca., Ročník*, 8 (4), 223-227.
- Susan-Resiga, D. (2009) "A rheological model for magneto-rheological fluids. *J. Intell. Mater. Syst. Struct.*, 20(8), 1001-1010.

Susan-Resiga, D. and Vékás, L. (2016). “Ferrofluid-based magnetorheological fluids: tuning the properties by varying the composition at two hierarchical levels.” *Rheol Acta*, 55(7), 581-595.

Talib, A., Hussin, M., Darns, M. and Zaurah, I. (2013). “Self-tuning PID controller for active suspension system with hydraulic actuator.” *In IEEE Symposium on Computers and Informatics*, 86-91.

Truong, D. Q. and Ahn, K. K. (2011). “Nonlinear black-box models and force-sensorless damping control for damping systems using magneto-rheological fluid dampers.” *Sens. Actuators A Phys*, 167(2), 556-573.

Tu, F., Yang, Q., He, C. and Wang, L. (2012). “Experimental study and design on automobile suspension made of magneto-rheological damper.” *Energy Procedia*, 16, 417-425.

Tu, S. H. and Jeng, W. S. (2007). “Finite Element Analysis of a Magnetorheological Fluid Damper.” *CSME Conf.*

Tyan, F., Hong, Y.F., Tu, S.H. and Jeng, W.S. (2009). “Generation of random road profiles.” *Int. J. Adv. Eng.*, 4(2), 1373-1378.

Wang, D. H. and Liao, W. H. (2004). “Modeling and control of magnetorheological fluid dampers using neural networks.” *Smart Mater. Struct.*, 14(1), 111.

Wang, E. R., Ma, X. Q., Rakheja, S. and Su, C. Y. (2003). “Modelling the hysteretic characteristics of a magnetorheological fluid damper.” *Proc. Inst. Mech. Eng. D.*, 217, 537–50.

Wang, J. and Meng, G. (2001). “Magnetorheological fluid devices: principles, characteristics and applications in mechanical engineering.” *Proc. Inst. Mech. Eng. L J. Mater. Des. Appl.*, 215(3), 165-174.

Wang, X. and Gordaninejad, F. (2006). “Study of magnetorheological fluids at high shear rates.” *Rheo. acta*, 45(6), 899-908.

- Wen, Y. K. (1976). "Method for random vibration of hysteretic systems." *J. Eng. Mech. Div.-ASCE*, 102, 249–63.
- Weng, W.C. and Olutunde, S.O. (2008). "Design, modelling and testing of magnetorheological dampers using analytical flow solutions". *Comp. and Struct.*, 86, 473-482.
- Wereley, N. M. and Pang, L. (1998). "Nondimensional analysis of semi-active electrorheological and magnetorheological dampers using approximate parallel plate models." *Smart Mater. Struct.*, 7(5), 732.
- Wereley, N. M., Kamath, G. M. and Madhavan, V. (1999). "Hysteresis modeling of semi-active magnetorheological helicopter dampers." *J. Intell. Mater. Syst. Struct.*, 10, 624–33.
- Wereley, N. M., Pang, L. and Kamath, G. M. (1998). "Idealized hysteresis modelling of electrorheological and magnetorheological dampers." *J. Intell Mater Syst Struct.*, 9(8), 642-649.
- Xiu, S., Wang, R., Sun, B., Ma, L. and Song, W. (2017). "Preparation and experiment of magnetorheological polishing fluid in reciprocating magnetorheological polishing process." *J. Intell Mater Syst Struct.*, 1045389X17698247.
- Xu, Z. D., Sha, L. F., Zhang, X. C. and Ye, H. H. (2013). "Design, performance test and analysis on magnetorheological damper for earthquake mitigation." *Struct. Control Hlth.*, 20(6), 956-970.
- Yang, G., Spencer Jr, B. F., Jung, H. J. and Carlson, J. D. (2004). "Dynamic modeling of large-scale magnetorheological damper systems for civil engineering applications." *J. Eng. Mech. ASCE.*, 130, 1107-1114.
- Yang, G., Spencer, B. F., Carlson, J. D. and Sain, M. K. (2002). "Large-scale MR fluid dampers: modeling and dynamic performance considerations." *Eng. Struct.*, 24(3), 309-323.

- Yang, M. G., Chen, Z. Q. and Hua, X. G. (2011). "An experimental study on using MR damper to mitigate longitudinal seismic response of a suspension bridge." *Soil. Dyn. Earthq. Eng.*, 31(8), 1171-1181.
- Yang, S. M. and Lee, G. S. (1997). "Vibration control of smart structures by using neural networks." *J. Dyn Syst Meas. Control*, 119(1), 34-39.
- Yang, Y., Li, L. and Chen, G. (2009). "Static yield stress of ferrofluid-based magnetorheological fluids." *Rheo. acta*, 48(4), 457-466.
- Yao, G. Z., Yap, F. F., Chen, G., Li, W. and Yeo, S. H. (2002). "MR damper and its application for semi-active control of vehicle suspension system." *Mechatronics*, 12(7), 963-973.
- Yasrebi, N., Ghazavi, A., Mashhadi, M. M. and Yousefi-Koma, A. (2006). "Magneto-rheological fluid dampers modelling: numerical and experimental." *Int. Mech.Eng. Conf.*, 1, 75.
- Yazid, I. I. M., Mazlan, S. A., Kikuchi, T., Zamzuri, H. and Imaduddin, F. (2014). "Design of magnetorheological damper with a combination of shear and squeeze modes". *Mater. Des.*, 54, 87-95.
- Yeh, E.C. and Tsao, Y.J. (1994). "A fuzzy preview control scheme of active suspension for rough road." *Int. J. Veh. Des.*, 15(1-2), 166-180.
- Yu, G. J., Du, C. B. and Sun, L. G. (2007). "The design of a new-style composite MR damper and magnetic circuit simulation analysis." *Machine Design and Research*, 23(3), 113-117.
- Zhang, H., Wang, E., Min, F., Subhash, R. and Su, C. (2013). "Skyhook-based semi-active control of full-vehicle suspension with magneto-rheological dampers." *Chin. J. Mech. Eng.*, 26(3), 498-505.
- Zhang, J. Q., Feng, Z. Z. and Jing, Q. (2009). "Optimization analysis of a new vane MRF damper." *J. Phys. Conf. Ser.*, 149 (1), 012087.

Zhang, X., Li, W. and Gong, X. L. (2008). “Study on magnetorheological shear thickening fluid.” *Smart Mater. Struct.*, 17(1), 015051.

Zheng, J., Li, Z., Koo, J. and Wang, J. (2014). “Magnetic circuit design and multi-physics analysis of a novel MR damper for applications under high velocity.” *Adv. Mech. Eng.*, 6, 402501.

Zhou, Q., Nielsen, S. R. K. and Qu, W. L. (2006). “Semi-active control of three-dimensional vibrations of an inclined sag cable with magnetorheological dampers.” *J. Sound Vib.*, 296,1–22.

Zhou, Y. and Zhang, Y. L. (2013). “Optimal design of a shear magnetorheological damper for turning vibration suppression.” *Smart Mater. Struct.*, 22(9), 095012.

Zhu, C. (2005). “A disk-type magneto-rheological fluid damper for rotor system vibration control.” *J. Sound Vib.*, 283(3), 1051–1069.

Zschunke, F., Brunn, P. O. and Steven, M. (2004). “Simulation of a magnetorheological damper with a combination of a commercial CFD and FEA code.” *ASME/JSME 2004 Pressure Vessels and Piping Conference.*, 119-124.

Zuzhi, T., Fei, C., Xiangfan, W. and Jian, W. (2016). “A Novel Preparation Process for Magnetorheological Fluid with High Sedimentation Stability.” *J. Mater. Process.*, 31(15), 2030-2036.

APPENDIX-A

Parallel plate model

To calculate the damper force of MR damper working under flow mode of operation, an axisymmetric model of annular fluid flow gap can be derived and used. The model is based on the Navier stokes equation. for an incompressible flow it can be expressed as, (Guglielmino et al. 2008)

For axisymmetric flow $u_x = u(r)$, $u_r = 0$, $u_w = 0$,

$$\frac{\partial u_x}{\partial x} = 0 \quad \text{Continuity equation (1)}$$

$$\rho \frac{\partial u_x}{\partial t} = \rho F_x - \frac{\partial P}{\partial x} + \frac{\partial}{\partial x} \left(2\eta \frac{\partial u_x}{\partial x} + \lambda \nabla \cdot V \right) + \frac{1}{r} \frac{\partial}{\partial r} (r \tau_{xr}) \quad \text{Navier-Stoke equation (2)}$$

where ρ and η are constant, $F_x =$ External force, $r =$ radial co-ordinates, $x =$ Longitudinal co-ordinates, $u_x =$ Velocity, and $\frac{\partial P}{\partial x} =$ Pressure gradient.

Neglecting inertia terms, equation becomes,

$$-\frac{\partial P}{\partial x} + \frac{\partial \tau_{xr}(r)}{\partial r} + \frac{\tau_{xr}(r)}{r} = 0 \quad (3)$$

$$\tau_{xr} = \frac{1}{2} \frac{dP(x)}{dx} r + \frac{C_1}{r} \quad (4)$$

Where C_1 is constant which can be evaluated by using boundary conditions.

Considering the Bingham viscoplastic model

$$\tau_{xr}(r) = \tau_y(H, r) \text{sgn} \left(\frac{\partial u_x(r)}{\partial r} \right) + \eta \frac{\partial u_x(r)}{\partial r} \quad (5)$$

The velocity profile of MR fluid flow through annular channel is as show in figure

The velocity profile from equation (4) and (5) in region I with boundary conditions

At $r = R_1$, $u_x(r) = v_0$

$$u_x(r) = \frac{1}{4\eta} \frac{dP}{dx} (r^2 - R_1^2) + \frac{C_1}{\eta} \ln \frac{r}{R_1} - \frac{1}{\eta} \int_{R_1}^r \tau_y(r) dr - v_0 \quad (6)$$

For $R_1 \leq r \leq r_1$

In Region II, At $r = R_2$, $u_x(r) = 0$ Boundary conditions

$$u_x(r) = -\frac{1}{4\eta} \frac{dP}{dx} (R_2^2 - r^2) - \frac{C_1}{\eta} \ln \frac{R_1}{r} - \frac{1}{\eta} \int_r^{R_2} \tau_y(r) dr \quad (7)$$

For $r_2 \leq r \leq R_2$

In region C, the variation in the yield stress with respect to r is neglected. Hence it can be written as,

$$\tau_y(r) = \tau_y(r_2) = \tau_y(H) \quad (8)$$

$$C_1 = \frac{r_1 r_2}{r_2 - r_1} \tau_y(H) \quad (9)$$

$$\frac{dP}{dx} (r_2 - r_1) = 2\tau_y(H) \quad (10)$$

$$(r_2 - r_1) = \frac{2\tau_y(H)}{\frac{dP}{dx}} \quad (11)$$

where $\tau_y(H)$ = yield stress, H = Applied magnetic field and $r_2 - r_1$ = plug thickness.

With conditions of (8) and (12) it can be written as,

$$u_x(r_1) = \frac{1}{4\eta} \frac{dP}{dx} (r_1^2 - r_2^2) + \frac{C_1}{\eta} \ln \frac{r_1}{R_1} - \frac{1}{\eta} \tau_y (r_1 - R_1) - v_0 \quad (12)$$

$$u_x(r_2) = -\frac{1}{4\eta} \frac{dP}{dx} (R_2^2 - r_2^2) - \frac{C_1}{\eta} \ln \frac{R_2}{r_2} - \frac{1}{\eta} \tau_y (r_1 - R_1) \quad (13)$$

From equation (12) and (13) with boundary conditions at $u_x(r) = \text{Constant}$ $u_x(r_1) = u_x(r_2)$

$$\frac{dp}{dx} \left[hR_m - \frac{1}{2}(r_2 - r_1)(r_2 + r_1) \right] + 2\tau_y \frac{r_1 r_2}{r_2 - r_1} \ln \frac{r_1 R_2}{R_1 r_2} + 2\tau_y(2R_m - r_1 - r_2) - 2\eta v_0 = 0 \quad (14)$$

Volumetric flow rate Q is given by,

$$Q = 2\pi \int_{R_1}^{R_2} r u_x(r) dr$$

Hence,

$$Q = Q_I + Q_{II} + Q_{III}$$

$$Q = 2\pi \left[\int_{R_1}^{r_1} r u_x^I(r) dr + \int_{r_2}^{R_2} r u_x^{II}(r) dr + \int_{r_1}^{r_2} r u_x^{III}(r) dr \right] \quad (15)$$

On substituting equations (6) and (7) into equation (15)

$$Q = \pi R_1^2 v_0 - \pi \left[\int_{R_1}^{r_1} r^2 \frac{du_x^I(r)}{dr} dr + \int_{r_2}^{R_2} r^2 \frac{du_x^{II}(r)}{dr} dr \right] \quad (16)$$

Hence

$$Q = \pi R_1^2 v_0 - \frac{\pi}{8\eta} \left\{ \frac{dp}{dx} [2hR_m(h^2 + 2R_1 R_2) - (r_2^4 - r_1^4)] + \frac{4r_1 r_2}{r_2 - r_1} [2gR_m - (r_2^2 - r_1^2)] + \frac{8\tau_y}{3} [2R_m(h^2 + R_1 R_2) - (r_2^3 + r_1^3)] \right\} \quad (17)$$

By considering the dimensionless number

$$N_1 = -\frac{\pi R_m h v_0}{Q} = -\frac{\pi R_m h}{A_p} \quad (18)$$

$$N_2 = -\frac{\pi R_m h^3}{6\eta A_p V_p} \left(\frac{dp}{dx} \right) \quad (19)$$

$$N_3 = \frac{\pi R_m h^3 \tau_y}{6\eta A_p V_p} \quad (20)$$

Following equation given as,

$$3(N_2 - 2N_3)^2 [N_2^3 - (1 + 3N_3 - N_1)N_2 + 4N_3] + N_1^2 \times N_2^2 N_3 = 0 \quad (21)$$

when $|N_1| > 3(N_2 - 2N_3)^2/N_2$, the pressure gradient is independent of dimensionless yield stress N_3 . For conditions $0 < N_3 < 1000$ and $0.5 < N_1 < 0$ an approximate solution can be given for pressure gradient as,

The total pressure drop in a working device is given by,

$$\Delta P = \Delta P_\eta + \Delta P_\tau = \frac{6v_p(A_p + \pi R_m h)}{\pi R_m h^3} \eta L + \frac{c}{h} \tau_y(H) L \quad (22)$$

Where ΔP_η pressure drop viscous component and ΔP_τ pressure drop yield stress component.

$$c = 2.07 + \frac{1}{1+N_3} = \left(2.07 + \frac{12\eta A_p v_p}{12\eta A_p v_p + 0.4A_g h \tau_y} \right) \quad (23)$$

The force induced in the device is expressed as,

$$F = \Delta P_\eta A_p + \Delta P_\tau A_p \quad (24)$$

Hence,

$$F_\eta = \frac{12\eta A_{Rm} v_p}{A_g h^2} A_p L \quad \text{and} \quad F_\tau = \frac{c \tau_y(H) A_p}{h} L \quad (25)$$

APPENDIX-B

Particle Swarm Optimization

To evaluate the optimal proportion of iron particle volume fraction in the MR fluid for MR damper application, particle swarm optimization technique was used. The MATLAB code for solving the problem is as below,

```
function z=Function name(x)
z=- Objective function;
end
%% Parameters and objective
ObjtFunction=@(x) MRF(x);
nVar=3;
VarSize=[1 nVar];
VarMin=[0.25 25 0.5];
VarMax=[1 35 2];
MaxIt=1000;
nPop=100;
w=1;
wdamp=0.99;
c1=2.0;
c2=3.0;
%% Population initialization
Initial_prtl.Loc=[];
Initial_prtl.Vel=[];
Initial_prtl.Objt=[];
Initial_prtl.B.Loc=[];
Initial_prtl.B.Objt=[];
prtl= repmat(Initial_prtl, nPop, 1);
GB.Objt=inf;
for i=1:nPop
```

```

prtl(i).Loc = unifrnd(VarMin, VarMax, VarSize);
prtl(i).Vel = zeros(VarSize);
prtl(i).Objt = ObjtFunction(prtl(i).Loc);
prtl(i).B.Loc = prtl(i).Loc;
prtl(i).B.Objt = prtl(i).Objt;
if prtl(i).B.Objt < GB.Objt
    GB = prtl(i).B;
end
end
% pso main program
BObjts = zeros(MaxIt, 1);
for it=1:MaxIt
    for i=1:nPop
        prtl(i).Vel = w*prtl(i).Vel...
            +c1*rand(VarSize).*(prtl(i).B.Loc - prtl(i).Loc)
            +c2*rand(VarSize).*(GB.Loc - prtl(i).Loc);
        prtl(i).Loc = prtl(i).Loc + prtl(i).Vel;
        prtl(i).Loc = max(prtl(i).Loc, VarMin);
        prtl(i).Loc = min(prtl(i).Loc, VarMax);
        prtl(i).Objt = ObjtFunction(prtl(i).Loc);
        if prtl(i).Objt < prtl(i).B.Objt
            prtl(i).B.Loc = prtl(i).Loc;
            prtl(i).B.Objt = prtl(i).Objt;
            if prtl(i).B.Objt < GB.Objt
                GB = prtl(i).B;
            end
        end
    end
end

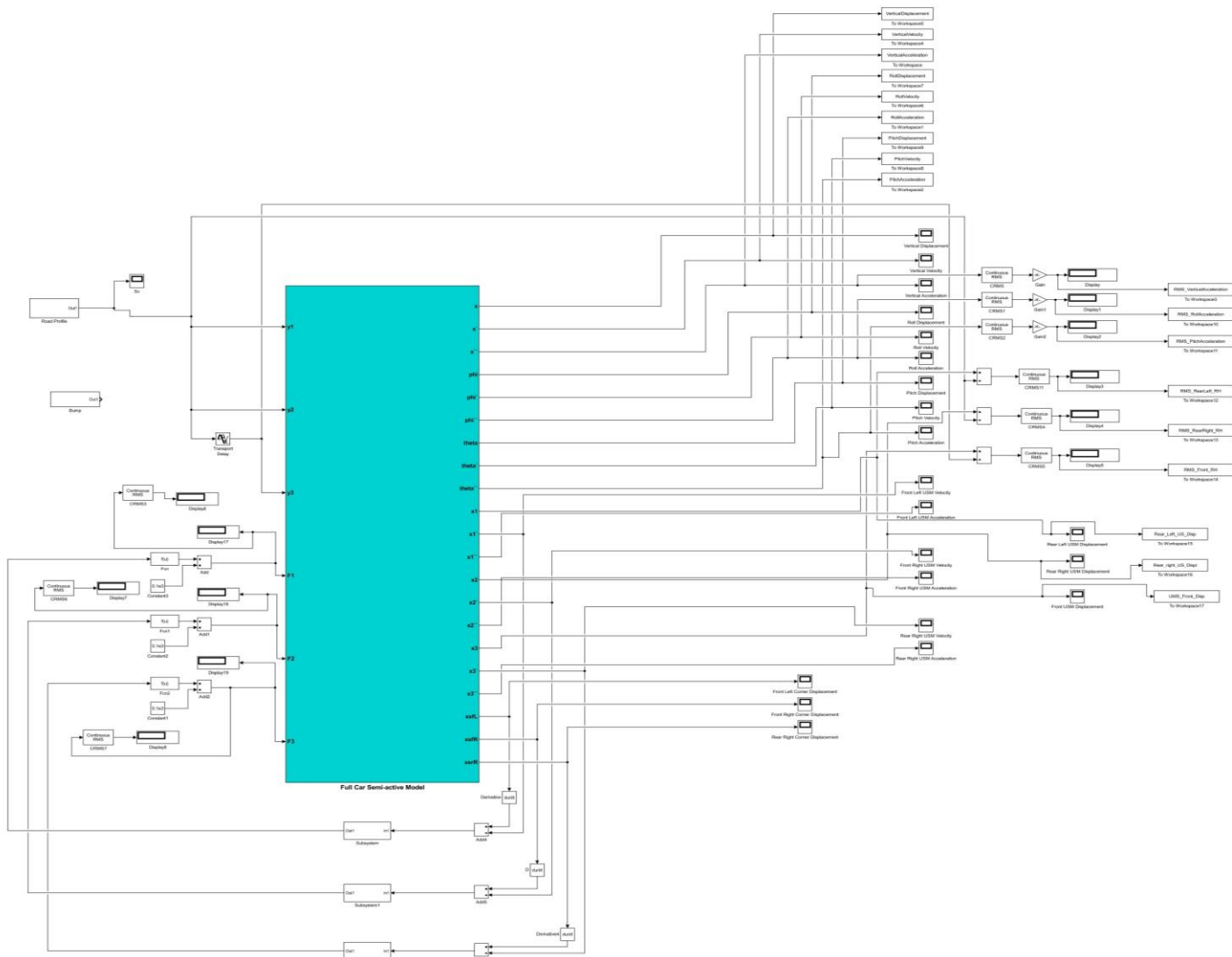
BObjts(it) = GB.Objt;
disp(['Iteration ' num2str(it) ': B Objt = ' num2str(BObjts(it))]);

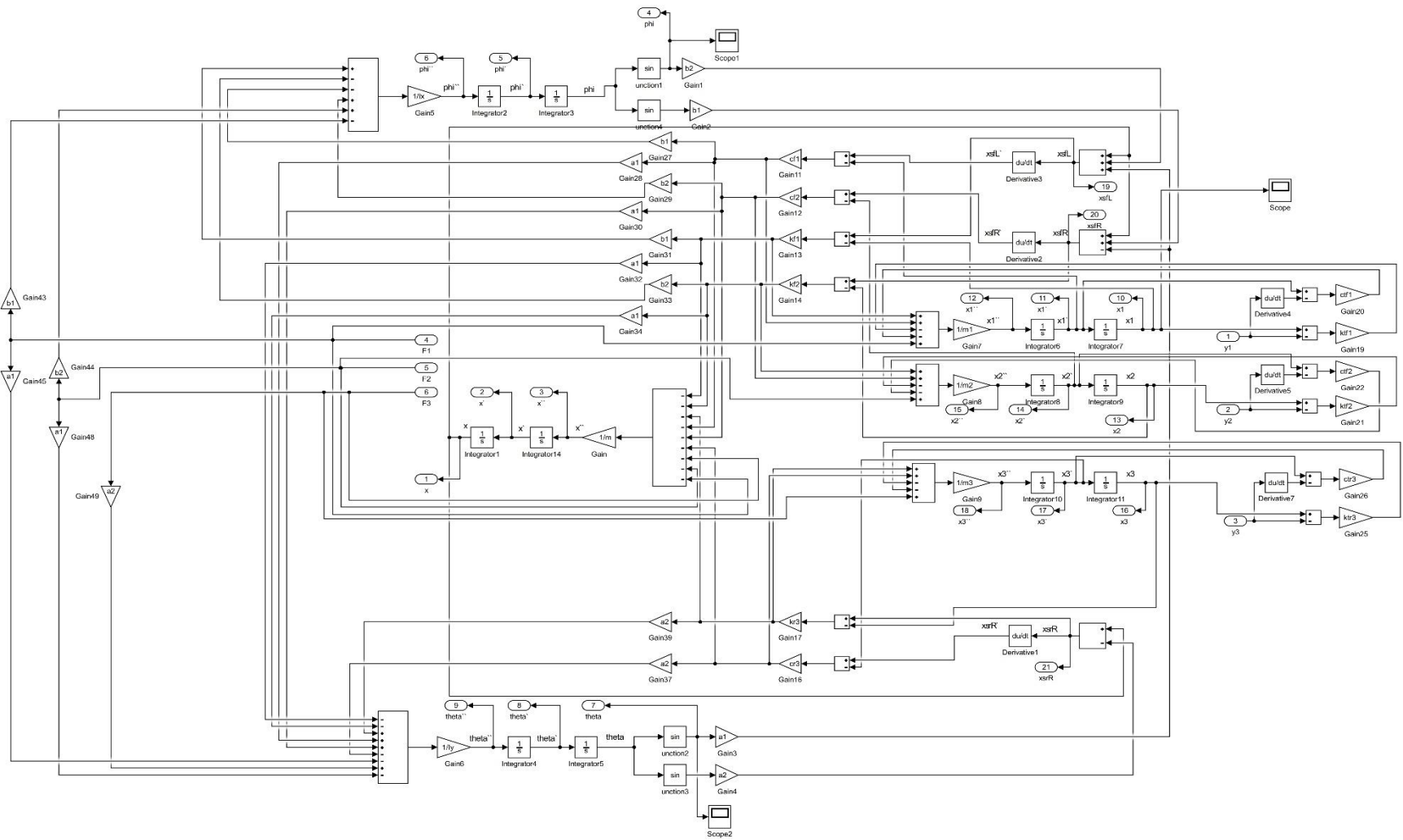
```

```
w=w*wdamp;  
end  
figure;  
semilogy(BObjts, 'LineWidth', 2);  
xlabel('Iteration');  
ylabel('B Objt');
```


APPENDIX-C

Simulink model of three-wheeler vehicle





APPENDIX-D

Multi-objective optimisation or pareto optimisation involves the optimisation problems statement with more than one objective function. It is concerned with mathematical optimisation of several objective simultaneously. MOGA used in ANSYS software is a hybrid variant of NAGA-II (Non-dominated sorted genetic algorithm II). It supports all types of input parameters.

Non-dominance principle is used to handling constraints, hence penalty function or lagrangian multiplier are not necessary and assumes a feasible solution.

MOGA procedure:

1. Population of MOGA: Initial population is generated and used to run the MOGA
2. New population generation: Population is generated by cross over and mutation after each iteration each population is run until it attains the number of samples defined initially.
3. Design point update: Design points for newly generated population are updated.
4. Convergence validation: MOGA converges when the maximum allowable pareto percentage or convergence stability is reached. Non-convergence: Process continuous to next step.
5. Stopping criteria: If the optimisation has not converged it is validated for fulfilment of stopping criteria. When maximum number if iteration criteria is met the process is stopped without having reached convergence. If the stopping criteria not met. MOGA run again to converge a new population.

The process MOGA uses to generate a new population is comprised of two main steps: Cross-over and Mutation.

Cross-over: Cross-over combines (mates) two chromosomes (parents) to produce a new chromosome (offspring). The idea behind cross-over is that the new chromosome may be better than both of the parents if it takes the best characteristics from each of the parents. Cross-over occurs during evolution according to a user-definable cross-over probability.

Cross-over for Continuous Parameters: A cross-over operator that linearly combines two parent chromosome vectors to produce two new offspring according to the following equations:

$$\text{Offspring1} = a * \text{parent1} + (1 - a) * \text{parent2}$$

$$\text{Offspring2} = (1 - a) * \text{parent1} + a * \text{parent2}$$

Mutation: Mutation alters one or more gene values in a chromosome from its initial state. This can result in entirely new gene values being added to the gene pool. With these new gene values, the genetic algorithm may be able to arrive at a better solution than was previously possible. Mutation is an important part of the genetic search, as it helps to prevent the population from stagnating at any local optima. Mutation occurs during evolution according to a user-defined mutation probability.

Mutation for Continuous Parameters: For continuous parameters, a polynomial mutation operator is applied to implement mutation.

$$C = P + (\text{Upper Bound} - \text{Lower Bound}) \delta$$

where C is the child, P is the parent, and δ is a small variation calculated from a polynomial distribution.

List of Publications based on PhD Research Work

Sl. No.	Title of the paper	Authors (in the same order as in the paper. Underline the Research Scholar's name)	Name of the Journal/ Conference/ Symposium, Vol., No., Pages	Month & Year of Publication	Category *
1	Performance analysis of a semi-active suspension system using coupled CFD-FEA based non-parametric modelling of low capacity shear mode monotube MR damper	Gurubasavaraju T.M , Hemantha Kumar and Arun M.	Proc. Inst. Mech. Eng. Part D - Journal of Automobile Engineering- (Science citation expanded index-IF 1.25. Sage Publication. DOI. 10.1177/0954407018765899	March-2018	1
2	An approach for characterizing twin tube shear mode magnetorheological damper through coupled FE and CFD analysis	Gurubasavaraju T.M , Hemantha Kumar and Arun M.	Journal of the Brazilian Society of Mechanical Sciences and Engineering, (Science citation expanded index-IF 1.23)- Springer publication 10.1007/s40430-018-1066-z	Feb-2018	1
3	Optimisation of monotube magnetorheological damper under shear mode	Gurubasavaraju T.M , Hemantha Kumar and Arun M.	Journal of the Brazilian Society of Mechanical Sciences and Engineering, Volume 39, Issue 6, pp 2225–2240 (Science citation expanded index-IF 1.23)-Springer publication	June 2017	1
4	Evaluation of optimal parameters of MR fluids for damper application using particle swarm and response surface optimisation	Gurubasavaraju T.M , Hemantha Kumar and Arun M.	Journal of the Brazilian Society of Mechanical Sciences and Engineering, Volume 39, Issue 9, pp 3683–3694 (Science citation expanded index-IF 1.23)-Springer publication	September 2017	1
5	Effect of rheological properties of MR fluid on dynamic performance of semi-active suspension with MR damper	Gurubasavaraju T.M , Hemantha Kumar and Arun M.	International Conference on Vibration Problem IIT Guwahati 2017	November 2017	3
6	A study of influence of material properties on magnetic flux density induced in magneto rheological damper through finite element analysis.	Gurubasavaraju T.M , Hemantha Kumar and Arun M	International Conference on Research in Mechanical Engineering Sciences, MIT Manipal.	December 2017	3

[to be filled-in by the Research Scholar and to be enclosed with Synopsis Submission Form

* Category: 1 : Journal paper, full paper reviewed, 2 : Journal paper, Abstract reviewed, 3 : Conference/Symposium paper, full paper reviewed, 4 : Conference/Symposium paper, abstract reviewed, 5 : others (including papers in Workshops, NITK Research Bulletins, Short notes etc.) (If the paper has been accepted for publication but yet to be published, the supporting documents must be attached.)

Research Scholar
Name & Signature, with Date

Research Guide
Name & Signature, with Date

Research Guide
Name & Signature, with Date

List of papers under review

Gurubasavaraju T.M., Hemantha Kumar and Arun M, “Dynamic response analysis of three-wheeler vehicle model equipped with dual annular mixed mode MR damper” *Journal: Proc. Inst. Mech. Eng. Part I - Journal of Systems and control Engineering- Sage Publication..* (**Revised and submitted**)- Sage publication IF-1.42

Gurubasavaraju T.M., Hemantha Kumar and Arun M “Evaluation of MR damper force through rheological characterization of magnetorheological fluids” *Journal of Engineering Science and Technology* (**under review**)- Malaysia.

BIO-DATA

1. **Name** : Gurubasavaraju T. M.
2. **Father's Name** : Thippeswamy T. M
3. **Date of Birth** : 24/04/1988
4. **Nationality** : Indian
5. **Marital Status** : Single
6. **Address** :

Permanent Address

s/o Thippeswamy T. M.
Tharehalli
Pallagatte, Jagaluru Taluk
Davanagere, Karnataka 577513

7. **Mobile Number** : +91 8762722404
8. **Email id** : gbrajtm@gmail.com / gbrajtm@yahoo.in

9. Educational Qualification:

Qualification	College/School	University/Board	Year of passing	Performance
Ph.D in Mechanical Engineering	National Institute of Technology Karnataka, Surathkal	National Institute of Technology Karnataka	Persuing	8.3 CGPA
M.Tech in Computer Aided Engineering	VTU center for post graduation studies Bengaluru	VTU Bengaluru	2014	73.4 %
BE in Mechanical Engineerin	Dr.Ambedkar Institute of Technology Bengaluru	VTU Belagavi	2010	71.3 %

I here by declare that above information is true and correct to best of my knowledge and belief.

Gurubasavaraju T. M.